



# Potentiel thérapeutique des S-nitrosothiols dans la prévention de l'athérosclérose : modulation de la métaplasie des monocytes et cellules musculaires lisses en cellules spumeuses

Justine Bonetti

## ► To cite this version:

Justine Bonetti. Potentiel thérapeutique des S-nitrosothiols dans la prévention de l'athérosclérose : modulation de la métaplasie des monocytes et cellules musculaires lisses en cellules spumeuses. Médecine humaine et pathologie. Université de Lorraine; Università degli studi (Sienne, Italie), 2021. Français. NNT : 2021LORR0172 . tel-03559981

**HAL Id: tel-03559981**

**<https://hal.univ-lorraine.fr/tel-03559981>**

Submitted on 7 Feb 2022

**HAL** is a multi-disciplinary open access archive for the deposit and dissemination of scientific research documents, whether they are published or not. The documents may come from teaching and research institutions in France or abroad, or from public or private research centers.

L'archive ouverte pluridisciplinaire **HAL**, est destinée au dépôt et à la diffusion de documents scientifiques de niveau recherche, publiés ou non, émanant des établissements d'enseignement et de recherche français ou étrangers, des laboratoires publics ou privés.



## AVERTISSEMENT

Ce document est le fruit d'un long travail approuvé par le jury de soutenance et mis à disposition de l'ensemble de la communauté universitaire élargie.

Il est soumis à la propriété intellectuelle de l'auteur. Ceci implique une obligation de citation et de référencement lors de l'utilisation de ce document.

D'autre part, toute contrefaçon, plagiat, reproduction illicite encourt une poursuite pénale.

Contact : [ddoc-theses-contact@univ-lorraine.fr](mailto:ddoc-theses-contact@univ-lorraine.fr)

## LIENS

Code de la Propriété Intellectuelle. articles L 122. 4

Code de la Propriété Intellectuelle. articles L 335.2- L 335.10

[http://www.cfcopies.com/V2/leg/leg\\_droi.php](http://www.cfcopies.com/V2/leg/leg_droi.php)

<http://www.culture.gouv.fr/culture/infos-pratiques/droits/protection.htm>

**Ecole Doctorale BioSE (Biologie-Santé-Environnement)**  
**Doctorate in GenOMeC (Genetics, Oncology and Clinical Medicine)**

**Thèse**

Présentée et soutenue publiquement pour l'obtention du titre de

**DOCTEUR DE L'UNIVERSITE DE LORRAINE**

**Mention : « Sciences de la Vie et de la Santé »**

par **Justine BONETTI**

**Potentiel thérapeutique des *S*-nitrosothiols dans la prévention de  
l'athérosclérose : modulation de la métaplasie des monocytes et  
des cellules musculaires lisses en cellules spumeuses**

**3 novembre 2021**

**Membres du jury :**

<b>Rapporteurs :</b>	<b>Lars-Oliver KLOTZ</b>	<b>Pr., Nutrigenomics section, Institute of Nutritional Sciences, Friedrich Schiller University, Jena, Germany</b>
	<b>Valérie SCHINI-KERTH</b>	<b>Pr., UMR 1260 INSERM Nanomédecine Régénérative, Faculté de Pharmacie, Université de Strasbourg</b>
<b>Examineurs :</b>	<b>Caroline GAUCHER</b>	<b>MCU, HDR, CITHEFOR EA 3452, Université de Lorraine. Directeur de thèse</b>
	<b>Alfonso POMPELLA</b>	<b>Pr., Department of Translational Research NTMC, University of Pisa, Italy. Co-directeur de thèse</b>
<b>Membres invités :</b>	<b>Alessandro CORTI</b>	<b>Dr., Department of Translational Research NTMC, University of Pisa, Italy. Co-directeur de thèse</b>
	<b>Nathalie AUCHET-MERCIER</b>	<b>MCU, HDR, U1116, INSERM, Université de Lorraine</b>

---

**CITHEFOR EA 3452 « Cibles Thérapeutiques, Formulation et Expertise Pré-clinique du Médicament »,  
Campus Brabois Santé, 9 avenue de la Forêt de Haye – BP 20199, 54505 Vandœuvre-lès-Nancy, France  
Department of Translational Research and New Technologies in Medicine and Surgery: Redox Signalling  
Laboratory, Medical School, University of Pisa, Via Roma 55, 56126 Pisa, Italy**

# Acknowledgements

---

The completion of this PhD thesis would not have been possible without many people whom I would like to thank for their implication, support and help. It is not easy for me to express my feelings, I apologize for these concise acknowledgements.

I wish express my sincere thanks to Pr. Lars-Oliver Klotz (University of Jena) and Pr. Valérie Schini-Kerth (University of Strasbourg) for accepting to be the reviewers of this work.

I would like to sincerely thank Dr. Caroline Gaucher, my French supervisor. Thanks for your implication, your patience with me, your support and trust in me. Thanks for your help in the research and experimental parts and the writing of this manuscript (and I know the amount of patience you needed). Finally, thanks to tolerate me since my Master's degree, you are a model for me.

I gratefully acknowledge Pr. Alfonso Pompella, my Italian supervisor, for his help in this international project, for all his precious knowledges and tips. Thanks guiding me in this crazy Italian life.

I wish also thank Dr. Alessandro Corti, my Italian co-supervisor, for his huge support, implication in the experiment part and also in the theoretical part of this work.

I also thank Dr. Nathalie Mercier for your implication in my thesis committee and your advices in this project. To Dr. Natacha Dreumont for your help and advices in the experimental part.

I would like to express my thanks Pr. Ariane Boudier (director of CITHEFOR) for your welcome, Pr. Anne Sapin-Minet, Pr. Isabelle Lartaud, Pr. Igor Clarot and Dr. Marianne Parent for all your advices and kindness.

To Pr. Pierre Leroy, the previous director of CITHEFOR, thanks you for teaching me the chromatography even if I was not a chemist and never learn chemistry my myself.

A special thank for Isabelle Fries, the best colleague, to follow me in my experiments, for all your advices in the experimentation and for your happiness. It was a pleasure to work with you.



To Marine, thank you to support me since the Master's degree and to proofread all my manuscripts from Québec. Next year, it will be your turn...

To Arnaud, Eugenia, Jordan, Margaux, Célia, Rama, Haiyan and Yi, you are the best colleagues and friends. Thanks for all the crazy moments in the lab and outside... And a last thanks for all my colleagues in IMoPA laboratory.

Finally, an immense thank to my parents, my sister and my brother, who always support me in my projects.

To my Italian grandfather who was so proud to know me in his country...

# List of contents

---

<b>Scientific works</b> .....	6
Publications .....	6
Presentations .....	7
Summer school .....	7
Formation.....	7
Teaching .....	8
<b>List of figures</b> .....	9
<b>List of tables</b> .....	12
<b>List of abbreviations</b> .....	13
 <b>Introduction générale</b> .....	 18
<b>CHAPTER 1: INTRODUCTION</b> .....	<b>21</b>
I. Atherosclerosis.....	22
1. General description .....	22
2. Nitric oxide in atherosclerosis.....	25
a. Nitric oxide and vascular homeostasis .....	25
b. Nitric oxide and the development of atherosclerosis disease .....	28
3. Phenotypic modulation of macrophages and SMCs: a link between NO depletion and activation of signaling pathways.....	28
4. Other cell types implicated.....	50
5. Atherosclerosis, oxidative stress and glutathione homeostasis .....	51
II. Atherosclerosis prevention and associated treatments.....	75
III. Animal models of atherosclerosis .....	77
IV. NO donors administration routes .....	79
<b>CHAPTER 2: S-NITROSOTHIOLS POTENTIAL vs. MACROPHAGES DERIVED FOAM CELLS FORMATION AND MONOCYTES/MACROPHAGES DIFFERENTIATION/POLARIZATION</b> .....	<b>94</b>
I. Production of oxidized low-density lipoproteins .....	95
1. Oxidation of low-density lipoproteins.....	95
2. Peroxidised lipids quantification .....	96
II. Article 4: S-nitrosoglutathione impact on oxLDLs phagocytosis by M0-macrophages .....	98
III. Development of a primary model of monocytes differentiation into macrophages and their polarization.....	119

1. Differentiation of monocytes into M0-macrophages .....	119
a. Polarization of M0-macrophages.....	120
b. Antioxidant defences .....	121
<b>CHAPTER 3: DEVELOPMENT OF A SMOOTH MUSCLE CELLS MODEL OF DEDIFFERENTIATION.....</b>	<b>125</b>
I. Validation of vascular smooth muscle cells contractile phenotype .....	127
II. Development of the smooth muscle cells dedifferentiation model.....	129
1. Synchronisation of the cells and impact of Angiotensin II .....	130
a. NOX species production.....	132
b. Cell redox status .....	133
<b>DISCUSSION GENERALE, CONCLUSIONS ET PERSPECTIVES .....</b>	<b>134</b>
I. Discussion générale .....	135
II. Conclusions et perspectives .....	139
<b>REFERENCES .....</b>	<b>142</b>
<b>Appendix 1 .....</b>	<b>149</b>

## Scientific works

---

### Publications

#### Published:

- **J. Bonetti**, A. Corti, L. Lerouge, A. Pompella, C. Gaucher, Phenotypic modulation of macrophages and vascular smooth muscle cells in atherosclerosis – Nitro-redox interconnections, *Antioxidants (Basel)* (2021); 10(4):516. **IF = 6.31 (Review)**
- A. Corti, **J. Bonetti**, S. Dominici, S. Piaggi, V. Fierabracci, R. Foddìs, A. Pompella, Induction of gamma-glutamyltransferase activity and consequent prooxidant reactions in human macrophages exposed to crocidolite asbestos, *Toxicol. Sci. Off. J. Soc. Toxicol.* (2019); 177(2):476-482. **IF = 3.85 (Original article)**
- M. Parent, Y. Zhou, **J. Bonetti**, C. Perrin-Sarrado, I. Lartaud, A. Sapin-Minet, C. Gaucher, Antioxidant Properties of S-nitrosoglutathione and Nanotechnologies, *Proceedings*. 11 (2019). **IF = None (Congress article)**
- C. Gaucher, A. Boudier, **J. Bonetti**, I. Clarot, P. Leroy, M. Parent, Glutathione: Antioxidant Properties Dedicated to Nanotechnologies, *Antioxid. Basel Switz.* 7 (2018); 7(5):62. **IF = 4.52 (Review)**
- R. Alhasan, A. Kharmah, M.J. Nasim, A.Y. Abidin, **J. Bonetti**, P. Giummelly, C.E.C.C. Ejike, P. Leroy, C. Gaucher, C. Jacob, Flush with a flash: natural three-component antimicrobial combinations based on S-nitrosothiols, controlled superoxide formation and “domino” reactions leading to peroxynitrite, *MedChemComm.* 9 (2018); 9(12):1994–1999. **IF = 2.34 (Original article)**
- H. Yu, **J. Bonetti**, C. Gaucher, I. Fries, L. Vernex-Loiset, P. Leroy, P. Chaimbault, Higher-energy collision-induced dissociation for the quantification by liquid chromatography/tandem ion trap mass spectrometry of nitric oxide metabolites coming from S-nitrosoglutathione in an in vitro model of the intestinal barrier, *Rapid Commun. Mass Spectrom. RCM.* 33 (2019); 33(1):1–11. **IF = 1.97 (Original article)**
- **J. Bonetti**, Y. Zhou, M. Parent, I. Clarot, H. Yu, I. Fries-Raeth, P. Leroy, I. Lartaud, C. Gaucher, Intestinal absorption of S-nitrosothiols: Permeability and transport mechanisms, *Biochem. Pharmacol.* 155 (2018); 155:21–31. **IF = 4.58 (Original article)**

### **To be submitted:**

**J. Bonetti**, A. Corti, I. Fries, A. Pompella, C. Gaucher, *S*-nitrosoglutathione impact on oxLDLs phagocytosis by M0-macrophages. *To be submitted in Nitric Oxide Journal* (IF = 4.23)

## **Presentations**

### **Oral communications**

- **October 2019** › “*Therapeutic potential of S-nitrosothiols in the prevention of atherosclerosis: Modulation of monocytes and smooth muscle cells metaplasia into foam cells*” – The NutRedOx COST Action CA16112, Lisbon (Portugal)
- **November 2018** › “*Therapeutic potential of S-nitrosothiols in the prevention of atherosclerosis: Modulation of monocytes and smooth muscle cells metaplasia into foam cells*” – Riunione Scientifica Scuola Dianzani, Torino (Italy)
- **September 2017** › “*Permeability and transport mechanisms of S-nitrosothiols in cellular model of intestinal barrier*” – The NutredOx COST Action CA16112 & the 6<sup>th</sup> NutriOx Atelier 2017, Strasbourg (France)

### **Poster presentations**

- **March 2020** › “*Therapeutic potential of S-nitrosothiols in the prevention of atherosclerosis: modulation of monocytes metaplasia into foam cells*” – The NutRedOx COST Action CA16112, Belgrade (Serbia) → **1<sup>st</sup> price of Poster**
- **June 2017** › P 168 – “*Intestine permeability of S-nitrosoglutathione as a potential nitric oxide donor via oral administration*” – *Free Radical Biology and Medicine*, Abstracts of the OCC World Congress and Annual SFRR-E Conference 2017 Metabolic Stress and Redox Regulation Berlin, Germany – **IF = 5.65**

## **Summer school**

**Cell Migration Workshop:** concepts, mechanisms and techniques › The lectured at the School of Health Sciences and Technologies (ECTS) from Lusófona University (Portugal)

## **Formation**

**2018** › UNIVERSITY DEGREE IN ANIMAL EXPERIMENTATION – Design and implementation of procedures – Faculty of Pharmacy, Université de Lorraine

## Teaching

- 2017-2020** › DCCE in microbiology, Faculty of Sciences and Techniques, Université de Lorraine
- 1<sup>st</sup> year of Bachelor's Degree in Life Sciences and Environment (UE 2.02A – Bacteriology): **16 h TD + 62 h TP**
- 2019-2020** › DCCE in biochemistry, Faculty of Pharmacy, Université de Lorraine
- DFG-SP2: - UEB BIO (Biological Sciences): **9 h TP**
- UEL BMI (Integrated Molecular Biology): **12 h TP**
- DFG-SP3: - UEL PGP (From Pharmacogenetic/Pharmacogenomic to personal therapy): **9 h TP**
- DFA-SP1: - UEL MOP (Markers of hereditary pathologies from molecular mechanisms): **3 h TP**

# List of figures

---

## Introduction générale

**Fig. 1:** Les différents acteurs impliqués dans le développement de l'athérosclérose ..... 18

## CHAPTER 1

**Fig. 2:** Synthesis of endogenous nitric oxide by nitric oxide synthase [22]. NADPH: nicotinamide adenine dinucleotide phosphate; NO: nitric oxide ..... 25

**Fig. 3:** NO signaling in the cardiovascular system, under physiological condition [30] ..... 27

**Fig. 4:** NO in the cardiovascular system, under pathological conditions [30] ..... 28

**Fig. 5:** Endothelial cells metabolism in atherosclerosis from Theodorou *et al.* [42] ..... 50

**Fig. 6:** Systems producing reactive oxygen species in atherosclerosis [46]. MIT: mitochondrial oxidative; eNOS: endothelial nitric oxide synthase ..... 51

## CHAPTER 2

### Article 4

**Fig. 7:** Optical microscopy monocytes (picture from ATCC) (A) and M0-like macrophages (Magnification: 40x, scale bar: 10  $\mu$ m) (B); fluorescent microscopy of CD68 in M0-like macrophages (Magnification: 40x, scale bar: 10  $\mu$ m) ..... 107

**Fig. 8:** Optical microscopy of M0-like macrophages before and after pre-treatment with 25  $\mu$ M of GSNO and 25  $\mu$ g/mL of oxLDLs (Magnification: 40x, scale bar: 10  $\mu$ m) ..... 108

**Fig. 9:** Fluorescent microscopy of M0-macrophages pre-treated with GSNO at 25  $\mu$ M and incubated with 25  $\mu$ g/mL of DiI-oxLDLs (Magnification: 40x) (n=1) ..... 108

**Fig. 10:** Immunofluorescent detection of CD36 in M0-macrophages. Cells were pre-treated with GSH or GSNO for 6 h and incubated with oxLDLs at 25  $\mu$ g/mL for 48 h in fresh complete medium. Cells were fixed with paraformaldehyde and incubated first with CD36 primary antibody followed by a secondary antibody coupled to Alexa<sup>®</sup> 488. Finally, nuclei were labelled with Hoechst 33258 (Magnification: 40x, scale bar: 20  $\mu$ m) ..... 109

**Fig. 11:** Expression of CD36 after M0-macrophages pre-treatment with 25  $\mu$ M of GSNO and incubation with 25  $\mu$ g/mL of oxLDLs. Ratio of proteins of CD36 *vs.*  $\alpha$ -actin bands were quantified by ImageJ. Results are presented as mean  $\pm$  SEM of 3 independent experiments and analysed by One-way ANOVA and Bonferroni's post-test; . \* *vs.* control; # *vs.* oxLDLs;  $p < 0.05$  ..... 109

**Fig. 12:** Extracellular quantification of peroxynitrite ions. Cells were pre-treated with GSH or GSNO for 6 h and incubated with oxLDLs at 25 µg/mL for 48 h in fresh complete medium. Results are presented as mean ± SEM of 2-3 independent experiments and analysed by Two-way ANOVA..... 110

**Fig. 13:** Thiol redox status of M0-macrophages. Cells were pre-treated with GSH or GSNO for 6 h and incubated with oxLDLs at 25 µg/mL for 48 h in fresh complete medium. **A:** intracellular low molecular weight (LMW) thiols concentration; **B:** intracellular GSH concentration; **C:** intracellular GSH/GSSG ratio; **D:** extracellular GSH concentration and **E:** intracellular protein thiols concentration. Results are presented as mean ± SEM of 3 independent experiments and analysed by Two-way ANOVA and Tukey's multiple comparison; \* *vs.* control without oxLDLs; # *vs.* control with oxLDLs; † *vs.* GSH without oxLDLs; \$ *vs.* GSNO with oxLDLs;  $p < 0.05$ ..... 111

**Figure 14:** **A:** Intracellular formation of nitrite ions ( $\text{NO}_2^-$ ) and **B:** S-nitrosothiols (RSNOs), quantified by DAN and DAN-Hg<sup>2+</sup> assay. N.D.: not detected. Cells were pre-treated with GSH or GSNO for 6 h and incubated with oxLDLs at 25 µg/mL for 48 h in fresh complete medium. Results are presented as mean ± SEM of 3 independent experiments and analysed by Two-way ANOVA;  $p < 0.05$  ..... 113

---

**Fig. 15:** Enzyme activity of the γ-glutamyl transferase (GGT) (**A**), the glutathione peroxidase (GPx) (**B**), the glutathione reductase (GR) (**C**) and the glutathione S-transferase (GST) (**D**). Results are presented as mean ± SEM of 3-4 independent experiments and analysed by One-way ANOVA – Tukey's post test; \* *vs.* IL-4 or IFNγ;  $p < 0.05$ ..... 123

### CHAPTER 3

**Fig. 16:** Optical microscopy of Human Aortic smooth muscle cells – CC2571 Lonza® (pictures from Lonza®)..... 127

**Fig. 17:** Immunofluorescent detection of differentiation markers of vSMCs: α-actin, transgelin, vimentin and reference protein: GAPDH. Cells were fixed with paraformaldehyde 4% (w/v) and labelled with 1:50 α-actin/transgelin/vimentin for 45 minutes in blocking solution (Triton 0.1% (w/v), PBS/BSA 0.5% (w/v)). Then, secondary antibody Alexa® 488 diluted at 1:100 was incubated 45 minutes. Finally, nuclei are labelled by Hoechst 33258 for 15 minutes (Magnification: 40x, scale bar: 10 µm)..... 127

**Fig. 18:** Quantification of the expression of differentiation markers of vSMCs by Western blot analysis; GAPDH, α-actin, transgelin and vimentin (n=3) ..... 128

**Fig. 19:** Impact of cell passages of the expression of differentiation markers: α-actin, transgelin and vimentin (n=1) ..... 128

**Fig. 20:** Protocol for SMC dedifferentiation based on Tang *et al.* [82] ..... 130



<b>Fig. 21:</b> Effect of passage and AngII stimulation on GAPDH expression in AoSMCs. Analysis were performed by Western-blot and bands quantify by ImageJ; Mean $\pm$ SEM (n=3) .....	130
<b>Fig. 22:</b> Optical microscopy of vSMCs. Cells are synchronised at J+1 during 24 h with complete medium by FBS deprivation (0.5% FBS) and are treated with AngII at 100 nM for 48 h (Magnification: 20x, scale bar: 100 $\mu$ m) .....	131
<b>Fig. 23:</b> Expression of differentiation markers after 48h of AngII stimulation. Ratio of protein of interest vs. GAPDH after Western-blot: $\alpha$ -actin ( <b>A</b> ), transgelin ( <b>B</b> ) and vimentin ( <b>C</b> ). Results are presented as mean $\pm$ SEM of 3 independent experiments and analysed by <i>t</i> -test; Mann-Whitney test .....	131
<b>Fig. 24:</b> Extracellular quantification of nitrite ions by Griess assay ( <b>A</b> ). vSMCs were synchronised 24 h with FBS 0.5% and incubated for 48 h with AngII; Extracellular ( <b>B</b> ) and intracellular ( <b>C</b> ) quantification of peroxynitrite ions in vSMCs after incubation with 100 nM of AngII for 48 h. Results are presented as mean $\pm$ SEM of 2-3 independent experiments and analysed by One-way ANOVA .....	132
<b>Fig. 25:</b> Intracellular thiols status after incubation with 100 nM of AngII (n=1 in triplicate) .....	133

# List of tables

---

## CHAPTER 1

<b>Table 1:</b> overview of large and small animals used as atherosclerotic models .....	78
--	----

## CHAPTER 2

<b>Table 2:</b> protocol of LDLs oxidation by copper sulfate .....	96
--	----

<b>Table 3:</b> expression of M1- and M2-macrophages markers after analysis by flow-cytometry .....	120
---	-----

## CHAPTER 3

<b>Table 4:</b> Synthesis of dedifferentiation protocols in literature .....	129
--	-----

## List of abbreviations

---

ABBREVIATION	FULL NAME
AAPH	2,2'-azobis(2-methylpropionamidine) dihydrochloride
ALDH2	Mitochondrial aldehyde dehydrogenase-2
AngII	Angiotensin II
AoSMC	Aortic smooth muscle cell
apo-E	Apolipoprotein-E
AT <sub>1</sub> R and AT <sub>2</sub> R	Angiotensin-II receptors
ATCC	American type culture collection
BCA	Bicinchoninic acid
BKCa	Large-conductance calcium-sensitive potassium channel
CAM	Cell adhesion molecule
CD	Cluster of differentiation
CDNB	Chloro-2,4 dinitrobenzene
cGMP	Cyclic guanosine monophosphate
Cys	Cysteine
DAN	2,3-diaminonaphthalene
DNA	Deoxyribonucleic acid
DTNB	5-5'-dithio-bis(2-nitrobenzoic) acid
EC	Endothelial cells
EDTA	Ethylenediaminetetraacetic acid
eNOS	Endothelial nitric oxide synthase
FAO	Fatty acid oxidation

FBS	Foetal bovine serum
GAPDH	Glyceraldehyde-3-phosphate dehydrogenase
GGT	$\gamma$ -glutamyltransferase
Glygly	Glycylglycine
GM-CSF	Granulocyte macrophage colony-stimulating factor
GPNA	Gamma-glutamyl-p-nitroanilide
GPx	Glutathione peroxidase
GR	Glutathione reductase
GS-DNB	GS-dinitrobenzene
GSH	Glutathione
GSNO	<i>S</i> -nitrosoglutathione
GSNO-NP	<i>S</i> -nitrosoglutathione nanoparticles
GSSG	Glutathione disulfide
GST	Glutathione <i>S</i> -transferase
HIF1 $\alpha$	Hypoxia inducible factor 1 alpha
HMG-CoA	3-hydroxy-3-methyl-glutaryl-coenzyme A
HMW	High molecular weight
HO-1	Heme oxygenase-1
HRP	Horseradish peroxidase
ICAM-1	Intercellular adhesion molecule-1
IL	Interleukin
iNOS	Inducible nitric oxide synthase
KLF-2	Krüppel-like factor 2
LDLs	Low-density lipoproteins

LMW	Low molecular weight
Lox-1	Lox-density lipoprotein receptor-1
LPS	Lipopolysaccharide
LRP-1	Low-density lipoprotein receptor-related protein-1
LTCC	L-type calcium channel
M0-macrophage	Native macrophage
M1-macrophage	Pro-inflammatory macrophage
M2-macrophage	Anti-inflammatory macrophage
MCP-1	Monocytes chemoattractant protein-1
M-CSF	Macrophage colony-stimulating factor
MDA	Malondialdehyde
MIT	Mitochondrial oxidative
MMP	Matrix metalloproteinase
Mox	Oxidized phospholipid-derived macrophage
MWCO	Molecular weight cut-off
NACNO	<i>S</i> -nitroso- <i>N</i> -acetylcysteine
NADPH	Nicotinamide adenine dinucleotide phosphate
NAT	2,3-naphtotriazole
NDA	2,3-naphthalene dicarboxaldehyde probe
NF-kB	Nuclear factor-kappa B
nNOS	Neuronal nitric oxide synthase
NO	Nitric oxide
NOX	NADPH oxidase
oxLDLs	Oxidized low-density lipoproteins

oxPAPC	Oxidized 1-palmitoyl-2-arachidonoyl-sn-glycero-3-phosphocholine
PAPC	1-palmitoyl-2-arachidonoyl-sn-glycero-3-phosphocholine
PBS	Phosphate buffered saline
PDE	Cyclic nucleotide phosphodiesterase
PGE2	Prostaglandin E2
PGPC	1-palmitoyl-2-glutaroyl-sn-glycero-3-phosphocholine
PKG	Protein kinase G
PLA2	Phospholipase A2
PMA	Phorbol 12-myristate 13-acetate
PMCA	Plasma membrane calcium-transporting ATPase
POVPC	1-palmytoyl-2-(5-oxovaleroyl)-sn-glycero-3-phosphocholine
PPAR $\gamma$	Peroxisome proliferator-activated receptor gamma
Rh-123	Rhodamine 123
ROCK	Rho-associated protein kinase
ROS	Reactive oxygen species
RPMI	Roswell park memorial institute
RSNO	S-nitrosothiols
SDS-PAGE	Sodium dodecylsulfate polyacrylamide gel electrophoresis
SERCA	Sarcoplasmic/endoplasmic reticulum calcium-ATPase
sGC	Soluble guanylyl cyclase
SIN-1	5-amino-3-(4-morpholinyl)-1,2,3-oxadiazolium chloride
SM	Smooth muscle
SM-MHC	Smooth muscle-myosin heavy chain

SNAP	<i>S</i> -nitroso- <i>N</i> -acetylpenicillamine
TAZ	PDZ-binding motif
TBA	2-thiobarbituric acid
TBARS	Thiobarbituric acid reactive substances
TMP	1,1,3,3-tetramethoxypropane <sup>3</sup>
TNF $\alpha$	Tumor necrosis factor alpha
VCAM-1	Vascular adhesion molecule-1
VEGF	Vascular endothelial growth factor
vSMCs	Vascular smooth muscle cells
YAP	Yes-associated protein

# Introduction générale

Selon l'Organisation Mondiale de la Santé (OMS), les maladies cardiovasculaires sont la première cause de mortalité dans le monde avec environ 17,7 millions de décès en 2017. L'athérosclérose est caractérisée par un dépôt de lipides au niveau de la paroi artérielle. Elle est décrite comme une maladie chronique, silencieuse et complexe associée à une inflammation et un stress oxydant ayant un impact sur la progression des lésions. L'hypertension artérielle, le diabète, le tabac, l'obésité, le manque d'activité physique ou encore la génétique sont autant de facteurs augmentant le risque de développer une pathologie cardiovasculaire associée à l'athérosclérose telle que l'infarctus du myocarde ou des accidents vasculaires cérébraux.

Le développement de l'athérosclérose (**Fig. 1**) se fait *via* une succession de stades évolutifs, *i*) les stries lipidiques apparaissant dès l'enfance, *ii*) les lésions athéromateuses et pour finir *iii*) les plaques d'athérome avec présence d'un cœur nécrotique fibreux (avec ou sans calcifications). Les lipoprotéines circulantes ainsi que quatre types cellulaires sont principalement impliqués dans la formation des plaques d'athérome : les monocytes/macrophages, les cellules musculaires lisses (CML), les cellules endothéliales (CE) et les lymphocytes. Au cours de ces travaux, nous nous sommes focalisés sur les deux premiers types cellulaires. L'infiltration des lipoprotéines de basse densité (LDL) dans le sous-endothélium marque le début de la formation de la strie lipidique. L'oxydation de ces LDL (oxLDL) a un rôle majeur dans la mise en place d'un environnement pro-inflammatoire.

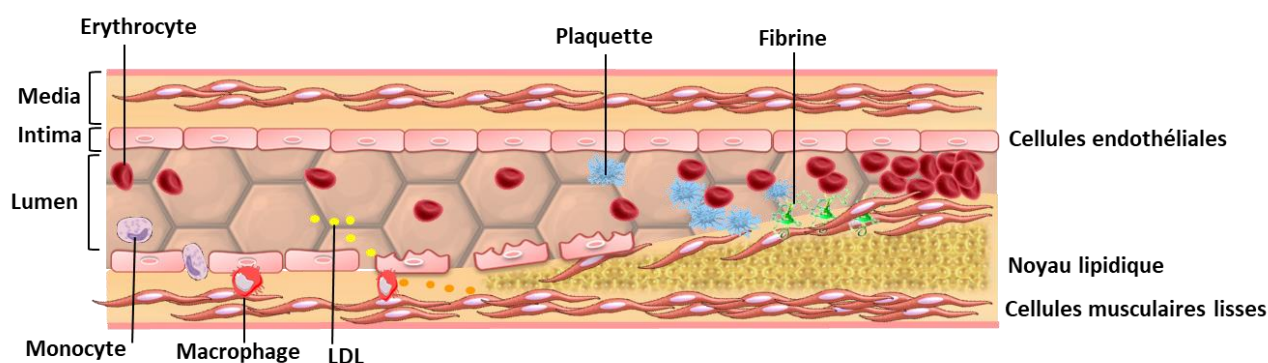


**Figure 1** : Les différents acteurs impliqués dans le développement de l'athérosclérose

En parallèle, une dysfonction de l'endothélium associée à une diminution de la biodisponibilité en monoxyde d'azote (NO) et à une augmentation du stress oxydant ainsi que de l'inflammation sont observés. Ce mécanisme, lié à la présence des oxLDL, augmente l'expression de molécules d'adhérence à la surface des CE et entraîne l'adhésion des monocytes à la surface de



l'endothélium artériel. En condition physiologique, NO produit par l'endothélium possède des propriétés anti-proliférative et anti-inflammatoire. La diminution de la biodisponibilité en NO est liée à la production d'espèces réactives de l'oxygène (ERO) ainsi qu'à la réduction de l'activité des enzymes impliquées dans sa synthèse, l'ensemble ayant pour conséquences une diminution des capacités antioxydantes et un stress oxydant. Suite à leur infiltration dans le sous-endothélium, les monocytes se différencient en macrophages M0 (natifs), M1 (pro-inflammatoires) ou M2 (anti-inflammatoires). L'environnement pro-inflammatoire ainsi que l'augmentation du stress oxydant induit également un switch phénotypique des CML, perdant leur phénotype contractile en faveur d'un phénotype prolifératif/sécrétoire avec capacités macrophagiques. L'ensemble de ces phénomènes couplés à la présence de oxLDL conduisent à la formation de cellules spumeuses directement dérivées de la métaplasie des macrophages et des CML. Ces cellules sont les composants clé du développement de la plaque athéromateuse.

Actuellement, aucun médicament n'a l'athérosclérose comme indication thérapeutique. L'observation de règles hygiéno-diététiques strictes et le traitement de la dyslipidémie par les hypolipémiants tels que les statines représentent les seules possibilités de limiter la formation des plaques d'athérome.

Dans ce contexte, il paraît important d'étudier l'effet d'une supplémentation en NO sur la formation des cellules spumeuses et donc, à plus long terme, du cœur nécrotique. L'application thérapeutique directe de NO sous forme de gaz radicalaire (Kinox<sup>®</sup>) est limitée au traitement de l'hypertension artérielle pulmonaire du fait de sa demi-vie trop courte (quelques secondes). Des donneurs de NO comme les sydnonimines (Molsidomine) ont déjà fait l'objet d'essais cliniques sans montrer d'amélioration de la dysfonction de l'endothélium. D'autres donneurs de NO, les *S*-nitrosothiols ont montré des résultats encourageants dans la limitation du développement de l'athérosclérose. Parmi les différents *S*-nitrosothiols existants, nous nous sommes focalisés sur le *S*-nitrosoglutathion (GSNO) et son impact sur les cellules spumeuses. GSNO constitue une forme physiologique de transport et de stockage NO. Son utilisation comme potentiel thérapeutique est intéressante du fait de son squelette composé de glutathion, qui permettrait en plus de l'apport de NO, d'apporter du glutathion, l'un des antioxydants naturels les plus répandus.

Ainsi, ce travail de thèse a été divisé en trois parties :

- Développer un modèle de différenciation des monocytes en macrophages et leur polarisation en M1- et M2- macrophages
- Étudier l'impact de NO, et plus particulièrement du GSNO, sur la formation des cellules spumeuses
- Développer un modèle de dédifférenciation des CML en utilisant différents stimuli tels que l'Angiotensine II et les oxLDL.

# CHAPTER 1

## INTRODUCTION

# I. Atherosclerosis

## 1. General description

According to the World Health Organization, cardiovascular diseases are the first cause of mortality in the world with around 17.7 million of deaths in 2017 [1]. In France, they are the second one for men, after cancer, and the first one for women. Risk factors like high blood pressure, diabetes, smoking, obesity, the lack of physical activity or genetic increase the risk to develop a cardiovascular pathology such as coronary artery diseases, venous thrombosis, angina pectoris and atherosclerosis.

In 1755, Von Haller used for the first time the Greek term “*atheroma*” to describe “a space filled with gruel-like materiel”. In 1833, Jean Frederic Martin Lobstein used, for the first time, the term “arteriosclerosis” to describe calcified lesions [2]. Today, atherosclerosis is described as a complex chronic disease associated with inflammation and oxidative stress, which modulate the initiation and the progression of lesions. There are different steps in the evolution of the atherosclerotic disease, *i.e.* atherosclerosis evolution, *i)* the fatty streak, appearing since childhood in the inner layers of artery walls, *ii)* the atheromatous *core* and finally *iii)* the necrotic *core* or fibroatheroma (with or without calcification). Atherosclerotic lesions are localised in artery walls mainly at the bifurcation/branching of vessels, where the atheroma plaque creates and increases a turbulent blood flow. During decades, lesions grow progressively reducing vascular lumen and blood perfusion with morphological modifications. In most cases, atherosclerotic plaques are silent with a slow development and patients are asymptomatic until acute events – like myocardial infraction or stroke – occur. These events are due to a sudden obstruction of the vessel after a plaque rupture leading to the formation of a thrombus.

Low-density lipoproteins (LDLs) associated with different cell types such as monocytes/macrophages, vascular smooth muscle cells (vSMCs), lymphocytes and endothelial cells are involved in the development of atherosclerotic lesions. LDLs infiltration under the intima is the starting point of atherosclerotic plaques formation.

The first step of atherosclerosis development occurs with the infiltration of lipids, and more specifically LDLs, in the arterial wall inducing the formation of fatty streaks. These LDLs undergo oxidation phenomenon to form oxidized LDLs (oxLDLs). OxLDLs increase the expression of adherence molecules like the intercellular adhesion molecule 1 (ICAM-1) and the vascular adhesion molecule 1 (VCAM-1) on endothelial cells. The expression of those

molecules results in monocytes recruitment, adhesion and transmigration, and in the production of chemokines by the endothelial layer of the vessel. Monocytes recruitment is also due to a perturbation of the blood flow in atherosclerotic areas. This induces a local production of pro-inflammatory molecules like monocyte chemoattractant protein-1 (MCP-1) and interleukine-8 (IL-8) by endothelial cells. Monocytes infiltrate the vessel wall from the intima where they differentiate into macrophages. Macrophages show a high plasticity reflected by a functional polarization and a dynamic switch between two macrophage phenotypes *i)* pro-inflammatory M1 and *ii)* anti-inflammatory M2. According to the literature, macrophages express specific phenotypic markers like LDLs surface receptors for M1-macrophages *i.e* CD80 [3] or the mannose receptor CD206 for M2-macrophages, which is enhanced by anti-inflammatory cytokines such as IL-4 or IL-10 [4]. Under physiological condition, the M1/M2 population remains in a mixed state while their balance is altered in atherosclerosis, varying from M2 prevalence in stable plaques to M1 prevalence in vulnerable ones. M2 subtype internalizes more lipids than M1 due to a lower expression of cholesterol efflux proteins [5]. This oxLDLs loading in M2 causes a shift towards a M1 phenotype [6,7]. In contrast, other studies found an increased uptake and storage of oxLDLs in M1 macrophages even if cholesterol efflux proteins are upregulated [8]. OxLDLs phagocytosis by macrophages lead to the formation of foam cells and may drive cell death, thus contributing to the formation of the necrotic core within atherosclerotic plaques.

Scavenger receptors like CD36 or Lox-1 expressed on the surface of macrophages are also responsible for oxLDLs binding and uptake. CD36, a membrane glycoprotein and class B scavenger receptor with a molecular weight of 88 kDa, interacts with oxLDLs and triggers the inflammatory response. CD36 expression on macrophages is increased by oxLDLs through the activation of PPAR $\gamma$ , a nuclear receptor implicated in adipogenesis. Foam cells formation is directly linked to CD36 expression. Indeed, Febbraio *et al.* [9] showed in CD36-apoE double null mice, a lack of foam cells formation after oxLDLs exposure. Another publication confirms that CD36 upregulation by oxLDLs, contributes to macrophage trapping inside atherosclerotic lesions [10].

The accumulation of M1 macrophages potentiates inflammation and oxidative stress within the vessel wall [11]. This environment associated with the internalization of oxLDLs by vSMCs *via* the low-density lipoprotein receptor-related protein 1 (LRP1) increases the nucleic localization of NF- $\kappa$ B and leads to pro-inflammatory cytokines secretion and to the promotion of vSMCs de-differentiation. Pro-inflammatory switch of vSMCs is followed by the loss of

contractile markers ( $\alpha$ -actin, myosin heavy chain, calponin (*i.e.* transgelin) and smoothelin) and matrix metalloproteases (MMP-2, MMP-9) secretion, inducing vSMCs proliferation and migration [12] with a modification of the extracellular matrix composition (from collagen IV to collagen I).

The renin-angiotensin system implicated in the regulation of vascular and renal homeostasis plays also a key role in the inflammatory and oxidative context of atherosclerosis. This system is composed of three major compounds: renin, angiotensin II (AngII) and aldosterone. In response to a decreased renal blood pressure, these three compounds act to elevate arterial pressure. In kidney arterioles, activation of juxtaglomerular cells in response to decreased blood pressure causes the cleavage of prorenin (inactive form) into renin. Renin is released into the blood and act on its target, angiotensinogen [13]. Angiotensinogen is produced by the liver and circulates continuously in the plasma. Renin cleaves angiotensinogen into angiotensin I, an inactive precursor of AngII. This reaction is catalysed by the angiotensin converting enzyme. AngII will have effects on kidneys, adrenal cortex, arterioles... by binding the type 1 and type 2 Angiotensin-II receptors ( $AT_1R$  and  $AT_2R$ ) inducing a vasoconstriction and a vasodilation, respectively. AngII has a half-life of 1-2 minutes and mediates many effects like vasoconstriction, angiogenesis... All these effects are linked to the  $AT_1R$ , found on monocytes, endothelial cells, vSMC or fibroblasts. AngII also activates NADPH oxidase (NOX), responsible for oxidative stress increase [14]. In vSMCs, AngII fixation on  $AT_1R$  activates the phospholipase  $A_2$  ( $PLA_2$ ), which acts on NOX that produces  $O_2^{\bullet-}$  [15]. The increase of intracellular oxidative stress activates the NF- $\kappa$ B pathway [16]. The translocation of this complex in the nucleus activates the transcription of genes coding for pro-inflammatory factors and cell adherence molecules (CAM) in vascular endothelial cells [17]. The renin-angiotensin system is also known to stimulate NF- $\kappa$ B activation in human monocytes [18], to stimulate macrophage-mediated LDLs oxidation [19] and to increase the expression of MCP-1 [20]. In atherosclerosis, the renin-angiotensin system is upregulated, so the activation of NOX by AngII is increased leading to ROS production and oxidative stress development. During all these steps,  $O_2^{\bullet-}$  is able to react with nitric oxide (NO), leading the formation of peroxynitrite ions ( $ONOO^-$ ) or hydroperoxyl radical ( $H_2O^{\bullet}$ ), implicated in lipid peroxidation. Therefore, atherosclerosis is associated with a decrease of NO bioavailability. Indeed, NO plays a central role in vascular homeostasis and its biosynthesis decreases during physiopathological processes like ageing, endothelial dysfunction or oxidative stress.

## 2. Nitric oxide in atherosclerosis

### a. Nitric oxide and vascular homeostasis

NO is a free-radical gas, with a short half-life (less than 5 seconds) [21] and one of the smallest endogenous molecules. NO is a chemical messenger, playing a critical role in the regulation of a wide range of physiological processes, including vascular relaxation, inflammation and neurotransmission. It is one of the most important substance produced by the endothelium, and its biosynthesis starts with the enzymatic conversion of *L*-arginine by three distinct nitric oxide synthases (**Fig. 2**). Endothelial (eNOS) and neuronal (nNOS) isoforms are constitutively expressed and generate a low concentration of NO (10 nM) for signaling, while the inducible isoform (iNOS) is induced by inflammation and generates a high concentration of NO (more than 1  $\mu$ M) inducing cytotoxic effects.

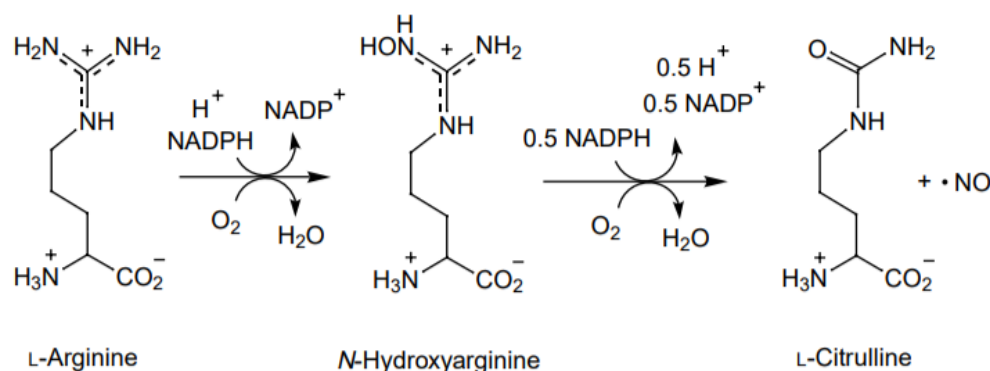


**Figure 2:** Synthesis of endogenous nitric oxide by nitric oxide synthase [22]. NADPH: nicotinamide adenine dinucleotide phosphate; NO: nitric oxide

NO signaling acts through three distinct mechanisms:

- **Nitrosylation:** the coordination of NO to a transition metal ion in enzymes [23]. NO activates the soluble guanylyl cyclase (sGC)/cGMP pathway in vSMCs and modify prosthetic metal of functional proteins (*i.e.*  $\text{Fe}^{2+}$ ,  $\text{Cu}^{2+}$ ), such as ferrous heme prosthetic groups within sGC enzyme.
- **Proteins S-nitrosation:** the formation of a covalent bond between NO and a cysteine residue of proteins (S-NO) that originates a *S*-nitrosoprotein. This reversible post-translational modification of proteins implicates both chemical and functional modifications of proteins and is a form of redox modulation in diverse tissues. It has been demonstrated several times that denitrosation signals initiated at the plasma membrane play an important role in the regulation of *S*-nitrosated proteins [24]. Under physiological or pathological oxidative stress, NO might provide protection to cells by

S-nitrosation of critical protein, preventing them from further oxidative modifications by ROS [25,26].

- **Nitration:** introduction of a nitro group ( $-\text{NO}_2$  group) covalently bound to the aromatic ring of tyrosine or tryptophan residues. This modification is irreversible and often related to a loss of protein function. It is also considered as a marker of nitrosative stress, inflammation and cell damage. Nitration leads to the formation of nitrotyrosine by peroxynitrite ions in a context of oxidative stress and inflammation [27]. Some studies have demonstrated that nitrotyrosine levels are associated with the presence of coronary artery disease and appears to be modulated by statin therapy [28].

NO plays different functions in the body, mainly depending on its concentration, its site of formation and the targeted tissue. In particular, NO regulates cardiovascular functions through two distinct pathways, *i.e.* the classical sGC/cGMP pathway and proteins S-nitrosation leading the modification of signaling pathways.

- The classical sGC/cGMP pathway originates by the release of NO by the endothelium. NO stimulates sGC and increases cyclic guanosine monophosphate (cGMP) concentrations. cGMP effects are dependent or independent to protein phosphorylation. cGMP activates two types of intracellular proteins: cGMP-dependent protein kinase (PKGs), cGMP-regulated ion channels, and is catabolized by cGMP-regulated cyclic nucleotide phosphodiesterases (PDEs). Depending on NO release and the site of cGMP activation, different biological effects can be observed [29]. In vessels, under physiological condition, cGMP inhibits thrombosis and platelet aggregation [30]. In vSMCs, cGMP activates the PKG that stimulates the sarcoplasmic/endoplasmic reticulum calcium-ATPase (SERCA) resulting in a lower  $\text{Ca}^{2+}$  concentration in the cytosol.  $\text{Ca}^{2+}$  is also released (efflux) through the plasma membrane calcium-transporting ATPase (PMCA). PKG also triggers  $\text{K}^+$  efflux *via* the large-conductance  $\text{Ca}^{2+}$ -sensitive potassium channel (BKCa) to hyperpolarize the cell, thereby reducing  $\text{Ca}^{2+}$  entry through the L-type calcium channel (LTCC). All these modifications mediate vessels vasodilation (**Fig. 3**).
- Modifications of signaling pathways through proteins S-nitrosation. Protein S-nitrosation has multiple roles, *i.e.* *i)* modification of the protein function/activity, *ii)* mechanism of NO storage and transport *i.e.* S-nitrosoalbumin, S-nitrosohemoglobin



and *S*-nitrosoglutathione or *iii*) protection of the cysteine thiol function from oxidation (*i.e.* by ROS or peroxynitrite ions) [30,31].

As already mentioned, NO synthesized by eNOS induces vSMCs relaxation and inhibits their proliferation. Through its diffusion to the vessel lumen, NO inhibits platelet aggregation and thrombosis. Some observations suggest eNOS expression in erythrocytes but these pieces of evidence are still debated [32,33]. NO, produced by endothelial cells, diffuses luminally to circulating erythrocytes where it reacts with the  $\text{Fe}^{2+}$  heme of oxyhaemoglobin and produces nitrate ions ( $\text{NO}_3^-$ ). Nitrate ions are reduced in nitrite ions ( $\text{NO}_2^-$ ) by nitrate reductase, present in mammalian tissues. In hypoxic and acidic environment, deoxygenated haemoglobin has a nitrite reductase activity to reduce  $\text{NO}_2^-$  into NO. This phenomenon suggests a role of erythrocytes in the transport of NO metabolites and NO release in hypoxic tissues, leading to vasodilation. Moreover, haemoglobin reversible *S*-nitrosation on the Cys 93 might transport and release NO in hypoxic tissues. In vSMCs, NO diffusion and bioavailability are regulated by haemoglobin- $\alpha$  at the myoendothelial junction and by cytoglobin in SMCs. NO synthesized by nNOS also contributes to regulate the vascular tone. In cardiac myocytes, cardiac contractility is modulated by autocrine and paracrine effects of NO (from eNOS and nNOS), with a regulation of excitation-contraction coupling, relaxation and mitochondrial respiration. The heart rate is also regulated by nNOS and eNOS. nNOS is expressed in cardiac nerves and postsynaptic eNOS modulates the ortho-parasympathetic balance, reinforcing parasympathetic transmission (vagal) (**Fig. 3**).

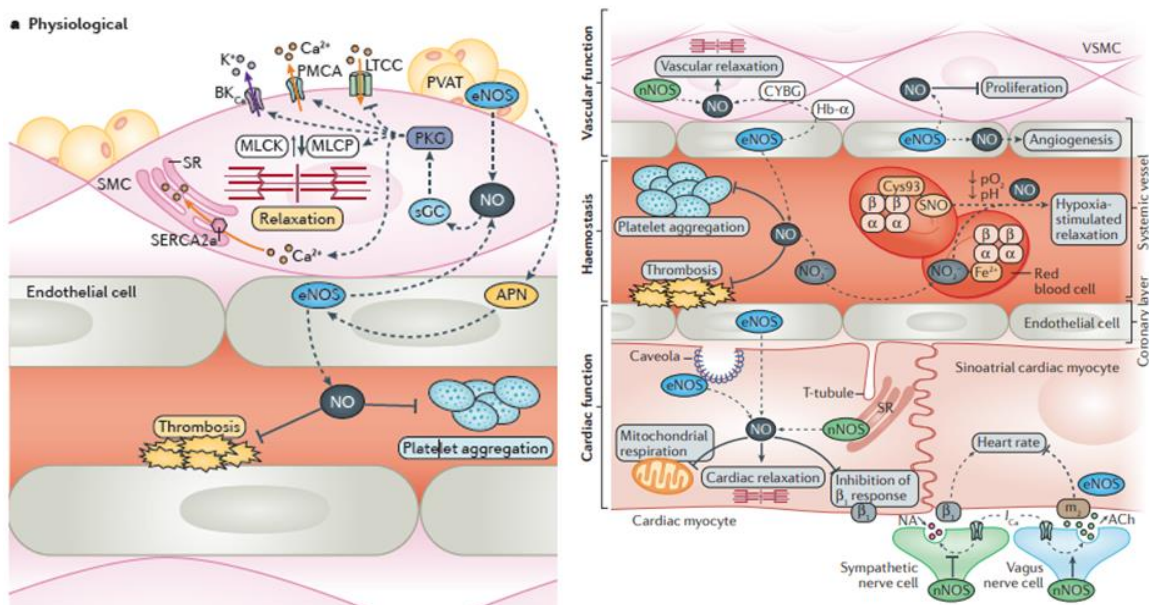


**Figure 3:** NO signaling in the cardiovascular system, under physiological condition [30]

Endothelial dysfunction is the earliest event of atherosclerosis plaque formation and may have different origins. The decrease of NO bioavailability seems to facilitate vascular inflammation, leading to LDLs oxidation and foam cells formation, vSMCs proliferation, extracellular modifications and platelet activation.

#### b. Nitric oxide and the development of atherosclerosis disease

NO deficiency induced either by the reduction of eNOS activity or its degradation by oxidative stress as well as antioxidant enzymes decrease of activity are the consequences of endothelial dysfunction (**Fig. 4**).

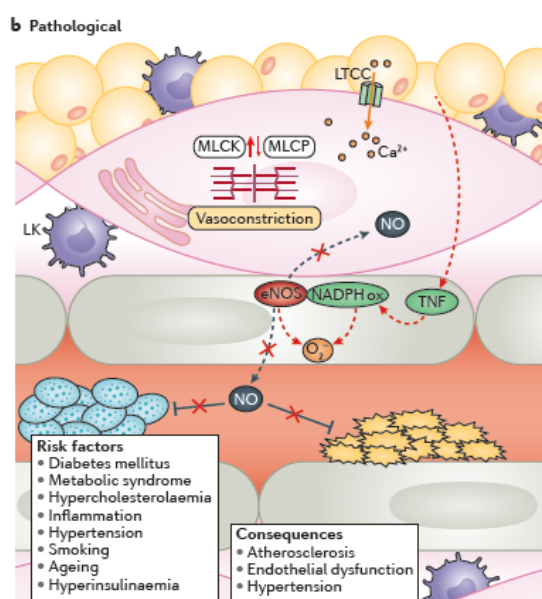


**Figure 4:** NO in the cardiovascular system, under pathological conditions [30]

NO depletion during atherosclerosis favours SMCs migration/proliferation and their switch from a contractile to a secreting phenotype. These changes in SMC characteristics are implicated in vascular wall hyperplasia observed in atherosclerotic plaques. Furthermore, SMCs undergoing phenotypic switch also express macrophage markers like CD68 [34] and acquire macrophage properties. This switch to macrophage-like phenotype may be driven by lipids accumulation leading to the formation of foam cells and participating to the formation of the necrotic core [35]. In fact, foam cells encountered in atherosclerotic plaques have been shown to derive, through oxLDLs accumulation, from macrophages and SMCs metaplasia [36–38].

### 3. Phenotypic modulation of macrophages and SMCs: a link between NO depletion and activation of signaling pathways

**Article 1: Phenotypic modulation of macrophages and vascular smooth muscle cells in atherosclerosis – Nitro redox interconnexions**

**Modulation phénotypique des macrophages et des cellules musculaires lisses au sein de l'athérosclérose – Interconnexions nitro redox**




Justine Bonetti, Alessandro Corti, Lucie Lerouge, Alfonso Pompella, Caroline Gaucher

*Antioxidants* **2021**, 10, 516

La diminution de la biodisponibilité en monoxyde d'azote (NO), sous forme libre ou liée à des fonctions thiol (stockage), au cours du développement de l'athérosclérose, induit une diminution de la signalisation NO-dépendante. Les monocytes/macrophages ainsi que les cellules musculaires lisses (vSMCs) sont les principales cellules impliquées dans le développement de l'athérosclérose. Contrairement à d'autres types cellulaires, ces cellules ont conservé une importante plasticité. En effet, en réponse à la modification de leur environnement (inflammation ou stress oxydant), les vSMCs évoluent d'un phénotype contractile vers un phénotype sécrétoire. Elles acquièrent également un phénotype « macrophage-like » alliant expression de marqueurs macrophagiques et capacité d'internalisation de lipides oxydés (oxLDL). De plus, la dysfonction de l'endothélium entraîne l'adhésion des monocytes à l'endothélium qui s'infiltrent dans le sous-endothélium et se différencient en macrophages. Il s'ensuit une polarisation fonctionnelle en macrophages M1 (pro-inflammatoires), en macrophages M2 (anti-inflammatoires) ou en macrophages Mox (suite à un stress oxydant). Macrophages et vSMCs « macrophage-like » ont la capacité d'internaliser des oxLDL entraînant la formation de cellules spumeuses. La diminution de la biodisponibilité de NO contribue à altérer les voies de signalisation impliquées dans les modifications phénotypiques des macrophages et des vSMCs et donc dans le développement de l'athérosclérose. Mieux comprendre l'ensemble de ces phénomènes permettrait d'identifier de nouvelles cibles thérapeutiques. Cette revue a pour but de répertorier les différents facteurs et voies de signalisation impliqués dans la formation des plaques d'athérome et d'identifier le rôle de NO au niveau moléculaire lors de la modification phénotypique des macrophages et des vSMCs.

## Review

# Phenotypic Modulation of Macrophages and Vascular Smooth Muscle Cells in Atherosclerosis—Nitro-Redox Interconnections

Justine Bonetti <sup>1</sup>, Alessandro Corti <sup>2</sup> , Lucie Lerouge <sup>1</sup>, Alfonso Pompella <sup>2,\*</sup>  and Caroline Gaucher <sup>1</sup> 
<sup>1</sup> CITHEFOR, Université de Lorraine, F-54000 Nancy, France; justine.bonetti@univ-lorraine.fr (J.B.); lucie.lerouge@etu.univ-lorraine.fr (L.L.); caroline.gaucher@univ-lorraine.fr (C.G.)

<sup>2</sup> Department of Translational Research NTMS, University of Pisa Medical School, 56126 Pisa, Italy; alessandro.corti@med.unipi.it

\* Correspondence: alfonso.pompella@med.unipi.it; Tel.: +39-050-2218-537



**Citation:** Bonetti, J.; Corti, A.; Lerouge, L.; Pompella, A.; Gaucher, C. Phenotypic Modulation of Macrophages and Vascular Smooth Muscle Cells in Atherosclerosis—Nitro-Redox Interconnections. *Antioxidants* **2021**, *10*, 516. <https://doi.org/10.3390/antiox10040516>

**Academic Editors:**  
Stefania Pizzimenti, Giuliana Muzio  
and Giuseppina Barrera

Received: 1 March 2021  
Accepted: 22 March 2021  
Published: 26 March 2021

**Publisher's Note:** MDPI stays neutral with regard to jurisdictional claims in published maps and institutional affiliations.



**Copyright:** © 2021 by the authors. Licensee MDPI, Basel, Switzerland. This article is an open access article distributed under the terms and conditions of the Creative Commons Attribution (CC BY) license (<https://creativecommons.org/licenses/by/4.0/>).

**Abstract:** Monocytes/macrophages and vascular smooth muscle cells (vSMCs) are the main cell types implicated in atherosclerosis development, and unlike other mature cell types, both retain a remarkable plasticity. In mature vessels, differentiated vSMCs control the vascular tone and the blood pressure. In response to vascular injury and modifications of the local environment (inflammation, oxidative stress), vSMCs switch from a contractile to a secretory phenotype and also display macrophagic markers expression and a macrophagic behaviour. Endothelial dysfunction promotes adhesion to the endothelium of monocytes, which infiltrate the sub-endothelium and differentiate into macrophages. The latter become polarised into M1 (pro-inflammatory), M2 (anti-inflammatory) or Mox macrophages (oxidative stress phenotype). Both monocyte-derived macrophages and macrophage-like vSMCs are able to internalise and accumulate oxLDL, leading to formation of “foam cells” within atherosclerotic plaques. Variations in the levels of nitric oxide (NO) can affect several of the molecular pathways implicated in the described phenomena. Elucidation of the underlying mechanisms could help to identify novel specific therapeutic targets, but to date much remains to be explored. The present article is an overview of the different factors and signalling pathways implicated in plaque formation and of the effects of NO on the molecular steps of the phenotypic switch of macrophages and vSMCs.

**Keywords:** atherosclerosis; macrophages; vascular smooth muscle cells; differentiation/de-differentiation; signalling pathways; nitric oxide

## 1. Introduction

Cardiovascular diseases are the major cause of death worldwide, being responsible for 17.9 million deaths (31% of the global death rate) in 2016 [1]. From these deaths, 85% were caused by heart attacks and strokes, which can be the consequence of atherosclerosis progression and plaque rupture. Atherosclerosis—the leading coronary arteries disease—is a chronic, silent and slowly developing pathology, mainly affecting arteries of medium-large diameter and characterised by the formation of atheroma plaques as a result of excess plasmatic low-density lipoprotein (LDL) concentrations. The accumulation of LDLs in the blood stream results in their infiltration and oxidation in the sub-endothelium, leading to vascular wall inflammation and oxidative stress. This deleterious environment induces endothelial dysfunction, in turn leading to decreased bioavailability of nitric oxide (NO) due to both decreased synthesis and increased catabolism. NO is a gaseous, lipophilic, free radical mediator with a short half-life (<5 s), synthesised by endothelial NO synthases (eNOS) and involved in the maintenance of vascular homeostasis. Endothelial dysfunction and decreased NO bioavailability induce adhesion/infiltration in the sub-endothelium of circulating monocytes, as well as migration/proliferation of vascular smooth muscle cells (vSMCs) from the arterial tunica media (Figure 1). Oxidised low-density lipoproteins (oxLDLs) are then phagocytised by macrophages or internalised by



vSMCs, thus originating the typical “foam cells” participating in the development of the plaque necrotic core (Figure 1).

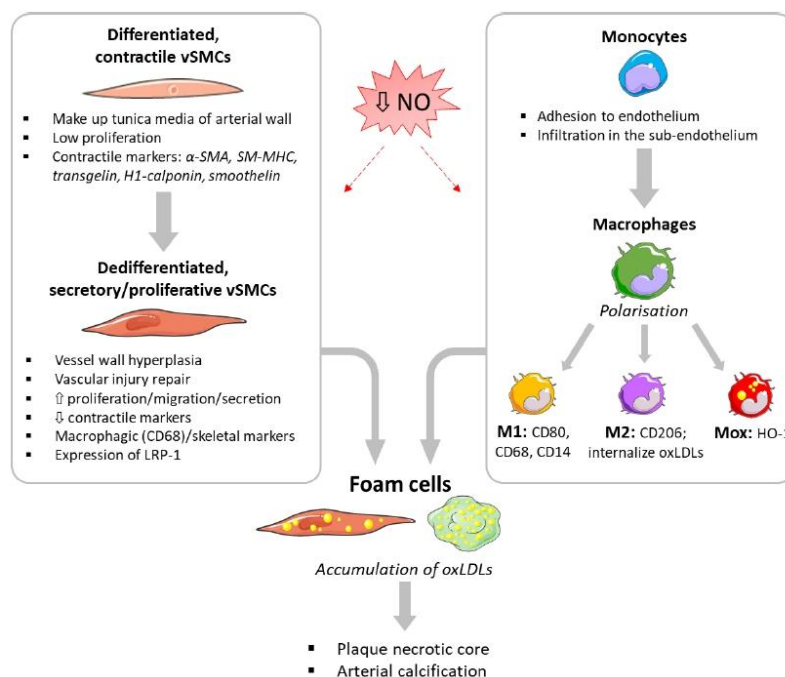


**Figure 1.** Summary of the main steps in formation of foam cells in atherosclerotic plaques. vSMCs: vascular smooth muscle cells;  $\alpha$ -SMA: alpha-smooth muscle actin; SM-MHC: smooth muscle-myosin heavy chain; LRP-1: pro-low density lipoprotein receptor-related protein 1; M1: M1 macrophages; M2: M2 macrophages; oxLDLs: oxidized low-density proteins; Mox: Mox macrophages; HO-1: heme oxygenase 1.

NO displays antiaggregant and vasorelaxant properties, concurring to maintain the anti-inflammatory phenotype of endothelial cells as well as the non-proliferative and non-migratory phenotype of vSMCs. The classical NO mechanism of action is mediated by the nitrosylation (coordination of NO to a metal) of haemoproteins, such as soluble guanylyl cyclase (sGC) producing cyclic guanosine monophosphate (cGMP), which is mostly responsible for the antiaggregant and vasorelaxant properties of NO. However, NO signalling is also mediated through protein S-nitrosation, a post-translational modification of high or low molecular weight proteins or peptides involving the formation of a covalent bond between NO and a reduced thiol of a cysteine residue. S-Nitrosated proteins and peptides are also storage and transport forms of NO: indeed, despite its short half-life, in this way NO is able to act at a distance from its sites of synthesis. The S-nitrosation process extends the NO half-life from 45 min up to several hours and limits the oxidative/nitrosative stress caused by NO oxidation into peroxynitrite ions ( $\text{ONOO}^-$ ). In vivo, S-nitrosothiols, such as S-nitrosoalbumin, S-nitrosohemoglobin and S-nitrosoglutathione (GSNO), are the main physiological forms of NO storage and transport. Finally, NO action can also be mediated through protein or lipid nitration, a marker of nitrosative stress characterized by the addition of a nitro group to a tyrosine residue or a fatty acid chain.

NO has anti-inflammatory and anti-proliferative actions, and its depletion during atherosclerosis will favour monocyte adhesion and infiltration in the sub-endothelium,

as well as vSMCs migration/proliferation and their switch from a contractile to a secreting phenotype. Monocytes infiltrating the sub-endothelium are exposed to oxLDLs, and differentiate into macrophages of different subtypes depending on the prevalent microenvironment. At first monocytes differentiate into naïve M0 macrophages, which can then become polarised into M1 (pro-inflammatory), M2 (anti-inflammatory) or Mox macrophages (oxidative stress phenotype). Indeed, macrophages show a high plasticity, and a dynamic switch between the mentioned phenotypes. M1 and M2 macrophages express specific phenotypic markers, e.g., LDL surface receptors CD80, CD68 and CD14 for the M1 phenotype [2]; the CD206 mannose receptor for the M2 phenotype [3]; or heme oxygenase 1 (HO-1) for Mox phenotype [4] (Figure 1). The balance of the M1/M2 population is modified along the atherosclerotic plaque development, varying from a M2 prevalence in stable plaques to a M1 prevalence in vulnerable ones [5–7]. Phagocytosis of oxLDLs by macrophages leads to the formation of foam cells, composing the lipidic necrotic core of plaques (Figure 1). M2 macrophages internalise more lipids than M1 macrophages, due to a lower expression of cholesterol efflux proteins [7]. The higher oxLDLs loading of M2 causes eventually a shift towards an M1 phenotype [8,9]. However, other studies found an increased oxLDLs uptake in M1-like macrophages, even when cholesterol efflux proteins are upregulated [10]. Mox macrophages, a distinct phenotype from M1 and M2 macrophages, derived from M0 macrophages, phagocytosed oxLDLs and protect from oxidative stress. Treatment of M1 or M2 macrophages with oxLDLs causes also a further switch to the a specific Mox phenotype [11].

In healthy arteries, vSMCs are located in the tunica media of the vessel wall where they are responsible of vasoactivity (contraction/relaxation), vascular diameter and blood pressure. Differentiated contractile vSMCs have low migration and proliferation abilities. They express specific contractile markers like  $\alpha$ -smooth muscle actin ( $\alpha$ -SMA), smooth muscle myosin heavy chain (SM-MHC), transgelin, H1-calponin and smoothelin (Figure 1). However, unlike other muscle cells, vSMCs do not terminally differentiate and retain a high level of plasticity while remaining in a quiescent phenotype. In response to vascular injury and inflammatory stimuli, such as during atherosclerosis, contractile vSMCs are able to undergo de-differentiation to a secretory/proliferative (“pro-atherosclerotic”) phenotype, which is implicated in vascular wall hyperplasia occurring during progression of atherosclerotic plaques [12]. Indeed, such de-differentiation has a physiological function in helping vascular repair after injury and is the same mechanism as observed in embryonic angiogenesis, neovascularisation and vascular remodelling [13]. De-differentiated vSMCs are characterised by a decreased expression of contractile markers and increased proliferation, migration and secretory abilities, and can even express markers of macrophagic as well as skeletal muscle phenotypes. De-differentiated vSMCs act in all steps of atherosclerosis development, until the formation of advanced plaques presenting a necrotic core and varying degrees of calcification. The vSMCs’ phenotypic switch allows their migration and infiltration from the media to intima due to secretion of matrix metalloproteinases (MMP-2, MMP-9) [14], as well as their capacity to internalise oxLDLs through the expression of the pro-low density lipoprotein receptor-related protein 1 (LRP-1) (Figure 1). During this process, the nuclear localisation of NF- $\kappa$ B is increased, leading to secretion of pro-inflammatory cytokines and promotion of vSMCs dedifferentiation.

During their phenotypic switch, vSMCs acquire macrophagic properties and express macrophage markers, such as CD68 [15], as well as mesenchymal stem cells markers (e.g., Sca1 and CD105) [16,17], suggesting the presence of a vSMC progenitor population within the vessel wall that proliferates and accumulates along with the development of atherosclerosis (Figure 1). The switch to a macrophage-like phenotype is likely driven by lipids accumulation and is the main step in the formation of foam cells and the necrotic core of plaques [16]. Foam cells encountered in plaques have been shown in fact to derive from both macrophages and vSMCs, through oxLDLs accumulation [18–20]. Allahverdian et al. previously demonstrated that, of the foam cells present in human plaques, 40% are of vSMC origin vs. 60% of a macrophagic one [21].

Many signalling pathways triggered by inflammatory and/or oxidative stimuli are implicated in the phenotypic switch of vSMCs, as well as in the differentiation of monocytes and the polarisation of macrophages. Activation of these signalling pathways occurs in parallel to a decrease in NO bioavailability. NO is known to promote M1 polarisation toward the M2 phenotype [22,23], and has been held responsible for the maintenance of the non-proliferative/non-migratory phenotype of vSMCs. However, no direct proof was provided for the alleged ability of NO to counteract the vSMCs' phenotypic switch. The present review is an overview and an appraisal of the current knowledge on the signalling pathways involved in vSMC and monocyte/macrophage differentiation/polarisation, with particular reference to NO-dependent signalling.

## 2. Modulation of Key Determinants of Cell Phenotype by Redox/Inflammatory Signalling

Under physiological conditions, reactive oxygen species (ROS) produced at low concentration are key redox regulators of cell functions in response to extracellular and intracellular stimuli. At first, cell cycle phases as well as assembly of the mitotic spindle were associated with variations in concentration of soluble thiols [24,25]. In particular, glutathione was shown to accumulate during the G<sub>2</sub> phase and the mitotic phase [26], in which the ROS concentration was shown to be 3-fold higher than in the G<sub>1</sub> phase [27]. The redox environment as well as inflammatory stimuli appear thus to control the cell cycle, especially transitions between phases [28–31].

The implications of ROS generating as well as antioxidant systems along the different steps of atherosclerosis progression (endothelial dysfunction, LDLs oxidation and accumulation, plaque formation) have been recently reviewed [32]. Paracrine signalling by growth factors, cytokines and hormones, such as platelet-derived growth factor (PDGF) [33,34], epithelial growth factor (EGF), transforming growth factor  $\beta$  (TGF- $\beta$ ), tumour necrosis factor- $\alpha$  (TNF- $\alpha$ ) [35] and angiotensin II [36], activates specific cell membrane receptors and induce ROS production. ROS can then reversibly oxidise thiol groups on regulatory proteins to disulfides, mixed disulfides or sulfoxides, as well as zinc-fingers to disulfides, or methionine residues to methionine [37].

### 2.1. Platelet-Derived Growth Factor (PDGF)

PDGF is one of the most robust phenotype-modulating agents, and a primary regulator of vSMCs proliferation in response to a multitude of stimuli like hypoxia, thrombin, growth factors (including PDGF itself) or cytokines. PDGF is produced as a dimer of four polypeptide chains, linked by disulphide bonds and encoded by four different genes. Five possible dimeric forms of PDGF have been identified: PDGF-AA, PDGF-AB, PDGF-BB, PDGF-CC and PDGF-DD. PDGF-A and PDGF-B monomers undergo activation (N-terminal pro-domain removed) during their intracellular transport for secretion [38]. PDGF-C and PDGF-D monomers are secreted as latent factors, requiring an activation by extracellular proteases [39,40].

Among the PDGF isoforms, PDGF-BB dimer is known to drive the Raf/Ras/MEK/ERK signalling pathway. Vascular injury and chronic arterial diseases result in PDGF-BB production as a signal for vSMCs de-differentiation, helping the remodelling of blood vessels. Indeed, PDGF-BB decreases the expression of contractile phenotype markers (calponin and  $\alpha$ -smooth muscle actin) and upregulates the expression of synthetic markers osteopontin and vimentin. Furthermore, PDGF-BB prevents oxidative stress-induced protein damage and cell death by promoting vSMC autophagy, essential for cell survival [41]. PDGF-BB is central for vSMC proliferation and migration regulation linked with ROS signalling and JAK/STAT signalling. NADPH oxidase (NOX), producing superoxide anions, in fact participates in signalling cascades regulating PDGF-BB-induced proliferation, while JAK inhibition abolishes PDGF-stimulated vSMCs growth [42].

PDGF-BB is also implicated in the modification of the extracellular matrix surrounding vSMCs. Contractile vSMCs are surrounded by type I and IV collagens and proteoglycans. However, along atherosclerosis development, vSMCs secrete type I, VI and VIII collagens,



as well as MMPs promoting their migration, followed by upregulation of synthesis of interstitial matrix components such as elastin, fibronectin, osteopontin or tenascin. Collagen deposits account for 60% of the total protein in atherosclerotic plaques, and drive vSMC migration [43]. PDGF-BB promotes the synthesis of type VI collagen  $\alpha 1$  chain, increasing vSMCs viability and migration capacity, as well as fibronectin and MMPs through the activation of Akt/mTOR signalling [44].

Addition of PDGF-BB to vSMCs suppresses SM-MHC mRNA/protein expression, but treatment with NO donors (FK409 or *S*-nitroso-*N*-acetylpenicillamine (SNAP)) can reverse this effect [45]. A study with short- (SNAP) and long-term (DETA/NO) NO donors showed that both compounds could inhibit PDGF-induced vSMCs migration in a dose-dependent manner, via blockade of the RhoA pathway [46,47]. De Oliveira et al. also showed that cyclamNO, a NO donor, can inhibit PDGF-BB-induced cell proliferation and migration [48]. CyclamNO prevents vSMCs' phenotypic switch by reducing ( $\approx 60\%$ ) the expression of  $\alpha$ -SMA induced by PDGF-BB. After a long exposure to SNAP, NO contributed to decrease vSMC proliferation by the attenuation of PDGF-BB-induced PKB- $\alpha$  activation [49]. Moreover, the loss of eNOS activity (eNOS<sup>-/-</sup> mice) is associated with the activation of the PDGF signalling pathway and with the induction of survivin, an apoptosis inhibitor. eNOS negatively regulates the PDGF-survivin axis, so that proportional flow-dependent luminal remodelling and vascular quiescence are maintained [50].

## 2.2. Transforming Growth Factor-B (TGF-B) Superfamily

### 2.2.1. TGF- $\beta$

TGF- $\beta$  is important in the maintenance of vascular homeostasis and integrity and is produced by all cell types in the arterial wall following a vascular lesion [51]. TGF- $\beta$  was initially recognised as a de-activating factor for macrophages, with the ability to suppress iNOS expression and to inhibit the production of pro-inflammatory mediators [52], resulting in the suppression of differentiation of monocytes to macrophages [53]. Three isoforms are comprised in the TGF- $\beta$  family, TGF- $\beta 1$ , - $\beta 2$  and - $\beta 3$ , secreted as precursors whose biological function is activated by enzymatic cleavage. TGF- $\beta 1$  and TGF- $\beta 3$  are expressed in vSMCs, macrophages and foam cells of early human vascular lesions [54]. Indeed, TGF- $\beta$  contributes to the progression of lipid-rich atherosclerotic lesions by stimulating the production of lipoprotein-trapping proteoglycans, inhibiting vSMCs proliferation and activating proteolytic mechanisms in macrophages [54]. TGF- $\beta$  regulates CD36 or apolipoprotein E (ApoE) genes implicated in oxLDLs uptake and in cholesterol efflux from foam cells [55]. In addition, TGF- $\beta$  inhibits foam cells formation and controls cholesterol homeostasis in macrophages via Smad-2 and Smad-3 phosphorylation in macrophages.

Regarding inflammation, TGF- $\beta 1$  exerts a protective role by inhibiting vSMC proliferation and migration by inhibiting signal transducer and activator of transcription 3 (STAT3) and NF- $\kappa$ B pathways, while at the same time inducing expression of contractile genes and actin re-organisation through an increased p38 MAPK activity [56–60]. Such TGF- $\beta 1$ -driven effects are blocked by inhibitors of RhoA kinase and its target PKN (also known as protein kinase C-related kinase 1 or PRK-1). The TGF- $\beta 1$ /RhoA/PKN triad in fact is the key component of an important intracellular signalling pathway promoting vSMC differentiation. The antiproliferative effects of NO on vSMCs are explained by its interactions with RhoA: *S*-nitrosation of the cysteine residues present in RhoA GTP-binding domain decreases its affinity for GTP, thus suppressing RhoA activity [61,62]. RhoA inhibition by *S*-nitrosation modulates the phosphorylation of myosin light chain, suggesting an implication of cGMP-independent effects of NO on vascular tone as well.

### 2.2.2. Bone Morphogenetic Proteins (BMPs) and Gremlin-1

BMPs are inflammatory mediators produced by the endothelium in response to shear stress, pro-inflammatory cytokines and oxidative stress [63]. They are members of the TGF- $\beta$  superfamily, and participate in bone formation, haematopoiesis and cell differentiation during embryogenesis.



In 1993, BMP-2 was first implicated in calcification of human atherosclerotic lesions [64]. Nakaoka et al. demonstrated then that BMP-2 can inhibit vSMC proliferation, and suggested the therapeutic application of BMP-2 to prevent vascular proliferative disorders [65]. On the other hand, BMP-2, BMP-4 and BMP-6 have also been shown to increase plaque formation, oxidative stress, inflammation and endothelial dysfunction [66,67], through the activation of their specific BMP type I and type II (serine/threonine kinase) receptors. BMP receptor signalling has been involved in endothelial dysfunction via inhibition of the Akt-eNOS pathway after induction of phosphatase and tensin homolog (PTEN), as well as in vSMC osteogenic differentiation [68].

BMPs modulate the vSMCs' phenotype via cross-talk with RhoA/MRTFs pathways, which may contribute to the development of pathological features. Indeed, BMPs promote the nuclear localisation and recruitment of myocardin-related transcription factors (MRTF-A and MRTF-B) to the promoter of the smooth muscle  $\alpha$ -actin gene [69]. In particular, BMP-4 decreases SM22- $\alpha$  and  $\alpha$ -actin gene expression, indicating vSMC de-differentiation [70].

The inhibition of BMP-2, BMP-4 and BMP-7 binding to BMP type II receptors by Gremlin-1, the physiological antagonist of BMP receptors, reduces Smad activation in the cytoplasm and induces VEGFR-2 expression of VEGFR-2. Gremlin-1 also prevents the recruitment and the activation of macrophages in atherosclerotic plaques by inhibiting the inflammatory mediator MIF [71]. Within vSMC de-differentiation, Gremlin-1 appears to act also independently of the BMP pathway, by reducing the expression of SM22- $\alpha$ ,  $\alpha$ -actin and calponin genes, as well as by efficiently promoting VEGFR-2-dependent angiogenesis [72].

### 2.3. Fibroblast Growth Factors (FGFs)

The FGFs family comprises 22 members divided into 7 subgroups. FGFs act as signal molecules that bind and activate FGF receptors (FGFRs), a family of tyrosine kinase receptors including four members.

In 1996, Hughes documented FGF/FGFR involvement in atherogenesis and atherosclerotic plaque progression [73]. Indeed, FGF is one of the growth factors released by vSMCs, implicated in their proliferation and phenotypic switch by inducing the secretion of chemokines (e.g., CCL2), a mechanism that could explain the infiltration of leukocytes during atherosclerosis development [74]. In vSMCs, FGF activation of FGFR-1 signalling also upregulates via Src/MEK/MAP kinases the expression of osteopontin, which is implicated in the migration of adventitial fibroblasts [75]. The FGF-2/FGFR-1 interaction increases atherosclerotic plaque instability through NF- $\kappa$ B potentiation and the consequent increase in MMP-9 and iNOS expression in vSMCs [76].

Low concentrations of NO were found to inhibit FGF-2-mediated vSMC migration [77]. On the other hand, high levels of NO induce vSMCs death, resulting in the release of FGF-2, in turn stimulating the proliferation of adjacent endothelial cells. Thus, vSMC damages induced by a high NO concentration may be a trigger of neovascularisation in atherosclerotic plaques [78]. The FGF-2 binding affinity for FGFR-1 is increased by H<sub>2</sub>O<sub>2</sub>, and thus oxidative stress can stimulate vSMC proliferation [79]. FGF-21 in particular has been shown to regulate lipid metabolism, foam cell formation, macrophage migration and inflammatory response by repressing NF- $\kappa$ B signalling [80]. FGF-21 could thus exert a cardioprotective action by inhibiting the initial steps in atherosclerosis.

Finally, a crosstalk between FGF and TGF- $\beta$  has been observed both in vitro and in vivo, likely contributing to the modulation of the vSMCs' phenotypic switch. In vitro, the inhibition of FGF signalling increases TGF- $\beta$  activity, promoting vSMCs differentiation and decreasing their proliferation. In vivo, FGF receptor knock-out mice crossed with ApoE<sup>-/-</sup> mice present a significant inhibition of atherosclerotic plaque growth [81].

### 2.4. Angiotensin II (AngII)

AngII is the main player in the renin-angiotensin system, regulating renal and vascular homeostasis. The main AngII effects are mediated by the angiotensin II type 1 receptor (AT<sub>1</sub>R) expressed on monocytes, endothelial cells, vSMCs and fibroblasts. Preclinical stud-

ies demonstrated that the administration of the AT<sub>1</sub>R antagonist telmisartan for 20 weeks to ApoE<sup>−/−</sup> mice reduces atherosclerosis progression, with decreased lipid deposition and accumulation of macrophages [82]. In parallel, the plaque collagen content was increased, indicating plaque stabilisation and an overall protective effect of telmisartan [82]. It seems, therefore, that the AngII/AT<sub>1</sub>R signalling can promote progression of atherosclerosis.

Interestingly, NO may counteract AT<sub>1</sub>R function. AT<sub>1</sub>R S-nitrosation was in fact shown to decrease its affinity for AngII [83], and to inhibit both AngII-dependent and -independent activation of AT<sub>1</sub>R [84]. AngII also plays a role in atherosclerosis progression by enhancing inflammation, endothelial dysfunction and vSMCs proliferation, thus favouring plaque vulnerability and rupture [85,86]. Decreased NO bioavailability and increased ROS levels can explain the pro-atherogenic effects of AngII [87]. Indeed, AngII activates endothelial NOX and p22phox, leading to the production of superoxide/H<sub>2</sub>O<sub>2</sub>, which, in turn, activates H<sub>2</sub>O<sub>2</sub>-sensitive signalling pathways, leading to vSMC proliferation [88,89]. AngII-induced hypertension in rats was associated with increased NOX-derived O<sub>2</sub><sup>•−</sup>, endothelial dysfunction and upregulation of AngII receptors [90]. All these effects were blocked by the AT<sub>1</sub>R antagonist losartan, and, in particular, NO can suppress NOX-dependent superoxide production through S-nitrosation of the p47phox subunit, resulting in suppression of vascular oxidative stress [91]. Similarly, the knockdown of p22phox, a subunit of the NOX complex, essential for its stability and activity, was shown to inhibit AngII-induced vSMC de-differentiation, proliferation and migration through the inhibition of H<sub>2</sub>O<sub>2</sub> production, Krüppel-like factor 4 (KLF-4) expression as well as phosphorylation of Akt and activation of ERK1/2 signalling [92]. Indeed, KLF-4 is one of the main transcriptional regulators of vSMCs' phenotypic switch, and is the end effector of the Akt/ERK1/2 signalling pathway (see Section 4.5).

#### 2.5. Oxidized Low Density Lipoproteins (oxLDLs)

Increased levels of circulating oxLDLs are known to promote monocytes adhesion to the endothelium. However, their effects are not limited to the luminal surface, as oxLDLs can penetrate the vascular wall and enhance oxidative stress and inflammation [93]. The latter is responsible for monocytes infiltration in the sub-endothelium and their differentiation into macrophages, expressing the scavenger receptors CD36 as well as lectin-like oxLDL receptor-1 (Lox-1) responsible for oxLDLs binding and uptake. Moreover, oxLDLs induce the phenotypic switch of M1 and M2 macrophages towards the Mox phenotype, i.e., macrophages with a decreased phagocytic activity expressing a panel of antioxidant enzymes under the control of the KLF-2 transcription factor [4]. Mox macrophages represent around 30% of all macrophages found in advanced atherosclerotic lesions of LDLR<sup>−/−</sup> mice [4].

The majority of foam cells found in plaques are derived from macrophages; however, oxLDLs also promote the vSMCs' phenotypic switch up to a final metaplasia into typical foam cells. Indeed, oxLDLs, such as oxPAPC (oxidized 1-palmitoyl-2-arachidonoyl-sn-glycero-3-phosphocholine), cause a dose-dependent downregulation of mRNA transcription for  $\alpha$ -actin and SM-MHC, two vSMCs phenotypic markers [93]. Moreover, POPVC (1-palmytoyl-2-(5-oxovaleroyl)-sn-glycero-3-phosphocholine) induces pro-inflammatory gene expression, such as chemokine ligand-2 (CCL2), MCP3 and the TNF superfamily, and induces the nuclear translocation of the KLF-4 transcription factor implicated in the repression of vSMC differentiation [93]. De-differentiated vSMCs acquire macrophage-like markers, such as CD68, as well as antigen presentation capacity. On the other hand, such de-differentiated vSMCs cannot perform phagocytosis (only internalisation, lacking digestion steps) and maintain low expression levels of SM-specific markers, such as SM- $\alpha$ -actin [12].

With respect to NO homeostasis, oxLDLs produce a modification of the eNOS/iNOS balance with downregulation of eNOS and sur-expression of iNOS, leading to sur-activation of Lox-1 receptor and NF- $\kappa$ B. The latter originates high concentrations of NO (>1  $\mu$ M) capable of promoting atherosclerosis progression by increasing LDL oxidation and inflammation, decreasing protective autophagic responses and accelerating the apoptosis



of endothelial cells [94]. iNOS inhibition results in the decreased of NO and peroxynitrite ions concentrations after oxLDL treatment, while generation of superoxide is increased, reversing the oxLDL-induced migratory arrest of foam cells [95]. Moreover, high NO concentrations (100  $\mu$ M) were shown to decrease cholesterol efflux from macrophages through the downregulation of ATP-binding cassette transporter A-1 (ABCA-1), thus increasing the oxLDLs and cholesterol accumulation [96]. The concentration and the type of NO donor used in these experiments is of importance: indeed, SNAP—a S-nitrosothiol NO donor—is unable to oxidize LDLs, whereas NO donors sodium nitroprusside and 3-morpholiniosydnonimine (SIN-1) induce a strong LDLs oxidation [97].

Overall, the restoration of NO bioavailability at physiological concentrations might be protective against atherosclerosis progression, and pharmacological treatments are obtaining the first results in this perspective. Indeed, treatment of LDLR<sup>−/−</sup> mice with 0.51  $\mu$ mol/kg/day with S-nitroso-N-acetylcysteine allowed a decreased extent of atherosclerotic plaques, of oxidative stress as well as of free circulating cholesterol [98]. Furthermore, NCX6560, a NO-releasing derivative of atorvastatin (a lipid-lowering drug), presented better anti-thrombotic and anti-inflammatory effects than atorvastatin alone [99].

### 3. Signalling Pathways Implicated in Phenotypic Modulation

#### 3.1. PI3K/Akt/mTOR Signalling

The phosphatidylinositol-3-kinase (PI3K)/protein kinase B (Akt) signalling pathway, as well as the downstream targets of Akt, play a central role in several cellular processes, such as growth, proliferation, death and differentiation [100,101], and are also implicated in the regulation of vSMC proliferation and contractility. Insulin as well as insulin-like growth factor (IGF) signalling suppress the de-differentiation programme in vSMCs and maintain their contractile phenotype via the classical PI3K/Akt pathway [102]. Active nuclear Akt phosphorylates FOXO-4, a co-repressor protein that interacts with the CarG/SRF/myocardin complex and blocks the expression of differentiation genes FOXO-4 is then exported from the nucleus, allowing the re-establishment of a functional CarG/SRF/myocardin complex and the expression of differentiation genes [103].

In spontaneously hypertensive (SHR) rats, aerobic exercise suppresses the vSMCs' phenotypic switch via Akt and mitogen-activated protein kinase (MAPK) signalling. Aerobic exercise decreases blood pressure and reverses the decreased expression of the vSMC protein markers (calponin, SM  $\alpha$ -actin and osteopontin) induced by hypertension. Thus, hypertension, sedentary habits and a lack of exercise in the general population might promote atherogenesis due to an inhibition of Akt/MAPK signalling pathways. Akt inhibition in fact significantly inhibits the expression of contractile proteins, which is instead increased by p38 MAPK and ERK inhibition. The latter in addition downregulates the expression of the synthetic phenotype marker, osteopontin [104]. The effects of aerobic exercise suggest the implication of redox signalling in the maintenance of the vSMC contractile phenotype as well as in the hyperplastic response associated with vascular injury. Kinases are downstream targets of ROS produced by enzymes, such as the NOX complex, and NOX-4 was in fact shown to contribute to the activation of MAPK-14 and the suppression of the vSMCs contractile phenotype [105].

The important role of PI3K/Akt signalling in survival, proliferation, polarisation and migration of macrophages has been previously reviewed [106]. The activity of Akt signalling determines monocyte/macrophage viability and their resistance to pro-apoptotic stimuli in atherosclerotic lesions. A selective inhibition of Akt and mTOR was indeed shown to increase plaque stability through the promotion of macrophage autophagy in a rabbit model of atherosclerosis [107].

The PI3K/Akt/mTOR pathway is implicated in vSMC autophagy as well. In ApoE<sup>−/−</sup> mice, the inhibition of P2Y<sub>12</sub> purinergic receptor promotes vSMC autophagy through the PI3K/Akt/mTOR pathway. Conversely, the P2Y<sub>12</sub> receptor activation can block cholesterol efflux and macrophage autophagy, thus promoting the formation of vSMC-derived foam cells [108]. The activation of the PI3K/Akt/mTOR pathway induced by

homocysteinaemia was also prevented by miR-145, thus inhibiting vSMC proliferation, migration and phenotypic switch [109].

NO signalling is intimately linked to the PI3K/Akt/mTOR pathway. Liu et al. demonstrated that a NO donor, PABA/NO ( $O^2$ -[2,4-dinitro-5-[4-(N-methylamino) benzoyloxy] phenyl]-1-(N,N-dimethylamino) diazen-1-ium-1,2-diolate) induces apoptosis in hepatocarcinoma cells through the inhibition of the PI3K/Akt/mTOR and MEK/ERK pathways. Data suggest that PABA/NO could be used as a potential therapeutic through the regulation of this pathway also in other pathologies, such as atherosclerosis [110]. Moreover, it was shown both in vivo and in vitro that the specific inhibition of PI3K effected by high levels of luteinizing hormone (LH) results in the suppression of eNOS-dependent production of NO, which is accompanied by promotion of atherosclerosis progression [111].

### 3.2. Raf/Ras/MEK/ERK Signalling

The Raf/Ras/MEK/ERK pathway—driven by the MAPK cascade as well as by ubiquitous growth factors such as PDGF-BB, epidermal growth factor (EGF) or fibroblast growth factor (FGF)—is considered as the master inducer of de-differentiation. It in fact promotes Elk-1 phosphorylation, leading to the expression of genes implicated in vSMC growth and proliferation and to the repression of genes coding for vSMC markers [112]. The Raf/Ras/MEK/ERK pathway has an important role in the maintenance of lipid balance and foam cells formation. Hu et al. investigated the activity, abundance and localisation of ERK1/2 in atherosclerotic lesions of cholesterol-fed rabbits [113]. Immunofluorescent analysis revealed an abundant and heterogeneous distribution of ERK1/2 in the cap and basal regions of atheromas. ERK1/2 was heavily phosphorylated on tyrosyl residues and co-expressed with proliferating cell nuclear antigen in atherosclerotic lesions. Furthermore, vSMCs derived from atherosclerotic lesions showed increased migratory/proliferative ability and higher ERK activity in response to LDL stimulation, compared to cells extracted from non-atherosclerotic vessels. These results suggest that a persistent activation and overexpression of ERK1/2 could be an initiator of cell proliferation during atherosclerosis progression and perpetuate the process in time [113]. The inhibition of ERK1/2 is a promising treatment because it reduces lipid deposition, upregulates the expression of ABCA1/G1 lipid efflux transporters and suppresses the expression of CD36 in oxLDL-stimulated macrophages [114].

## 4. Transcriptional Regulation of Phenotypes

### 4.1. Activator Protein-1 (AP-1)

AP-1 is the main physiological inhibitor of tissue-type plasminogen activator (t-PA), and therefore an important inhibitor of fibrinolysis. AP-1 controls several cellular events including cell proliferation, differentiation and apoptosis [115]. Previous studies showed that AP-1 activity is negatively affected by S-nitrosation and increased by antioxidants. AP-1 activity is in fact related with thioredoxin levels, suggesting a redox regulation of AP-1 [116]. Another study showed that the downregulation of NF- $\kappa$ B and AP-1 in vSMCs allows the inhibition of MMP-9 expression and induces G1-cell cycle arrest via PTEN [117]. PTEN is an inhibitor of the PI3K/Akt pathway and an inositol phosphatase, known to inhibit PDGF-mediated vSMC proliferation and migration [118]. Overexpression of PTEN inhibits growth factor-induced activation of Akt and p70 and proliferation, migration and survival of vSMCs. Furthermore, a critical role of AP-1 was shown in the atherosclerosis-associated process termed called arteriogenesis. The latter consists of wall remodelling and proliferation of collateral arterioles and is promoted by monocytes recruited from blood by the monocyte chemoattractant protein-1 (MCP-1). AP-1 in fact mediates an increased MCP-1 expression in vSMCs under stretch stress [119].



#### 4.2. Nuclear Factor Erythroid 2-Related Factor (Nrf-2)

Nrf-2 is a transcription factor, member of the cap'n'collar (CNC) subfamily, mediating the induction by antioxidants and electrophiles of detoxifying enzymes such as glutathione *S*-transferases or NAD(P)H:quinone oxidoreductase-1 (NQO-1) [120,121].

During atherogenesis, Nrf-2 can play a twofold role. On the one hand, it is pro-atherogenic, since Nrf-2 is the second transcription factor—after PPAR- $\gamma$ —involved in oxLDL-induced expression of CD36 and antioxidant stress proteins (A170, heme oxygenase-1, peroxiredoxin I) in macrophages [122]. Furthermore, Nrf-2 is a key regulator of Mox macrophages developed in response to oxidative tissue damage [4]. Treatment of M1 and M2 macrophages with oxidized phospholipids in fact induces their phenotypic switch to Mox macrophages through a marked Nrf-2-mediated expression of redox-regulatory genes.

On the other hand, there are anti-atherosclerotic mechanisms. Both Nrf-2 and Keap-1 are key components of the oxidative stress response for the maintenance of vascular homeostasis, through the induction of vSMC apoptosis and inhibition of neointimal hyperplasia [123]. Nrf-2 also participates in anti-atherosclerotic adaptive defence mechanisms, by inducing heme oxygenase-1 (HO-1) expression [124]. Monocyte-derived macrophages of healthy subjects in fact exhibit a lower oxidative stress status as compared to coronary artery disease patients, along with lower levels of Nrf-2 and HO-1. The latter are instead highly expressed in macrophages of active plaques. Thus, the HO-1 levels may reflect plaque vulnerability and allow the identification of patients with rupture-prone plaques [124].

As far as NO connections are concerned, earlier studies documented that NO itself is a potent inducer of HO-1 in vSMCs [125,126], and the effect was indeed shown to be mediated through activation of the Nrf-2/ARE axis [127]. It was suggested that the phenomenon may represent a critical adaptive response to maintain cell viability at sites of vascular inflammation during atherosclerosis.

#### 4.3. Nuclear Factor- $\kappa$ B (NF- $\kappa$ B)

NF- $\kappa$ B is a key regulator of the inflammatory response. It is usually sequestered in the cytoplasm in complexes with I $\kappa$ Bs, a family of inhibitory proteins. NF- $\kappa$ B translocation to the nucleus is thus prevented, avoiding the expression of genes encoding inflammatory and immuno-modulatory proteins, as well as of genes regulating cell differentiation, survival and proliferation [128]. The NF- $\kappa$ B family, encoded by the Rel gene family, is composed of five members—p50, p52, p65 (RelA), c-Rel and RelB—as well as six I $\kappa$ B members, which emphasizes its complex regulation. c-Rel allows macrophages to scale the inflammatory response after a transient or persistent stimulation of toll like receptor 4 (TLR-4), which also depends on macrophages localisation in tissue vs. blood [129,130]. p65 signalling was shown to directly upregulate the promoter activity of miR-17, an inducer of cell cycle G1/S transition and vSMCs proliferation. As NF- $\kappa$ B is both activated by inflammation and regulates inflammation, p65-dependent miR-17 upregulation could represent a mechanism explaining the excessive proliferation of vSMCs [131].

Chylomicron remnants and oxLDLs, both inducing foam cells formation, have been implicated in the suppression of NF- $\kappa$ B activity in macrophages [132]. Indeed, oxLDLs mediate oxidative modifications of NF- $\kappa$ B, such as carbonylation of the p65 subunit [133]. The uptake of oxLDLs is highly reduced in activated p50-deficient macrophages, along with a prolonged production of TNF- $\alpha$  in response to lipopolysaccharides (LPS) [134].

The effects of NO on NF- $\kappa$ B functions are biphasic. In the first place, high NO concentrations can be pro-apoptotic and pro-atherosclerotic, by inhibiting NF- $\kappa$ B activation in macrophages, monocytes and neutrophils. NF- $\kappa$ B DNA-binding is in fact inhibited by *S*-nitrosation of the p50 subunit (Figure 2). NO also inhibits NF- $\kappa$ B activation in rat vSMCs via a cGMP-independent inhibition of I $\kappa$ B phosphorylation. NF- $\kappa$ B activity is also stimulated through the nitration of I $\kappa$ B.str $\alpha$  following activation of NO synthase [135]. On the other hand, NO can also have anti-apoptotic effects, through modulation of several

proteins of the Bcl-2 family via sGC activation or inhibition by S-nitrosation of a large number of apoptotic proteins (e.g., caspases) [136].

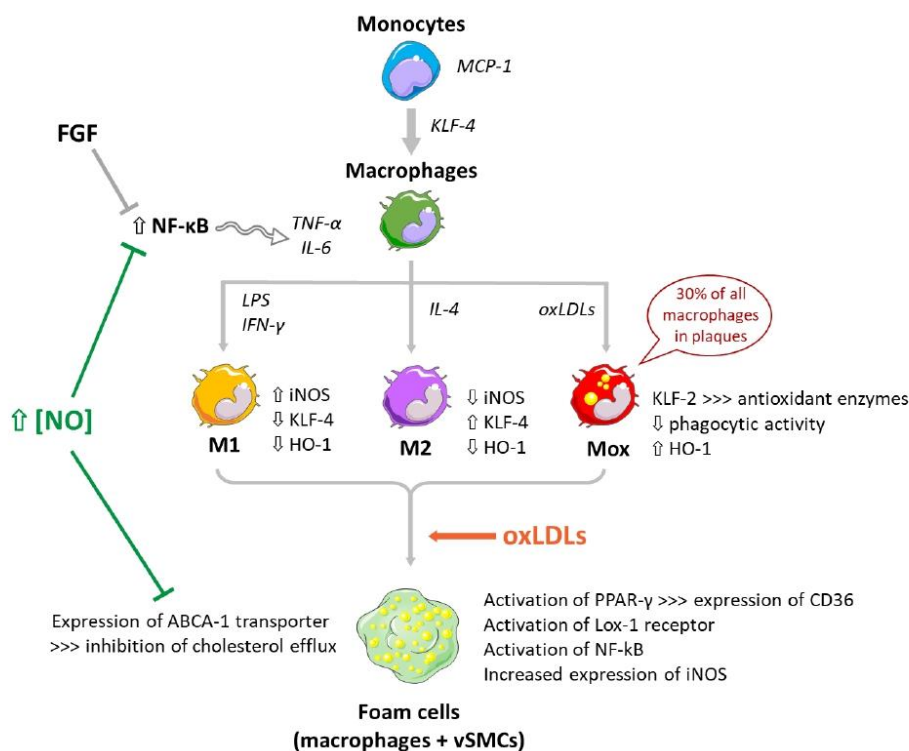


**Figure 2.** Involvement of NO and oxLDLs in the differentiation of monocytes to different subtypes of macrophages and formation of foam cells. NO: nitric oxide; iNOS: inducible NO synthase; FGF: fibroblast growth factor; NF-κB: nuclear factor-κB; TNF-α: tumour necrosis factor alpha; IL-6: interleukin-6; TLR4: toll-like receptor 4; MCP-1: monocyte chemoattractant protein 1; KLF-4: Krüppel-like factor 4; LPS: lipopolysaccharide, IFN-γ: interferon-γ; IL-4: interleukin-4; HO-1: heme oxygenase 1; KLF-2: Krüppel-like factor 2; LDLs: low-density lipoproteins; oxLDLs: oxidized low-density lipoproteins; PPAR-γ: proliferator-activated receptor γ.

#### 4.4. Myocardin/Serum Response Factor (SRF)

Myocardin is a powerful myogenic transcriptional regulator and co-activator, specifically expressed during adulthood in smooth muscle and myocardium. It negatively regulates vSMC inflammatory activation and reduces monocytes infiltration [137]. Myocardin is closely associated with SRF, considered as a docking platform for its activity. SRF is a ubiquitous DNA-binding transcription factor binding to a 10-base-pair CarG-box sequence (CC(A/T-rich)<sub>6</sub>CC), and activate the transcription of genes implicated in muscle differentiation and proliferation [138,139]. The myocardin/SRF/CarG complex is disrupted during the vSMC de-differentiation process. KLF-4, Elk-1 or FOXO-4 transcription factors act as co-repressor proteins, which compete with the myocardin/SRF/CarG complex and prevent the expression of differentiation genes [103] (Figure 3). Phosphorylated Elk-1 displaces myocardin from its SRF docking site and replaces it to form a nuclear factor activating the transcription of growth and proliferation genes.

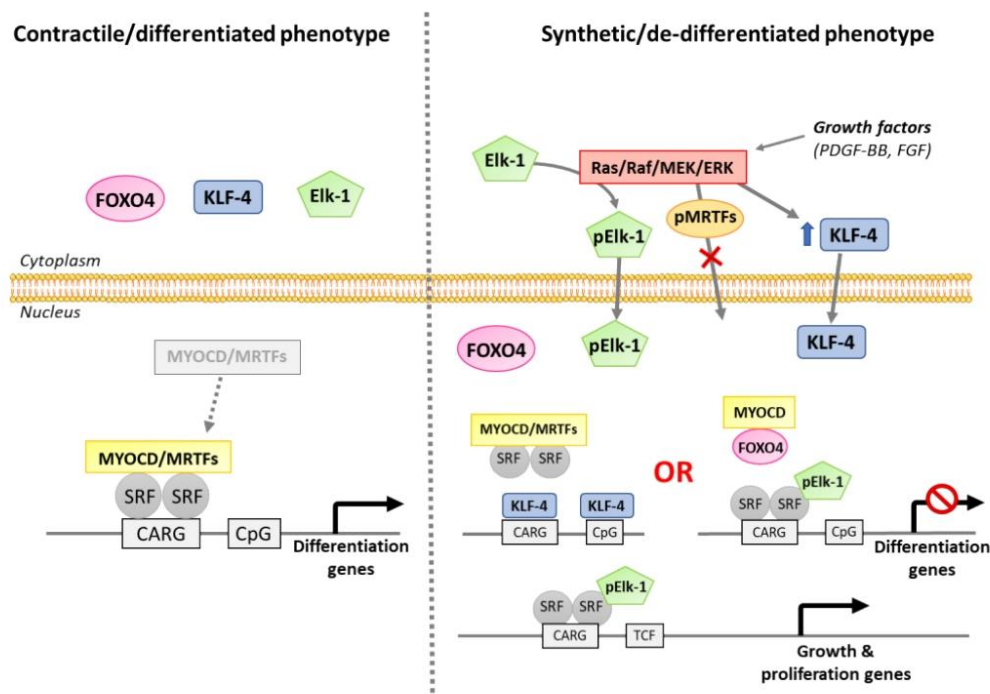


**Figure 3.** Impact of the myocardin–SRF–CarG complex and its cofactors in the maintenance vs. de-differentiation of the vSMCs' phenotype. CARG: CarG-box sequence; MYOCD: myocardin; MRTFs: myocardin-related transcription factors; SRF: serum response factor; KLF-4: Krüppel-like factor 4; PDGF-BB: platelet-derived growth factor-BB; FGF: fibroblast growth factor; TCF: ternary complex factor.

Myocardin levels are associated with the vSMCs' phenotypic switch and are decreased during progression of atherosclerosis. In  $\text{ApoE}^{-/-}$  mice, myocardin deficiency was shown to accelerate atherosclerosis. On the contrary, increased myocardin levels can prevent the expression of inflammatory cytokines, chemokines and adhesion molecules in vSMCs [137]. Thus, endogenous levels of myocardin are an important regulator of vessel inflammation, which identifies this transcriptional regulator as “the guardian” of the vSMCs' contractile phenotype.

NO can participate in the modulation of myocardin functions, with important bearings on vSMCs phenotypic switch and neo-angiogenesis. Vascular endothelial growth factor A (VEGF-A) was in fact shown to promote myocardin S-nitrosation, resulting in STAT-3 activation and vSMC proliferation, along with the inhibition of the vSMC markers' expression, such as ACTA-2, SM-22 and Myh-11. In addition, in experiments using GSNO as a NO donor, it was shown that myocardin can dose-dependently enhance the expression of GSNO reductase (GSNOR, also known as alcohol dehydrogenase class III), the enzyme effecting the catabolism GSNO into GSNHOH, thus downregulating NO bioavailability within the cell [140].

#### 4.5. Krüppel-Like Factor 4 (KLF-4)

KLF-4 is a pluripotent transcription factor, physiologically absent from contractile vSMCs but rapidly upregulated in response to vascular injury [141]. KLF-4 is a transcriptional target of BMPs 2, 4 and 6 as well as TGF- $\beta$ 1, resulting in the modulation of vSMC differentiation. Under vascular injury, KLF-4 is upregulated and mediates the vSMCs'



phenotypic switch in response to TGF- $\beta$ 1 through the activation of Smad2/3 and p38 MAPK signalling. KLF-4-promoted vSMC de-differentiation proceeds through the inhibition of SM- $\alpha$ -actin, SM22 $\alpha$  and SM-MHC expression, inducing vascular remodelling and plaque progression [142,143]. Furthermore, KLF-4 represses vSMC genes through the downregulation of myocardin and prevents the association of the SRF/myocardin complex with gene promoters of phenotypic vSMC markers (SM22 $\alpha$ , SM-MHC). Vendrov et al. demonstrated in mice that KLF-4 activates pro-inflammatory genes and allows vSMCs to acquire a pro-inflammatory, macrophage-like phenotype [144]. They also studied the effect of NOX activator A (NOXA1) deletion on the vSMCs' phenotype. NOXA1 is a functional homolog of p67-phox in activation of NADPH oxidase, and its deletion therefore decreases vascular levels of ROS and the size of the atherosclerotic lesions. The SMC-specific deletion of NOXA1 in mice produced a marked decrease in ROS generation, in TNF- $\alpha$ -induced vSMCs proliferation and migration, as well as in CD68<sup>+</sup> cells, myosin expression and levels of KLF-4 with its downstream targets (VCAM, MMP2). These results support an important role of NOXA1-dependent NADPH oxidase activity in vSMC plasticity, acting by increasing vSMC proliferation and migration, KLF-4-mediated transition to a macrophage-like phenotype and plaque inflammation. The stimulating protein-1 (Sp-1) transcription factor was shown to be essential for KLF-4 activation by PDGF-BB [145]. Indeed, Sp-1 overexpression can itself increase KLF-4 promoter activity and vSMCs phenotype modulation. In addition, following activation by oxidized phospholipids, KLF-4 mediates the upregulation of several extracellular matrix genes, such as type VIII collagen, and promotes vSMCs migration, contributing to progression of atherosclerosis [146].

During the differentiation of monocytes into macrophages, KLF-4 is regulated through demethylation of its promoter by a cytidine deaminase [147]. KLF-4 upregulates ApoE, an important anti-atherosclerotic factor [148], and is a critical regulator of macrophage polarisation [149], being highly expressed in M2 macrophages and downregulated in M1 macrophages (Figure 2). It has been recently shown in endothelial cells that KLF-4 can undergo S-nitrosation in response to a nitrosative stress, which impairs its activity [150]. Indeed, after a treatment with the physiological NO-donor S-nitrosoglutathione (GSNO), the KLF-4-dependent vasodilatory response in pulmonary arteries is impaired.

## 5. Conclusions

vSMCs and macrophages are the main cells implicated in atherosclerosis development, and their phenotypes are modified/switched upon various stimuli. Differentiation or de-differentiation processes implicate a large number of mechanisms and signalling pathways. In the last decade, several studies attempted to better understand these processes and to explore their possible utilisation in therapeutics. From this perspective, studies have highlighted the importance of NO in the progression of atherosclerosis, with a biphasic effect on cells depending on its concentration. NO can act through S-nitrosation to modulate the pathways discussed above (Figure 4). The differentiation of monocytes/macrophages and their phenotypic switch are sufficiently well characterised, while the signalling pathways driving the de-differentiation of the vSMCs remain partly unclear. While the implication of NO in atherosclerosis progression is indubitable, the interconnections between NO signalling and other relevant signalling pathways remain poorly understood. The identification of these interconnections could help to identify novel specific therapeutic targets, to be possibly exploited in synergy with other current anti-atherosclerotic strategies (hypolipidemic agents or antiplatelet drugs).



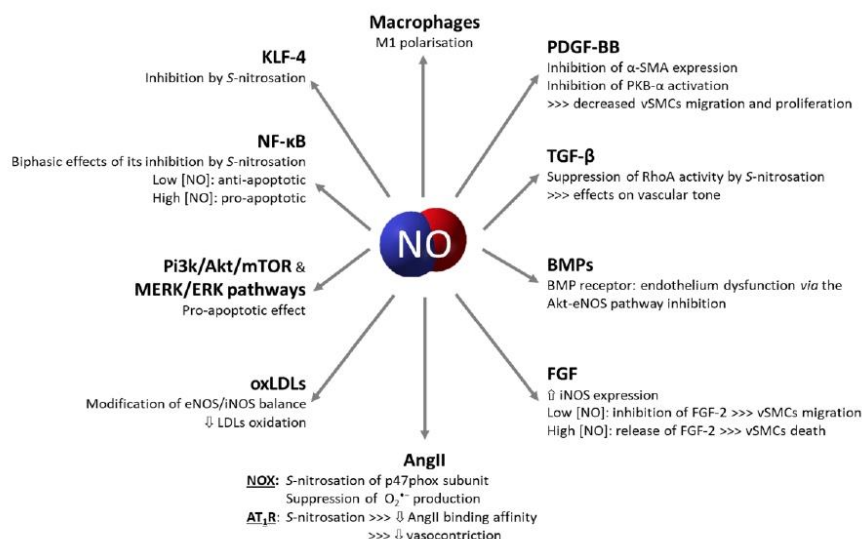


**Figure 4.** Mechanisms and pathways impacted by NO bioavailability. NO: nitric oxide; PDGF-BB: platelet-derived growth factor-BB; vSMCs: vascular smooth muscle cells; TGF- $\beta$ : transforming growth factor- $\beta$ ; iNOS: inducible NO synthase; BMPs: bone morphogenic proteins; eNOS: endothelial NO synthase; FGF: fibroblast growth factor; AngII: angiotensin II; AT<sub>1</sub>R: angiotensin II type I receptor; NOX: NAPDH oxidase; O<sub>2</sub><sup>•−</sup>: superoxide anion; oxLDLs: oxidized low-density lipoproteins; LDLs: low-density lipoproteins; NF- $\kappa$ B: nuclear factor- $\kappa$ B; KLF-4: Krüppel-like factor 4.

**Author Contributions:** Conceptualization, C.G. and J.B.; writing—original draft preparation, J.B. and L.L.; writing—review and editing, C.G., A.P. and A.C.; supervision, C.G. All authors have read and agreed to the published version of the manuscript.

**Funding:** The CITHEFOR EA3452 lab was supported by the “Impact Biomolecules” project of the “Lorraine Université d’Excellence” (Investissements d’avenir—ANR) and Programme VINCI 2018—Université Franco Italienne (Project no. C2-796). The authors acknowledge the COST Action NutRedOx-CA16112 supported by the COST (European Cooperation in Science and Technology). Additional funds were provided by Fondazione per lo studio della Fibrosi Cistica (FFC, Verona, Italy) and Università di Pisa, Italy (PRA funds).

**Acknowledgments:** The Servier Medical Art by Servier, licensed under a Creative Commons Attribution 3.0 Unported License was used to create Figures 1–3.

**Conflicts of Interest:** The authors declare no conflict of interest.

## References

1. World Health Organization. *World Health Statistics 2017: Monitoring Health for the SDGs, Sustainable Development Goals*; World Health Organization: Geneva, Switzerland, 2017; ISBN 978-92-4-156548-6.
2. Martinez, F.O.; Gordon, S. The M1 and M2 paradigm of macrophage activation: Time for reassessment. *F1000Prime Rep.* **2014**, *6*, 13. [CrossRef] [PubMed]
3. Stein, M.; Keshav, S.; Harris, N.; Gordon, S. Interleukin 4 potently enhances murine macrophage mannose receptor activity: A marker of alternative immunologic macrophage activation. *J. Exp. Med.* **1992**, *176*, 287–292. [CrossRef] [PubMed]
4. Kadl, A.; Meher, A.K.; Sharma, P.R.; Lee, M.Y.; Doran, A.C.; Johnstone, S.R.; Elliott, M.R.; Gruber, F.; Han, J.; Chen, W.; et al. Identification of a Novel Macrophage Phenotype That Develops in Response to Atherogenic Phospholipids via Nrf2. *Circ. Res.* **2010**, *107*, 737–746. [CrossRef] [PubMed]
5. De Gaetano, M.; Crean, D.; Barry, M.; Belton, O. M1- and M2-Type Macrophage Responses Are Predictive of Adverse Outcomes in Human Atherosclerosis. *Front. Immunol.* **2016**, *7*, 275. [CrossRef]

6. Chinetti-Gbaguidi, G.; Baron, M.; Bouhelle, M.A.; Vanhoutte, J.; Copin, C.; Sebti, Y.; Derudas, B.; Mayi, T.; Bories, G.; Tailleux, A.; et al. Human Atherosclerotic Plaque Alternative Macrophages Display Low Cholesterol Handling but High Phagocytosis Because of Distinct Activities of the PPAR $\gamma$  and LXR $\alpha$  Pathways. *Circ. Res.* **2011**, *108*, 985–995. [\[CrossRef\]](#) [\[PubMed\]](#)
7. Waldo, S.W.; Li, Y.; Buono, C.; Zhao, B.; Billings, E.M.; Chang, J.; Kruth, H.S. Heterogeneity of Human Macrophages in Culture and in Atherosclerotic Plaques. *Am. J. Pathol.* **2008**, *172*, 1112–1126. [\[CrossRef\]](#) [\[PubMed\]](#)
8. Sierra-Filardi, E.; Vega, M.A.; Sánchez-Mateos, P.; Corbí, A.L.; Puig-Kröger, A. Heme Oxygenase-1 expression in M-CSF-polarized M2 macrophages contributes to LPS-induced IL-10 release. *Immunobiology* **2010**, *215*, 788–795. [\[CrossRef\]](#)
9. van Tits, L.; Stienstra, R.; van Lent, P.; Netea, M.; Joosten, L.; Stalenhoef, A. Oxidized LDL enhances pro-inflammatory responses of alternatively activated M2 macrophages: A crucial role for Krüppel-like factor 2. *Atherosclerosis* **2011**, *214*, 345–349. [\[CrossRef\]](#)
10. Kazawa, T.; Kawasaki, T.; Sakamoto, A.; Imamura, M.; Ohashi, R.; Jiang, S.; Tanaka, T.; Iwanari, H.; Hamakubo, T.; Sakai, J.; et al. Expression of liver X receptor  $\alpha$  and lipid metabolism in granulocyte-macrophage colony-stimulating factor-induced human monocyte-derived macrophage. *Pathol. Int.* **2009**, *59*, 152–160. [\[CrossRef\]](#)
11. Chistiakov, D.A.; Bobryshev, Y.V.; Orekhov, A.N. Changes in transcriptome of macrophages in atherosclerosis. *J. Cell. Mol. Med.* **2015**, *19*, 1163–1173. [\[CrossRef\]](#)
12. Allahverdian, S.; Chaabane, C.; Boukais, K.; Francis, G.; Bochaton-Piallat, M.-L. Smooth muscle cell fate and plasticity in atherosclerosis. *Cardiovasc. Res.* **2018**, *114*, 540–550. [\[CrossRef\]](#)
13. Chistiakov, D.A.; Orekhov, A.N.; Bobryshev, Y.V. Vascular smooth muscle cell in atherosclerosis. *Acta Physiol.* **2015**, *214*, 33–50. [\[CrossRef\]](#)
14. Gomez, D.; Owens, G.K. Smooth muscle cell phenotypic switching in atherosclerosis. *Cardiovasc. Res.* **2012**, *95*, 156–164. [\[CrossRef\]](#)
15. Feil, S.; Fehrenbacher, B.; Lukowski, R.; Essmann, F.; Schulze-Osthoff, K.; Schaller, M.; Feil, R. Transdifferentiation of Vascular Smooth Muscle Cells to Macrophage-Like Cells during Atherogenesis. *Circ. Res.* **2014**, *115*, 662–667. [\[CrossRef\]](#) [\[PubMed\]](#)
16. Bennett, M.R.; Sinha, S.; Owens, G.K. Vascular Smooth Muscle Cells in Atherosclerosis. *Circ. Res.* **2016**, *118*, 692–702. [\[CrossRef\]](#) [\[PubMed\]](#)
17. Shankman, L.S.; Gomez, D.; Cherepanova, O.A.; Salmon, M.; Alencar, G.F.; Haskins, R.M.; Swiatlowska, P.; Newman, A.A.C.; Greene, E.S.; Straub, A.C.; et al. KLF4-dependent phenotypic modulation of smooth muscle cells has a key role in atherosclerotic plaque pathogenesis. *Nat. Med.* **2015**, *21*, 628–637. [\[CrossRef\]](#) [\[PubMed\]](#)
18. Yu, X.-H.; Fu, Y.-C.; Zhang, D.-W.; Yin, K.; Tang, C.-K. Foam cells in atherosclerosis. *Clin. Chim. Acta* **2013**, *424*, 245–252. [\[CrossRef\]](#) [\[PubMed\]](#)
19. Chaabane, C.; Coen, M.; Bochaton-Piallat, M.-L. Smooth muscle cell phenotypic switch. *Curr. Opin. Lipidol.* **2014**, *25*, 374–379. [\[CrossRef\]](#) [\[PubMed\]](#)
20. Chistiakov, D.A.; Melnichenko, A.A.; Myasoedova, V.A.; Grechko, A.V.; Orekhov, A.N. Mechanisms of foam cell formation in atherosclerosis. *J. Mol. Med.* **2017**, *95*, 1153–1165. [\[CrossRef\]](#)
21. Allahverdian, S.; Chehroudi, A.C.; McManus, B.M.; Abraham, T.; Francis, G.A. Contribution of Intimal Smooth Muscle Cells to Cholesterol Accumulation and Macrophage-Like Cells in Human Atherosclerosis. *Circulation* **2014**, *129*, 1551–1559. [\[CrossRef\]](#)
22. Tang, D.; Chen, S.; Hou, D.; Gao, J.; Jiang, L.; Shi, J.; Liang, Q.; Kong, D.; Wang, S. Regulation of macrophage polarization and promotion of endothelialization by NO generating and PEG-YIGSR modified vascular graft. *Mater. Sci. Eng. C* **2018**, *84*, 1–11. [\[CrossRef\]](#)
23. Lee, W.J.; Tateya, S.; Cheng, A.M.; Rizzo-DeLeon, N.; Wang, N.F.; Handa, P.; Wilson, C.L.; Clowes, A.W.; Sweet, I.R.; Bomsztyk, K.; et al. M2 Macrophage Polarization Mediates Anti-inflammatory Effects of Endothelial Nitric Oxide Signaling. *Diabetes* **2015**, *64*, 2836–2846. [\[CrossRef\]](#) [\[PubMed\]](#)
24. Rapkine, L. Sur les processus chimiques au cours de la division cellulaire. *J. Chim. Phys.* **1936**, *33*, 493–506. [\[CrossRef\]](#)
25. Kawamura, N. Cytochemical and quantitative study of protein-bound sulfhydryl and disulfide groups in eggs of Arbacia during the first cleavage. *Exp. Cell Res.* **1960**, *20*, 127–138. [\[CrossRef\]](#)
26. Cierny, M.; Sicinski, P. Cell cycle in mouse development. *Oncogene* **2005**, *24*, 2877–2898. [\[CrossRef\]](#) [\[PubMed\]](#)
27. Goswami, P.C.; Sheren, J.; Albee, L.D.; Parsian, A.; Sim, J.E.; Ridnour, L.A.; Higashikubo, R.; Gius, D.; Hunt, C.R.; Spitz, D.R. Cell Cycle-coupled Variation in Topoisomerase II $\alpha$  mRNA Is Regulated by the 3'-Untranslated Region. *J. Biol. Chem.* **2000**, *275*, 38384–38392. [\[CrossRef\]](#) [\[PubMed\]](#)
28. Menon, S.G.; Goswami, P.C. A redox cycle within the cell cycle: Ring in the old with the new. *Oncogene* **2006**, *26*, 1101–1109. [\[CrossRef\]](#) [\[PubMed\]](#)
29. Menon, S.G.; Sarsour, E.H.; Kalen, A.L.; Venkataraman, S.; Hitchler, M.J.; Domann, F.E.; Oberley, L.W.; Goswami, P.C. Superoxide Signaling Mediates N-acetyl-L-cysteine-Induced G1 Arrest: Regulatory Role of Cyclin D1 and Manganese Superoxide Dismutase. *Cancer Res.* **2007**, *67*, 6392–6399. [\[CrossRef\]](#) [\[PubMed\]](#)
30. Sarsour, E.H.; Venkataraman, S.; Kalen, A.L.; Oberley, L.W.; Goswami, P.C. Manganese superoxide dismutase activity regulates transitions between quiescent and proliferative growth. *Aging Cell* **2008**, *7*, 405–417. [\[CrossRef\]](#) [\[PubMed\]](#)
31. Sarsour, E.H.; Agarwal, M.; Pandita, T.K.; Oberley, L.W.; Goswami, P.C. Manganese Superoxide Dismutase Protects the Proliferative Capacity of Confluent Normal Human Fibroblasts. *J. Biol. Chem.* **2005**, *280*, 18033–18041. [\[CrossRef\]](#) [\[PubMed\]](#)
32. Negre-Salvayre, A.; Guerby, P.; Gayral, S.; Laffargue, M.; Salvayre, R. Role of reactive oxygen species in atherosclerosis: Lessons from murine genetic models. *Free. Radic. Biol. Med.* **2020**, *149*, 8–22. [\[CrossRef\]](#) [\[PubMed\]](#)



33. Chen, K.C.-W.; Zhou, Y.; Zhang, W.; Lou, M.F. Control of PDGF-induced reactive oxygen species (ROS) generation and signal transduction in human lens epithelial cells. *Mol. Vis.* **2007**, *13*, 374–387. [\[PubMed\]](#)
34. Raines, E.W. PDGF and cardiovascular disease. *Cytokine Growth Factor Rev.* **2004**, *15*, 237–254. [\[CrossRef\]](#) [\[PubMed\]](#)
35. Morgan, M.J.; Kim, Y.-S.; Liu, Z.-G. TNF $\alpha$  and reactive oxygen species in necrotic cell death. *Cell Res.* **2008**, *18*, 343–349. [\[CrossRef\]](#) [\[PubMed\]](#)
36. Dzau, V.J.; Gibbons, G.H.; Pratt, R.E. Molecular mechanisms of vascular renin-angiotensin system in myointimal hyperplasia. *Hypertension* **1991**, *18*, II100. [\[CrossRef\]](#) [\[PubMed\]](#)
37. Jones, D.P.; Sies, H. The Redox Code. *Antioxid. Redox Signal.* **2015**, *23*, 734–746. [\[CrossRef\]](#)
38. Andrae, J.; Gallini, R.; Betsholtz, C. Role of platelet-derived growth factors in physiology and medicine. *Genes Dev.* **2008**, *22*, 1276–1312. [\[CrossRef\]](#)
39. Siegbahn, A.; Hammacher, A.; Westermarck, B.; Heldin, C.H. Differential effects of the various isoforms of platelet-derived growth factor on chemotaxis of fibroblasts, monocytes, and granulocytes. *J. Clin. Investig.* **1990**, *85*, 916–920. [\[CrossRef\]](#) [\[PubMed\]](#)
40. Fredriksson, L.; Li, H.; Eriksson, U. The PDGF family: Four gene products form five dimeric isoforms. *Cytokine Growth Factor Rev.* **2004**, *15*, 197–204. [\[CrossRef\]](#) [\[PubMed\]](#)
41. Salabei, J.K.; Cummins, T.D.; Singh, M.; Jones, S.P.; Bhatnagar, A.; Hill, B.G. PDGF-mediated autophagy regulates vascular smooth muscle cell phenotype and resistance to oxidative stress. *Biochem. J.* **2013**, *451*, 375–388. [\[CrossRef\]](#)
42. Jay, D.B.; Papaharalambus, C.A.; Seidel-Rogol, B.; Dikalova, A.E.; Lassègue, B.; Griendling, K.K. Nox5 mediates PDGF-induced proliferation in human aortic smooth muscle cells. *Free Radic. Biol. Med.* **2008**, *45*, 329–335. [\[CrossRef\]](#) [\[PubMed\]](#)
43. Chistiakov, D.A.; Sobenin, I.A.; Orekhov, A.N. Vascular Extracellular Matrix in Atherosclerosis. *Cardiol. Rev.* **2013**, *21*, 270–288. [\[CrossRef\]](#)
44. Chen, Z.; Wu, Q.; Yan, C.; Du, J. COL6A1 knockdown suppresses cell proliferation and migration in human aortic vascular smooth muscle cells. *Exp. Ther. Med.* **2019**, *18*, 1977–1984. [\[CrossRef\]](#)
45. Itoh, S.; Katoh, Y.; Konishi, H.; Takaya, N.; Kimura, T.; Periasamy, M.; Yamaguchi, H. Nitric Oxide Regulates Smooth-muscle-specific Myosin Heavy Chain Gene Expression at the Transcriptional Level—Possible Role of SRF and YY1 Through CARC Element. *J. Mol. Cell. Cardiol.* **2001**, *33*, 95–107. [\[CrossRef\]](#) [\[PubMed\]](#)
46. Seymour, K.; Han, X.; Sadowitz, B.; Maier, K.G.; Gahtan, V. Differential effect of nitric oxide on thrombospondin-1-, PDGF- and fibronectin-induced migration of vascular smooth muscle cells. *Am. J. Surg.* **2010**, *200*, 615–619. [\[CrossRef\]](#)
47. Largiadèr, T.; Eto, M.; Payeli, S.K.; Greutert, H.; Viswambharan, H.; Lachat, M.; Zünd, G.; Yang, Z.; Tanner, F.C.; Lüscher, T.F. Endothelial Nitric Oxide Synthase Gene Transfer Inhibits Human Smooth Muscle Cell Migration via Inhibition of Rho A. *J. Cardiovasc. Pharmacol.* **2008**, *52*, 369–374. [\[CrossRef\]](#)
48. de Oliveira, M.G.; Doro, F.G.; Tfouni, E.; Krieger, M.H. Phenotypic switching prevention and proliferation/migration inhibition of vascular smooth muscle cells by the ruthenium nitrosyl complex trans-[Ru(NO)Cl(cyclam)](PF<sub>6</sub>)<sub>2</sub>. *J. Pharm. Pharmacol.* **2017**, *69*, 1155–1165. [\[CrossRef\]](#) [\[PubMed\]](#)
49. Sandrasegarane, L.; Charles, R.; Bourbon, N.; Kester, M. NO regulates PDGF-induced activation of PKB but not ERK in A7r5 cells: Implications for vascular growth arrest. *Am. J. Physiol. Physiol.* **2000**, *279*, C225–C235. [\[CrossRef\]](#)
50. Yu, J.; Zhang, Y.; Zhang, X.; Rudic, R.D.; Bauer, P.M.; Altieri, D.C.; Sessa, W.C. Endothelium Derived Nitric Oxide Synthase Negatively Regulates the PDGF-Survivin Pathway during Flow-Dependent Vascular Remodeling. *PLoS ONE* **2012**, *7*, e31495. [\[CrossRef\]](#) [\[PubMed\]](#)
51. Toma, I.; McCaffrey, T.A. Transforming growth factor- $\beta$  and atherosclerosis: Interwoven atherogenic and atheroprotective aspects. *Cell Tissue Res.* **2011**, *347*, 155–175. [\[CrossRef\]](#) [\[PubMed\]](#)
52. Mallat, Z.; Tedgui, A. The role of transforming growth factor beta in atherosclerosis: Novel insights and future perspectives. *Curr. Opin. Lipidol.* **2002**, *13*, 523–529. [\[CrossRef\]](#) [\[PubMed\]](#)
53. Tsunawaki, S.; Sporn, M.B.; Ding, A.; Nathan, C. Deactivation of macrophages by transforming growth factor- $\beta$ . *Nat. Cell Biol.* **1998**, *334*, 260–262. [\[CrossRef\]](#)
54. Bobik, A.; Agrotis, A.; Kanellakis, P.; Dilley, R.; Krushinsky, A.; Smirnov, V.; Tararak, E.; Condrón, M.; Kostolias, G. Distinct Patterns of Transforming Growth Factor- $\beta$  Isoform and Receptor Expression in Human Atherosclerotic Lesions. *Circulation* **1999**, *99*, 2883–2891. [\[CrossRef\]](#)
55. Michael, D.R.; Salter, R.C.; Ramji, D.P. TGF- $\beta$  inhibits the uptake of modified low density lipoprotein by human macrophages through a Smad-dependent pathway: A dominant role for Smad-2. *Biochim. Biophys. Acta (BBA) Mol. Basis Dis.* **2012**, *1822*, 1608–1616. [\[CrossRef\]](#)
56. Gao, P.; Wu, W.; Ye, J.; Lu, Y.W.; Adam, A.P.; Singer, H.A.; Long, X. Transforming growth factor  $\beta$ 1 suppresses proinflammatory gene program independent of its regulation on vascular smooth muscle differentiation and autophagy. *Cell. Signal.* **2018**, *50*, 160–170. [\[CrossRef\]](#) [\[PubMed\]](#)
57. Zhu, S.-B.; Zhu, J.; Zhou, Z.-Z.; Xi, E.-P.; Wang, R.-P.; Zhang, Y. TGF- $\beta$ 1 induces human aortic vascular smooth muscle cell phenotype switch through PI3K/AKT/ID2 signaling. *Am. J. Transl. Res.* **2015**, *7*, 2764–2774. [\[PubMed\]](#)
58. Deaton, R.A.; Su, C.; Valencia, T.G.; Grant, S.R. Transforming Growth Factor- $\beta$ 1-induced Expression of Smooth Muscle Marker Genes Involves Activation of PKN and p38 MAPK. *J. Biol. Chem.* **2005**, *280*, 31172–31181. [\[CrossRef\]](#) [\[PubMed\]](#)
59. Tang, Y.; Yang, X.; Friesel, R.E.; Vary, C.P.; Liaw, L. Mechanisms of TGF- $\beta$ -Induced Differentiation in Human Vascular Smooth Muscle Cells. *J. Vasc. Res.* **2011**, *48*, 485–494. [\[CrossRef\]](#)

60. Edlund, S.; Landström, M.; Heldin, C.-H.; Aspenström, P. Transforming Growth Factor- $\beta$ -induced Mobilization of Actin Cytoskeleton Requires Signaling by Small GTPases Cdc42 and RhoA. *Mol. Biol. Cell* **2002**, *13*, 902–914. [\[CrossRef\]](#)
61. Lin, L.; Xu, C.; Carraway, M.S.; Piantadosi, C.A.; Whorton, A.R.; Li, S. RhoA inactivation by S-nitrosylation regulates vascular smooth muscle contractile signaling. *Nitric Oxide* **2018**, *74*, 56–64. [\[CrossRef\]](#)
62. Zuckerbraun, B.S.; Stoyanovsky, D.A.; Sengupta, R.; Shapiro, R.A.; Ozanich, B.A.; Rao, J.; Barbato, J.E.; Tzeng, E. Nitric oxide-induced inhibition of smooth muscle cell proliferation involves S-nitrosation and inactivation of RhoA. *Am. J. Physiol. Physiol.* **2007**, *292*, C824–C831. [\[CrossRef\]](#)
63. Yao, Y.; Bennett, B.J.; Wang, X.; Rosenfeld, M.E.; Giachelli, C.M.; Lusis, A.J.; Boström, K.I. Inhibition of Bone Morphogenetic Proteins Protects Against Atherosclerosis and Vascular Calcification. *Circ. Res.* **2010**, *107*, 485–494. [\[CrossRef\]](#)
64. Boström, K.; Watson, K.; Horn, S.; Wortham, C.; Herman, I.M.; Demer, L.L. Bone morphogenetic protein expression in human atherosclerotic lesions. *J. Clin. Investig.* **1993**, *91*, 1800–1809. [\[CrossRef\]](#)
65. Nakaoka, T.; Gonda, K.; Ogita, T.; Otawara-Hamamoto, Y.; Okabe, F.; Kira, Y.; Harii, K.; Miyazono, K.; Takuwa, Y.; Fujita, T. Inhibition of rat vascular smooth muscle proliferation in vitro and in vivo by bone morphogenetic protein-2. *J. Clin. Investig.* **1997**, *100*, 2824–2832. [\[CrossRef\]](#)
66. Li, X.; Yang, H.-Y.; Giachelli, C.M. BMP-2 promotes phosphate uptake, phenotypic modulation, and calcification of human vascular smooth muscle cells. *Atherosclerosis* **2008**, *199*, 271–277. [\[CrossRef\]](#)
67. Yung, L.-M.; Sánchez-Duffhues, G.; Dijke, P.T.; Yu, P.B. Bone morphogenetic protein 6 and oxidized low-density lipoprotein synergistically recruit osteogenic differentiation in endothelial cells. *Cardiovasc. Res.* **2015**, *108*, 278–287. [\[CrossRef\]](#) [\[PubMed\]](#)
68. Kajimoto, H.; Kai, H.; Aoki, H.; Uchiwa, H.; Aoki, Y.; Yasuoka, S.; Anegawa, T.; Mishina, Y.; Suzuki, A.; Fukumoto, Y.; et al. BMP type I receptor inhibition attenuates endothelial dysfunction in mice with chronic kidney disease. *Kidney Int.* **2015**, *87*, 128–136. [\[CrossRef\]](#)
69. Lagna, G.; Ku, M.M.; Nguyen, P.H.; Neuman, N.A.; Davis, B.N.; Hata, A. Control of Phenotypic Plasticity of Smooth Muscle Cells by Bone Morphogenetic Protein Signaling through the Myocardin-related Transcription Factors. *J. Biol. Chem.* **2007**, *282*, 37244–37255. [\[CrossRef\]](#)
70. De Barros, R.S.; Dias, G.S.; Rosario, A.P.D.; Paladino, F.V.; Lopes, G.H.; Campos, A.H. Gremlin-1 potentiates the dedifferentiation of VSMC in early stages of atherosclerosis. *Differentiation* **2019**, *109*, 28–33. [\[CrossRef\]](#) [\[PubMed\]](#)
71. Müller, I.I.; Chatterjee, M.; Schneider, M.; Borst, O.; Seizer, P.; Schönberger, T.; Vogel, S.; Müller, K.A.; Geisler, T.; Lang, F.; et al. Gremlin-1 inhibits macrophage migration inhibitory factor-dependent monocyte function and survival. *Int. J. Cardiol.* **2014**, *176*, 923–929. [\[CrossRef\]](#) [\[PubMed\]](#)
72. Grillo, E.; Ravelli, C.; Corsini, M.; Ballmer-Hofer, K.; Zammataro, L.; Oreste, P.; Zoppetti, G.; Tobia, C.; Ronca, R.; Presta, M.; et al. Monomeric gremlin is a novel vascular endothelial growth factor receptor-2 antagonist. *Oncotarget* **2016**, *7*, 35353–35368. [\[CrossRef\]](#) [\[PubMed\]](#)
73. Hughes, S.E. Localisation and Differential Expression of the Fibroblast Growth Factor Receptor (FGFR) Multigene Family in Normal and Atherosclerotic Human Arteries. *Cardiovasc. Res.* **1996**, *32*, 557–569. [\[CrossRef\]](#)
74. Qi, M.; Xin, S. FGF signaling contributes to atherosclerosis by enhancing the inflammatory response in vascular smooth muscle cells. *Mol. Med. Rep.* **2019**, *20*, 162–170. [\[CrossRef\]](#)
75. Li, G.; Oparil, S.; Kelpke, S.S.; Chen, Y.-F.; Thompson, J.A. Fibroblast growth factor receptor-1 signaling induces osteopontin expression and vascular smooth muscle cell-dependent adventitial fibroblast migration in vitro. *Circulation* **2002**, *106*, 854–859. [\[CrossRef\]](#)
76. Sigala, F.; Savvari, P.; Lontos, M.; Sigalas, P.; Pateras, I.S.; Papalampros, A.; Basdra, E.K.; Kolettas, E.; Kotsinas, A.; Papavassiliou, A.G.; et al. Increased expression of bFGF is associated with carotid atherosclerotic plaques instability engaging the NF- $\kappa$ B pathway. *J. Cell. Mol. Med.* **2010**, *14*, 2273–2280. [\[CrossRef\]](#) [\[PubMed\]](#)
77. Alfke, H.; Kleb, B.; Klose, K.J. Stickstoffmonoxid inhibiert die durch basischen Fibroblastenwachstumsfaktor induzierte Migration von bovinen, glatten Gefäßmuskulzellen in vitro. *Vasa* **2000**, *29*, 99–102. [\[CrossRef\]](#) [\[PubMed\]](#)
78. Fukuo, K.; Inoue, T.; Morimoto, S.; Nakahashi, T.; Yasuda, O.; Kitano, S.; Sasada, R.; Ogihara, T. Nitric oxide mediates cytotoxicity and basic fibroblast growth factor release in cultured vascular smooth muscle cells. A possible mechanism of neovascularization in atherosclerotic plaques. *J. Clin. Investig.* **1995**, *95*, 669–676. [\[CrossRef\]](#) [\[PubMed\]](#)
79. Herbert, J.-M.; Bono, F.; Savi, P. The mitogenic effect of H<sub>2</sub>O<sub>2</sub> for vascular smooth muscle cells is mediated by an increase of the affinity of basic fibroblast growth factor for its receptor. *FEBS Lett.* **1996**, *395*, 43–47. [\[CrossRef\]](#)
80. Wang, N.; Li, J.-Y.; Li, S.; Guo, X.-C.; Wu, T.; Wang, W.-F.; Li, D.-S. Fibroblast growth factor 21 regulates foam cells formation and inflammatory response in Ox-LDL-induced THP-1 macrophages. *Biomed. Pharmacother.* **2018**, *108*, 1825–1834. [\[CrossRef\]](#)
81. Chen, P.; Qin, L.; Li, G.; Tellides, G.; Simons, M. Smooth muscle FGF/TGF  $\beta$  cross talk regulates atherosclerosis progression. *EMBO Mol. Med.* **2016**, *8*, 712–728. [\[CrossRef\]](#) [\[PubMed\]](#)
82. Fukuda, D.; Enomoto, S.; Hirata, Y.; Nagai, R.; Sata, M. The angiotensin receptor blocker, telmisartan, reduces and stabilizes atherosclerosis in ApoE and AT1aR double deficient mice. *Biomed. Pharmacother.* **2010**, *64*, 712–717. [\[CrossRef\]](#)
83. Leclerc, P.C.; Lanctot, P.M.; Auger-Messier, M.; Escher, E.; LeDuc, R.; Guillemette, G. S-nitrosylation of cysteine 289 of the AT1 receptor decreases its binding affinity for angiotensin II. *Br. J. Pharmacol.* **2006**, *148*, 306–313. [\[CrossRef\]](#) [\[PubMed\]](#)



84. Bouressam, M.-L.; Lecat, S.; Raoul, A.; Gaucher, C.; Perrin-Sarrado, C.; Lartaud, I.; Dupuis, F. S-nitrosoglutathione inhibits cerebrovascular angiotensin II-dependent and -independent AT1 receptor responses: A possible role of S-nitrosation. *Br. J. Pharmacol.* **2019**, *176*, 2049–2062. [\[CrossRef\]](#) [\[PubMed\]](#)
85. Durante, A.; Peretto, G.; Laricchia, A.; Ancona, F.; Spartera, M.; Mangieri, A.; Cianflone, D. Role of the Renin-Angiotensin-Aldosterone System in the Pathogenesis of Atherosclerosis. *Curr. Pharm. Des.* **2012**, *18*, 981–1004. [\[CrossRef\]](#)
86. Da Silva, A.R.; Fraga-Silva, R.A.; Stergiopoulos, N.; Montecucco, F.; Mach, F. Update on the role of angiotensin in the pathophysiology of coronary atherothrombosis. *Eur. J. Clin. Investig.* **2015**, *45*, 274–287. [\[CrossRef\]](#) [\[PubMed\]](#)
87. Sata, M.; Fukuda, D. Crucial role of renin-angiotensin system in the pathogenesis of atherosclerosis. *J. Med. Investig.* **2010**, *57*, 12–25. [\[CrossRef\]](#) [\[PubMed\]](#)
88. Madiraju, P.; Hossain, E.; Anand-Srivastava, M.B. Natriuretic peptide receptor-C activation attenuates angiotensin II-induced enhanced oxidative stress and hyperproliferation of aortic vascular smooth muscle cells. *Mol. Cell. Biochem.* **2018**, *448*, 77–89. [\[CrossRef\]](#) [\[PubMed\]](#)
89. Griendling, K.K.; Minieri, C.; Ollerenshaw, J.D.; Alexander, R.W. Angiotensin II stimulates NADH and NADPH oxidase activity in cultured vascular smooth muscle cells. *Circ. Res.* **1994**, *74*, 1141–1148. [\[CrossRef\]](#) [\[PubMed\]](#)
90. Cat, A.N.D.; Montezano, A.C.; Burger, D.; Touyz, R.M. Angiotensin II, NADPH Oxidase, and Redox Signaling in the Vasculature. *Antioxid. Redox Signal.* **2013**, *19*, 1110–1120. [\[CrossRef\]](#)
91. Selemidis, S.; Dusting, G.J.; Peshavariya, H.; Kemp-Harper, B.K.; Drummond, G.R. Nitric oxide suppresses NADPH oxidase-dependent superoxide production by S-nitrosylation in human endothelial cells. *Cardiovasc. Res.* **2007**, *75*, 349–358. [\[CrossRef\]](#)
92. Tang, Y.; Huang, Q.; Liu, C.; Ou, H.; Huang, D.; Peng, F.; Liu, C.; Mo, Z. p22phox promotes Ang-II-induced vascular smooth muscle cell phenotypic switch by regulating KLF4 expression. *Biochem. Biophys. Res. Commun.* **2019**, *514*, 280–286. [\[CrossRef\]](#) [\[PubMed\]](#)
93. Pidkova, N.A.; Cherepanova, O.A.; Yoshida, T.; Alexander, M.R.; Deaton, R.A.; Thomas, J.A.; Leitinger, N.; Owens, G.K. Oxidized Phospholipids Induce Phenotypic Switching of Vascular Smooth Muscle Cells In Vivo and In Vitro. *Circ. Res.* **2007**, *101*, 792–801. [\[CrossRef\]](#) [\[PubMed\]](#)
94. Gliozzi, M.; Scicchitano, M.; Bosco, F.; Musolino, V.; Carresi, C.; Scarano, F.; Maiuolo, J.; Nucera, S.; Maretta, A.; Paone, S.; et al. Modulation of Nitric Oxide Synthases by Oxidized LDLs: Role in Vascular Inflammation and Atherosclerosis Development. *Int. J. Mol. Sci.* **2019**, *20*, 3294. [\[CrossRef\]](#) [\[PubMed\]](#)
95. Huang, H.; Koelle, P.; Fendler, M.; Schrotte, A.; Czihal, M.; Hoffmann, U.; Conrad, M.; Kuhlencordt, P. Induction of inducible nitric oxide synthase (iNOS) expression by oxLDL inhibits macrophage derived foam cell migration. *Atherosclerosis* **2014**, *235*, 213–222. [\[CrossRef\]](#) [\[PubMed\]](#)
96. Zhao, J.-F.; Shyue, S.-K.; Lin, S.-J.; Wei, J.; Lee, T.-S. Excess nitric oxide impairs liver X receptor  $\alpha$ -ATP-binding cassette transporter A1-dependent cholesterol efflux in macrophage foam cells. *J. Cell. Physiol.* **2013**, *229*, 117–125. [\[CrossRef\]](#) [\[PubMed\]](#)
97. Jaworski, K.; Kinard, F.; Goldstein, D.; Holvoet, P.; Trouet, A.; Schneider, Y.-J.; Remacle, C. S-nitrosothiols do not induce oxidative stress, contrary to other nitric oxide donors, in cultures of vascular endothelial or smooth muscle cells. *Eur. J. Pharmacol.* **2001**, *425*, 11–19. [\[CrossRef\]](#)
98. Krieger, M.; Santos, K.; Shishido, S.; Wanschel, A.; Estrela, H.; Santos, L.; De Oliveira, M.G.; Franchini, K.; Spadari-Bratfisch, R.; Laurindo, F. Antiatherogenic effects of S-nitroso-N-acetylcycteine in hypercholesterolemic LDL receptor knockout mice. *Nitric Oxide* **2006**, *14*, 12–20. [\[CrossRef\]](#) [\[PubMed\]](#)
99. Momi, S.; Impagnatiello, F.; Guzzetta, M.; Caracchini, R.; Guglielmini, G.; Olivieri, R.; Monopoli, A.; Gesele, P. NCX 6560, a nitric oxide-releasing derivative of atorvastatin, inhibits cholesterol biosynthesis and shows anti-inflammatory and anti-thrombotic properties. *Eur. J. Pharmacol.* **2007**, *570*, 115–124. [\[CrossRef\]](#)
100. Abeyrathna, P.; Su, Y. The critical role of Akt in cardiovascular function. *Vasc. Pharmacol.* **2015**, *74*, 38–48. [\[CrossRef\]](#)
101. Mathew, O.P.; Ranganna, K.; Mathew, J.; Zhu, M.; Yousefipour, Z.; Selvam, C.; Milton, S.G. Cellular Effects of Butyrate on Vascular Smooth Muscle Cells are Mediated through Disparate Actions on Dual Targets, Histone Deacetylase (HDAC) Activity and PI3K/Akt Signaling Network. *Int. J. Mol. Sci.* **2019**, *20*, 2902. [\[CrossRef\]](#) [\[PubMed\]](#)
102. Hayashi, K.; Saga, H.; Chimori, Y.; Kimura, K.; Yamanaka, Y.; Sobue, K. Differentiated Phenotype of Smooth Muscle Cells Depends on Signaling Pathways through Insulin-like Growth Factors and Phosphatidylinositol 3-Kinase. *J. Biol. Chem.* **1998**, *273*, 28860–28867. [\[CrossRef\]](#) [\[PubMed\]](#)
103. Frisantiene, A.; Philippova, M.; Erne, P.; Resink, T.J. Smooth muscle cell-driven vascular diseases and molecular mechanisms of VSMC plasticity. *Cell. Signal.* **2018**, *52*, 48–64. [\[CrossRef\]](#)
104. Zhang, L.; Zhang, Y.; Wu, Y.; Yu, J.; Zhang, Y.; Zeng, F.; Shi, L. Role of the Balance of Akt and MAPK Pathways in the Exercise-Regulated Phenotype Switching in Spontaneously Hypertensive Rats. *Int. J. Mol. Sci.* **2019**, *20*, 5690. [\[CrossRef\]](#) [\[PubMed\]](#)
105. Wu, W.; Zhang, W.; Choi, M.; Zhao, J.; Gao, P.; Xue, M.; Singer, H.A.; Jourdain, D.; Long, X. Vascular smooth muscle-MAPK14 is required for neointimal hyperplasia by suppressing VSMC differentiation and inducing proliferation and inflammation. *Redox Biol.* **2019**, *22*, 101137. [\[CrossRef\]](#)
106. Linton, M.F.; Moslehi, J.J.; Babaev, V.R. Akt Signaling in Macrophage Polarization, Survival, and Atherosclerosis. *Int. J. Mol. Sci.* **2019**, *20*, 2703. [\[CrossRef\]](#) [\[PubMed\]](#)
107. Zhai, C.; Cheng, J.; Mujahid, H.; Wang, H.; Kong, J.; Yin, Y.; Li, J.; Zhang, Y.; Ji, X.; Chen, W. Selective Inhibition of PI3K/Akt/mTOR Signaling Pathway Regulates Autophagy of Macrophage and Vulnerability of Atherosclerotic Plaque. *PLoS ONE* **2014**, *9*, e90563. [\[CrossRef\]](#) [\[PubMed\]](#)

108. Pi, S.; Mao, L.; Chen, J.; Shi, H.; Liu, Y.; Guo, X.; Li, Y.; Zhou, L.; He, H.; Yu, C.; et al. The P2RY12 receptor promotes VSMC-derived foam cell formation by inhibiting autophagy in advanced atherosclerosis. *Autophagy* **2020**, 1–21. [\[CrossRef\]](#)
109. Zhang, M.; Li, F.; Wang, X.; Gong, J.; Xian, Y.; Wang, G.; Zheng, Z.; Shang, C.; Wang, B.; He, Y.; et al. MiR-145 alleviates Hcy-induced VSMC proliferation, migration, and phenotypic switch through repression of the PI3K/Akt/mTOR pathway. *Histochem. Cell Biol.* **2020**, *153*, 357–366. [\[CrossRef\]](#) [\[PubMed\]](#)
110. Liu, L.; Chen, J.; Cao, M.; Wang, J.; Wang, S. NO donor inhibits proliferation and induces apoptosis by targeting PI3K/AKT/mTOR and MEK/ERK pathways in hepatocellular carcinoma cells. *Cancer Chemother. Pharmacol.* **2019**, *84*, 1303–1314. [\[CrossRef\]](#) [\[PubMed\]](#)
111. Meng, X.; Li, X.; Xu, X.; Li, P.; Chen, Y.; Fu, X.; Xu, X. Elevated luteinizing hormone contributes to atherosclerosis formation by inhibiting nitric oxide synthesis via PI3K/Akt pathway. *Vasc. Pharmacol.* **2019**, *121*, 106582. [\[CrossRef\]](#)
112. Wang, Z.; Wang, D.-Z.; Hockemeyer, D.; McAnally, J.; Nordheim, A.; Olson, E.N. Myocardin and ternary complex factors compete for SRF to control smooth muscle gene expression. *Nat. Cell Biol.* **2004**, *428*, 185–189. [\[CrossRef\]](#) [\[PubMed\]](#)
113. Hu, Y.; Dietrich, H.; Metzler, B.; Wick, G.; Xu, Q. Hyperexpression and activation of extracellular signal-regulated kinases (ERK1/2) in atherosclerotic lesions of cholesterol-fed rabbits. *Arter. Thromb. Vasc. Biol.* **2000**, *20*, 18–26. [\[CrossRef\]](#)
114. Xue, X.-H.; Shi, F.-F.; Chen, T.; Wei, W.; Zhou, X.-M.; Chen, L.-D. Inhibition of ERK1/2 improves lipid balance in rat macrophages via ABC A1/G1 and CD36. *Mol. Med. Rep.* **2016**, *13*, 1533–1540. [\[CrossRef\]](#)
115. Ameyar, M.; Wisniewska, M.; Weitzman, J. A role for AP-1 in apoptosis: The case for and against. *Biochimistry* **2003**, *85*, 747–752. [\[CrossRef\]](#) [\[PubMed\]](#)
116. Marshall, H.E.; Merchant, K.; Stamler, J.S. Nitrosation and oxidation in the regulation of gene expression. *FASEB J.* **2000**, *14*, 1889–1900. [\[CrossRef\]](#) [\[PubMed\]](#)
117. Moon, S.-K.; Kim, H.-M.; Kim, C.-H. PTEN induces G1 cell cycle arrest and inhibits MMP-9 expression via the regulation of NF- $\kappa$ B and AP-1 in vascular smooth muscle cells. *Arch. Biochem. Biophys.* **2004**, *421*, 267–276. [\[CrossRef\]](#) [\[PubMed\]](#)
118. Huang, J.; Kontos, C.D. Inhibition of Vascular Smooth Muscle Cell Proliferation, Migration, and Survival by the Tumor Suppressor Protein PTEN. *Arter. Thromb. Vasc. Biol.* **2002**, *22*, 745–751. [\[CrossRef\]](#)
119. Demicheva, E.; Hecker, M.; Korff, T. Stretch-Induced Activation of the Transcription Factor Activator Protein-1 Controls Monocyte Chemotactic Protein-1 Expression during Arteriogenesis. *Circ. Res.* **2008**, *103*, 477–484. [\[CrossRef\]](#) [\[PubMed\]](#)
120. Itoha, K.; Chibab, T.; Takahashia, S.; Ishiia, T.; Igarashia, K.; Katoha, Y.; Oyaked, T.; Hayashid, N.; Satohe, K.; Hatayamae, I.; et al. An Nrf2/Small Maf Heterodimer Mediates the Induction of Phase II Detoxifying Enzyme Genes through Antioxidant Response Elements. *Biochem. Biophys. Res. Commun.* **1997**, *236*, 313–322. [\[CrossRef\]](#) [\[PubMed\]](#)
121. Venugopal, R.; Jaiswal, A.K. Nrf1 and Nrf2 positively and c-Fos and Fra1 negatively regulate the human antioxidant response element-mediated expression of NAD(P)H:quinone oxidoreductase1 gene. *Proc. Natl. Acad. Sci. USA* **1996**, *93*, 14960–14965. [\[CrossRef\]](#) [\[PubMed\]](#)
122. Ishii, T.; Itoh, K.; Ruiz, E.; Leake, D.S.; Unoki, H.; Yamamoto, M.; Mann, G.E. Role of Nrf2 in the Regulation of CD36 and Stress Protein Expression in Murine Macrophages. *Circ. Res.* **2004**, *94*, 609–616. [\[CrossRef\]](#) [\[PubMed\]](#)
123. Ashino, T.; Yamamoto, M.; Numazawa, S. Nrf2/Keap1 system regulates vascular smooth muscle cell apoptosis for vascular homeostasis: Role in neointimal formation after vascular injury. *Sci. Rep.* **2016**, *6*, 26291. [\[CrossRef\]](#) [\[PubMed\]](#)
124. Fiorelli, S.; Porro, B.; Cosentino, N.; Di Minno, A.; Manega, C.M.; Fabbicchi, F.; Niccoli, G.; Fracassi, F.; Barbieri, S.; Marenzi, G.; et al. Activation of Nrf2/HO-1 Pathway and Human Atherosclerotic Plaque Vulnerability: An In Vitro and In Vivo Study. *Cells* **2019**, *8*, 356. [\[CrossRef\]](#)
125. Durante, W.; Kroll, M.H.; Christodoulides, N.; Peyton, K.J.; Schafer, A.I. Nitric Oxide Induces Heme Oxygenase-1 Gene Expression and Carbon Monoxide Production in Vascular Smooth Muscle Cells. *Circ. Res.* **1997**, *80*, 557–564. [\[CrossRef\]](#)
126. Hartsfield, C.L.; Alam, J.; Cook, J.L.; Choi, A.M.K. Regulation of heme oxygenase-1 gene expression in vascular smooth muscle cells by nitric oxide. *Am. J. Physiol. Content* **1997**, *273*, L980–L988. [\[CrossRef\]](#) [\[PubMed\]](#)
127. Liu, X.-M.; Peyton, K.J.; Ensenat, D.; Wang, H.; Hannink, M.; Alam, J.; Durante, W. Nitric oxide stimulates heme oxygenase-1 gene transcription via the Nrf2/ARE complex to promote vascular smooth muscle cell survival. *Cardiovasc. Res.* **2007**, *75*, 381–389. [\[CrossRef\]](#)
128. Hayden, M.S.; Ghosh, S. Shared Principles in NF- $\kappa$ B Signaling. *Cell* **2008**, *132*, 344–362. [\[CrossRef\]](#) [\[PubMed\]](#)
129. Litvak, V.; Ramsey, S.A.; Rust, A.G.; Zak, D.E.; Kennedy, K.A.; Lampano, A.E.; Nykter, M.; Shmulevich, I.; Aderem, A. Function of C/EBP $\delta$  in a regulatory circuit that discriminates between transient and persistent TLR4-induced signals. *Nat. Immunol.* **2009**, *10*, 437–443. [\[CrossRef\]](#)
130. Grigoriadis, G.; Zhan, Y.; Grumont, R.J.; Metcalf, D.; Handman, E.; Cheers, C.; Gerondakis, S. The Rel Subunit of NF-KappaB-like Transcription Factors Is a Positive and Negative Regulator of Macrophage Gene Expression: Distinct Roles for Rel in Different Macrophage Populations. *EMBO J.* **1996**, *15*, 7099–7107. [\[CrossRef\]](#) [\[PubMed\]](#)
131. Yang, D.; Sun, C.; Zhang, J.; Lin, S.; Zhao, L.; Wang, L.; Lin, R.; Lv, J.; Xin, S. Proliferation of vascular smooth muscle cells under inflammation is regulated by NF- $\kappa$ B p65/microRNA-17/RB pathway activation. *Int. J. Mol. Med.* **2017**, *41*, 43–50. [\[CrossRef\]](#) [\[PubMed\]](#)
132. De Pascale, C.; Graham, V.; Fowkes, R.C.; Wheeler-Jones, C.P.D.; Botham, K.M. Suppression of nuclear factor- $\kappa$ B activity in macrophages by chylomicron remnants: Modulation by the fatty acid composition of the particles. *FEBS J.* **2009**, *276*, 5689–5702. [\[CrossRef\]](#)



133. Muroya, T.; Ihara, Y.; Ikeda, S.; Yasuoka, C.; Miyahara, Y.; Urata, Y.; Kondo, T.; Kohno, S. Oxidative modulation of NF- $\kappa$ B signaling by oxidized low-density lipoprotein. *Biochem. Biophys. Res. Commun.* **2003**, *309*, 900–905. [\[CrossRef\]](#)
134. Kanters, E.; Gijbels, M.J.J.; Van Der Made, I.; Vergouwe, M.N.; Heeringa, P.; Kraal, G.; Hofker, M.H.; De Winther, M.P.J. Hematopoietic NF- $\kappa$ B1 deficiency results in small atherosclerotic lesions with an inflammatory phenotype. *Blood* **2004**, *103*, 934–940. [\[CrossRef\]](#) [\[PubMed\]](#)
135. Yakovlev, V.A.; Barani, I.J.; Rabender, C.S.; Black, S.M.; Leach, J.K.; Graves, P.R.; Mikkelsen, R.B. Tyrosine Nitration of I $\kappa$ B $\alpha$ : A Novel Mechanism for NF- $\kappa$ B Activation. *Biochemistry* **2007**, *46*, 11671–11683. [\[CrossRef\]](#)
136. Taylor, E.L.; Megson, I.L.; Haslett, C.; Rossi, A.G. Nitric oxide: A key regulator of myeloid inflammatory cell apoptosis. *Cell Death Differ.* **2003**, *10*, 418–430. [\[CrossRef\]](#)
137. Ackers-Johnson, M.; Talasila, A.; Sage, A.P.; Long, X.; Bot, I.; Morrell, N.W.; Bennett, M.R.; Miano, J.M.; Sinha, S. Myocardin Regulates Vascular Smooth Muscle Cell Inflammatory Activation and Disease. *Arter. Thromb. Vasc. Biol.* **2015**, *35*, 817–828. [\[CrossRef\]](#)
138. Minty, A.; Kedes, L. Upstream regions of the human cardiac actin gene that modulate its transcription in muscle cells: Presence of an evolutionarily conserved repeated motif. *Mol. Cell. Biol.* **1986**, *6*, 2125–2136. [\[CrossRef\]](#) [\[PubMed\]](#)
139. McDonald, O.G.; Wamhoff, B.R.; Hoofnagle, M.H.; Owens, G.K. Control of SRF binding to CArG box chromatin regulates smooth muscle gene expression in vivo. *J. Clin. Investig.* **2005**, *116*, 36–48. [\[CrossRef\]](#) [\[PubMed\]](#)
140. Liao, X.H.; Xiang, Y.; Li, H.; Zheng, D.L.; Xu, Y.; Yu, C.X.; Li, J.P.; Zhang, X.Y.; Bin Xing, W.; Cao, D.S.; et al. VEGF-A Stimulates STAT3 Activity via Nitrosylation of Myocardin to Regulate the Expression of Vascular Smooth Muscle Cell Differentiation Markers. *Sci. Rep.* **2017**, *7*, 2660. [\[CrossRef\]](#) [\[PubMed\]](#)
141. Liu, Y.; Sinha, S.; McDonald, O.G.; Shang, Y.; Hoofnagle, M.H.; Owens, G.K. Kruppel-like Factor 4 Abrogates Myocardin-induced Activation of Smooth Muscle Gene Expression. *J. Biol. Chem.* **2005**, *280*, 9719–9727. [\[CrossRef\]](#) [\[PubMed\]](#)
142. Owens, G.K. Molecular Control of Vascular Smooth Muscle Cell Differentiation and Phenotypic Plasticity. *Novartis Found. Symp.* **2007**, *283*, 174–193. [\[CrossRef\]](#)
143. Kawai-Kowase, K.; Owens, G.K. Multiple repressor pathways contribute to phenotypic switching of vascular smooth muscle cells. *Am. J. Physiol. Physiol.* **2007**, *292*, C59–C69. [\[CrossRef\]](#) [\[PubMed\]](#)
144. Vendrov, A.E.; Sumida, A.; Canugovi, C.; Lozhkin, A.; Hayami, T.; Madamanchi, N.R.; Runge, M.S. NOXA1-dependent NADPH oxidase regulates redox signaling and phenotype of vascular smooth muscle cell during atherogenesis. *Redox Biol.* **2019**, *21*, 101063. [\[CrossRef\]](#) [\[PubMed\]](#)
145. Deaton, R.A.; Gan, Q.; Owens, G.K. Sp1-dependent activation of KLF4 is required for PDGF-BB-induced phenotypic modulation of smooth muscle. *Am. J. Physiol. Circ. Physiol.* **2009**, *296*, H1027–H1037. [\[CrossRef\]](#) [\[PubMed\]](#)
146. Cherepanova, O.A.; Pidkovka, N.A.; Sarmiento, O.F.; Yoshida, T.; Gan, Q.; Adiguzel, E.; Bendeck, M.P.; Berliner, J.; Leitinger, N.; Owens, G.K. Oxidized Phospholipids Induce Type VIII Collagen Expression and Vascular Smooth Muscle Cell Migration. *Circ. Res.* **2009**, *104*, 609–618. [\[CrossRef\]](#) [\[PubMed\]](#)
147. Karpurapu, M.; Ranjan, R.; Deng, J.; Chung, S.; Lee, Y.G.; Xiao, L.; Nirujogi, T.S.; Jacobson, J.R.; Park, G.Y.; Christman, J.W. Krüppel Like Factor 4 Promoter Undergoes Active Demethylation during Monocyte/Macrophage Differentiation. *PLoS ONE* **2014**, *9*, e93362. [\[CrossRef\]](#)
148. Ghaleb, A.M.; Yang, V.W. Krüppel-like factor 4 (KLF4): What we currently know. *Gene* **2017**, *611*, 27–37. [\[CrossRef\]](#) [\[PubMed\]](#)
149. Liao, X.; Sharma, N.; Kapadia, F.; Zhou, G.; Lu, Y.; Hong, H.; Paruchuri, K.; Mahabeshwar, G.H.; Dalmas, E.; Venter, N.; et al. Krüppel-like factor 4 regulates macrophage polarization. *J. Clin. Investig.* **2011**, *121*, 2736–2749. [\[CrossRef\]](#)
150. Ban, Y.; Liu, Y.; Li, Y.; Zhang, Y.; Xiao, L.; Gu, Y.; Chen, S.; Zhao, B.; Chen, C.; Wang, N. S-nitrosation impairs KLF4 activity and instigates endothelial dysfunction in pulmonary arterial hypertension. *Redox Biol.* **2019**, *21*, 101099. [\[CrossRef\]](#)

#### 4. Other cell types implicated

Endothelial cells (ECs) are the third cell type implicated in atherosclerosis development. They form the intima, a single layer of cells at the interface between the blood stream and the vessel wall. The endothelium plays a role in the maintenance of vascular homeostasis. It is a semipermeable barrier, regulating macromolecules transport between the vascular lumen and vSMCs. Under pathological conditions, the permeability of this layer is modified. Indeed, some molecules, like thrombin or inflammatory mediators, stimulate intercellular junctions opening. Vascular endothelial growth factors (VEGFs) are key modulators of vascular permeability *via* NOS regulation. Indeed, VEGF is able to increase vascular permeability and hemodynamic changes *via* eNOS phosphorylation, thus supporting NO production [39,40].

Lipopolysaccharides (LPS) induce endothelium hyperpermeability by the stimulation of small GTPases like RhoA and ROCK. Therefore, LDLs accumulation is increased in permeable areas exposed to low wall shear stress of the vessels wall, where atherosclerotic lesions are preferentially developed [41].

ECs exposed to high unidirectional laminar shear stress, activate atheroprotective signaling *via* KLF-2 upregulation (**Fig. 5**).

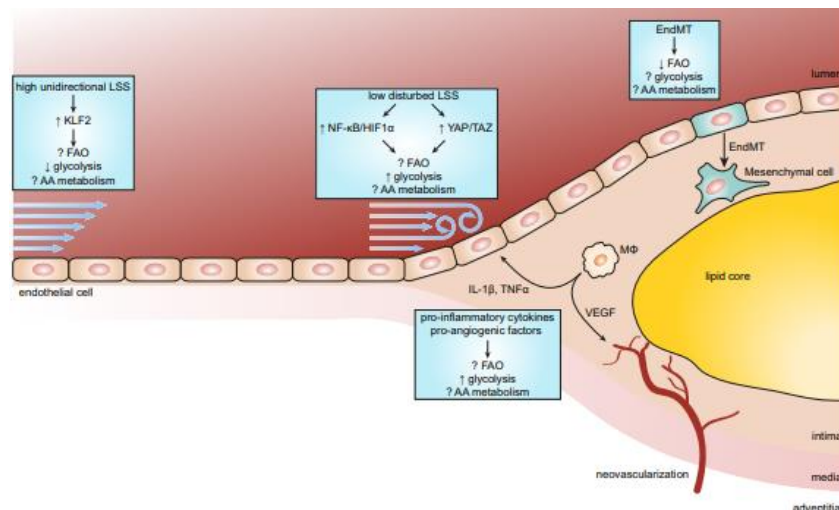


**Figure 5:** Endothelial cells metabolism in atherosclerosis from Theodorou *et al.* [42]

KLF-2 is a transcription factor known to maintain endothelial barrier integrity and EC in a quiescent state, reducing glycolysis and resulting in an anti-inflammatory and anti-thrombotic phenotype. Indeed, during atherosclerosis development, EC are exposed to a pro-inflammatory environment (IL-1 $\beta$ , TNF- $\alpha$ ) and low disturbed laminar shear stress, which enhances glycolysis through NF- $\kappa$ B/HIF1 $\alpha$  pathway, Yes-associated protein (YAP) and transcriptional coactivator



with PDZ-binding motif (TAZ). In advanced lesions, macrophages secrete pro-angiogenic factors, like VEGFs, inducing the neovascularization of atheroma plaques to support proliferation and migration. Moreover, reduced fatty acid oxidation (FAO) [42] can affect plaque stability allowing the transition of EC into mesenchymal cells.

## 5. Atherosclerosis, oxidative stress and glutathione homeostasis

Oxidative stress, characterised by an increase of free oxygen and nitrogen radicals, plays a major role in the atherosclerotic disease with the induction of numerous cellular/molecular modifications. Indeed, oxidative stress is involved in the progression of the disease, being associated with endothelial dysfunction and the promotion of vascular inflammation through the destruction of well-balanced homeostatic mechanisms. Under physiological conditions, reactive oxygen species (ROS) are produced at low concentration mainly by the electron transport chain reactions from mitochondria [43]. They are key regulators of redox-sensitive signaling pathways implicated in the maintenance of cellular homeostasis [44] and modify molecules, enzymes, DNA or transcriptions factors [44,45].

An excess of ROS production leads to an excess of antioxidants consumption resulting in oxidative stress [46]. Several ROS-producing systems such as NADPH oxidase, xanthine oxidase, mitochondrial oxidative or uncoupled eNOS are responsible of superoxide anions, hypochlorite ion,  $\text{H}_2\text{O}_2$ , NO or  $\text{ONOO}^-$  generation, (**Fig. 6**).

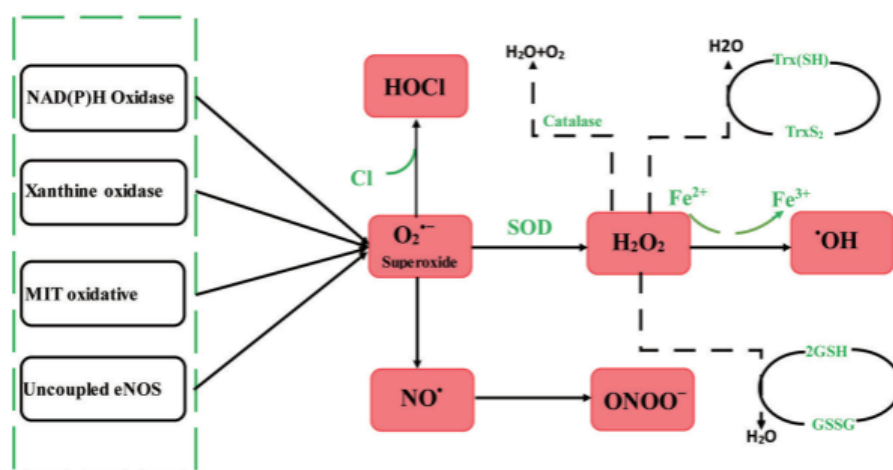


**Figure 6:** Systems producing reactive oxygen species in atherosclerosis [46].

MIT: mitochondrial oxidative; eNOS: endothelial nitric oxide synthase

Glutathione (GSH), a low-molecular weight tripeptide, is considered as the major antioxidant, found in every cells in the body. It is synthesised and degraded by Meister's cycle. Briefly, the

addition of *L*-cystine to glutamate followed by the addition of *L*-glycine. GSH maintain redox homeostasis with its interaction with ROS and reactive nitrogen species. GSH and its oxidised form, GSSG, act collectively with other redox compounds to regulate and maintain cell redox status.

## **Article 2: Glutathione: Antioxidant Properties Dedicated to Nanotechnologies**

### **Glutathion : propriétés antioxydantes dédiées aux nanotechnologies**



Caroline Gaucher, Ariane Boudier, Justine Bonetti, Igor Clarot, Pierre Leroy, Marianne Parent

*Antioxidants* **2018**, 7, 62

Le glutathion (GSH), tripeptide de faible masse molaire composé d'acide glutamique, de cystéine et de glycine est retrouvé dans l'ensemble des organismes vivants (des bactéries aux Mammifères). C'est l'un des antioxydants naturels les plus répandus, ayant un rôle dans la détoxification des cellules et dans le contrôle des espèces réactives de l'oxygène (EROs). En fonction de sa concentration et de son état redox, GSH aura un rôle dans la maintenance et la régulation du statut redox-thiol. Dans cette revue, il est question des capacités antioxydantes et pro-oxydantes du GSH en lien avec des enzymes redox. Différentes enzymes participent à l'homéostasie (synthèse, dégradation et activité antioxydante) du GSH : la gamma-glutamyl transférase (GGT), la glutathion réductase (GR), la glutathion peroxydase (GPx) et enfin la glutathion *S*-transférase (GST). Le but étant de maintenir de faibles concentrations en espèces réactives de l'oxygène et de l'azote ainsi qu'en GSSG (forme oxydée du GSH) et un taux élevé de glutathion réduit (GSH). GSH a un rôle antioxydant, cependant au cours de son catabolisme *via* la (GGT), il peut induire un stress oxydant. Ensuite, cette revue décrit le rôle du GSH dans la signalisation redox *via* deux mécanismes : la modification du potentiel redox intracellulaire activant des facteurs de transcription dont dépendent des gènes codant pour des enzymes antioxydantes et la glutathionylation des protéines correspondant à la formation du pont disulfure entre la fonction thiol réduit d'une protéine et celle du GSH. Enfin, différentes méthodes analytiques de dosage du GSH et des protéines glutathionylées sont décrites. Finalement, l'intérêt de GSH en tant qu'outil thérapeutique (cancer, athérosclérose, diabète...) ou stratégie de ciblage pour les systèmes d'administration des médicaments est abordé.

Review

# Glutathione: Antioxidant Properties Dedicated to Nanotechnologies

Caroline Gaucher <sup>\*</sup>, Ariane Boudier, Justine Bonetti, Igor Clarot, Pierre Leroy and Marianne Parent 

Université de Lorraine, CITHEFOR, F-54000 Nancy, France; ariane.boudier@univ-lorraine.fr (A.B.); justine.bonetti@univ-lorraine.fr (J.B.); igor.clarot@univ-lorraine.fr (I.C.); pierre.leroy@univ-lorraine.fr (P.L.); marianne.parent@univ-lorraine.fr (M.P.)

<sup>\*</sup> Correspondence: caroline.gaucher@univ-lorraine.fr; Tel.: +33-3-7274-7349

Received: 28 March 2018; Accepted: 25 April 2018; Published: 27 April 2018



**Abstract:** Which scientist has never heard of glutathione (GSH)? This well-known low-molecular-weight tripeptide is perhaps the most famous natural antioxidant. However, the interest in GSH should not be restricted to its redox properties. This multidisciplinary review aims to bring out some lesser-known aspects of GSH, for example, as an emerging tool in nanotechnologies to achieve targeted drug delivery. After recalling the biochemistry of GSH, including its metabolism pathways and redox properties, its involvement in cellular redox homeostasis and signaling is described. Analytical methods for the dosage and localization of GSH or glutathiolated proteins are also covered. Finally, the various therapeutic strategies to replenish GSH stocks are discussed, in parallel with its use as an addressing molecule in drug delivery.

**Keywords:** glutathione; antioxidant; redox signaling; nanotechnologies; repletion; targeted drug delivery

## 1. Introduction: Biochemical Implication of Glutathione in Redox Homeostasis

Reduced glutathione (GSH; Figure 1) is the main low-molecular-weight thiol-containing peptide present in most living cells from bacteria to mammals (except some bacteria and amoebae) [1]. Since its discovery 130 years ago in baker's yeast (*Saccharomyces cerevisiae*) by J. de Rey Pailhade, who named it “philothion”, many works have tried to establish and have elucidated its pivotal role in aerobic life. Its structure and redox role were established by Sir Frederick Gowland Hopkins in 1922 [2]. Glutathione was first claimed to be a dipeptide, and then a tripeptide, that is,  $\gamma$ -L-glutamyl-L-cysteinylglycine [3].

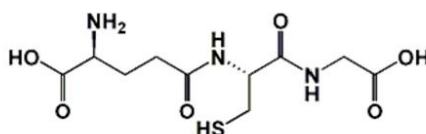


**Figure 1.** Condensed structural chemical formula of glutathione (IUPAC name: (2S)-2-amino-4-[[[(1R)-1-[(carboxymethyl)carbamoyl]-2-sulfanylethyl] carbamoyl]butanoic acid).

In the 1970s, the cellular glutathione cycle, involving two ATP-dependent enzymatically catalyzed steps for its synthesis, was established by Meister (Figure 2) [4,5]. The first enzyme, the  $\gamma$ -glutamylcysteinyl ligase (EC 6.3.2.3; GCL), is a heterodimeric rate-limiting enzyme. In animals

and humans, the transcription of the GCL gene is regulated by nuclear factor erythroid-derived 2-like 2 (NFE2L2), which is sensitive to oxidative stress. Indeed, NFE2L2 activates the transcription of genes under the control of the antioxidant responsive element in various cell types [6]. The second enzyme, the glutathione synthase (EC 6.3.2.2; GS), catalyzes the formation of the covalent bond between the glycine residue and the  $\gamma$ -glutamyl-cysteine dipeptide. The rate of GSH synthesis is controlled by the cell content of L-cysteine [5] and ATP, and the ratio between the two subunits of the GCL [7], as well as its feedback inhibition by GSH [8] and oxidative stimulation of GCL enzymatic activity [9]. Although all cell types synthesize GSH, the main GSH source in the body remains the liver [10,11].

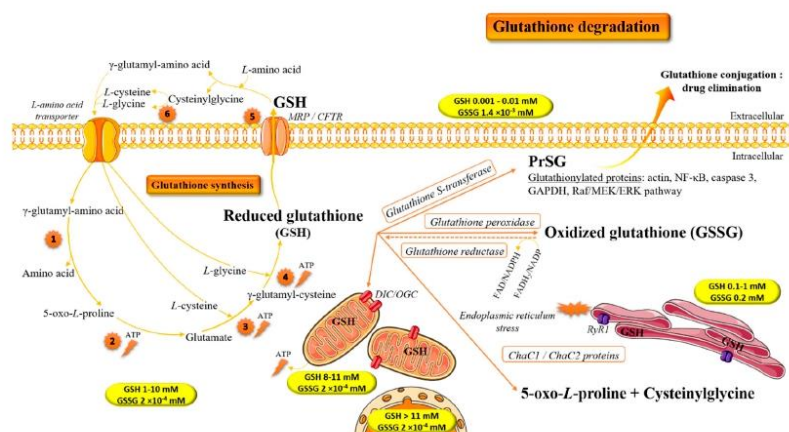


**Figure 2.** The homeostasis of reduced (GSH) and oxidized/disulfide (GSSG) glutathione within cells [12–17].

The synthesis of GSH is controlled by enzymes of Meister's cycle: 1.  $\gamma$ -Glutamyl cyclotransferase. 2. 5-Oxoprolinase. 3.  $\gamma$ -Glutamyl-cysteine ligase. 4. GS; 5.  $\gamma$ -Glutamyl transferase. 6. Dipeptidase. These last two enzymes contribute to extracellular GSH catabolism, whereas glutathione-specific  $\gamma$ -glutamylcyclotransferases, the ChaC1 and ChaC2 proteins (EC 4.3.2.7) handle its intracellular catabolism. After synthesis, GSH is distributed between intracellular organelles by transporters such as the dicarboxylate carrier (DIC) and the oxoglutarate carrier (OGC) on the mitochondria and the ryanodine receptor type 1 (RyR1) on the endoplasmic reticulum. The multidrug resistance-associated proteins (MRPs) and the cystic fibrosis transmembrane conductance regulator (CFTR) are in charge of GSH cell efflux.

The  $\gamma$ -bond between the two amino acids, glutamic acid and cysteine, provides peculiar characteristics, such as insusceptibility to proteolysis. Moreover, the thiol-containing cysteine residue confers redox catalytic properties. Glutathione indeed resists hydrolysis of most of the proteases and peptidases, except  $\gamma$ -glutamyltransferase (EC 2.3.2.2; GGT) and the enzymes from the ChaC family. GGT, an exofacial plasmic membrane, is able to transfer the  $\gamma$ -glutamyl residue of glutathione to an acceptor (e.g., peptides) and release the dipeptide cysteinylglycine. It is the only known enzyme able to catabolize both GSH and GSH adducts (e.g., oxidized glutathione, glutathione S-conjugates and glutathione complexes) [18,19]. The glutathione catabolism is controlled by GGT, and the released cysteinylglycine is next degraded by a dipeptidase; then resulting free amino acids enter the cell to permit the de novo GSH synthesis. GGT is a glycosylated glycoprotein that shows multiple sites of N-glycosylation depending on the species and localization of the enzyme. For example, seven N-glycosylation sites have been identified in human GGT [20]. Furthermore, GGT is redox-regulated at the transcriptional and translational levels as well as in its enzymatic



activity [20,21]. Other cytosolic enzymes from the ChaC family have recently been reported to catalyze the cleavage of glutathione. The ChaC enzymes, ChaC1 and ChaC2, are cytosolic glutathione-specific  $\gamma$ -glutamylcyclotransferases, cleaving the amide bond via transamidation using the  $\alpha$ -amine of the L-glutamyl residue, releasing it as cyclic 5-oxo-L-proline and cysteinylglycine dipeptide. The ChaC1 and ChaC2 enzymes show around 50% of sequence homology and specifically degrade glutathione but no other  $\gamma$ -glutamyl peptides or oxidized glutathione [22,23]. The ChaC2 proteins are characterized by a lower catalytic efficiency than ChaC1 and are constitutively expressed [23]. ChaC1 is a proapoptotic enzyme under the regulation of CHOP (C/EBP homologue protein) transcription factor during the unfolding protein response of endoplasmic reticulum stress [24].

Therefore, the intracellular and extracellular GSH concentrations are determined by the balance between its synthesis and catabolism, as well as by its transport between the cytosol and the different organelles or the extracellular space. The mechanisms of GSH transport into the mitochondria and the endoplasmic reticulum have not been established. However, the DIC and the OGC seem to contribute to the transport of GSH across the mitochondrial inner membrane [25], and RyR1 participates in the accumulation of GSH in the endoplasmic reticulum [26,27]. Although some of the GSH synthesized within cells is delivered to intracellular compartments, much of it is exported across the plasma membrane into the extracellular spaces, especially under oxidative stress [28]. Plasma membrane proteins such as MRPs and the CFTR are implicated in the GSH export from cells essentially under oxidative stress [29,30]. The ability to export both GSH and oxidized derivatives of GSH endows these transporters with the capacity to directly regulate the cellular thiol-redox status and therefore the ability to influence many key signaling and biochemical pathways.

The physiological functions of glutathione range from (i) the maintenance of cysteine under a reduced state within proteins; (ii) the formation of a cysteine pool; (iii) the metabolism of oestrogens, leukotrienes, and prostaglandins and the production of deoxyribonucleotides; (v) the maturation of iron-sulfur clusters in proteins; and (vi) the transduction of redox signals to the cell transcription machinery; to (vii) the maintenance of the cell redox potential [31]. Indeed, as a result of its ability to exist in different redox states, GSH is implicated in processes of the maintenance and regulation of the thiol-redox status [32].

## 2. Glutathione and Antioxidant/Pro-Oxidant Properties

Even if the glutathione reducing power was described early on by reacting with the redox probe methylene blue [2], its redox role corresponding to a Nernstian response was clearly established in this century [33]. From a thermodynamic point of view (Gibbs free energy of redox reactions at the equilibrium, excluding enzyme activity in the redox buffering), two molecules of GSH simultaneously exchange two electrons and two protons with its disulfide form (GSSG). Taking into account the high concentration of glutathione in cells (in the millimolar range) and the high proportion of its reduced form (more than 98% in healthy cells), the GSSG/2 GSH redox couple is considered as the main cellular redox buffer. The standard potential value  $E^\circ$  of the couple GSSG/2 GSH is equal to +197 mV, and because of its pH dependence according to the Nernst equation (Equation (1)), its apparent potential  $E^{\circ'}$  at the physiological pH is equal to −240 mV.

$$E^{\circ'} = E^\circ - 0.059 \times pH \times \log \frac{[GSH]^2}{[GSSG]} \quad (1)$$

The redox metabolism of the cells depends also on redox enzymes working under steady-state conditions instead of the equilibrium defining thermodynamic systems. From this point of view, the enzymes' reaction rate and kinetic constants ( $k_{cat}$  and  $K_m$  values), as well as GSH concentration and localization, are fundamental to highlight kinetic competition and to completely understand the GSH metabolism [17,34].

Therefore, the concentration of GSH as well as the  $[GSH]/[GSSG]$  ratio is a marker of oxidative stress and of the cell redox homeostasis. Regarding GSH reducing properties, it plays the role of

an antioxidant as a scavenger of electrophilic and oxidant species either in a direct way or through enzymatic catalysis: (i) it directly quenches reactive hydroxyl free radicals, other oxygen-centered free radicals, and radical centers on DNA as well as on other biomolecules such as methylglyoxal and 4-hydroxynonenal; and (ii) GSH is the co-substrate of glutathione peroxidase (EC 1.11.1.9; GPx), permitting the reduction of peroxides (hydrogen and lipid peroxides) and producing GSSG. In turn, GSSG is reduced to 2 GSH by using NADPH reducing equivalents and glutathione disulfide reductase (EC 1.6.4.2; GR) catalysis. Electrophilic endogenous compounds and xenobiotics (drugs, pollutants and their phase I metabolites) are conjugated with GSH through activation by glutathione-S-transferases (EC 2.5.1.18; GSTs). The resulting conjugates are substrates of GGT, which initiates the mercapturic acid pathway and facilitates toxic elimination.

The overall cellular redox homeostasis is aimed at maintaining harmful reactive oxygen and nitrogen species and GSSG at very low levels and GSH at a high level. However, GSH can play a pro-oxidant role, which occurs to a lesser extent than its antioxidant role. This process has been reported during the GSH catabolism via GGT catalysis (Figure 3) [35,36]. The mechanism relies upon a shift of pKa of the SH group in the cysteine residue between GSH (pKa of 8.7) and its breakdown product cysteinylglycine (pKa of 6.4). Consequently, the proportion of the more reactive thiolate form is higher in cysteinylglycine than in GSH at the physiological pH value: the reduction rate of ferric ions to ferrous ions is higher, and the production of hydroxyl radicals and superoxide anions through Fenton and Haber–Weiss reactions is more abundant. The GSH pro-oxidant effect occurs, at least initially, on the outer side of the plasma membrane inducing lipid peroxidation, which destabilizes the cell membrane structure. Then, pro-oxidant effects, which are not stopped by the antioxidant defense systems [36], are propagated inside the cell through a signaling process. The pro-oxidant action of GGT is linked to the presence of redox active metals in the extracellular space. The reactivity of free redox active metals is strongly prevented in vivo by complexation with ferritin, transferrin or ceruloplasmin, for example. In this regard, the GGT activity can be postulated as able to reduce and to promote the release of iron ions from transferrin [37,38] as well as copper ions from ceruloplasmin [39]. An excess production of reactive oxygen species through GSH catabolism will produce DNA damages [40,41] or trigger the lipid peroxidation, already documented in vitro for linoleic acid [42] and for low-density lipoproteins (LDLs). Indeed, LDLs' oxidation process catalyzed during the reduction of iron ( $\text{Fe}^{3+}$  to  $\text{Fe}^{2+}$ ) is known to play a central role in atherogenesis and vascular damage. Moreover, thiol-containing residues such as cysteine and homocysteine are known to reduce  $\text{Fe}^{3+}$  and promote  $\text{Fe}^{2+}$ -dependent LDL oxidation [43]. The  $\gamma$ -glutamate residue of GSH decreases the interactions between the thiol function of the cysteine residue and iron, precluding  $\text{Fe}^{3+}$  reduction and hence LDL oxidation [44,45]. The catabolism of GSH by GGT removing the  $\gamma$ -glutamate residue from the cysteine residue increases the iron reduction and LDL oxidation remarkably [38].

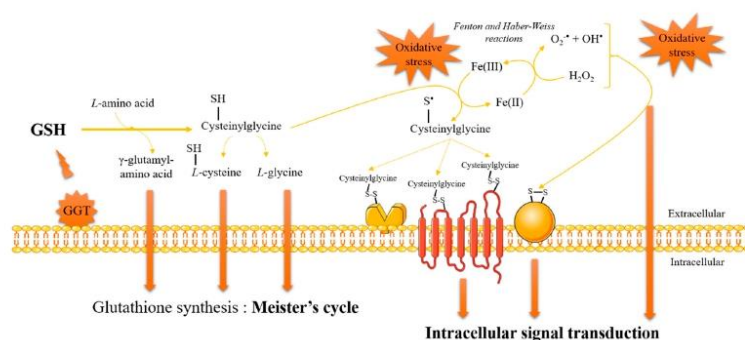


Figure 3. The pro-oxidant activity of  $\gamma$ -glutamyltransferase (GGT) adapted from [35].



### 3. Glutathione and Redox Signaling

Glutathione plays a crucial role in cell signaling via two pathways: (i) the modification of the redox potential toward oxidative values linked to the GSH concentration decrease and/or GSSG increase can activate transcription factors, which provokes gene activation and the synthesis of proteins with antioxidant properties; and (ii) the formation of the disulfide bond between protein thiol groups (PSHs) and GSH generates mixed (protein/non-protein) disulfides, that is, S-glutathiolated proteins (PSSGs).

Three main redox systems, the GSSG/2 GSH couple, the NADP<sup>+</sup>/NADPH couple and the thioredoxin system, regulate the intracellular redox potential [33]. However, as the intracellular concentration of GSH is very high, the ratio of the concentration of GSSG and GSH is fundamental for signal transductions, such as in the cell-cycle regulation [33]. Depending on the conditions, the *in vivo* redox potential of the GSSG/2 GSH couple ranges from −260 to −150 mV [46]. In fact, shifting the GSSG/2 GSH ratio toward the oxidizing state (redox potential of up to −150 mV) reduces cell proliferation and increases apoptosis through the activation of several signaling pathways, including calcineurin, NF-κB, protein kinase B, c-Jun N-terminal kinase, apoptosis signal-regulated kinase 1, and mitogen-activated protein kinase [47]. Furthermore, the cellular redox environment fluctuates during the cell cycle. Indeed, the cellular GSH content is significantly higher in the G2 and M phases compared with G1, while cells in the S-phase show an intermediate redox state [48]. Pharmacologic and genetic manipulations of the cellular redox environment perturb normal cell-cycle progression [49,50].

The process S-glutathiolation, a reversible post-translational modification of proteins, may have a role in the protection of PSHs from irreversible oxidation and in the redox regulation of the protein function, serving for cell signaling [51]. Indeed, if the modified cysteine is critical for the protein function, the S-glutathiolation will also either inactivate the protein or compromise cellular functions. Several S-glutathiolation mechanisms have been proposed: the direct reaction of GSH with partially oxidized reactive PSHs (thiyl radicals or sulfenic acids), thiol–disulfide exchange between PSHs and GSSG or between PSHs and oxidized GSH (sulfenic acid (GSOH)), nucleophilic attack of a protein thiolate on S-nitrosoglutathione (GSNO), and finally, PSHs' S-nitrosation followed by S-glutathiolation by GSH to yield the rate of mixed disulfides' formation. Protein S-glutathiolation can also change the protein activity and have a role in redox signaling. Under normal physiological conditions, the glutathiolation status of some proteins is important for many vital functions such as actin polymerization, transcription factor activation, and apoptosis [51]. Glutaredoxin, whose major isoforms in mammals are Grx1, Grx2, and Grx5, as well as thioredoxin, catalyzes S-glutathiolation and deglutathiolation of proteins to protect SH-groups from oxidation and restore functionally active thiols [52].

### 4. Methodologies for Dosage of Glutathione/Glutathiolated Proteins

As glutathione plays a fundamental role in cellular homeostasis, the changes in the GSH/GSSG ratio and concentrations are especially important in the evaluation and diagnosis of many redox-related pathologies, such as cancers [53], neurodegenerative diseases [54] or stroke [55], and cardiovascular diseases [56]. Glutathione in biological fluids (e.g., plasma) is known to demonstrate great instability, with a half-life of about 20 min [57]. The methodology used for GSH or GSSG quantification is therefore essential to achieve (i) the specificity required to discriminate between the various forms of glutathione and other endogenous thiols present in the biological matrices (cells, tissues, fluids, etc.), as well as (ii) the mandatory selectivity to separate the reduced and oxidized glutathione forms. Another important methodological criterion is sensitivity. For GSH, this parameter is often not critical because of its high concentration in cells (from 1 to 10 mM) and plasma (from 1 to 6 μM [58]). This will often be a problem for GSSG, which is present at low concentrations under physiological conditions, at around 1% of intracellular GSH levels.

At present, there are many methods for evaluating GSH and GSSG in biological samples, from the classical enzyme-colorimetric method developed by Tietze in 1969 [59], to spectrophotometric [60] or spectrofluorimetric [61] methods. The lack of chromophores and

fluorophores in the glutathione family has led to the development of numerous derivatization methods (e.g., *N*-pyrenemalimide or *O*-phthalaldehyde (OPA) [62–66]) or the use of electrochemical methods [67], mass spectrometry [68], chemiluminescence [69], nuclear magnetic resonance [70] or surface-enhanced Raman scattering [71]. Separation methods are also in full extension for this type of application, using chromatographic techniques (ultra-performance liquid chromatography [72], high-performance liquid chromatography [73], and gas chromatography [74]) or electrophoretic techniques [75], such as, for example, the quality control of GSH produced by microorganisms for pharmaceutical use [76].

The different methodologies mentioned above can be very effective but require specific equipment and an important analysis time, as well as peculiar sample processing or treatment. In this context, the use of nanotechnologies (essentially gold and silver metallic nanoparticles (NPs)) appears to be an interesting solution to quantify glutathiolated species. Gold and other metallic species are indeed characterized by an important avidity to bind sulfhydryl compounds [77–79]. In an organism, these atoms, including those under a NP state, form a bond with the thiol function of glutathione, even if the sulfur–metal interfacial chemistry remains controversial in the literature [77,80]. Over the past years, quantification on the basis of NPs has been largely developed to evaluate GSH in intracellular and/or extracellular concentrations in various biological matrices such as plasma, urine or saliva. Many colorimetric methods using gold NPs (AuNPs) (sensor or probes) [81] have been developed on the basis of their high molar absorbance coefficient associated with a specific plasmonic resonance-band shift (the maximum wavelength moves from a dispersed to an aggregated state or vice versa; see, e.g., [82]). The development of such nanosystems is very interesting but can lead to many problems of interference as a result, in particular, of chemical structures close to glutathione in large quantities in the body, such as cysteine or homocysteine [83]. Current methods make it possible to reach nanomolar concentrations, such as capillary electrophoresis coupled laser-induced fluorescence, as described by Shen et al. [84]. To a lesser extent, silver NPs are also used to evaluate glutathione in a biological medium with the same advantages as AuNPs described previously [85,86]. Other, more marginal examples of NPs developed specifically to quantify GSH or GSSG, such as NPs of alumina or zinc, can be found in the literature [87,88].

All the examples mentioned above show that nanotechnology is the future of the determination of many biological molecules, glutathione clearly being a part of it.

## 5. Repletion of Glutathione: Therapeutic Opportunities and Challenges

In cancer therapy, the depletion of glutathione has emerged as a valuable strategy to increase the sensitivity of cancer cells to radiations and toxic drugs, especially for aggressive and/or metastatic cancers [89–91]. However, a great majority of diseases (diabetes [92], cardiovascular diseases [56], HIV/AIDS [93], sepsis [94], cystic fibrosis [95], stroke [55], and brain disorders such as Alzheimer's and Parkinson's diseases or schizophrenia [96–98]), are associated with a decrease in GSH, combined with various oxidative stress states. Similarly, it has been demonstrated that the GSH antioxidant defenses of the body decrease linearly with age (oxidation of the GSSG/2 GSH couple in plasma: +0.7 mV/year after 45 years of age [99]), leaving us vulnerable to many age-related diseases. As a result, therapeutic strategies to restore the GSH pool are needed, ideally through oral administration for such chronic conditions. This is especially challenging because of the physicochemical properties of GSH (low partition coefficient; PubChem's calculated log *P* = −4.5) and its high degradation rate in the gastrointestinal tract through bacterial and epithelial GGT catalysis [100]. Two complementary approaches might increase GSH bioavailability: one is based on chemistry and the other is based on drug delivery technology (Figure 4a).

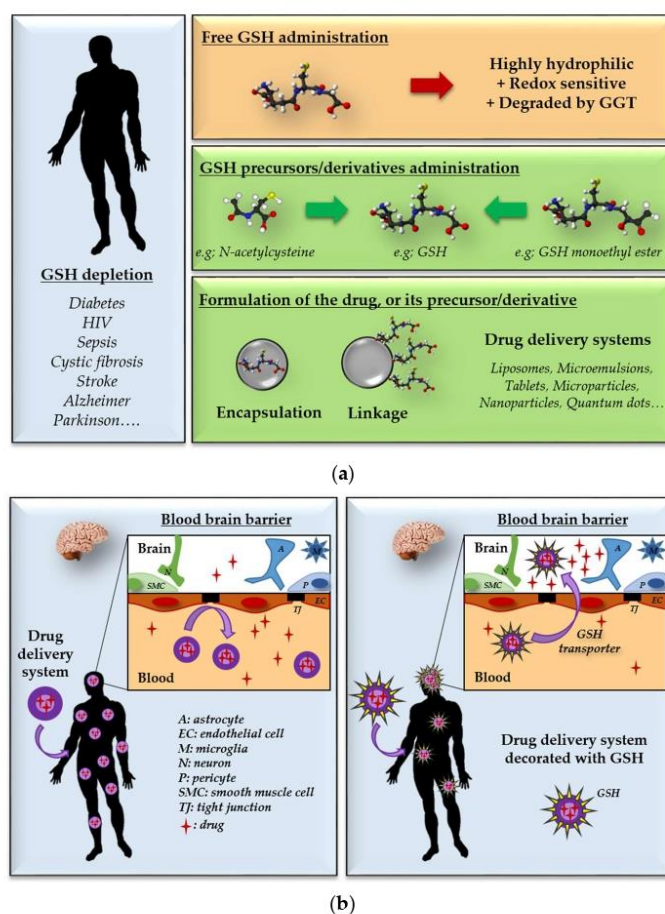


**Figure 4.** Schematic representations of the links between nanotechnologies and glutathione. (a) How nanotechnologies can help to reconstitute the glutathione pool? (b) How GSH can help nanotechnologies to reach their target? The example of Brain delivery.

The administration of prodrugs of GSH (or GSH precursors such as cysteine) is a first option. However, cysteine cannot be administered directly because of its toxicity and instability [101]; therefore precursors of cysteine, for example, the well-known *N*-acetylcysteine (NAC), are used. NAC is a potent antioxidant and an established antidote for acetaminophen overdose (which depletes hepatic GSH). Both parenteral and oral administrations are approved by the Food and Drug Administration for this indication, with different therapeutic schemes: loading dose followed by 17 additional doses over 72 h for oral NAC versus loading dose and 2 additional doses over 21 h for parenteral NAC [102]. Although several human clinical trials have investigated the potential of oral NAC to replenish GSH in chronic depletions (e.g., in HIV patients), all have failed to give sufficient benefits to gain regulatory approval, even at high doses (up to 2 g/day) [103]. These results can be explained by different mechanisms of GSH depletion between acute and chronic conditions and/or by the low NAC bioavailability when given per os (6–10% [104]). To improve tissue



distribution, lipophilic derivatives of NAC were prepared: they gave encouraging results in cells (NAC amide [105]) or after peritoneal (NAC amide [106]) or oral administration in rats (NAC ethyl ester [107]). This strategy was also extended to GSH, creating more lipophilic derivatives through esterification. Glutathione esters (mainly mono- and di-methylesters) have been investigated as potential oral delivery compounds because they present a higher hydrophobicity and less sensitivity toward GGT degradation [108–111], but no conclusive data on their ability to restore the GSH pool in humans are currently reported in the literature. Furthermore, other cysteine or glutathione precursors have been evaluated with varying results: L-methionine; S-adenosylmethionine (SAME) [112]; L-2-oxothiazolidine-4-carboxylate (OTC, procysteine), which is enzymatically converted to cysteine within liver cells [113]; 2-(RS)-n-propylthiazolidine-4(R)-carboxylic-acid (PTCA); D-ribose-L-cysteine; L-cysteine-glutathione mixed disulphide [114]; and  $\gamma$ -glutamylcysteine [115].

The second option for improving the bioavailability of GSH (or its derivatives) is to use a drug delivery system. In the literature, GSH has been encapsulated into various galenic forms for oral administration: liposomes [116], water-in-oil microemulsions [117], pellets of montmorillonite and glutathione [118], polymeric NPs and microparticles prepared with natural or synthetic polymers [119–121], hydrogels [122], and mucoadhesive films for sublingual delivery [123], as well as orobuccal tablets in combination with L-cystine, vitamin C and selenium [124]. Only this latter form has been tested per os in humans, with promising results: the GSH blood level increased significantly with time after administration of this tablet containing 250 mg of GSH to 15 healthy volunteers (both sexes, 20–40 years old) [124]. Aside from improving bioavailability, an additional benefit of formulations is to increase patient compliance while hiding the undesirable organoleptic (odor and flavor) properties of the thiol drugs.

The GSH can also be chemically linked to the carrier surface (instead of being passively encapsulated into the carrier). The main problem encountered with GSH conjugation on molecules remains the preservation of the thiol function, that is, to avoid formation of a disulfide. Many works use GSH as a stabilizer for metallic (mainly gold or silver) NPs [125–127] or nanoclusters [128] by the interaction between sulfur and metallic atoms, as previously explained. However, this prevents their use for the peptide repletion event if these particles seem to be well-tolerated by cells and the organism [129]. Only few works have reported the synthesis of GSH conjugates with a preservation of its antioxidant property. Two main strategies were led, grafting GSH either to polymers used as raw material for NP preparation, or to preformed NPs. First, GSH was covalently linked to chitosan [130] and polyethylene glycol [131]. Yields of grafting were 99% for polyethylene glycol–GSH oligomers [131] and 111  $\mu\text{mol}$  GSH/g of functionalized chitosan [130]. In an in vitro model of oxidative stress (human brain neuroblastoma cells' SH-SY5Y cell line; exposed to  $\text{H}_2\text{O}_2$  for 24 h), cells pre-treated by oligomers (polyethylene glycol conjugated to GSH) were protected from oxidative damage [131]. Second, GSH was anchored to core shell (CdSe/ZnS) quantum dots (up to 40 GSH moieties per quantum dot [132]). These quantum dots were tested in an in vivo model using *Hydra vulgaris* [132]. The authors showed the localization of GSH binding proteins inside the animals after internalization, as a result of the fluorescent properties of the quantum dots. GSH was also conjugated to gold NPs (AuNPs) via a linker (lipoic acid), which was previously shown to passivate the NP surface [133,134], and which limited the access of the thiol function to the gold core [135]. In this work, the authors report the possible oligomerization of GSH during the process, which could explain the high grafting density (ca. 7500 GSH moieties per AuNP) on AuNPs. The preservation of GSH properties was demonstrated using classical redox tests. Compared to non-conjugated GSH AuNPs, an activity enhanced by factors of 10,000 and 36,000 was reported for AuNPs functionalized by GSH using 2,2'-azino-bis(3-ethylbenzothiazoline-6-sulphonic) acid (ABTS) and ferric reducing antioxidant power (FRAP), respectively [135].

To conclude, very few of these works have moved from research into clinic applications (apart from precursors/prodrugs of GSH such as NAC, and one GSH-containing orobuccal tablet), especially for

oral GSH supplementation. The collaboration between the chemical and galenic approaches seems nevertheless to offer promising opportunities in the future.

## 6. GSH Decoration as a Tool for Targeted Drug Delivery Systems

Glutathione is now also being investigated as a molecular tool in the hand of chemists and pharmacists to specifically deliver drugs to the brain (Figure 4b) or to obtain controlled drug release in the intracellular compartment. These two aspects are discussed in this section.

### 6.1. Brain-Targeted Drug Delivery

Drug delivery to the central nervous system represents one of the major pharmaceutical challenges, as the passage of macromolecules as well as 98% of small molecules is prevented by the blood–brain barrier under physiological conditions [136]. However, brain drug delivery can be achieved by taking advantage of the numerous endogenous specialized transport systems of this biological barrier. In the last years, GSH has emerged as a potential candidate to facilitate the receptor-mediated transcytosis of nanocarriers. The sodium-dependent (active) glutathione transporter is indeed present in all mammalian species, with a preferential expression in the central nervous system and the blood–brain barrier [137–139]. The conjugation of GSH on several pharmaceutical forms safely enhanced the delivery of various encapsulated drugs and nucleic acids to the brain. The story of G-technology, a liposomal system with a polyethylene glycol (PEG) coating modified with GSH, is developed as an example of the successful transfer from the pre-clinic to the clinic. Rip et al. evaluated the uptake of GSH-coated–PEGylated liposomes encapsulating carboxyfluorescein (an autoquenched fluorescent tracer) by brain endothelial cells, as well as their pharmacokinetic behavior and brain distribution after intraperitoneal or intravenous administration to rats [140]. The results demonstrated a temperature-dependent uptake of liposomes by the endothelial cells (about 2 times higher for GSH–PEG liposomes compared to uncoated liposomes). In rats, both administration routes gave comparable circulating levels and tissue distribution, and the brain levels of the fluorescent tracer were increased 4-fold by the GSH coating. This technology was used to deliver amyloid-targeting antibody fragments to the brain in a mouse model of Alzheimer’s disease after intravenous bolus [141]. The liposomes were prepared by the ethanol injection method, with cholesterol, mPEG-2000-1,2-distearoyl-sn-glycero-3-phosphoethanolamine, and different lipids: the brain accumulation was higher for egg-yolk phosphatidylcholine liposomes than 1,2-dimyristoyl-sn-glycero-3-phosphocholine liposomes. Maussang et al. studied the mechanisms of increased in vivo brain delivery of the model drug ribavirin when encapsulated into PEGylated liposomes conjugated with GSH, intravenously administered to rats [142]. They demonstrated that this brain-specific uptake was positively correlated with increasing amounts of GSH coating and involved a receptor-mediated mechanism. These GSH–PEG liposomes (G-technology) have also demonstrated brain targeting as well as therapeutic efficacy in murine models of brain cancer (2B3-101; drug: doxorubicin [143,144]) and neuroinflammation (2B3-201; drug: methylprednisolone [145]). As an example, the major results obtained with 2B3-101 in cells and animals are presented in Figure 5. The 2B3-201 product has recently completed a phase I trial in healthy volunteers [146], while the 2B3-101 product has completed a phase I/IIa trial in patients with various forms of brain cancer (ClinicalTrials.gov Identifier: NCT01386580 [147,148]) and is currently being tested in a phase II trial in patients with breast cancer and leptomeningeal metastases (ClinicalTrials.gov Identifier: NCT01818713).

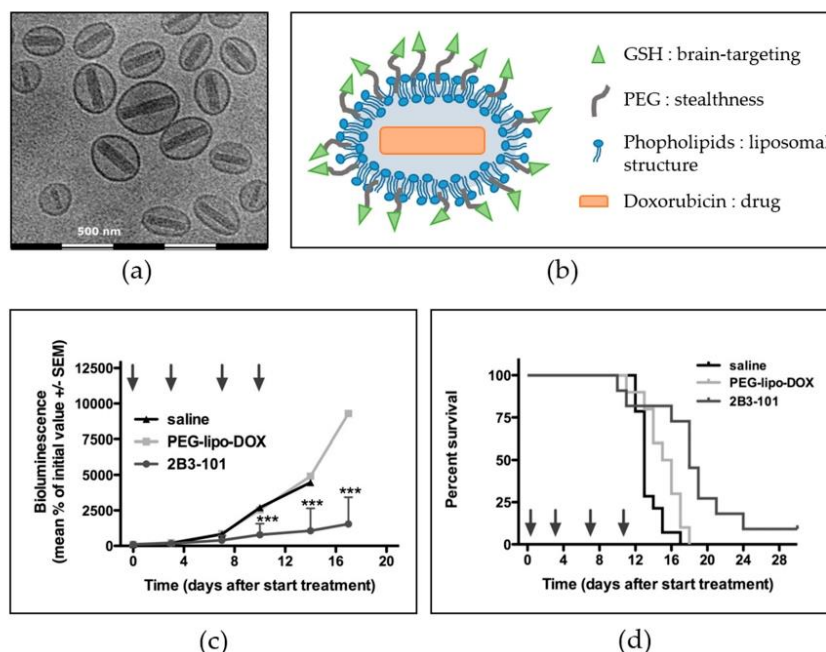


**Figure 5.** Brain targeting with reduced glutathione (GSH) decoration: example of the 2B3-101 product (GSH-coated–polyethylene glycol (PEG)ylated liposome containing doxorubicin). (a) Cryo-electron microscopy image of 2B3-101; (b) schematic representation of the liposomal structure; (c) inhibition of brain tumor growth in mice with experimental brain tumors; (d) increased survival of mice with experimental brain tumors. Animals received twice-weekly IV administrations (arrows on the graph) of saline ( $n = 14$ ), 2B3-101 ( $n = 10$ ) or PEGylated liposomal doxorubicin (PEG-lipo-DOX;  $n = 10$ ), all at 5 mg/kg doxorubicin equivalents. \*\*\*  $p < 0.001$ , 2B3-101 vs saline and PEG-lipo-DOX; (a,c,d) are reproduced with permission from [144].

GSH-coating is also under investigation to obtain the brain delivery of drugs encapsulated into NPs. Veszelka et al. have, for example, demonstrated on cells that GSH coating leads to a higher cell uptake of polystyrene NPs than biotin coating [149]. GSH-coated poly(lactic-co-glycolic acid) (PLGA)–PEG NPs containing docetaxel [150], doxorubicin [151] or paclitaxel [152] have also been developed and characterized for drug release, cytotoxicity and blood–brain barrier permeation. In animals, bovine serum albumin (BSA) NPs with a GSH ligand led to 10-fold higher brain concentrations of a neuroprotective agent than the drug solution, 5 h after intravenous injection [153]. In another study, a hydrophilic model drug was 3 times more concentrated in the brain after intravenous injection of GSH-coated BSA NPs, compared to the same uncoated NPs [154]. Finally, in a middle cerebral artery occlusion model of stroke, GSH-coated PLGA–PEG NPs containing the thyroid T3 hormone showed better therapeutic efficacy than T3 solution or uncoated NPs, on both tissue infarction (reduction of 58%, 34%, and 51%, respectively) and brain edema (reduction of 75%, 59% and 68%, respectively) [155]. Although these GSH-coated NPs are not already in use in clinical trials, they highlight that GSH-mediated brain targeting can be used with different galenic forms, for various drugs. Recently, this strategy has also been proved to be successful in vitro for gene delivery to brain endothelial cells [156], thus opening another wide field of applications.



## 6.2. Intracellular-Targeted Drug Delivery

Because of the difference in GSH concentrations between plasma and cytosol (0.001 mM vs. 1 to 10 mM), the intracellular compartment is a more reductive environment than plasma. As a result, the difference in redox potential has been exploited by researchers to create stimuli-sensitive NPs. Using this strategy, a drug is not only protected in the blood flow but is also released specifically in this reductive environment, thus achieving intracellular targeting. Other external stimuli have been described on the basis of physical (light and electromagnetic field), chemical (pH and temperature) or even biochemical (enzyme) signals. To go further, there is growing research to develop sequential or simultaneous multi-stimuli responsive delivery systems. Interesting reviews on this topic can be found in the literature (e.g., [157–159]). As far as the redox stimulus is concerned, two main strategies are usually described, based either on the reduction of disulfide bounds structuring the NPs or on ligand exchange at the surface of inorganic NPs. An extensive literature deals with the design of new bio-reducible polymers (such as poly(ethylenimine), poly(amido amine) or polymers based on peptide or nucleic acid derivatives) [159,160]. In these works, the authors use the reduction of disulfide bounds (introduced into the polymer structure) by intracellular GSH to trigger the drug release through NP disorganization or disassembly. Another approach focuses on di-selenide or carbon–selenide bonds, which are more sensitive to the GSH concentration than disulfide bonds [161]. Chemical and pre-clinical proofs of concept have been brought forward for applications in gene silencing and imaging [162], as well as in the delivery of genes [160], proteins and anti-proliferative drugs [159,162]. None of these objects has nevertheless reached the clinical level so far.

Apart from disulfide reduction by GSH, another strategy using ligand exchange at the surface of AuNPs has been described (Figure 6). As previously explained, there is a strong avidity of AuNPs towards the thiol function of GSH. After internalization of AuNPs into the cellular cytoplasm, the drug grafted on the surface of the gold core is progressively released and replaced by GSH through thiol–gold binding. This was used to deliver the drug (e.g., paclitaxel) or for cell imaging [162,163]. However, intracellular GSH may be depleted, which could lead to oxidative stress in addition to other redox side-effects that may be induced by AuNPs [164].

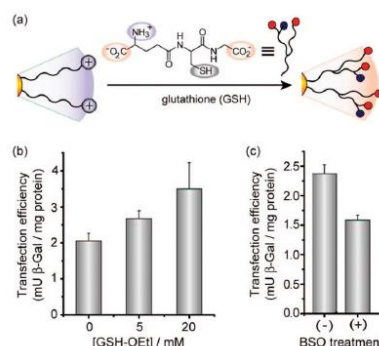


**Figure 6.** Example of ligand exchange strategy involving reduced glutathione (GSH) for targeted intracellular gene delivery. (a) Scheme of the ligand exchange reaction between native cationic ligands and cellular glutathione on gold nanoparticles' surface. (b) Elevation in transfection level depending on dose of glutathione monoester (GSH–Oet). Monkey kidney cells were preincubated with GSH–Oet for 1 h then washed prior to transfection, to transiently increase the GSH level. (c) Decrease in transfection efficiency upon L-buthionine-[S,R]-sulfoximine (BSO) treatment. Cells were plated in BSO-containing (2 mM) media and incubated for 24 h. BSO is an inhibitor of  $\gamma$ -glutamylcysteine synthetase and thus suppresses baseline GSH production. Reprinted with permission from [163]. Copyright (2008) American Chemical Society.



## 7. Conclusions

Since its discovery, GSH has been shown to play ubiquitous roles in most living cells, from prokaryotic to eukaryotic organisms. GSH was defined as the intracellular redox buffer, and its major function, either free or associated to proteins, is tightly connected to redox reactions, mainly acting as a reductant versus oxygen and its derived reactive species. From physico-chemical and biochemical points of view, GSH redox properties are well defined and act in cell signaling through post-translational modifications. Disturbance of redox homeostasis related to the depletion of GSH has been shown more and more to be implicated in many pathophysiological states, opening a means for its use as a drug. Glutathione has clearly penetrated fields other than biology, such as therapeutics, with associated nanotechnology approaches for improving its bioavailability and targeting ability. Indeed, growing research considers GSH not only as a drug, but also as a tool for stimuli responsive in drug delivery systems.

**Acknowledgments:** The authors acknowledge support of EA 3452 CITHEFOR by the “Impact Biomolecules” project of the “Lorraine Université d’Excellence” (Investissements d’avenir—ANR).

**Conflicts of Interest:** The authors declare no conflict of interest.

## Abbreviations

ABTS	2,2'-Azino-bis(3-éthylbenzothiazoline-6-sulphonic) acid
AuNP	Gold nanoparticle
BSA	Bovine serum albumin
BSO	L-Buthionine-[S,R]-sulfoximine
CFTR	Cystic fibrosis transmembrane conductance regulator
DIC	Dicarboxylate carrier
FRAP	Ferric reducing antioxidant power
GCL	$\gamma$ -Glutamylcysteinyl ligase
GGT	$\gamma$ -Glutamyltransferase
GPx	Glutathione peroxidase
GR	Glutathione disulfide reductase
GS	Glutathione synthase
GSH	Reduced glutathione
GSH-Oet	Glutathione monoester
GSNO	S-Nitrosoglutathione
GSOH	Glutathione sulfenic acid
GSSG	Disulfide glutathione
GSTs	Glutathione-S-transferases
LDL	Low-density lipoprotein
MRP	Multidrug resistance-associated protein
NAC	N-Acetylcysteine
NFE2L2	Nuclear factor erythroid-derived 2-like 2
NP	Nanoparticle
OGC	Oxoglutarate carrier
OPA	O-Phthalaldehyde
OTC	L-2-Oxothiazolidine-4-carboxylate
PEG	Poly(ethylene)glycol
PLGA	Poly(lactic-co-glycolic acid)
PSHs	Protein thiol groups
PSSGs	S-Glutathiolated proteins
PTCA	2-(RS)-n-Propylthiazolidine-4(R)-carboxylic-acid
RyR1	Ryanodine receptor type 1
SAMe	S-Adenosylmethionine

## References

- Hamilton, C.J.; Arbach, M.; Groom, M. Beyond Glutathione: Different Low Molecular Weight Thiols as Mediators of Redox Regulation and Other Metabolic Functions in Lower Organisms. In *Recent Advances in Redox Active Plant and Microbial Products*; Jacob, C., Kirsch, G., Slusarenko, A., Winyard, P., Burkholz, T., Eds.; Springer: Dordrecht, The Netherlands, 2014; ISBN 978-94-017-8925-3.
- Gowland Hopkins, F.; Dixon, M. On glutathione. II. A thermostable oxidation-reduction system. *J. Biol. Chem.* **1922**, *54*, 527–563.
- Hunter, G.; Eagles, B.A. Glutathione: A critical study. *J. Biol. Chem.* **1927**, *72*, 147–166.
- Meister, A.; Tate, S.S. Glutathione and related gamma-glutamyl compounds: Biosynthesis and utilization. *Annu. Rev. Biochem.* **1976**, *45*, 559–604. [[CrossRef](#)] [[PubMed](#)]
- Meister, A.; Anderson, M.E. Glutathione. *Annu. Rev. Biochem.* **1983**, *52*, 711–760. [[CrossRef](#)] [[PubMed](#)]
- Baldelli, S.; Aquilano, K.; Ciriolo, M.R. Punctum on two different transcription factors regulated by PGC-1 $\alpha$ : Nuclear factor erythroid-derived 2-like 2 and nuclear respiratory factor 2. *Biochim. Biophys. Acta* **2013**, *1830*, 4137–4146. [[CrossRef](#)] [[PubMed](#)]
- Chen, Y.; Shertzer, H.G.; Schneider, S.N.; Nebert, D.W.; Dalton, T.P. Glutamate cysteine ligase catalysis: Dependence on ATP and modifier subunit for regulation of tissue glutathione levels. *J. Biol. Chem.* **2005**, *280*, 33766–33774. [[CrossRef](#)] [[PubMed](#)]
- Taylor, C.G.; Nagy, L.E.; Bray, T.M. Nutritional and hormonal regulation of glutathione homeostasis. *Curr. Top. Cell. Regul.* **1996**, *34*, 189–208. [[PubMed](#)]
- Krejsa, C.M.; Franklin, C.C.; White, C.C.; Ledbetter, J.A.; Schieven, G.L.; Kavanagh, T.J. Rapid Activation of Glutamate Cysteine Ligase following Oxidative Stress. *J. Biol. Chem.* **2010**, *285*, 16116–16124. [[CrossRef](#)] [[PubMed](#)]
- Lauterburg, B.H.; Adams, J.D.; Mitchell, J.R. Hepatic glutathione homeostasis in the rat: Efflux accounts for glutathione turnover. *Hepatology* **1984**, *4*, 586–590. [[CrossRef](#)] [[PubMed](#)]
- DeLeve, L.D.; Kaplowitz, N. Glutathione metabolism and its role in hepatotoxicity. *Pharmacol. Ther.* **1991**, *52*, 287–305. [[CrossRef](#)]
- Cooper, A.J.; Pinto, J.T.; Callery, P.S. Reversible and irreversible protein glutathionylation: Biological and Clinical aspects. *Expert Opin. Drug Metab. Toxicol.* **2011**, *7*, 891–910. [[CrossRef](#)] [[PubMed](#)]
- Pineda-Molina, E.; Klatt, P.; Vázquez, J.; Marina, A.; García de Lacoba, M.; Pérez-Sala, D.; Lamas, S. Glutathionylation of the p50 subunit of NF-kappaB: A mechanism for redox-induced inhibition of DNA binding. *Biochemistry* **2001**, *40*, 14134–14142. [[CrossRef](#)] [[PubMed](#)]
- Huang, Z.; Pinto, J.T.; Deng, H.; Richie, J.P. Inhibition of caspase-3 activity and activation by protein glutathionylation. *Biochem. Pharmacol.* **2008**, *75*, 2234–2244. [[CrossRef](#)] [[PubMed](#)]
- Pastore, A.; Piemonte, F. Protein glutathionylation in cardiovascular diseases. *Int. J. Mol. Sci.* **2013**, *14*, 20845–20876. [[CrossRef](#)] [[PubMed](#)]
- Circu, M.L.; Aw, T.Y. Glutathione and modulation of cell apoptosis. *Biochim. Biophys. Acta* **2012**, *1823*, 1767–1777. [[CrossRef](#)] [[PubMed](#)]
- Deponte, M. The Incomplete Glutathione Puzzle: Just Guessing at Numbers and Figures? *Antioxid. Redox Signal.* **2017**, *27*, 1130–1161. [[CrossRef](#)] [[PubMed](#)]
- Taniguchi, N.; Ikeda, Y. Gamma-glutamyl transpeptidase: Catalytic mechanism and gene expression. *Adv. Enzymol. Relat. Areas Mol. Biol.* **1998**, *72*, 239–278. [[PubMed](#)]
- Ohkama-Ohtsu, N.; Radwan, S.; Peterson, A.; Zhao, P.; Badr, A.F.; Xiang, C.; Oliver, D.J. Characterization of the extracellular gamma-glutamyl transpeptidases, GGT1 and GGT2, in Arabidopsis. *Plant J.* **2007**, *49*, 865–877. [[CrossRef](#)] [[PubMed](#)]
- Hanigan, M.H. Gamma-glutamyl transpeptidase: Redox regulation and drug resistance. *Adv. Cancer Res.* **2014**, *122*, 103–141. [[CrossRef](#)] [[PubMed](#)]
- Zhang, H.; Forman, H.J. Redox regulation of gamma-glutamyl transpeptidase. *Am. J. Respir. Cell Mol. Biol.* **2009**, *41*, 509–515. [[CrossRef](#)] [[PubMed](#)]
- Kumar, A.; Tikoo, S.; Maity, S.; Sengupta, S.; Sengupta, S.; Kaur, A.; Bachhawat, A.K. Mammalian proapoptotic factor ChaCl and its homologues function as  $\gamma$ -glutamyl cyclotransferases acting specifically on glutathione. *EMBO Rep.* **2012**, *13*, 1095–1101. [[CrossRef](#)] [[PubMed](#)]

23. Kaur, A.; Gautam, R.; Srivastava, R.; Chandel, A.; Kumar, A.; Karthikeyan, S.; Bachhawat, A.K. ChaC2, an Enzyme for Slow Turnover of Cytosolic Glutathione. *J. Biol. Chem.* **2017**, *292*, 638–651. [[CrossRef](#)] [[PubMed](#)]
24. Mungrue, I.N.; Pagnon, J.; Kohannim, O.; Gargalovic, P.S.; Lusis, A.J. CHAC1/MGC4504 is a novel proapoptotic component of the unfolded protein response, downstream of the ATF4-ATF3-CHOP cascade. *J. Immunol.* **2009**, *182*, 466–476. [[CrossRef](#)] [[PubMed](#)]
25. Lash, L.H. Mitochondrial glutathione transport: Physiological, pathological and toxicological implications. *Chem. Biol. Interact.* **2006**, *163*, 54–67. [[CrossRef](#)] [[PubMed](#)]
26. Bánhegyi, G.; Csala, M.; Nagy, G.; Sorrentino, V.; Fulceri, R.; Benedetti, A. Evidence for the transport of glutathione through ryanodine receptor channel type 1. *Biochem. J.* **2003**, *376*, 807–812. [[CrossRef](#)] [[PubMed](#)]
27. Csala, M.; Fulceri, R.; Mandl, J.; Benedetti, A.; Bánhegyi, G. Ryanodine receptor channel-dependent glutathione transport in the sarcoplasmic reticulum of skeletal muscle. *Biochem. Biophys. Res. Commun.* **2001**, *287*, 696–700. [[CrossRef](#)] [[PubMed](#)]
28. Belcastro, E.; Wu, W.; Fries-Raeth, I.; Corti, A.; Pompella, A.; Leroy, P.; Lartaud, I.; Gaucher, C. Oxidative stress enhances and modulates protein S-nitrosation in smooth muscle cells exposed to S-nitrosoglutathione. *Nitric Oxide Biol. Chem.* **2017**, *69*, 10–21. [[CrossRef](#)] [[PubMed](#)]
29. Ballatori, N.; Krance, S.M.; Marchan, R.; Hammond, C.L. Plasma membrane glutathione transporters and their roles in cell physiology and pathophysiology. *Mol. Asp. Med.* **2009**, *30*, 13–28. [[CrossRef](#)] [[PubMed](#)]
30. Muanprasat, C.; Wongborisuth, C.; Pathomthongtawechai, N.; Satitsri, S.; Hongeng, S. Protection against oxidative stress in beta thalassemia/hemoglobin E erythrocytes by inhibitors of glutathione efflux transporters. *PLoS ONE* **2013**, *8*, e55685. [[CrossRef](#)] [[PubMed](#)]
31. Dickinson, D.A.; Forman, H.J. Cellular glutathione and thiols metabolism. *Biochem. Pharmacol.* **2002**, *64*, 1019–1026. [[CrossRef](#)]
32. Forman, H.J.; Zhang, H.; Rinna, A. Glutathione: Overview of its protective roles, measurement, and biosynthesis. *Mol. Asp. Med.* **2009**, *30*, 1–12. [[CrossRef](#)] [[PubMed](#)]
33. Schafer, F.Q.; Buettner, G.R. Redox environment of the cell as viewed through the redox state of the glutathione disulfide / glutathione couple. *Free Radic. Biol. Med.* **2001**, *30*, 1191–1212. [[CrossRef](#)]
34. Nagy, P. Kinetics and mechanisms of thiol-disulfide exchange covering direct substitution and thiol-oxidation pathways. *Antioxid. Redox Signal.* **2013**, *18*, 1623–1641. [[CrossRef](#)] [[PubMed](#)]
35. Paolicchi, A.; Dominici, S.; Pieri, L.; Maellaro, E.; Pompella, A. Glutathione catabolism as a signaling mechanism. *Biochem. Pharmacol.* **2002**, *64*, 1027–1035. [[CrossRef](#)]
36. Dominici, S.; Paolicchi, A.; Corti, A.; Maellaro, E.; Pompella, A. Prooxidant reactions promoted by soluble and cell-bound gamma-glutamyltransferase activity. *Methods Enzymol.* **2005**, *401*, 484–501. [[CrossRef](#)] [[PubMed](#)]
37. Drozd, R.; Parmentier, C.; Hachad, H.; Leroy, P.; Siest, G.; Wellman, M. gamma-Glutamyltransferase dependent generation of reactive oxygen species from a glutathione/transferrin system. *Free Radic. Biol. Med.* **1998**, *25*, 786–792. [[CrossRef](#)]
38. Dominici, S.; Pieri, L.; Comporti, M.; Pompella, A. Possible role of membrane gamma-glutamyltransferase activity in the facilitation of transferrin-dependent and -independent iron uptake by cancer cells. *Cancer Cell Int.* **2003**, *3*, 7. [[CrossRef](#)] [[PubMed](#)]
39. Glass, G.A.; Stark, A.A. Promotion of glutathione-gamma-glutamyl transpeptidase-dependent lipid peroxidation by copper and ceruloplasmin: The requirement for iron and the effects of antioxidants and antioxidant enzymes. *Environ. Mol. Mutagen.* **1997**, *29*, 73–80. [[CrossRef](#)]
40. Schmidt, A.M.; Hori, O.; Brett, J.; Yan, S.D.; Wautier, J.L.; Stern, D. Cellular receptors for advanced glycation end products. Implications for induction of oxidant stress and cellular dysfunction in the pathogenesis of vascular lesions. *Arterioscler. Thromb. J. Vasc. Biol.* **1994**, *14*, 1521–1528. [[CrossRef](#)]
41. Gimbrone, M.A. Vascular endothelium: An integrator of pathophysiologic stimuli in atherosclerosis. *Am. J. Cardiol.* **1995**, *75*, 67B–70B. [[CrossRef](#)]
42. Ross, R. The pathogenesis of atherosclerosis: A perspective for the 1990s. *Nature* **1993**, *362*, 801–809. [[CrossRef](#)] [[PubMed](#)]
43. Bradley, J.R. TNF-mediated inflammatory disease. *J. Pathol.* **2008**, *214*, 149–160. [[CrossRef](#)] [[PubMed](#)]



44. Paolicchi, A.; Minotti, G.; Tonarelli, P.; Tongiani, R.; De Cesare, D.; Mezzetti, A.; Dominici, S.; Comporti, M.; Pompella, A. Gamma-glutamyl transpeptidase-dependent iron reduction and LDL oxidation—A potential mechanism in atherosclerosis. *J. Investig. Med.* **1999**, *47*, 151–160. [[PubMed](#)]
45. Berliner, J.A.; Heinecke, J.W. The role of oxidized lipoproteins in atherogenesis. *Free Radic. Biol. Med.* **1996**, *20*, 707–727. [[CrossRef](#)]
46. Jones, D.P. Redox potential of GSH/GSSG couple: Assay and biological significance. *Methods Enzymol.* **2002**, *348*, 93–112. [[PubMed](#)]
47. Sen, C.K. Cellular thiols and redox-regulated signal transduction. *Curr. Top. Cell. Regul.* **2000**, *36*, 1–30. [[PubMed](#)]
48. Conour, J.E.; Graham, W.V.; Gaskins, H.R. A combined in vitro/bioinformatic investigation of redox regulatory mechanisms governing cell cycle progression. *Physiol. Genom.* **2004**, *18*, 196–205. [[CrossRef](#)] [[PubMed](#)]
49. Menon, S.G.; Sarsour, E.H.; Spitz, D.R.; Higashikubo, R.; Sturm, M.; Zhang, H.; Goswami, P.C. Redox regulation of the G1 to S phase transition in the mouse embryo fibroblast cell cycle. *Cancer Res.* **2003**, *63*, 2109–2117. [[PubMed](#)]
50. Menon, S.G.; Sarsour, E.H.; Kalen, A.L.; Venkataraman, S.; Hitchler, M.J.; Domann, F.E.; Oberley, L.W.; Goswami, P.C. Superoxide signaling mediates N-acetyl-L-cysteine-induced G1 arrest: Regulatory role of cyclin D1 and manganese superoxide dismutase. *Cancer Res.* **2007**, *67*, 6392–6399. [[CrossRef](#)] [[PubMed](#)]
51. Belcastro, E.; Gaucher, C.; Corti, A.; Leroy, P.; Lartaud, I.; Pompella, A. Regulation of protein function by S-nitrosation and S-glutathionylation: Processes and targets in cardiovascular pathophysiology. *Biol. Chem.* **2017**, *398*, 1267–1293. [[CrossRef](#)] [[PubMed](#)]
52. Holmgren, A. Redox regulation by thioredoxin and thioredoxin reductase. *BioFactors* **2000**, *11*, 63–64. [[CrossRef](#)] [[PubMed](#)]
53. Pastore, A.; Federici, G.; Bertini, E.; Piemonte, F. Analysis of glutathione: Implication in redox and detoxification. *Clin. Chim. Acta* **2003**, *333*, 19–39. [[CrossRef](#)]
54. Schulz, J.B.; Lindenau, J.; Seyfried, J.; Dichgans, J. Glutathione, oxidative stress and neurodegeneration. *Eur. J. Biochem.* **2000**, *267*, 4904–4911. [[CrossRef](#)] [[PubMed](#)]
55. Anderson, M.F.; Nilsson, M.; Eriksson, P.S.; Sims, N.R. Glutathione monoethyl ester provides neuroprotection in a rat model of stroke. *Neurosci. Lett.* **2004**, *354*, 163–165. [[CrossRef](#)] [[PubMed](#)]
56. Vargas, F.; Rodríguez-Gómez, I.; Pérez-Abud, R.; Vargas Tendero, P.; Baca, Y.; Wangenstein, R. Cardiovascular and renal manifestations of glutathione depletion induced by buthionine sulfoximine. *Am. J. Hypertens.* **2012**, *25*, 629–635. [[CrossRef](#)] [[PubMed](#)]
57. Beutler, E.; Duron, O.; Kelly, B.M. Improved method for the determination of blood glutathione. *J. Lab. Clin. Med.* **1963**, *61*, 882–888. [[PubMed](#)]
58. Mansoor, M.A.; Svardal, A.M.; Ueland, P.M. Determination of the in vivo redox status of cysteine, cysteinylglycine, homocysteine, and glutathione in human plasma. *Anal. Biochem.* **1992**, *200*, 218–229. [[CrossRef](#)]
59. Tietze, F. Enzymic method for quantitative determination of nanogram amounts of total and oxidized glutathione: Applications to mammalian blood and other tissues. *Anal. Biochem.* **1969**, *27*, 502–522. [[CrossRef](#)]
60. Chen, Z.; Wang, Z.; Chen, J.; Wang, S.; Huang, X. Sensitive and selective detection of glutathione based on resonance light scattering using sensitive gold nanoparticles as colorimetric probes. *Analyst* **2012**, *137*, 3132–3137. [[CrossRef](#)] [[PubMed](#)]
61. Xu, H.; Hepel, M. “Molecular beacon”—Based fluorescent assay for selective detection of glutathione and cysteine. *Anal. Chem.* **2011**, *83*, 813–819. [[CrossRef](#)] [[PubMed](#)]
62. Piccoli, G.; Fiorani, M.; Biagiarelli, B.; Palma, F.; Potenza, L.; Amicucci, A.; Stocchi, V. Simultaneous high-performance capillary electrophoretic determination of reduced and oxidized glutathione in red blood cells in the femtomole range. *J. Chromatogr. A* **1994**, *676*, 239–246. [[CrossRef](#)]
63. Park, S.K.; Boulton, R.B.; Noble, A.C. Automated HPLC analysis of glutathione and thiol-containing compounds in grape juice and wine using pre-column derivatization with fluorescence detection. *Food Chem.* **2000**, *68*, 475–480. [[CrossRef](#)]
64. Parmentier, C.; Leroy, P.; Wellman, M.; Nicolas, A. Determination of cellular thiols and glutathione-related enzyme activities: Versatility of high-performance liquid chromatography-spectrofluorimetric detection. *J. Chromatogr. B. Biomed. Sci. Appl.* **1998**, *719*, 37–46. [[CrossRef](#)]



65. Parmentier, C.; Wellman, M.; Nicolas, A.; Siest, G.; Leroy, P. Simultaneous measurement of reactive oxygen species and reduced glutathione using capillary electrophoresis and laser-induced fluorescence detection in cultured cell lines. *Electrophoresis* **1999**, *20*, 2938–2944. [CrossRef]
66. Lewicki, K.; Marchand, S.; Matoub, L.; Lulek, J.; Coulon, J.; Leroy, P. Development of a fluorescence-based microtiter plate method for the measurement of glutathione in yeast. *Talanta* **2006**, *70*, 876–882. [CrossRef] [PubMed]
67. Rezaei, B.; Khosropour, H.; Ensafi, A.A.; Hadadzadeh, H.; Farrokhpour, H. A Differential Pulse Voltammetric Sensor for Determination of Glutathione in Real Samples Using a Trichloro(terpyridine)ruthenium(III)/Multiwall Carbon Nanotubes Modified Paste Electrode. *IEEE Sens. J.* **2015**, *15*, 483–490. [CrossRef]
68. Burford, N.; Eelman, M.D.; Mahony, D.E.; Morash, M. Definitive identification of cysteine and glutathione complexes of bismuth by mass spectrometry: Assessing the biochemical fate of bismuth pharmaceutical agents. *Chem. Commun.* **2003**, *1*, 146–147. [CrossRef]
69. Han, H.-Y.; He, Z.-K.; Zeng, Y.-E. Chemiluminescence method for the determination of glutathione in human serum using the Ru(phen)<sub>3</sub><sup>2+</sup>-KMnO<sub>4</sub> system. *Microchim. Acta* **2006**, *155*, 431–434. [CrossRef]
70. Mandal, P.K.; Tripathi, M.; Sugunan, S. Brain oxidative stress: Detection and mapping of anti-oxidant marker “Glutathione” in different brain regions of healthy male/female, MCI and Alzheimer patients using non-invasive magnetic resonance spectroscopy. *Biochem. Biophys. Res. Commun.* **2012**, *417*, 43–48. [CrossRef] [PubMed]
71. Huang, G.G.; Hossain, M.K.; Han, X.X.; Ozaki, Y. A novel reversed reporting agent method for surface-enhanced Raman scattering; highly sensitive detection of glutathione in aqueous solutions. *Analyst* **2009**, *134*, 2468–2474. [CrossRef] [PubMed]
72. Vallverdú-Queralt, A.; Verbaere, A.; Meudec, E.; Cheynier, V.; Sommerer, N. Straightforward method to quantify GSH, GSSG, GRP, and hydroxycinnamic acids in wines by UPLC-MRM-MS. *J. Agric. Food Chem.* **2015**, *63*, 142–149. [CrossRef] [PubMed]
73. Parent, M.; Dahboul, F.; Schneider, R.; Clarot, I.; Maincent, P.; Leroy, P.; Boudier, A. A Complete Physicochemical Identity Card of S-Nitrosoglutathione. Available online: <http://www.eurekaselect.com/105996/article> (accessed on 22 March 2018).
74. Neuschwander-Tetri, B.A.; Roll, F.J. Glutathione measurement by high-performance liquid chromatography separation and fluorometric detection of the glutathione-orthophthalaldehyde adduct. *Anal. Biochem.* **1989**, *179*, 236–241. [CrossRef]
75. Serru, V.; Baudin, B.; Ziegler, F.; David, J.P.; Cals, M.J.; Vaubourdolle, M.; Mario, N. Quantification of reduced and oxidized glutathione in whole blood samples by capillary electrophoresis. *Clin. Chem.* **2001**, *47*, 1321–1324. [PubMed]
76. European Department for the Quality of Medicines. *Glutathione, Monograph 01/2017: 1670, European Pharmacopoeia*; European Department for the Quality of Medicines: Strasbourg, France, 2018.
77. Pensa, E.; Cortés, E.; Corthey, G.; Carro, P.; Vericat, C.; Fonticelli, M.H.; Benítez, G.; Rubert, A.A.; Salvarezza, R.C. The chemistry of the sulfur-gold interface: In search of a unified model. *Acc. Chem. Res.* **2012**, *45*, 1183–1192. [CrossRef] [PubMed]
78. Lin, Z.; Monteiro-Riviere, N.A.; Riviere, J.E. Pharmacokinetics of metallic nanoparticles. *Wiley Interdiscip. Rev. Nanomed. Nanobiotechnol.* **2015**, *7*, 189–217. [CrossRef] [PubMed]
79. Bhattacharjee, A.; Chakraborty, K.; Shukla, A. Cellular copper homeostasis: Current concepts on its interplay with glutathione homeostasis and its implication in physiology and human diseases. *Metallomics* **2017**, *9*, 1376–1388. [CrossRef] [PubMed]
80. Reimers, J.R.; Ford, M.J.; Marcuccio, S.M.; Ulstrup, J.; Hush, N.S. Competition of van der Waals and chemical forces on gold-sulfur surfaces and nanoparticles. *Nat. Rev. Chem.* **2017**, *1*, 17. [CrossRef]
81. Tsogas, G.Z.; Kappi, F.A.; Vlessidis, A.G.; Giokas, D.L. Recent Advances in Nanomaterial Probes for Optical Biothiol Sensing: A Review. *Anal. Lett.* **2018**, *51*, 443–468. [CrossRef]
82. Li, Z.-J.; Zheng, X.-J.; Zhang, L.; Liang, R.-P.; Li, Z.-M.; Qiu, J.-D. Label-free colorimetric detection of biothiols utilizing SAM and unmodified Au nanoparticles. *Biosens. Bioelectron.* **2015**, *68*, 668–674. [CrossRef] [PubMed]
83. Li, J.-F.; Huang, P.-C.; Wu, F.-Y. Highly selective and sensitive detection of glutathione based on anti-aggregation of gold nanoparticles via pH regulation. *Sens. Actuators B Chem.* **2017**, *240*, 553–559. [CrossRef]

84. Shen, C.-C.; Tseng, W.-L.; Hsieh, M.-M. Selective enrichment of aminothiols using polysorbate 20-capped gold nanoparticles followed by capillary electrophoresis with laser-induced fluorescence. *J. Chromatogr. A* **2009**, *1216*, 288–293. [\[CrossRef\]](#) [\[PubMed\]](#)
85. Shen, L.-M.; Chen, Q.; Sun, Z.-Y.; Chen, X.-W.; Wang, J.-H. Assay of biothiols by regulating the growth of silver nanoparticles with C-dots as reducing agent. *Anal. Chem.* **2014**, *86*, 5002–5008. [\[CrossRef\]](#) [\[PubMed\]](#)
86. Kappi, F.A.; Papadopoulos, G.A.; Tsogas, G.Z.; Giokas, D.L. Low-cost colorimetric assay of biothiols based on the photochemical reduction of silver halides and consumer electronic imaging devices. *Talanta* **2017**, *172*, 15–22. [\[CrossRef\]](#) [\[PubMed\]](#)
87. Dringen, R.; Koehler, Y.; Derr, L.; Tomba, G.; Schmidt, M.M.; Treccani, L.; Colombi Ciacchi, L.; Rezwani, K. Adsorption and reduction of glutathione disulfide on  $\alpha$ -Al<sub>2</sub>O<sub>3</sub> nanoparticles: Experiments and modeling. *Langmuir* **2011**, *27*, 9449–9457. [\[CrossRef\]](#) [\[PubMed\]](#)
88. Barman, U.; Mukhopadhyay, G.; Goswami, N.; Ghosh, S.S.; Paily, R.P. Detection of Glutathione by Glutathione-S-Transferase-Nanoconjugate Ensemble Electrochemical Device. *IEEE Trans. Nanobiosci.* **2017**, *16*, 271–279. [\[CrossRef\]](#) [\[PubMed\]](#)
89. Estrela, J.; Obrador, E.; Navarro, J.; Delavega, M.; Pellicer, J. Elimination of Ehrlich Tumors by ATP-Induced Growth-Inhibition, Glutathione Depletion and X-Rays. *Nat. Med.* **1995**, *1*, 84–88. [\[CrossRef\]](#) [\[PubMed\]](#)
90. Mena, S.; Benlloch, M.; Ortega, A.; Carretero, J.; Obrador, E.; Asensi, M.; Petschen, I.; Brown, B.D.; Estrela, J.M. Bcl-2 and glutathione depletion sensitizes B16 melanoma to combination therapy and eliminates metastatic disease. *Clin. Cancer Res.* **2007**, *13*, 2658–2666. [\[CrossRef\]](#) [\[PubMed\]](#)
91. Rocha, C.R.R.; Garcia, C.C.M.; Vieira, D.B.; Quinet, A.; de Andrade-Lima, L.C.; Munford, V.; Belizario, J.E.; Menck, C.F.M. Glutathione depletion sensitizes cisplatin- and temozolomide-resistant glioma cells in vitro and in vivo. *Cell Death Dis.* **2014**, *5*, e1505. [\[CrossRef\]](#) [\[PubMed\]](#)
92. Lagman, M.; Ly, J.; Saing, T.; Kaur Singh, M.; Vera Tudela, E.; Morris, D.; Chi, P.-T.; Ochoa, C.; Sathananthan, A.; Venketaraman, V. Investigating the causes for decreased levels of glutathione in individuals with type II diabetes. *PLoS ONE* **2015**, *10*, e0118436. [\[CrossRef\]](#) [\[PubMed\]](#)
93. Herzenberg, L.A.; DeRosa, S.C.; Dubs, J.G.; Roederer, M.; Anderson, M.T.; Ela, S.W.; Deresinski, S.C.; Herzenberg, L.A. Glutathione deficiency is associated with impaired survival in HIV disease. *Proc. Natl. Acad. Sci. USA* **1997**, *94*, 1967–1972. [\[CrossRef\]](#) [\[PubMed\]](#)
94. Biolo, G.; Antonione, R.; De Cicco, M. Glutathione metabolism in sepsis. *Crit. Care Med.* **2007**, *35*, S591–S595. [\[CrossRef\]](#) [\[PubMed\]](#)
95. Day, B.J. Glutathione—A radical treatment for cystic fibrosis lung disease? *Chest* **2005**, *127*, 12–14. [\[CrossRef\]](#) [\[PubMed\]](#)
96. Martin, H.L.; Teismann, P. Glutathione—A review on its role and significance in Parkinson's disease. *FASEB J.* **2009**, *23*, 3263–3272. [\[CrossRef\]](#) [\[PubMed\]](#)
97. Pocernich, C.B.; Butterfield, D.A. Elevation of glutathione as a therapeutic strategy in Alzheimer disease. *Biochim. Biophys. Acta* **2012**, *1822*, 625–630. [\[CrossRef\]](#) [\[PubMed\]](#)
98. Gu, F.; Chauhan, V.; Chauhan, A. Glutathione redox imbalance in brain disorders. *Curr. Opin. Clin. Nutr. Metab. Care* **2015**, *18*, 89–95. [\[CrossRef\]](#) [\[PubMed\]](#)
99. Jones, D.P.; Mody, V.C.; Carlson, J.L.; Lynn, M.J.; Sternberg, P. Redox analysis of human plasma allows separation of pro-oxidant events of aging from decline in antioxidant defenses. *Free Radic. Biol. Med.* **2002**, *33*, 1290–1300. [\[CrossRef\]](#)
100. Witschi, A.; Reddy, S.; Stofer, B.; Lauterburg, B.H. The systemic availability of oral glutathione. *Eur. J. Clin. Pharmacol.* **1992**, *43*, 667–669. [\[CrossRef\]](#) [\[PubMed\]](#)
101. Shibui, Y.; Sakai, R.; Manabe, Y.; Masuyama, T. Comparisons of l-cysteine and d-cysteine toxicity in 4-week repeated-dose toxicity studies of rats receiving daily oral administration. *J. Toxicol. Pathol.* **2017**, *30*, 217–229. [\[CrossRef\]](#) [\[PubMed\]](#)
102. Greene, S.C.; Noonan, P.K.; Sanabria, C.; Peacock, W.F. Effervescent N-Acetylcysteine Tablets versus Oral Solution N-Acetylcysteine in Fasting Healthy Adults: An Open-Label, Randomized, Single-Dose, Crossover, Relative Bioavailability Study. *Curr. Ther. Res. Clin. Exp.* **2016**, *83*, 1–7. [\[CrossRef\]](#) [\[PubMed\]](#)
103. Dröge, W.; Breitzkreutz, R. N-acetyl-cysteine in the therapy of HIV-positive patients. *Curr. Opin. Clin. Nutr. Metab. Care* **1999**, *2*, 493–498. [\[CrossRef\]](#) [\[PubMed\]](#)
104. Borgström, L.; Kågedal, B.; Paulsen, O. Pharmacokinetics of N-acetylcysteine in man. *Eur. J. Clin. Pharmacol.* **1986**, *31*, 217–222. [\[CrossRef\]](#) [\[PubMed\]](#)



105. Grinberg, L.; Fibach, E.; Amer, J.; Atlas, D. N-acetylcysteine amide, a novel cell-permeating thiol, restores cellular glutathione and protects human red blood cells from oxidative stress. *Free Radic. Biol. Med.* **2005**, *38*, 136–145. [[CrossRef](#)] [[PubMed](#)]
106. Patel, S.P.; Sullivan, P.G.; Pandya, J.D.; Goldstein, G.A.; VanRooyen, J.L.; Yonutas, H.M.; Eldahan, K.C.; Morehouse, J.; Magnuson, D.S.K.; Rabchevsky, A.G. N-acetylcysteine amide preserves mitochondrial bioenergetics and improves functional recovery following spinal trauma. *Exp. Neurol.* **2014**, *257*, 95–105. [[CrossRef](#)] [[PubMed](#)]
107. Giustarini, D.; Milzani, A.; Dalle-Donne, I.; Tsikas, D.; Rossi, R. N-Acetylcysteine ethyl ester (NACET): A novel lipophilic cell-permeable cysteine derivative with an unusual pharmacokinetic feature and remarkable antioxidant potential. *Biochem. Pharmacol.* **2012**, *84*, 1522–1533. [[CrossRef](#)] [[PubMed](#)]
108. Anderson, M.E.; Powrie, F.; Puri, R.N.; Meister, A. Glutathione monoethyl ester: Preparation, uptake by tissues, and conversion to glutathione. *Arch. Biochem. Biophys.* **1985**, *239*, 538–548. [[CrossRef](#)]
109. Grattagliano, I.; Wieland, P.; Schranz, C.; Lauterburg, B.H. Effect of oral glutathione monoethyl ester and glutathione on circulating and hepatic sulfhydryls in the rat. *Pharmacol. Toxicol.* **1994**, *75*, 343–347. [[CrossRef](#)] [[PubMed](#)]
110. Minhas, H.S.; Thornalley, P.J. Comparison of the delivery of reduced glutathione into P388D1 cells by reduced glutathione and its mono- and diethyl ester derivatives. *Biochem. Pharmacol.* **1995**, *49*, 1475–1482. [[CrossRef](#)]
111. Zampagni, M.; Wright, D.; Cascella, R.; D'Adamio, G.; Casamenti, F.; Evangelisti, E.; Cardona, F.; Goti, A.; Nacmias, B.; Sorbi, S.; et al. Novel S-acyl glutathione derivatives prevent amyloid oxidative stress and cholinergic dysfunction in Alzheimer disease models. *Free Radic. Biol. Med.* **2012**, *52*, 1362–1371. [[CrossRef](#)] [[PubMed](#)]
112. Lieber, C.S. S-Adenosyl-L-methionine and alcoholic liver disease in animal models: Implications for early intervention in human beings. *Alcohol* **2002**, *27*, 173–177. [[CrossRef](#)]
113. Fawcett, J.P.; Schiller, B.; Jiang, R.; Moran, J.; Walker, R.J. Supplementation with L-2-oxothiazolidine-4-carboxylic acid, a cysteine precursor, does not protect against lipid peroxidation in puromycin aminonucleoside-induced nephropathy. *Exp. Nephrol.* **1996**, *4*, 248–252. [[PubMed](#)]
114. Oz, H.S.; Chen, T.S.; Nagasawa, H. Comparative efficacies of 2 cysteine prodrugs and a glutathione delivery agent in a colitis model. *Transl. Res. J. Lab. Clin. Med.* **2007**, *150*, 122–129. [[CrossRef](#)] [[PubMed](#)]
115. Zarka, M.H.; Bridge, W.J. Oral administration of  $\gamma$ -glutamylcysteine increases intracellular glutathione levels above homeostasis in a randomised human trial pilot study. *Redox Biol.* **2017**, *11*, 631–636. [[CrossRef](#)] [[PubMed](#)]
116. Rosenblat, M.; Volkova, N.; Coleman, R.; Aviram, M. Anti-oxidant and anti-atherogenic properties of liposomal glutathione: Studies in vitro, and in the atherosclerotic apolipoprotein E-deficient mice. *Atherosclerosis* **2007**, *195*, e61–e68. [[CrossRef](#)] [[PubMed](#)]
117. Wen, J.; Du, Y.; Li, D.; Alany, R. Development of water-in-oil microemulsions with the potential of prolonged release for oral delivery of L-glutathione. *Pharm. Dev. Technol.* **2013**, *18*, 1424–1429. [[CrossRef](#)] [[PubMed](#)]
118. Baek, M.; Choy, J.-H.; Choi, S.-J. Montmorillonite intercalated with glutathione for antioxidant delivery: Synthesis, characterization, and bioavailability evaluation. *Int. J. Pharm.* **2012**, *425*, 29–34. [[CrossRef](#)] [[PubMed](#)]
119. Trapani, A.; Laquintana, V.; Denora, N.; Lopodota, A.; Cutrignelli, A.; Franco, M.; Trapani, G.; Liso, G. Eudragit RS 100 microparticles containing 2-hydroxypropyl- $\beta$ -cyclodextrin and glutathione: Physicochemical characterization, drug release and transport studies. *Eur. J. Pharm. Sci.* **2007**, *30*, 64–74. [[CrossRef](#)] [[PubMed](#)]
120. Trapani, A.; Lopodota, A.; Franco, M.; Cioffi, N.; Ieva, E.; Garcia-Fuentes, M.; Alonso, M.J. A comparative study of chitosan and chitosan/cyclodextrin nanoparticles as potential carriers for the oral delivery of small peptides. *Eur. J. Pharm. Biopharm.* **2010**, *75*, 26–32. [[CrossRef](#)] [[PubMed](#)]
121. Naji-Tabasi, S.; Razavi, S.M.A.; Mehditabar, H. Fabrication of basil seed gum nanoparticles as a novel oral delivery system of glutathione. *Carbohydr. Polym.* **2017**, *157*, 1703–1713. [[CrossRef](#)] [[PubMed](#)]
122. Mandracchia, D.; Denora, N.; Franco, M.; Pitarresi, G.; Giammona, G.; Trapani, G. New Biodegradable Hydrogels Based on Inulin and alpha,beta-Polyaspartylhydrazide Designed for Colonic Drug Delivery: In Vitro Release of Glutathione and Oxytocin. *J. Biomater. Sci. Polym. Ed.* **2011**, *22*, 313–328. [[CrossRef](#)] [[PubMed](#)]

123. Chen, G.; Bunt, C.; Wen, J. Mucoadhesive polymers-based film as a carrier system for sublingual delivery of glutathione. *J. Pharm. Pharmacol.* **2015**, *67*, 26–34. [[CrossRef](#)] [[PubMed](#)]
124. Buonocore, D.; Grosini, M.; Giardina, S.; Michelotti, A.; Carrabetta, M.; Seneci, A.; Verri, M.; Dossena, M.; Marzatico, F. Bioavailability Study of an Innovative Orobuccal Formulation of Glutathione. *Oxid. Med. Cell. Longev.* **2016**, *2016*, 3286365. [[CrossRef](#)] [[PubMed](#)]
125. Beqa, L.; Singh, A.K.; Khan, S.A.; Senapati, D.; Arumugam, S.R.; Ray, P.C. Gold nanoparticle-based simple colorimetric and ultrasensitive dynamic light scattering assay for the selective detection of Pb(II) from paints, plastics, and water samples. *ACS Appl. Mater. Interfaces* **2011**, *3*, 668–673. [[CrossRef](#)] [[PubMed](#)]
126. Zhang, Z.; Jia, J.; Lai, Y.; Ma, Y.; Weng, J.; Sun, L. Conjugating folic acid to gold nanoparticles through glutathione for targeting and detecting cancer cells. *Bioorg. Med. Chem.* **2010**, *18*, 5528–5534. [[CrossRef](#)] [[PubMed](#)]
127. Valusová, E.; Svec, P.; Antalík, M. Structural and thermodynamic behavior of cytochrome c assembled with glutathione-covered gold nanoparticles. *J. Biol. Inorg. Chem.* **2009**, *14*, 621–630. [[CrossRef](#)] [[PubMed](#)]
128. Polavarapu, L.; Manna, M.; Xu, Q.-H. Biocompatible glutathione capped gold clusters as one- and two-photon excitation fluorescence contrast agents for live cells imaging. *Nanoscale* **2011**, *3*, 429–434. [[CrossRef](#)] [[PubMed](#)]
129. Simpson, C.A.; Salleng, K.J.; Cliffl, D.E.; Feldheim, D.L. In vivo toxicity, biodistribution, and clearance of glutathione-coated gold nanoparticles. *Nanomed. Nanotechnol. Biol. Med.* **2013**, *9*, 257–263. [[CrossRef](#)] [[PubMed](#)]
130. Koo, S.H.; Lee, J.-S.; Kim, G.-H.; Lee, H.G. Preparation, Characteristics, and Stability of Glutathione-Loaded Nanoparticles. *J. Agric. Food Chem.* **2011**, *59*, 11264–11269. [[CrossRef](#)] [[PubMed](#)]
131. Williams, S.R.; Lepene, B.S.; Thatcher, C.D.; Long, T.E. Synthesis and characterization of poly(ethylene glycol)-glutathione conjugate self-assembled nanoparticles for antioxidant delivery. *Biomacromolecules* **2009**, *10*, 155–161. [[CrossRef](#)] [[PubMed](#)]
132. Tortiglione, C.; Quarta, A.; Tino, A.; Manna, L.; Cingolani, R.; Pellegrino, T. Synthesis and biological assay of GSH functionalized fluorescent quantum dots for staining *Hydra vulgaris*. *Bioconjug. Chem.* **2007**, *18*, 829–835. [[CrossRef](#)] [[PubMed](#)]
133. Tournebise, J.; Boudier, A.; Sapin-Minet, A.; Maincent, P.; Leroy, P.; Schneider, R. Role of gold nanoparticles capping density on stability and surface reactivity to design drug delivery platforms. *ACS Appl. Mater. Interfaces* **2012**, *4*, 5790–5799. [[CrossRef](#)] [[PubMed](#)]
134. Tournebise, J.; Boudier, A.; Joubert, O.; Eidi, H.; Bartosz, G.; Maincent, P.; Leroy, P.; Sapin-Minet, A. Impact of gold nanoparticle coating on redox homeostasis. *Int. J. Pharm.* **2012**, *438*, 107–116. [[CrossRef](#)] [[PubMed](#)]
135. Luo, M.; Boudier, A.; Clarot, L.; Maincent, P.; Schneider, R.; Leroy, P. Gold Nanoparticles Grafted by Reduced Glutathione With Thiol Function Preservation. *Colloid Interface Sci. Commun.* **2016**, *14*, 8–12. [[CrossRef](#)]
136. Levin, V.A. Relationship of octanol/water partition coefficient and molecular weight to rat brain capillary permeability. *J. Med. Chem.* **1980**, *23*, 682–684. [[CrossRef](#)] [[PubMed](#)]
137. Kannan, R.; Kuhlenskamp, J.F.; Jeandidier, E.; Trinh, H.; Ookhtens, M.; Kaplowitz, N. Evidence for carrier-mediated transport of glutathione across the blood-brain barrier in the rat. *J. Clin. Invest.* **1990**, *85*, 2009–2013. [[CrossRef](#)] [[PubMed](#)]
138. Zlokovic, B.V.; Mackic, J.B.; McComb, J.G.; Weiss, M.H.; Kaplowitz, N.; Kannan, R. Evidence for transcapillary transport of reduced glutathione in vascular perfused guinea-pig brain. *Biochem. Biophys. Res. Commun.* **1994**, *201*, 402–408. [[CrossRef](#)] [[PubMed](#)]
139. Kannan, R.; Chakrabarti, R.; Tang, D.; Kim, K.J.; Kaplowitz, N. GSH transport in human cerebrovascular endothelial cells and human astrocytes: Evidence for luminal localization of Na<sup>+</sup>-dependent GSH transport in HCEC. *Brain Res.* **2000**, *852*, 374–382. [[CrossRef](#)]
140. Rip, J.; Chen, L.; Hartman, R.; van den Heuvel, A.; Reijerkerk, A.; van Kregten, J.; van der Boom, B.; Appeldoorn, C.; de Boer, M.; Maussang, D.; et al. Glutathione PEGylated liposomes: Pharmacokinetics and delivery of cargo across the blood-brain barrier in rats. *J. Drug Target.* **2014**, *22*, 460–467. [[CrossRef](#)] [[PubMed](#)]
141. Rotman, M.; Welling, M.M.; Bunschoten, A.; de Backer, M.E.; Rip, J.; Nabuurs, R.J.A.; Gaillard, P.J.; van Buchem, M.A.; van der Maarel, S.M.; van der Weerd, L. Enhanced glutathione PEGylated liposomal brain delivery of an anti-amyloid single domain antibody fragment in a mouse model for Alzheimer's disease. *J. Control. Release* **2015**, *203*, 40–50. [[CrossRef](#)] [[PubMed](#)]



142. Maussang, D.; Rip, J.; van Kregten, J.; van den Heuvel, A.; van der Pol, S.; van der Boom, B.; Reijerkerk, A.; Chen, L.; de Boer, M.; Gaillard, P.; et al. Glutathione conjugation dose-dependently increases brain-specific liposomal drug delivery in vitro and in vivo. *Drug Discov. Today Technol.* **2016**, *20*, 59–69. [[CrossRef](#)] [[PubMed](#)]
143. Birngruber, T.; Raml, R.; Gladdines, W.; Gatschelhofer, C.; Gander, E.; Ghosh, A.; Kroath, T.; Gaillard, P.J.; Pieber, T.R.; Sinner, F. Enhanced doxorubicin delivery to the brain administered through glutathione PEGylated liposomal doxorubicin (2B3-101) as compared with generic Caelyx,®/Doxil®—A cerebral open flow microperfusion pilot study. *J. Pharm. Sci.* **2014**, *103*, 1945–1948. [[CrossRef](#)] [[PubMed](#)]
144. Gaillard, P.J.; Appeldoorn, C.C.M.; Dorland, R.; van Kregten, J.; Manca, F.; Vugts, D.J.; Windhorst, B.; van Dongen, G.A.M.S.; de Vries, H.E.; Maussang, D.; et al. Pharmacokinetics, brain delivery, and efficacy in brain tumor-bearing mice of glutathione pegylated liposomal doxorubicin (2B3-101). *PLoS ONE* **2014**, *9*, e82331. [[CrossRef](#)] [[PubMed](#)]
145. Gaillard, P.J.; Appeldoorn, C.C.M.; Rip, J.; Dorland, R.; van der Pol, S.M.A.; Kooij, G.; de Vries, H.E.; Reijerkerk, A. Enhanced brain delivery of liposomal methylprednisolone improved therapeutic efficacy in a model of neuroinflammation. *J. Control. Release* **2012**, *164*, 364–369. [[CrossRef](#)] [[PubMed](#)]
146. Kanhai, K.M.S.; Zuiker, R.G.J.A.; Stavrakaki, I.; Gladdines, W.; Gaillard, P.J.; Klaassen, E.S.; Groeneveld, G.J. Glutathione-PEGylated liposomal methylprednisolone in comparison to free methylprednisolone: Slow release characteristics and prolonged lymphocyte depression in a first-in-human study. *Br. J. Clin. Pharmacol.* **2018**. [[CrossRef](#)] [[PubMed](#)]
147. Gaillard, P.J.; Kerklaan, B.M.; Aftimos, P.; Altintas, S.; Jager, A.; Gladdines, W.; Lonnqvist, F.; Soetekouw, P.; Verheul, H.; Awada, A.; et al. Abstract CT216: Phase I dose escalating study of 2B3-101, glutathione PEGylated liposomal doxorubicin, in patients with solid tumors and brain metastases or recurrent malignant glioma. *Cancer Res.* **2014**, *74*, CT216. [[CrossRef](#)]
148. Brandsma, D.; Kerklaan, B.M.; Diéras, V.; Altintas, S.; Anders, C.K.; Ballester, M.A.; Gelderblom, H.; Soetekouw, P.M.M.B.; Gladdines, W.; Lonnqvist, F.; et al. Phase 1/2a study of glutathione pegylated liposomal doxorubicin (2b3-101) in patients with brain metastases (BM) from solid tumors or recurrent high grade gliomas (HGG). *Ann. Oncol.* **2014**, *25*, iv157–iv158. [[CrossRef](#)]
149. Veszelka, S.; Meszaros, M.; Kiss, L.; Kota, Z.; Pali, T.; Hoyk, Z.; Bozso, Z.; Fulop, L.; Toth, A.; Rakhely, G.; et al. Biotin and Glutathione Targeting of Solid Nanoparticles to Cross Human Brain Endothelial Cells. *Curr. Pharm. Des.* **2017**, *23*, 4198–4205. [[CrossRef](#)] [[PubMed](#)]
150. Grover, A.; Hirani, A.; Pathak, Y.; Sutariya, V. Brain-targeted delivery of docetaxel by glutathione-coated nanoparticles for brain cancer. *AAPS PharmSciTech* **2014**, *15*, 1562–1568. [[CrossRef](#)] [[PubMed](#)]
151. Geldenhuys, W.; Wehrung, D.; Groshev, A.; Hirani, A.; Sutariya, V. Brain-targeted delivery of doxorubicin using glutathione-coated nanoparticles for brain cancers. *Pharm. Dev. Technol.* **2015**, *20*, 497–506. [[CrossRef](#)] [[PubMed](#)]
152. Geldenhuys, W.; Mbimba, T.; Bui, T.; Harrison, K.; Sutariya, V. Brain-targeted delivery of paclitaxel using glutathione-coated nanoparticles for brain cancers. *J. Drug Target.* **2011**, *19*, 837–845. [[CrossRef](#)] [[PubMed](#)]
153. Raval, N.; Mistry, T.; Acharya, N.; Acharya, S. Development of glutathione-conjugated asiatic acid-loaded bovine serum albumin nanoparticles for brain-targeted drug delivery. *J. Pharm. Pharmacol.* **2015**, *67*, 1503–1511. [[CrossRef](#)] [[PubMed](#)]
154. Patel, P.; Acharya, N.; Acharya, S. Development and characterization of glutathione-conjugated albumin nanoparticles for improved brain delivery of hydrophilic fluorescent marker. *Drug Deliv.* **2013**, *20*, 143–155. [[CrossRef](#)] [[PubMed](#)]
155. Mdzinarishvili, A.; Sutariya, V.; Talasila, P.K.; Geldenhuys, W.J.; Sadana, P. Engineering triiodothyronine (T3) nanoparticle for use in ischemic brain stroke. *Drug Deliv. Transl. Res.* **2013**, *3*, 309–317. [[CrossRef](#)] [[PubMed](#)]
156. Englert, C.; Trützschler, A.-K.; Raasch, M.; Bus, T.; Borchers, P.; Mosig, A.S.; Traeger, A.; Schubert, U.S. Crossing the blood-brain barrier: Glutathione-conjugated poly(ethylene imine) for gene delivery. *J. Control. Release* **2016**, *241*, 1–14. [[CrossRef](#)] [[PubMed](#)]
157. Yin, J.; Chen, Y.; Zhang, Z.-H.; Han, X. Stimuli-Responsive Block Copolymer-Based Assemblies for Cargo Delivery and Theranostic Applications. *Polymers* **2016**, *8*, 268. [[CrossRef](#)]
158. Liu, X.; Yang, Y.; Urban, M.W. Stimuli-Responsive Polymeric Nanoparticles. *Macromol. Rapid Commun.* **2017**, *38*, 13. [[CrossRef](#)] [[PubMed](#)]

159. Cheng, R.; Meng, F.; Deng, C.; Klok, H.-A.; Zhong, Z. Dual and multi-stimuli responsive polymeric nanoparticles for programmed site-specific drug delivery. *Biomaterials* **2013**, *34*, 3647–3657. [[CrossRef](#)] [[PubMed](#)]
160. Son, S.; Namgung, R.; Kim, J.; Singha, K.; Kim, W.J. Bioreducible polymers for gene silencing and delivery. *Acc. Chem. Res.* **2012**, *45*, 1100–1112. [[CrossRef](#)] [[PubMed](#)]
161. Ma, N.; Li, Y.; Xu, H.; Wang, Z.; Zhang, X. Dual redox responsive assemblies formed from diselenide block copolymers. *J. Am. Chem. Soc.* **2010**, *132*, 442–443. [[CrossRef](#)] [[PubMed](#)]
162. Han, L.; Zhang, X.-Y.; Wang, Y.-L.; Li, X.; Yang, X.-H.; Huang, M.; Hu, K.; Li, L.-H.; Wei, Y. Redox-responsive theranostic nanoplatfroms based on inorganic nanomaterials. *J. Control. Release* **2017**, *259*, 40–52. [[CrossRef](#)] [[PubMed](#)]
163. Ghosh, P.S.; Kim, C.-K.; Han, G.; Forbes, N.S.; Rotello, V.M. Efficient Gene Delivery Vectors by Tuning the Surface Charge Density of Amino Acid-Functionalized Gold Nanoparticles. *ACS Nano* **2008**, *2*, 2213–2218. [[CrossRef](#)] [[PubMed](#)]
164. Tournebise, J.; Sapin-Minet, A.; Bartosz, G.; Leroy, P.; Boudier, A. Pitfalls of assays devoted to evaluation of oxidative stress induced by inorganic nanoparticles. *Talanta* **2013**, *116*, 753–763. [[CrossRef](#)] [[PubMed](#)]



© 2018 by the authors. Licensee MDPI, Basel, Switzerland. This article is an open access article distributed under the terms and conditions of the Creative Commons Attribution (CC BY) license (<http://creativecommons.org/licenses/by/4.0/>).

GSH is also implicated in atherosclerosis development. Indeed, the presence of GSH-related enzymatic antioxidant defences (selenium-dependant or independent glutathione peroxidase (GPx), glutathione *S*-transferase (GST), glutathione reductase (GR)) was described in human atherosclerotic lesions and its specific antioxidant/prooxidant imbalance was described as a factor contributing to the atherogenic process [47]. Indeed, in ApoE<sup>-/-</sup> mice, a deficiency of GPx1 activity accelerates and modifies atherosclerosis lesions (increasing cellularity and ROS concentration) [48]. GSH is also implicated in macrophage polarization into M1 macrophages by stimulating the production of immune mediators like NO, PGE2 and inducing phagocytic activity through NF-κB pathway. Moreover, GSH up-regulates the production of pro-inflammatory cytokines (interleukins and TNF-α) and neutrophil-attracting chemokines. GSH decreased ROS generation induced by LPS with the activation of Nrf2/HO-1 signaling pathway [49]. The Akt signaling pathway is known to be regulated by the GSH/glutaredoxin (GRX)-dependent redox system. Sex hormones like oestrogens and oestradiol protect against oxidative stress *via* the protection of Akt signaling pathway. These hormones also upregulate the GSH/GRX1 redox status, suggesting a protection against atherosclerotic processes. Furthermore, an increase of *S*-glutathionylated serum proteins was found in patients with atherosclerosis obliterans and could be used as a marker of vascular dysfunction development [50].

## **II. Atherosclerosis prevention and associated treatments**

There is no drug indicated for atherosclerosis treatment. The primary prevention for patient with risk factors but without any symptom or complication is based on lifestyle and dietary advises like healthy (low fat) diet, exercise, blood pressure control, quit smoking. The secondary prevention for patients with symptoms and complications associated with atherosclerosis is to reduce the risk of new complications by treating dyslipidaemia using hypolipidemic drugs, like statins. This treatment can be associated with calcium inhibitors (inducing vasorelaxation), beta-blockers or antiplatelet drugs. Anti-platelet drugs prevent thrombosis and, cardiovascular or cerebrovascular complications (*i.e.* heart attack or stroke) associated with atherosclerosis in patients with high cardiovascular risk.

Statins are prescribed for patients with high cardiovascular risk (men ≥ 45 years old; women ≥ 55 years old; active smoking; pre-diabetes; high blood pressure (systolic blood pressure ≥ 140 mmHg and/or diastolic blood pressure ≥ 90 mmHg); dyslipidaemia; obesity; previous family history; sedentary lifestyle). These treatments allow the stabilisation of plaques evolution by decreasing the concentration of circulating LDLs. Statins are inhibitor of the

3-hydroxy-3-methyl-glutaryl-coenzyme A reductase (HMG-CoA reductase) implicated in cholesterol synthesis. Statins show pleiotropic effects such as NO production, which confirms the importance of NO to limit atherosclerosis development. With this in mind, the use of NO donors like *S*-nitrosothiols as another therapeutic/preventive option to restore NO bioavailability and to limit the formation/progression of atherosclerotic plaques seems to be appropriate [51]. Indeed, as already said, a decrease of NO bioavailability is often observed in cardiovascular diseases, this supports the use of NO repletion as a therapeutic opportunity to prevent plaques formation. The direct utilization of NO as gas (Kinox<sup>®</sup>) is limited by its short half-life and is used only for the treatment of arterial pulmonary hypertension. NO donors are already used in clinics to prevent angina pectoris with nitroglycerin administrated by sublingual pulverisation or by transdermal devices (Diafusor<sup>®</sup>, Trinipatch<sup>®</sup>) or with isosorbide dinitrate, an organic nitrate administrated by sublingual pulverisation or as capsules (Isocard<sup>®</sup>, Risordan<sup>®</sup>). However, these drugs are indirect NO donors or prodrugs that need to be metabolised to produce NO. Organic nitrates work exclusively on vSMCs where the mitochondrial aldehyde dehydrogenase-2 (ALDH2) or cytochrome P450 reduce them to NO [52]. NO may react with thiol residues to form *S*-nitrosothiols, which are able to stabilize and carry NO to the guanylyl cyclase. During a chronic treatment, organic nitrates are subject to a tolerance phenomenon linked with ALDH2 and P450 decrease of activity and thiols depletion amplifying the oxidative stress. Sydnominines (molsidomine; Corvasal<sup>®</sup>) are also used for the prevention of intimal hyperplasia and are also subjected to tolerance phenomenon.

*S*-nitrosothiols formed by *S*-nitrosation of high or low molecular weight proteins or peptides are interesting NO donor candidates. *S*-nitrosoalbumin, *S*-nitrosohemoglobin and *S*-nitrosoglutathione (GSNO) are physiological forms of NO storage and transport *in vivo*. Indeed, the formation of the S-NO bond extends NO half-life from few seconds (free NO) to several hours and limits the oxidative/nitrosative stress induced by NO oxidation into peroxynitrite ions (ONOO<sup>-</sup>). Therefore, *S*-nitrosothiols can be considered as drugs that mimic the physiological reservoir of NO and could counteract different steps of atherosclerosis development. It has been demonstrated that NO donors, such as *S*-nitroso-D-penicillamine (SNAP), are able to decrease LDLs oxidation rate and to deplete macrophages from atherosclerotic plaques [51]. Other studies showed a decrease of atheroma plaques size, oxidative stress and free circulating cholesterol following *S*-nitroso-N-acetylcysteine (NACNO) administration in a mice model (LDLR<sup>-/-</sup> mice) of atherosclerosis [35].



### III. Animal models of atherosclerosis

Atherosclerosis is a complex process. Cells of the vessel wall and cells of the immune system participate to its development. Plasma lipoproteins, genetic and arterial hemodynamic also participate to the process. To find potential therapeutic targets of this multifactorial disease (*i.e.* the alteration of lipid metabolism, increased oxidative stress and chronic inflammation) and check the efficacy of molecules, the utilization of animal models to increase our understanding of atherosclerosis mechanisms is necessary. Animal models need to be as close as possible to human hemodynamic parameters: 37 °C; 60-80 bpm; systolic blood pressure: 100-140 mmHg; diastolic blood pressure: 50-85 mmHg. Suitable small and large animal models have been developed (see **Table 1**). These models are mainly based on an accelerated formation of plaques through a cholesterol or Western-type diet associated (or not) with the deletion of genes implicated in cholesterol metabolism, or through the induction of other risk factors such as hypercholesterolemia and diabetes. Mouse and rabbit models have been the most used with their advantages and limitations. Murine models have a short life cycle but a high reproduction rate and are easy to manipulate. They are the most used model for experimental research. Rabbit models are phylogenetically closer to humans, with a short gestation period and a large number of young rabbits. Moreover, the rabbit genome sequencing and transcriptomic profiling of atheroma is completed. This model is used for experimental research and pre-clinic drug tests.

**Table 1:** overview of large and small animals used as atherosclerotic models

		Hemodynamic parameters	Advantages	Limitations	Utilizations
Non-human primates	Old World monkey African Green, Rhesus and Cynomolgus monkeys	36-38 °C 150-220 bpm > 60 mmHg (systolic) > 90 mmHg (diastolic)	Humanoid lipoprotein With high fat diet: more plaque for males than females Cynomolgus: rapid atherosclerotic development, lesions rich in foam cells	Expensive (food and life conditions)	Rhesus monkey: regression of coronary atherosclerosis with the return to a low fat diet Cynomolgus: used for extensive studies of the influence of social status on atherosclerosis
Pigs	/	37-38 °C 70-180 bpm > 60 mmHg (systolic) > 90 mmHg (diastolic)	Spontaneous development of plaques: accelerated with atherogenic diet Predominantly foam cells atherosclerotic lesions	Expensive (food and life conditions) Long period to develop complex atherosclerotic lesions	Elucidation of the heterogeneous interaction of hemodynamics and responses of arterial endothelial layer
Rabbits	New Zealand white (NZW) + cholesterol food	37-39 °C 140-180 bpm > 90 mmHg (systolic) > 75 mmHg (diastolic)		Non spontaneous development of plaques	Remnant lipoproteins predominate Predominantly macrophage-derived foam cells lesions
	Watanabe hereditary hypercholesterolemic (WHHL): defect of LDLR		Spontaneous development of plaques and hypercholesterolemia LDLs predominant lipoprotein		Predominantly smooth muscle cells origin for the lesions
	ApoE <sup>-/-</sup>		Mild hyperlipidaemia on normal diet		Promising alternative to ApoE <sup>-/-</sup> mice
Mice	ApoE <sup>-/-</sup>	≈ 37 °C 520-650 bpm > 130 mmHg (systolic) > 100 mmHg (diastolic)	Spontaneous development of vascular lesions on normal diet: comparable to human lesions with the presence of oxLDLs Rate of atherogenesis can be accelerate with a cholesterol diet (increase plasma lipids levels)		
	LDLR <sup>-/-</sup>		Lower lipoprotein profile alteration compared to ApoE <sup>-/-</sup> mice Time manner atherosclerotic lesions development		

#### IV. NO donors administration routes

Several preclinical studies have focused on the application of *S*-nitrosothiols as vascular therapeutic. For example, NACNO administrated intraperitoneally, showed anti-atherosclerotic effects in a LDLR<sup>-/-</sup> mouse model, preventing the early formation of atheroma plaques and moderately modifying circulating lipid profile [53]. However, intraperitoneal administration is not a suitable solution for the treatment of chronic pathologies. Indeed, the oral route might be favoured to improve patient compliance to the treatment. At this time, no study using the *S*-nitrosothiols oral administration has been designed for atherosclerosis treatment. Nevertheless, GSNO administered orally in the context of stroke [54] showed a neuroprotective effect by maintaining the integrity of the blood-brain barrier and reducing the neurological deficits caused by stroke [55]. In addition, during stroke, aberrant nNOS activity is observed as well as NO imbalance. Recently, GSNO has been shown to reduce the formation of peroxynitrite ions during stroke, confirming its neuroprotective effect. Currently, FDA-approved therapy for the treatment of stroke (hypothermia or thrombolysis (Actilyse®)) suffers from a lack of neuronal protection. Therefore, GSNO appears to be a good drug candidate as it has neuroprotective activity and improves stroke damage by stabilizing Hypoxia Inducible Factor 1 alpha (HIF-1 $\alpha$ ) via *S*-nitrosation [56,57]. Consequently, these studies support the potential of *S*-nitrosothiols as oral therapeutic without any proof of their intestinal permeability.

Only, Pinheiro *et al.* demonstrated that the oral administration of nitrite ions or nitrate ions (which are the NO-derived species stable in aqueous media) induces the formation of *S*-nitrosothiols under the action of stomach acidic [58]. These *S*-nitrosothiols, once in the bloodstream, produce antihypertensive effects with a decrease in mean blood pressure. The study therefore indirectly demonstrated the intestinal absorption of *S*-nitrosothiols after oral administration of nitrite ions or nitrate ions. Despite this, no information about *S*-nitrosothiols intestinal absorption mechanisms were available before our study published in 2018 [59].

### **Article 3: Intestinal absorption of S-nitrosothiols: permeability and transport mechanisms**

#### **Absorption intestinale des S-nitrosothiols : mécanismes de transport et de perméabilité**

Justine Bonetti<sup>1</sup>, Yi Zhou<sup>1</sup>, Marianne Parent, Igor Clarot, Haiyan Yu, Isabelle Fries-Raeth, Pierre Leroy, Isabelle Lartaud, Caroline Gaucher

<sup>1</sup>Les deux auteurs ont contribué à parts égales à ce travail

*Biochemical Pharmacology 155 (2018) 21–31*

Au cours du vieillissement ou du développement des pathologies cardiovasculaires comme l'athérosclérose ou l'angor, une diminution de la biodisponibilité du monoxyde d'azote (NO) est observée. Afin de restaurer une concentration physiologique de NO, les donneurs de NO comme les S-nitrosothiols (RSNO) sont envisagés. Les RSNO sont la forme physiologique de stockage et de transport de NO dans l'organisme, lui assurant ainsi une demi-vie supérieure à sa forme libre radicalaire (< 0,5 s). La plupart des pathologies cardiovasculaires nécessitent un traitement chronique pour lequel la voie orale est plébiscitée. Ainsi, l'absorption intestinale et les paramètres l'influençant (efflux, pH), sont les premiers facteurs à étudier pour l'évaluation de la biodisponibilité orale de ces donneurs de NO. Dans notre étude, trois différents S-nitrosothiols ont été évalués : le S-nitrosoglutathion (GSNO), la S-nitroso-N-acétylcystéine (NACNO), la S-nitroso-D-pénicillamine (SNAP), classés respectivement du plus au moins hydrophile. Chacun de ses S-nitrosothiols possède un squelette différent porteur de la liaison S-NO, conférant des propriétés physico-chimiques (lipophilie) et des activités biologiques (antioxydantes et/ou anti-inflammatoires) propres à chacun. Ces S-nitrosothiols sont susceptibles d'être absorbés sous forme moléculaire ou ionique, les ions nitrite et les ions nitrate, espèces stables en milieu aqueux dérivées de NO. L'absorption intestinale des S-nitrosothiols a été étudiée à partir d'un modèle d'épithélium intestinal différencié composé de cellules Caco-2 cultivées sur des inserts poreux permettant ainsi l'absorption sélective des molécules. Ce modèle permet également d'étudier les mécanismes d'absorption intestinale et de prédire le site préférentiel d'absorption intestinal des S-nitrosothiols. Le modèle a été validé en utilisant des molécules de référence, propranolol et furosémide, dont la perméabilité intestinale est connue. La perméabilité des S-nitrosothiols a été caractérisée selon les paramètres suivants *i)* espèces réellement absorbées (NO<sub>2</sub><sup>-</sup>, NO<sub>3</sub><sup>-</sup>, RSNO), *ii)* cinétiques de transport, *iii)* modes de perméabilité (passif *versus* actif) et *iv)* influence du pH sur le transport des S-nitrosothiols. L'évaluation bidirectionnelle de la perméabilité a démontré que les RSNO



étaient absorbés selon un mécanisme passif essentiellement sous forme d'espèces dérivées de NO. La perméabilité apparente moyenne ainsi que la forte solubilité des RSNO permet de les placer entre la classe I et la classe III du Système de Classification Biopharmaceutique (FDA, 2015). Il a également été démontré que GSNO et NACNO suivent préférentiellement une voie transcellulaire alors que SNAP privilégie une voie paracellulaire. Enfin, le squelette portant NO a montré une influence sur le site d'absorption des RSNO. La perméabilité de NACNO est favorisée à pH 6,4, pH se rapprochant de la partie proximale du jéjunum, alors que la perméabilité de GSNO et SNAP est meilleure à pH 7,4, pH proche de la partie distale de l'iléon. Selon la littérature, les médicaments de classe I et II présentent une bonne corrélation *in vivo/in vitro*. Ainsi, la projection de ces résultats vers la biodisponibilité orale des *S*-nitrosothiols *in vivo*, ouvre une possibilité quant à l'administration orale des *S*-nitrosothiols comme médicament du système cardiovasculaire avec une absorption majoritaire sous forme d'espèces dérivées de NO.



# Intestinal absorption of S-nitrosothiols: Permeability and transport mechanisms

Justine Bonetti<sup>1</sup>, Yi Zhou<sup>1</sup>, Marianne Parent, Igor Clarot, Haiyan Yu, Isabelle Fries-Raeth, Pierre Leroy, Isabelle Lartaud, Caroline Gaucher\*

Université de Lorraine, CITHEFOR, F-54000 Nancy, France

## ARTICLE INFO

**Keywords:**  
S-Nitrosothiols  
Nitric oxide  
Intestinal permeability  
Caco-2 cells  
Passive diffusion

## ABSTRACT

S-Nitrosothiols, a class of NO donors, demonstrate potential benefits for cardiovascular diseases. Drugs for such chronic diseases require long term administration preferentially through the oral route. However, the absorption of S-nitrosothiols by the intestine, which is the first limiting barrier for their vascular bioavailability, is rarely evaluated. Using an *in vitro* model of intestinal barrier, based on human cells, the present work aimed at elucidating the mechanisms of intestinal transport (passive or active, paracellular or transcellular pathway) and at predicting the absorption site of three S-nitrosothiols: S-nitrosoglutathione (GSNO), S-nitroso-N-acetyl-L-cysteine (NACNO) and S-nitroso-N-acetyl-D-penicillamine (SNAP). These S-nitrosothiols include different skeletons carrying the nitroso group, which confer different physico-chemical characteristics and biological activities (anti-oxidant and anti-inflammatory). According to the values of apparent permeability coefficient, the three S-nitrosothiols belong to the medium class of permeability. The evaluation of the bidirectional apparent permeability demonstrated a passive diffusion of the three S-nitrosothiols. GSNO and NACNO preferentially cross the intestinal barrier through the transcellular pathway, while SNAP followed both the trans- and paracellular pathways. Finally, the permeability of NACNO was favoured at pH 6.4, which is close to the pH of the jejunal part of the intestine. Through this study, we determined the absorption mechanisms of S-nitrosothiols and postulated that they can be administrated through the oral route.

## 1. Introduction

Nitric oxide (NO) is a gaseous mediator with a short half-life (less than 5 s [1]). Due to its radical nature and oxidative activity, NO is involved in various signalling pathways among different cellular types and physiological systems. NO is continuously synthesised by oxydoreductases, *i.e.* the three endothelial, inducible or neuronal isoforms of NO synthases. The decrease in NO bioavailability, linked to vascular endothelium dysfunction and oxidative stress, plays a major role in ageing and cardiovascular chronic diseases like atherosclerosis, angina pectoris and stroke. As a result, the restoration of NO bioavailability, using among NO donors the physiologically occurring S-nitrosothiols, is a therapeutic key to treat cardiovascular diseases [2–7]. S-Nitrosothiols are formed by S-nitrosation – *i.e.* formation of a covalent bond between NO and a reduced thiol function of a cysteine residue belonging to high or low molecular weight proteins or peptides. *In vivo*, S-nitrosothiols like S-nitrosoalbumin, S-nitrosohemoglobin and S-nitrosoglutathione (GSNO) are the physiological forms of NO storage and transport [8].

Indeed, the formation of the S-NO bond extends NO half-life from 45 min up to several hours [9–10] and limits the oxidative/nitrosative stress induced by NO oxidation into peroxynitrite ions (ONOO<sup>−</sup>) [11]. Despite the therapeutic potential of S-nitrosothiols, their half-life linked to their physico-chemical instability (heat, light, metallic cations,...) and/or enzymatic (redoxines or, for GSNO only,  $\gamma$ -glutamyltransferase) degradation, is too short for chronic diseases treatment [12].

Nowadays, many preclinical studies focused on cardiovascular therapeutics using S-nitrosothiols [6,13–17]. For example, daily intraperitoneal administration of S-nitroso-N-acetyl-L-cysteine (NACNO) for two weeks shows anti-atherosclerotic effects in mice [13]. However, compared to the oral route, the intraperitoneal administration is less suitable for chronic treatments. GSNO administration through the oral route in a context of stroke [14] results in neuroprotective effects: GSNO maintains the blood-brain barrier integrity, reduces peroxynitrite formation and stabilises several deleterious factors *via* S-nitrosation [13–16]. Despite such beneficial effects following oral administration, to the best of our knowledge, no study evaluated the mechanisms of

\* Corresponding author at: Université de Lorraine, CITHEFOR EA 3452, Faculté de Pharmacie, BP 80403, F-54001 Nancy Cedex, France.

E-mail address: [caroline.gaucher@univ-lorraine.fr](mailto:caroline.gaucher@univ-lorraine.fr) (C. Gaucher).

<sup>1</sup> Both authors contributed equally to this work.

<https://doi.org/10.1016/j.bcp.2018.06.018>

Received 12 April 2018; Accepted 19 June 2018

Available online 21 June 2018

0006-2952/ © 2018 Elsevier Inc. All rights reserved.

intestinal absorption of GSNO and other S-nitrosothiols. Only Pinheiro et al. [17] demonstrated that oral administration of nitrite and nitrate ions (stable NO derived species) to rats increased the concentration of circulating S-nitrosothiols, thus produced antihypertensive effects. This study indirectly proves the intestinal absorption of S-nitrosothiols without elucidated the underlying mechanisms. However, the understanding of the intestinal absorption mechanisms of S-nitrosothiols is a prerequisite to control the dose and the kinetic of NO reaching its action sites.

To predict the intestinal absorption of drugs, the Biopharmaceutical Classification System (BCS) [18] defines four classes based on the physico-chemical properties (solubility) and intestinal permeability of drugs. The intestinal permeability of a drug is characterised, using *in vitro* or *ex vivo* models, by apparent permeability coefficient (Papp) from low permeability ( $< 1 \times 10^{-6} \text{ cm.s}^{-1}$ ) to high permeability ( $\geq 10 \times 10^{-6} \text{ cm.s}^{-1}$ ) including also a medium permeability class [19]. Thus far, only one of our studies was interested in the improvement and the prolongation of GSNO intestinal absorption by proposing alginate/chitosan nanocomposite formulation [20]. Using an *in vitro* intestinal barrier model of differentiated Caco-2 cells, we showed low intestinal permeability for GSNO with a Papp of  $0.83 \times 10^{-7} \text{ cm.s}^{-1}$ . The nanocomposite formulation delayed GSNO absorption up to 24 h (1 h for free GSNO) and multiplied by four the Papp value ( $3.41 \times 10^{-7} \text{ cm.s}^{-1}$ ) even if GSNO stayed in the low class of permeability [20]. This study showed the ability for GSNO to cross the intestinal barrier model and the possibility to modulate its kinetics of absorption. This opens new therapeutic applications in the treatment of chronic pathologies linked to a decrease of NO bioavailability.

Intestinal absorption of low molecular weight molecules is mainly driven by their physico-chemical properties such as lipophilicity, correlated with the octanol/water partition coefficient, expressed as a logarithmic value (log P), and the ionisation constant (pKa). For S-nitrosothiols, the log P value is driven by the skeleton carrying NO. GSNO, NACNO and S-nitroso-N-acetyl-D-penicillamine (SNAP), the three main S-nitrosothiols described in the literature, are characterised by calculated log P value of  $-2.70$ ,  $-0.47$  and  $1.08$ , respectively [2]. The skeleton carrying NO presents also different therapeutic properties linked with its chemical structure. GSNO is a physiological S-nitrosothiol [21], present in the cytosol at a high concentration especially in erythrocytes [22], platelets and cerebral tissue. Its reduced glutathione (GSH) skeleton shows an antioxidant chemical structure thanks to its thiol functional group and forms, with the glutathione disulphide (GSSG), the intracellular redox buffer. NACNO and SNAP are synthetic S-nitrosothiols. NACNO with its N-acetyl-L-cysteine (NAC) skeleton possesses also an antioxidant activity in accordance with its chemical structure (thiol function). Furthermore, NAC is already used in human medicine as a mucolytic agent (oral administration) or as the antidote in acetaminophen intoxication [23]. SNAP shows in addition to its antioxidant properties (thiol function), an anti-inflammatory skeleton, N-acetyl-D-penicillamine (NAP) is used in the treatment of Wilson's disease (Trolvol®) and rheumatoid arthritis.

In this study, using an *in vitro* cell model of intestinal barrier, we propose to elucidate the intestinal transport mechanisms of S-nitrosothiols and NO in relation to their physico-chemical properties. Three different conditions were studied, i) permeability from the apical to the basolateral compartment, ii) permeability from the basolateral to the apical compartment to highlight an active transport such as drug influx/efflux, or a passive diffusion, and iii) permeability from an acidified apical compartment, mimicking the luminal intestinal pH of the jejunum, the major site of amino acid absorption [24].

## 2. Material and methods

### 2.1. Material and reagents

Eagle's Minimum Essential Medium (EMEM), foetal bovine serum

(FBS), sodium pyruvate, penicillin 10 000 U.mL<sup>-1</sup> and streptomycin 10 mg.mL<sup>-1</sup> mix, trypsin, non-essential amino acids, glutamine, Hank's Balanced Salt Solution (HBSS Ca<sup>2+</sup>/Mg<sup>2+</sup>), sodium nitrate (NaNO<sub>3</sub>), 2,3-diaminonaphthalene (DAN), 1.0 M hydrochloric acid (HCl) solution, propranolol hydrochloride, furosemide salt, triethylamine, 2-(N-morpholino)ethanesulfonic acid (MES), Tris base (Tris), sodium chloride (NaCl), Igepal CA-630, sodium dodecyl sulfate (SDS), ethylenediaminetetraacetic acid (EDTA), neocuproine and N-ethylmaleimide (NEM) were purchased from Sigma, France. Mercuric chloride (HgCl<sub>2</sub>), orthophosphoric acid and sodium tetraborate were purchased from Prolabo (VWR). Sodium nitrite (NaNO<sub>2</sub>) from Merck, sodium hydroxide (NaOH) from VWR Chemicals, methanol from Carlo Erba Reagents and acetonitrile was from Biosolve. Nitrite/nitrate fluorimetric kit was purchased from Cayman Chemical (Ref. 780051).

### 2.2. S-Nitrosothiols synthesis

GSNO, NACNO and SNAP were synthesised according to a previously described method [25]. Briefly, GSH, NAC or NAP were incubated with one equivalent of sodium nitrite under acidic condition. Then, the pH was shifted to 7.4 using a phosphate buffered saline (PBS 0.148 M) solution. The final concentration was assessed by UV-Vis. spectrophotometry (Shimadzu; UV-spectrophotometer; UV-1800) using the specific molar absorbance of the S-NO bond at 334 nm for GSNO and NACNO ( $\epsilon_{\text{GSNO}} = 922 \text{ M}^{-1} \text{ cm}^{-1}$ ;  $\epsilon_{\text{NACNO}} = 900 \text{ M}^{-1} \text{ cm}^{-1}$ ) and at 340 nm for SNAP ( $\epsilon_{\text{SNAP}} = 1020 \text{ M}^{-1} \text{ cm}^{-1}$ ).

### 2.3. Caco-2 cells culture and cytocompatibility

Intestinal Caco-2 cells (ATCC® HTB-37™) from passage 36 to 45 were grown in complete medium consisting of EMEM supplemented with 10% (v/v) of FBS, 4 mM of glutamine, 100 U/mL of penicillin, 100 U/mL of streptomycin, 1% (v/v) of non-essential amino acids. Cells were cultivated at 37 °C under 5% CO<sub>2</sub> (v/v) in a humidified incubator. Caco-2 cells were seeded in 96-wells plates at  $2 \times 10^4$  cells/well 24 h before experiment. They were then exposed to each S-nitrosothiol (from 10 to 100 μM) for 24 h at 37 °C, complete medium being used as control. Cytocompatibility was assessed through metabolic activity with the 3(4,5-dimethylthiazol-2-yl)-2,5-diphenyltetrazolium bromide (MTT) assay. The absorbance of extracted formazan crystals was read at 570 nm with a reference at 630 nm (EL 800 microplate reader, Bio-TEK Instrument, Inc®, France). Metabolic activity in control condition was considered as 100%.

### 2.4. Intestinal permeability of reference molecules and S-nitrosothiols

Caco-2 cells were seeded at  $2 \times 10^6$  cell/cm<sup>2</sup> on cell culture inserts (Transwell®, Corning, USA, membrane with 0.4 μm pore size, 1.12 cm<sup>2</sup> area or 4.97 cm<sup>2</sup>) disposed in a 12-wells or 6-wells plate, respectively. The complete medium was replaced every two days during the first week of cell proliferation. During the second week, the medium was replaced every day until the differentiated cell monolayer was formed (14–15 days). The formation of the barrier was followed by transepithelial electrical resistance (TEER) measurement using a Millicell®-Electrical Resistance system (Millipore, USA) and validated for TEER values higher than 500 Ω.cm<sup>2</sup>.

The bidirectional permeability of each S-nitrosothiol across the Caco-2 monolayer was evaluated from the apical to basolateral (A-B) compartment, mimicking physiological permeability conditions (intestinal lumen to blood compartment), and from the basolateral to the apical (B-A) (Fig. 1) compartment in HBSS at pH 7.4 to evaluate possible efflux mechanisms. A third condition evaluates the importance of the influence of luminal pH adjusted to 6.4 with 0.5 M MES solution in the apical compartment to determine the intestinal site of absorption (intestinal segment).

The concentration of S-nitrosothiols used to study the permeability



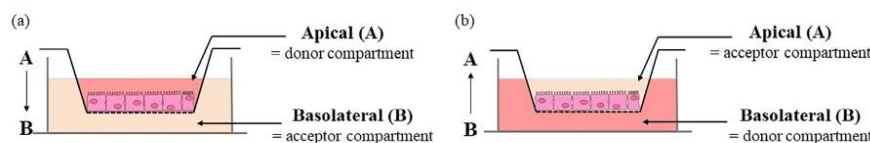


Fig. 1. Schematic representation of the bidirectional permeability of S-nitrosothiols across the Caco-2 monolayer. (a) From the apical (intestinal lumen) to the basolateral (bloodstream) compartment (on the left, A → B) to study physiological intestinal permeability, (b) from the basolateral to the apical compartment (on the right, B → A) to study S-nitrosothiol efflux.

in each direction was the same (100  $\mu\text{M}$ ). Since the apical and the basolateral compartments have different volumes (0.5 and 1.5 mL, respectively), the initial amounts of S-nitrosothiol for A-B and for B-A permeability studies were 50 and 150 nmol, respectively.  $\text{NaNO}_2$  treatment (100  $\mu\text{M}$ ) was used as a positive control for nitrite ions permeability. The bidirectional permeability of propranolol (50  $\mu\text{M}$ ) and furosemide (100  $\mu\text{M}$ ), two reference molecules belonging to the high and low permeability class, respectively, was also assessed to surround the permeability of S-nitrosothiols [26,27] and to validate our model faced to the literature.

Permeability tests were conducted during 4 h under orbital shaking (500 rpm) at 37 °C. In the acceptor compartment, S-nitrosothiols were considered as RSNO because the R skeleton carrying NO cannot be identified by the methodology of quantification used. Reference molecules as well as NOx species (RSNO, nitrite ions and nitrate ions) were quantified after 1 h (entire volume of acceptor compartment removed) in the acceptor compartment and after 4 h in both compartments (for methodologies, see Sections 2.5. and 2.6.). RSNO and nitrite ions were also quantified inside the cells after 1 h and 4 h of permeability study.

At the end of the study, the integrity of the intestinal cell monolayer was checked by measuring the TEER value and the permeability of sodium fluorescein (5  $\mu\text{M}$ ), a marker of low paracellular permeability. A TEER value higher than 300  $\Omega\cdot\text{cm}^2$  as well as a 5% of fluorescein permeability validated the integrity of the intestinal monolayer at the end of the experiment [28,29].

## 2.5. Quantification of S-nitrosothiols, nitrite and nitrate ions

S-Nitrosothiols and nitrite ions were immediately quantified using a fluorimetric method [30] with standard curves of GSNO and sodium nitrite, respectively (Table 1). Briefly,  $\text{N}_2\text{O}_3$  generated from acidified nitrite ions reacts with DAN in the presence (for RSNO) or absence (for nitrite ions) of  $\text{HgCl}_2$  producing 2,3-naphthotriazole that emits fluorescence at 415 nm after excitation at 375 nm (JASCO FP-8300, France). Nitrate ions quantification, using a standard curve of sodium nitrate included a reduction step to nitrite ions by reacting with nitrate reductase and its cofactors before the addition of DAN reagent (fluorimetric kit nitrite/nitrate Cayman Chemical) (Table 1). The concentration of nitrite ions (DAN assay) was subtracted from the value obtained by DAN- $\text{Hg}^{2+}$  quantification to obtain the RSNO concentration and from the nitrate reductase quantification to obtain the nitrate ions concentration. The cumulative amounts of RSNO,  $\text{NO}_2^-$  and  $\text{NO}_3^-$  crossing the Caco-2 monolayer were calculated from the concentrations measured at 1 h and 4 h of the permeability studies in the acceptor

compartment.

For intracellular quantifications, cells were lysed in 50 mM Tris buffer pH 6.8 added with 150 mM of NaCl, 1% of Igepal CA-630 (v/v), 0.1% of SDS (v/v), 1 mM of EDTA, 0.1 mM of neocuproine, 20 mM of sodium tetraborate and 10 mM of NEM.

## 2.6. Quantification of furosemide and propranolol

This procedure was adapted from [31–33] for propranolol and from [34] for furosemide. Briefly, the separation was performed on a C18 analytical column (Macherey-Nagel LiChrospher RP 18e; 5  $\mu\text{m}$ ; 125  $\times$  4 mm) eluted with a mobile phase composed of acetonitrile added with 14 mM triethylamine in water buffered with orthophosphoric acid, pH 2.5 (30/70; v/v) at a flow rate of 1.0 mL  $\text{min}^{-1}$  and with a column temperature of 40 °C. The injection volume was 20  $\mu\text{L}$ . Propranolol and furosemide were detected using a spectrofluorometric detector (model Jasco FP-920) set at  $\lambda_{\text{exc}} = 230 \text{ nm}$ / $\lambda_{\text{em}} = 340 \text{ nm}$ , and  $\lambda_{\text{exc}} = 235 \text{ nm}$ / $\lambda_{\text{em}} = 402 \text{ nm}$ , respectively. Standard curves of propranolol and furosemide were established between 0.5 and 10.0  $\mu\text{M}$  and 62.5 nM to 2.0  $\mu\text{M}$ , respectively.

## 2.7. Calculation of apparent permeability coefficients and recovery rates

### 2.7.1. Apparent permeability coefficient

The apparent permeability coefficient (Papp) values were calculated using the following equation (Eq. (1)):

$$P_{\text{app}} = \frac{dQ}{dt} \times \frac{1}{A \times C_0} \quad (1)$$

$dQ/dt$  ( $\text{mol.s}^{-1}$ ) refers to the permeability rate of reference molecules, RSNO or NOx species (mol) in the acceptor compartment at the time ( $s$ ) of quantification,  $A$  ( $\text{cm}^2$ ) refers to membrane diffusion area, and  $C_0$  ( $\text{mol.mL}^{-1}$  or  $\text{mol.cm}^{-3}$ ) refers to the initial concentration in the donor compartment.

### 2.7.2. Recovery rate

Mass balance was calculated as the addition of the amount of drug recovered in the acceptor compartment after each interval and in the donor compartment at the end of the experiment.

## 2.8. Statistical analysis

Results are shown as mean  $\pm$  standard deviation (SD), based on 3 or 4 independent experiments in duplicate. Values were compared with

Table 1

Standard curves validation parameters for S-nitrosothiols (RSNO), nitrite ions ( $\text{NO}_2^-$ ) and nitrate ions ( $\text{NO}_3^-$ ) in HBSS with  $\text{Ca}^{2+}/\text{Mg}^{2+}$ . Mean  $\pm$  SD;  $n = 3$ .

	Concentration range ( $\mu\text{M}$ )	Standard curves equation	Relative standard deviation (%)	$R^2$
RSNO	0.1–2.0	$y = (1451 \pm 236)x + (399 \pm 98)$	0.1 $\mu\text{M}$ : 12.3 2 $\mu\text{M}$ : 1.2	0.99
$\text{NO}_2^-$		$y = (1527 \pm 96)x + (435 \pm 89)$	0.1 $\mu\text{M}$ : 4.3 2 $\mu\text{M}$ : 3.2	
$\text{NO}_3^-$	0.01–3.75	$y = (264 \pm 22)x + (1719 \pm 116)$	0.01 $\mu\text{M}$ : 8.4 3.75 $\mu\text{M}$ : 5.1	



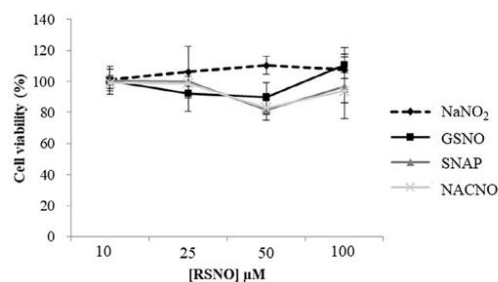


Fig. 2. Cytocompatibility of *S*-nitrosothiols with Caco-2 cells. Cell activity was assessed with the MTT test, 24 h after incubation with different *S*-nitrosothiols or NaNO<sub>2</sub>. Values are expressed as mean  $\pm$  SD of three independent experiments done in duplicate.

one-way ANOVA (treatments) or two-way ANOVA (treatment and time) followed by a Bonferroni's post-test using the Graphpad Prism 5 software;  $p < 0.05$  was considered as statistically significant. Statistics are analysed excluding NaNO<sub>2</sub> treatments, which too high permeability values interfered with the statistical comparison of *S*-nitrosothiols.

### 3. Results

#### 3.1. Cytocompatibility

Cell viability was not affected by any of the *S*-nitrosothiols presently tested and NaNO<sub>2</sub>, with more 80% of viability independently of the concentration used (Fig. 2). For all the forthcoming experiments, a concentration of 100  $\mu$ M of each *S*-nitrosothiol will be safely used.

Table 2

Values of apparent permeability coefficient (Papp) for NOx species (RSNO + NO<sub>2</sub><sup>-</sup> + NO<sub>3</sub><sup>-</sup>) and the RSNO molecular form after 4 h of permeation from the apical to the basolateral compartment. nd: not determined, LOQ: Limit of quantification. Mean  $\pm$  SD of four independent experiments done in duplicate.

Treatments	NOx Papp ( $\times 10^{-6}$ cm.s <sup>-1</sup> )	RSNO Papp ( $\times 10^{-6}$ cm.s <sup>-1</sup> )
GSNO	2.6 $\pm$ 0.9	0.2 $\pm$ 0.1
NACNO	5.0 $\pm$ 2.1	0.21 $\pm$ 0.08
SNAP	3.3 $\pm$ 1.6	0.13 $\pm$ 0.09
NaNO <sub>2</sub>	12.3 $\pm$ 3.2	Under LOQ
Propranolol	24.4 $\pm$ 1	nd
Furosemide	0.3 $\pm$ 0.1	nd

#### 3.2. *S*-Nitrosothiols permeability from the apical to the basolateral compartment

*S*-Nitrosothiols permeation through the intestinal barrier model, evaluated in the A-B direction, showed the same profile for each treatment (GSNO, NACNO and SNAP) (Fig. 3). Each *S*-nitrosothiol (treatment) was permeated under three different chemical species. The RSNO form (Fig. 3A) was less permeated (0.50%  $\pm$  0.14% of the initial amount deposited in the donor compartment) than the NO<sub>2</sub><sup>-</sup> (the first stable oxidation degree of NO in aqueous media) and NO<sub>3</sub><sup>-</sup> ionic forms (4.8%  $\pm$  1.9% and 7.9%  $\pm$  2.4% of the initial amount, respectively). The NACNO treatment led to a higher permeation under the RSNO form than the GSNO and SNAP treatments (Fig. 3A). The duration of the study has no impact on the permeability of each treatment under the RSNO form while the permeability under the nitrite ions and nitrate ions (the oxidation product of nitrite ions) forms depended on time (Fig. 3B and 3C,  $p_{\text{time}} < 0.05$ ) and on the treatment. Indeed, the NACNO treatment induced a higher absorption of NO<sub>2</sub><sup>-</sup> (and NO<sub>3</sub><sup>-</sup>) ionic forms than the GSNO and the SNAP treatments

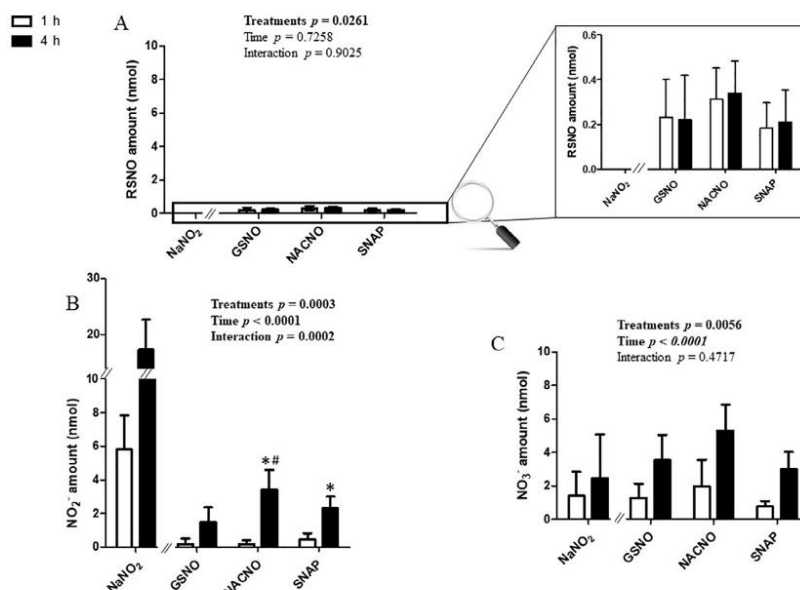


Fig. 3. Apical (pH 7.4) to basolateral compartment – Quantification in the basolateral compartment of permeated (A) RSNO, (B) NO<sub>2</sub><sup>-</sup> and (C) NO<sub>3</sub><sup>-</sup> after 1 h and 4 h of exposure to 50 nmol of each treatment. Results are shown as mean  $\pm$  SD of four independent experiments done in duplicate and are compared using two-way ANOVA ( $p_{\text{treatment}}$  (GSNO, NACNO, SNAP; excluding NaNO<sub>2</sub>),  $p_{\text{time}}$  (1 h, 4 h) and  $p_{\text{interaction}}$ ). \* vs. GSNO; # vs. SNAP at the same time;  $p < 0.05$  (Bonferroni's multiple comparisons test).

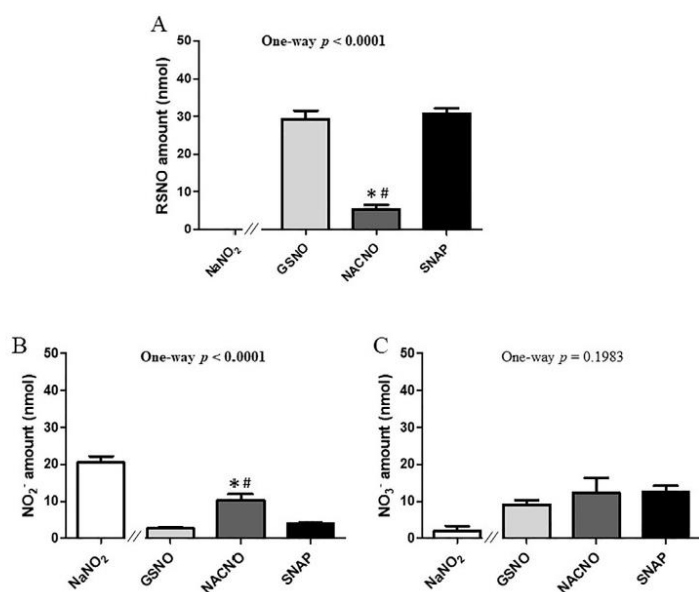


Fig. 4. Apical (pH 7.4) o basolateral compartment – Quantification in the apical compartment of remaining (A) RSNO, (B)  $\text{NO}_2^-$  and (C)  $\text{NO}_3^-$  and 4 h of exposure to 50 nmol of each treatment. Results are shown as mean  $\pm$  SD of four independent experiments done in duplicate and are compared using one-way ANOVA (excluding  $\text{NaNO}_2$ ) Bonferroni post-test. \* vs. GSNO; # vs. SNAP at the same time;  $p < 0.05$ .

Table 3

Mass balance for each treatment (initial amount: 50 nmol) after 4 h of permeation from the apical to the basolateral compartment. Mean  $\pm$  SD of four independent experiments done in duplicate.

Treatments	Amount (nmol)	Percentage of initial amount
GSNO	46 $\pm$ 4	92 $\pm$ 8
NACNO	38 $\pm$ 6	77 $\pm$ 12
SNAP	53 $\pm$ 7	106 $\pm$ 13
$\text{NaNO}_2$	41 $\pm$ 8	83 $\pm$ 16

( $p_{\text{treatment}} = 0.0003$  and  $p_{\text{interaction}} = 0.0002$ ), especially after 4 h ( $p_{\text{time}} < 0.0001$ ) (Fig. 3B).

The  $\text{NaNO}_2$  treatment led to the permeability of the two ionic species only (Fig. 3). The permeability under the  $\text{NO}_2^-$  form was time

dependent and 30% higher than the permeability of each S-nitrosothiol treatment under  $\text{NO}_2^-$  form (Fig. 3B). The permeability under the nitrate ionic form (Fig. 3C), representing 5% of the initial amount, supposes a spontaneous oxidation of nitrite ions into nitrate ions within our experimental conditions (presence of dioxygen).

The Papp values for the NOx species (addition of RSNO,  $\text{NO}_2^-$  and  $\text{NO}_3^-$ ) were situated within the medium class of permeability (BCS definition) for each S-nitrosothiol treatment and surrounded by the Papp values of the reference drugs, propranolol and furosemide (Table 2). The permeability of S-nitrosothiols under the RSNO form was 25–40 times lower ( $\text{Papp} \approx 0.17 \times 10^{-6} \text{ cm.s}^{-1}$ ) than that of NOx species, confirming the higher absorption of S-nitrosothiols under the  $\text{NO}_2^-$  and  $\text{NO}_3^-$  ionic forms. The  $\text{NaNO}_2$  treatment allowed to define a high permeability under the  $\text{NO}_2^-$  ionic form.

After 4 h of permeability, 60% of the initial amount (50 nmol) of S-

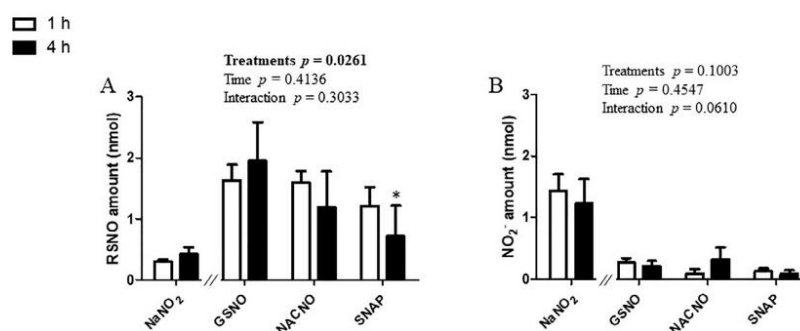
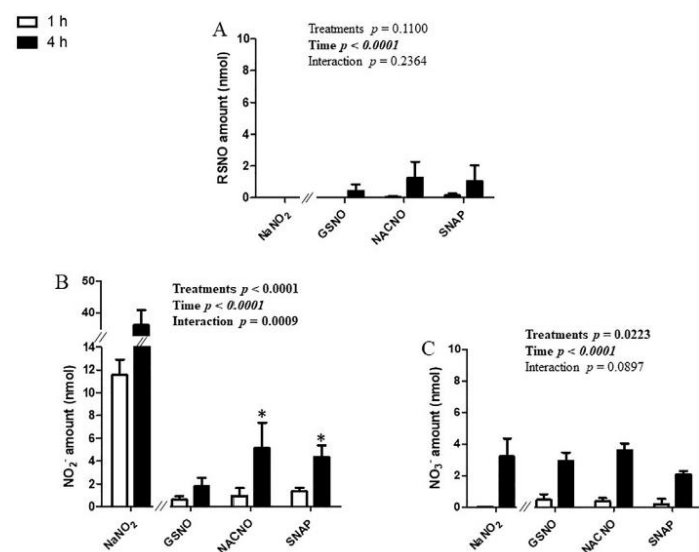


Fig. 5. Apical (pH 7.4) to basolateral permeability – Intracellular quantifications of (A) RSNO, (B)  $\text{NO}_2^-$ , (subtracted from the control cells) after 1 h and 4 h of exposure to 50 nmol of each treatment. Results are shown as mean  $\pm$  SD of four independent experiments done in duplicate and are compared using two-way ANOVA ( $p_{\text{treatment}}$  (GSNO, NACNO, SNAP; excluding  $\text{NaNO}_2$ ),  $p_{\text{time}}$  (1h, 4 h) and  $p_{\text{interaction}}$ ). \* vs. GSNO at the same time;  $p < 0.05$  (Bonferroni's multiple comparisons test).



**Fig. 6.** Basolateral to Apical permeability – Quantification in the apical compartment of permeated (A) RSNO, (B) NO<sub>2</sub><sup>-</sup> and (C) NO<sub>3</sub><sup>-</sup> after 1 h and 4 h from 150 nmol of each treatment. Results are shown as mean ± SD of four independent experiments done in duplicate and are compared using two-way ANOVA ( $p_{\text{treatment}}$  (GSNO, NACNO, SNAP; excluding NaNO<sub>2</sub>),  $p_{\text{time}}$  (1h, 4 h) and  $p_{\text{interaction}}$ ). \* vs. GSNO at the same time;  $p < 0.05$  (Bonferroni's multiple comparisons test).

**Table 4**

Values of apparent permeability coefficient (Papp) for NOx species (RSNO + NO<sub>2</sub><sup>-</sup> + NO<sub>3</sub><sup>-</sup>) and the RSNO form after 4 h of permeation from basolateral to apical compartment. nd: not determined, LOQ: Limit of quantification. Mean ± SD of four independent experiments done in duplicate.

Treatments	NOx Papp ( $\times 10^{-6}$ cm.s <sup>-1</sup> )	RSNO Papp ( $\times 10^{-6}$ cm.s <sup>-1</sup> )
GSNO	2.8 ± 1.2	0.3 ± 0.2
NACNO	4.5 ± 1.5	0.6 ± 0.6
SNAP	4.1 ± 0.7	0.5 ± 0.5
NaNO <sub>2</sub>	97.5 ± 16.4	Under LOQ
Propranolol	33.1 ± 0.8	nd
Furosemide	15.2 ± 0.8	nd

nitrosothiols remained in the apical compartment for the GSNO and SNAP treatments, and only 10% for the NACNO treatment (Fig. 4A). Furthermore, the NACNO treatment led to a higher amount of nitrite ions remaining in the apical compartment compared to the GSNO and SNAP treatments (Fig. 4B), suggesting a higher degradation of NACNO into NO<sub>2</sub><sup>-</sup>. Non-permeated nitrate ions amounts were around 23% for each treatment (Fig. 4C). The NaNO<sub>2</sub> treatment was still presenting 41% of non-permeated nitrite ions after 4 h (Fig. 4B) and lower spontaneous oxidation into nitrate ions (4%) within the apical compartment compared to S-nitrosothiol treatments (Fig. 4C).

Finally, the calculation of the mass balance (addition of all species quantified in the two compartments) after 4 h of permeability study, showed 83 ± 16% to 106 ± 13% of recovery for GSNO, SNAP and NaNO<sub>2</sub> (Table 3). Nevertheless, the NACNO treatment showed a loss of 23% of the initial amount deposited in the apical compartment. This missing can be trapped inside the cell monolayer, so cells were lysed and only RSNO and nitrite ions were quantified. Indeed, due to intracellular reducing power [35], the nitrate ions cannot exist inside cells. Quantities of RSNO found inside the cells were higher for S-nitrosothiol treatments than for the NaNO<sub>2</sub> treatment (Fig. 5A). This was the opposite for the NO<sub>2</sub><sup>-</sup> intake (Fig. 5B). For each S-nitrosothiol treatment, the intracellular incorporation of the RSNO form was higher than the nitrite ions form. Intracellular quantity of the RSNO form depended on the S-nitrosothiol chemical structure ( $p_{\text{treatment}} < 0.05$ )

with the lowest incorporation obtained for the SNAP treatment (< 2% of the initial amount) (Fig. 5A). Intracellular incorporation of nitrite ions was independent on time and treatments (Fig. 5B).

For intracellular quantification, the surface area of cells was increased 4.17 times (from 1.12 to 4.67 cm<sup>2</sup>) in order to be able to quantify NOx species inside the cells. So, the intracellular amounts of RSNO and NO<sub>2</sub><sup>-</sup> form were divided by 4.17 to calculate the mass balance (Table 2). The intracellular incorporation of RSNO and NO<sub>2</sub><sup>-</sup> represented only 1.1%, 1.0% and 0.4% of the initial amount, for the GSNO, NACNO and SNAP treatments, respectively. Therefore, 22% of the initial amount are still missing for the NACNO treatment.

### 3.3. S-Nitrosothiols permeability from the basolateral to apical compartment

In order to determine the permeability modality (passive vs. active) for each S-nitrosothiol, the study was carried out in the opposite direction, from the basolateral to the apical compartment.

In this condition, the permeability of the RSNO form (Fig. 6A) was only dependent on time for each S-nitrosothiol treatment. The permeability of the NO<sub>2</sub><sup>-</sup> and NO<sub>3</sub><sup>-</sup> ionic forms was dependent on time and treatment (Fig. 6B and 6C). Higher amounts were permeated under the NO<sub>2</sub><sup>-</sup> ionic form for the NACNO and SNAP treatments (≈ 3% of initial amounts) compared to the GSNO treatment (1.2% of initial amount, Fig. 6B). As in the experiments performed from the apical to the basolateral compartment (Section 3.2), NO<sub>2</sub><sup>-</sup> and NO<sub>3</sub><sup>-</sup> were the major permeated species.

For each S-nitrosothiol treatment, the Papp values in both directions (apical to basolateral versus basolateral to apical) were equivalent (Tables 2 and 4), the S-nitrosothiols intestinal permeability can be postulated as a passive diffusion [36]. This postulate is also based on the validation of our intestinal barrier model comparing the Papp values of reference molecules with the literature [19]. Propranolol with equivalent bidirectional Papp values follows a passive diffusion whereas furosemide with a higher Papp value from basolateral to apical than from apical to basolateral, follows an active efflux transport.

After 4 h of permeability study, 95% of the initial amount (150 nmol) of each S-nitrosothiol treatment remained unpermeated



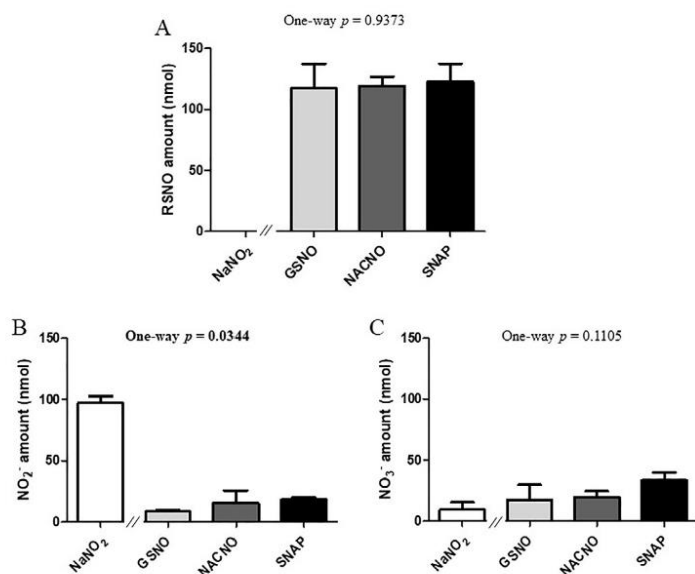


Fig. 7. Basolateral to apical permeability – Quantification in the basolateral compartment of remaining (A) RSNO, (B) NO<sub>2</sub><sup>-</sup> and (C) NO<sub>3</sub><sup>-</sup> after 4 h of exposure to 150 nmol of each treatment. Results are shown as mean  $\pm$  SD of four independent experiments done in duplicate and are compared using one-way ANOVA (excluding NaNO<sub>2</sub>).

Table 5

Mass balance for each tested treatment (initial amount 150 nmol) after 4 h of permeability from the basolateral to the apical compartment. Mean  $\pm$  SD of four independent experiments done in duplicate.

Treatments	Amount (nmol)	Percentage of the initial amount
GSNO	169 $\pm$ 40	113 $\pm$ 36
NACNO	159 $\pm$ 24	106 $\pm$ 21
SNAP	162 $\pm$ 49	108 $\pm$ 44
NaNO <sub>2</sub>	155 $\pm$ 18	103 $\pm$ 17

(Fig. 7). The amounts of unpermeated NO<sub>2</sub><sup>-</sup> ions (Fig. 7B) were the only form that depended on *S*-nitrosothiol chemical structure ( $p_{\text{treatment}} = 0.0344$ ). As *S*-nitrosothiols are separated from cells by the porous membrane of the device, they cannot be metabolised by cell membrane enzymes showing the great importance of *S*-nitrosothiol metabolism in their permeability. Furthermore, the high amount of remaining RSNO form (Fig. 7A) attested from the stability of each *S*-nitrosothiol in our operating conditions.

This also showed that the degradation of *S*-nitrosothiols into ionic forms observed in the apical to basolateral permeability study (Fig. 4) was due to cell membrane enzymes activity. Finally, the study of *S*-nitrosothiols permeability from the basolateral to the apical compartment showed a mass balance of 100% for each *S*-nitrosothiol treatment (Table 5).

### 3.4. Influence of the apical pH on *S*-nitrosothiols permeability

The principal site of absorption of small molecules including peptides and amino acids is the jejunum part of the intestine, which physiological pH ranges from 6 to 7. In order to study the permeability of *S*-nitrosothiols close to physiological conditions, the pH of the apical compartment mimicking the intestinal lumen was shifted of one log from pH 7.4 to pH 6.4. pH acidification has no impact on propranolol and furosemide permeability [27], so the experiment was not performed.

At pH 6.4, the permeability of each *S*-nitrosothiol under the RSNO

and the ionic forms (Fig. 8) followed the same profile than at pH 7.4 (Fig. 3). However, the NACNO treatment showed a 7 times increase of permeability under the RSNO form (Fig. 8A) compared to pH 7.4. The NaNO<sub>2</sub> treatment showed a permeability under the RSNO form (Fig. 8A) and a large (10 times at 1 h and 20 times at 4 h) increase of the permeability under the NO<sub>3</sub><sup>-</sup> form (Fig. 8C). So, at pH 6.4, the Papp values of NOx species and RSNO form rose for the NaNO<sub>2</sub> treatment (Table 6) compared to pH 7.4 (Table 2).

The Papp values at pH 6.4 (Table 6) maintained each *S*-nitrosothiol in the medium class of permeability for NOx species and in the low permeability class for the RSNO form. However, the Papp value of the NACNO treatment under the RSNO form increased from  $0.21 \pm 0.08 \times 10^{-6} \text{ cm.s}^{-1}$  (Table 2) at pH 7.4 to  $0.9 \pm 0.7 \times 10^{-6} \text{ cm.s}^{-1}$  at pH 6.4, bringing NACNO close to the medium permeability class (from 1 to  $10 \times 10^{-6} \text{ cm.s}^{-1}$ , [19]).

The distribution of non-permeated species remaining in the apical compartment after 4 h of permeability at pH 6.4 (Fig. 9) was similar to that at pH 7.4 (Fig. 4).

The absorption of *S*-nitrosothiols from the apical compartment at pH 6.4 to the basolateral compartment at pH 7.4 presented a mass balance from 58% to 78% of the initial amount (Table 7).

## 4. Discussion

The human intestinal barrier model based on Caco-2 cells is widely used in the pharmaceutical industry to determine the parameters of intestinal permeability of new drugs. The results obtained depend mainly on cell culture parameters (time, medium and age [29]). In the present study, we validated our conditions using two reference molecules, *i.e.* propranolol and furosemide, in comparison with already published Papp values. These Papp values, as well as TEER values ( $> 500 \Omega \cdot \text{cm}^2$ ), are quality guaranties of our model and results. From the literature, propranolol, with a Papp value between  $3.30 \times 10^{-6}$  and  $41.90 \times 10^{-6} \text{ cm.s}^{-1}$  [26,27] belongs to the high permeability class, and furosemide, with a Papp value varying from  $0.04 \times 10^{-6}$  to  $0.11 \times 10^{-6} \text{ cm.s}^{-1}$  [26,37] belongs to the low permeability class. Such a low permeability for furosemide was attributed to an efflux



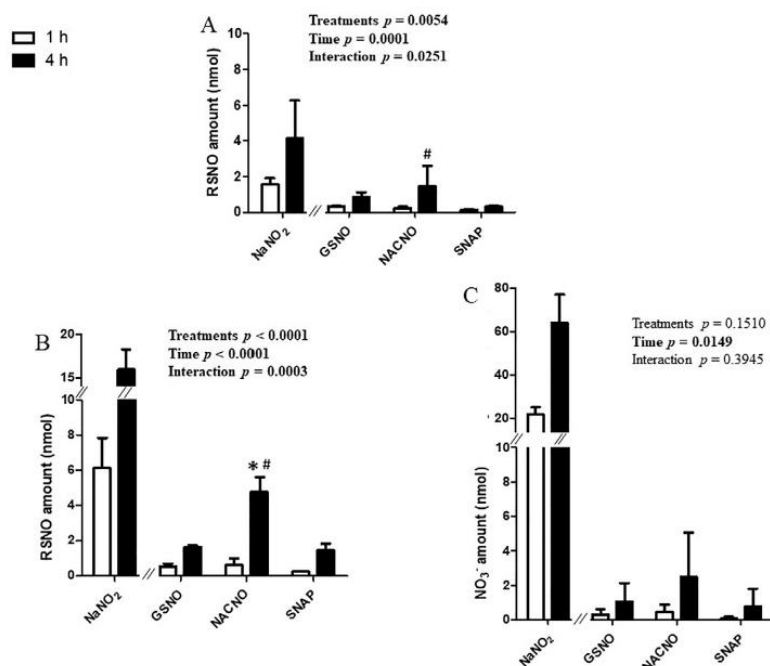


**Fig. 8.** Apical pH 6.4 to Basolateral permeability – Quantification in the basolateral compartment of remaining (A) RSNO, (B) NO<sub>2</sub><sup>-</sup> and (C) NO<sub>3</sub><sup>-</sup> after 1h and 4h of exposure to 50 nmol of each treatment. Results are shown as mean  $\pm$  SD of three independent experiments done in duplicate and are compared using two-way ANOVA ( $p_{\text{treatment}}$  (GSNO, NACNO, SNAP; excluding NaNO<sub>2</sub>),  $p_{\text{time}}$  (1h, 4h) and  $p_{\text{interaction}}$ ). \* vs. GSNO; # vs. SNAP at the same time;  $p < 0.05$  (Bonferroni's multiple comparisons test).

**Table 6**

Values of apparent permeability coefficient (Papp) for NO<sub>x</sub> species (RSNO + NO<sub>2</sub><sup>-</sup> + NO<sub>3</sub><sup>-</sup>) and the RSNO form after 4h of permeability study from the apical compartment (pH 6.4) to the basolateral compartment (pH 7.4). Mean  $\pm$  SD of three independent experiments done in duplicate.

Treatments	NO <sub>x</sub> Papp ( $\times 10^{-6}$ cm.s <sup>-1</sup> )	RSNO Papp ( $\times 10^{-6}$ cm.s <sup>-1</sup> )
GSNO	1.9 $\pm$ 0.6	0.5 $\pm$ 0.2
NACNO	4.8 $\pm$ 2.4	0.9 $\pm$ 0.7
SNAP	1.4 $\pm$ 0.8	0.20 $\pm$ 0.05
NaNO <sub>2</sub>	207.0 $\pm$ 37.9	7.7 $\pm$ 6.5

driven by the intestinal P-glycoprotein to the luminal direction [38]. The Papp values for propranolol ( $24.4 \times 10^{-6}$  cm.s<sup>-1</sup>) and furosemide ( $0.3 \times 10^{-6}$  cm.s<sup>-1</sup>) obtained using our intestinal barrier model confirm the already published values and probably attest for the presence and activity of the P-glycoprotein in this model.

S-Nitrosothiols are NO donors allowing the release of NO with a relative short half-life (within a few hours) [2]. Thereby, in aqueous medium, NO is spontaneously and quickly oxidized into nitrite and nitrate ions. So, it is mandatory to study the intestinal permeability of these ionic species as well as the permeability of the RSNO form to evaluate the bioavailability of NO in the blood stream after oral administration. In the present study, each S-nitrosothiol increased their permeability following time, in each of the three proposed conditions (apical to basolateral compartments at pH 7.4 direction, opposite direction, apical compartment at pH 6.4 to basolateral compartment at pH 7.4).

The study of S-nitrosothiols permeability from the compartment mimicking the intestinal lumen (apical compartment) to the compartment mimicking the lumen of blood vessels (basolateral compartment) revealed a weak absorption of each S-nitrosothiol treatment under the RSNO form compared to the ionic species, which are the major absorbed species (Fig. 10A). In a general point of view, the ionic species are more absorbed by the intestine than the neutral molecules. Indeed, specific ionic transporters such as the Organic Cation Transporters

(OCT) and the Zwitterion Transporters (OCTN), implied in the absorption of Na<sup>+</sup> and Ca<sup>2+</sup>, are expressed within the intestinal tissue and Caco-2 cells [39,40].

The Papp values of all permeated species placed each S-nitrosothiol studied within the medium permeability class for NO<sub>x</sub> species, class that was surrounded by our two reference molecules (propranolol and furosemide). The Papp value was the same for each S-nitrosothiol even if they presented different physico-chemical properties with a higher hydrophilicity for GSNO than SNAP [2]. In this way, the physico-chemical properties of the skeleton (R) carrying the nitroso group are not prevalent for the intestinal permeability of the S-nitrosothiols. The mass balance within both compartments allowed a recovery of 100% of the initial amount deposited for the SNAP treatment. The small missing amount for the GSNO treatment was recovered by the intracellular quantification, rising the mass balance to almost 100%. However, the NACNO treatment showed a mass balance of 75%, which was not completed to 100% after intracellular quantification.

The amount of NO<sub>x</sub> species found inside the cells was higher for the GSNO treatment than for the SNAP treatment, with the NACNO treatment situated between each other. SNAP promotes drug intestinal absorption [41] by opening tight junctions without affecting barrier integrity. Indeed, SNAP increases insulin rectal absorption, transepithelial transport of fluorescein sulfonic acid (low absorbable molecule) [41,42] and macromolecules absorption through the thickening by the reversible opening of tight junctions [41,43,44] and a thickening of ileal mucosal membrane [45]. So, in our study, paracellular absorption of SNAP can be speculated. GSNO and NACNO were partially absorbed via a trans-cellular pathway. The mass imbalance observed for the NACNO treatment can be attributed to its higher metabolism within the apical compartment. Moreover, the metabolism of each S-nitrosothiol was abolished in the donor compartment when studying the permeability from the basolateral to the apical compartments. This phenomenon is a proof of the intestinal barrier orientation with a brush border including metabolic enzymes like redoxins and gamma-glutamyl transferase [46], faced to the apical compartment, and a basal lamina without any metabolic activity faced to the basolateral compartment.

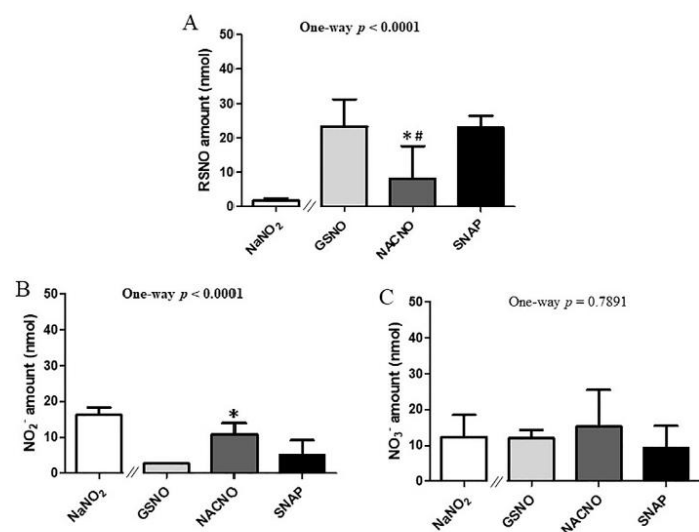


Fig. 9. Apical (pH 6.4) to basolateral compartment – Quantification in the apical compartment of remaining (A) RSNO, (B) NO<sub>2</sub><sup>-</sup> and (C) NO<sub>3</sub><sup>-</sup> after 1 h and 4 h of exposure to 50 nmol of each treatment. Results are shown as mean  $\pm$  SD of three independent experiments done in duplicate and are compared using one-way ANOVA (excluding NaNO<sub>2</sub>). \* vs. GSNO; # vs. SNAP at the same time;  $p < 0.05$  (Bonferroni post-test).

Table 7

Mass balance for all tested treatments (initial amount 50 nmol) after 4 h of permeability from the apical compartment at pH 6.4 to the basolateral compartment at pH 7.4. Mean  $\pm$  SD of three independent experiments done in duplicate.

Treatments	Amount (nmol)	Percentage of the initial amount
GSNO	34 $\pm$ 10	68 $\pm$ 20
NACNO	37 $\pm$ 10	78 $\pm$ 20
SNAP	31 $\pm$ 5	58 $\pm$ 8
NaNO <sub>2</sub>	114 $\pm$ 18	227 $\pm$ 35

The equal Papp values obtained permeability studies from the apical to the basolateral compartments and permeability studies from the basolateral to the apical compartments revealed that the absorption of S-nitrosothiols is driven by a passive diffusion through the intestinal barrier (Fig. 10B). This transport modality excluded the participation of all transport systems and energy consumption in the permeability of S-nitrosothiols [47]. In that way, S-nitrosothiols permeability may be improved using pharmaceutical formulations, which are aimed at opening tight junctions and increasing the local concentration and the residence time of the molecule.

Finally, the acidification (pH 6.4) of the apical compartment to mimic the physiological condition of the jejunum part of the intestine (Fig. 10C) showed a permeability dependent on the S-nitrosothiol treatment. The very low permeability of the RSNO form for the NACNO treatment at pH 7.4 was multiplied by ten at pH 6.4. However, this favoured permeability of NACNO seemed to be related neither to the lipophilic balance – as NACNO showed a log P intermediate between GSNO and SNAP – nor to the ionization state – as the isoelectric point (pI) of NACNO is intermediate (3.24) between GSNO and SNAP (4.8 and 4.85, respectively) and far away from the studied pHs. As the thiol functions are blocked by NO, their pKa values are not involved in the pI of the S-nitrosothiols. However, it may be involved in the stability of the S-NO bound, e.g. the S-nitrosocysteine (cysNO) is less stable than GSNO due to a lower pKa of the thiol function of the cysteine residue. The permeability of the RSNO form for the NaNO<sub>2</sub> treatment suggested that pH 6.4 favoured the formation of RSNO starting from NO<sub>2</sub><sup>-</sup>. This can also be postulated for all the experiments where permeability of the

RSNO forms was observed. However, the formation of RSNO following the NaNO<sub>2</sub> treatment should certainly occur thanks to intracellular thiols, which are the only available source of thiol in the experimental system. This phenomenon will lead to cell thiol depletion, which will induce tolerance at it was already seen in clinics for organic nitrate treatments [48]. However, our experiments showed that S-nitrosothiol treatments bringing the thiol function itself, won't induce thiol depletion neither tolerance phenomenon. Furthermore, Pinheiro and coworkers demonstrated that oral administration of nitrite ions allowed the formation of RSNO in the stomach leading to an increased plasma RSNO concentration [17]. Our work precises that the formation of RSNO may also occur in the jejunum part of the intestine at acidic pH.

Finally, according to the BCS, S-nitrosothiols can be classified between class I and class III, regarding their high solubility and medium permeability. From Le Ferrec et al. [49], the result obtained *in vitro* with high permeability molecules (class I and class II) can be easily transposed to *in vivo* intestinal absorption unlike results obtained for low permeability molecules (class III and class IV). So, the S-nitrosothiols included in the medium class of permeability can be considered as drugs suitable for oral administration. Thereafter, it would be interesting to study the permeability of S-nitrosothiols in the presence of albumin in the basolateral compartment to mimic the blood stream compartment [50]. Furthermore, albumin including a free reduced cysteine residue in position 34 will increase the amount of RSNO found in the basolateral compartment through S-nitrosation process.

In conclusion, our study suggested that S-nitrosothiols can be administered by the oral route to be absorbed at the intestinal level, mainly in the jejunum part. The passive diffusion of S-nitrosothiols under three different kinds of species such as nitrite and nitrate ions and the RSNO form was demonstrated using a model of human intestinal barrier. The permeation of the RSNO species will improve the interest for S-nitrosothiols oral administration compared to nitrite ions. Indeed, S-nitrosothiols would not deplete the intracellular stock of reduced thiols. Even if S-nitrosothiols are good candidates for NO oral supplementation, they will need appropriate protection from enzymatic degradation using nanotechnologies [20,51–53].



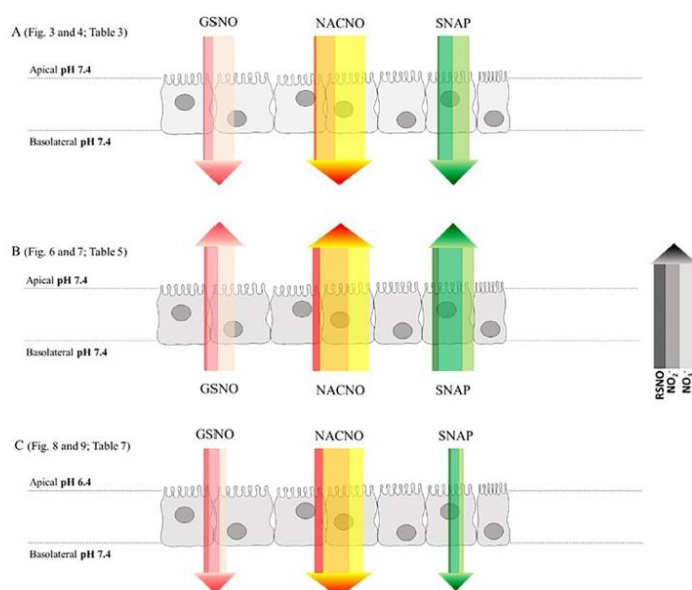


Fig. 10. Summary of NO<sub>x</sub> species permeability for each S-nitrosothiol treatment. The colour code of each arrow from the left to the right is the amount (width) of RSNO, NO<sub>2</sub><sup>-</sup> and NO<sub>3</sub><sup>-</sup>. The 4 h-permeability for each treatment is represented from (A) apical to basolateral compartment, (B) basolateral to apical compartment and (C) apical (pH 6.4) to basolateral compartment (pH 7.4).

## Acknowledgments

The authors acknowledge Dr Wen WU for her help in preliminary experiment settings. The CITHEFOR EA3452 lab was supported by the "Impact Biomolecules" project of the "Lorraine Université d'Excellence" (Investissements d'avenir – ANR).

## References

- [1] T.S. Hakim, K. Sugimori, E.M. Camporesi, G. Anderson, Half-life of nitric oxide in aqueous solutions with and without haemoglobin, *Physiol. Meas.* 17 (1996) 267–277.
- [2] C. Gaucher, A. Boudier, F. Dabboul, M. Parent, P. Leroy, S-nitrosation/denitrosation in cardiovascular pathologies: facts and concepts for the rational design of S-nitrosothiols, *Curr. Pharm. Des.* 19 (2013) 458–472.
- [3] Z. Kaposzta, P.A. Baskerville, D. Madge, S. Fraser, J.F. Martin, H.S. Markus, L-Arginine and S-nitrosoglutathione reduce embolization in humans, *Circulation* 103 (2001) 2371–2375.
- [4] Z. Kaposzta, A. Clifton, J. Molloy, J.F. Martin, H.S. Markus, S-nitrosoglutathione reduces asymptomatic embolization after carotid angioplasty, *Circulation* 106 (2002) 3057–3062.
- [5] Z. Kaposzta, J.F. Martin, H.S. Markus, Switching off embolization from symptomatic carotid plaque using S-nitrosoglutathione, *Circulation* 105 (2002) 1480–1484.
- [6] T. Rassaf, P. Kleinbongard, M. Preik, A. Dejam, P. Gharini, T. Lauer, J. Erckenbrecht, A. Duschin, R. Schulz, G. Heusch, M. Feelisch, M. Kelm, Plasma nitrosothiols contribute to the systemic vasodilator effects of intravenously applied NO: experimental and clinical study on the fate of NO in human blood, *Circ. Res.* 91 (2002) 470–477.
- [7] T. Rassaf, L.W. Poll, P. Brouzos, T. Lauer, M. Totzeck, P. Kleinbongard, P. Gharini, K. Andersen, R. Schulz, G. Heusch, U. Mödter, M. Kelm, Positive effects of nitric oxide on left ventricular function in humans, *Eur. Heart J.* 27 (2006) 1699–1705, <http://dx.doi.org/10.1093/eurheartj/ehl096>.
- [8] S. Moncada, A. Higgs, The L-arginine-nitric oxide pathway, *N. Engl. J. Med.* 329 (1993) 2002–2012, <http://dx.doi.org/10.1056/NEJM199312303292706>.
- [9] B. Meyer, A. Genoni, A. Boudier, P. Leroy, M.F. Ruiz-Lopez, Structure and stability studies of pharmacologically relevant S-nitrosothiols: a theoretical approach, *J. Phys. Chem. A* 120 (2016) 4191–4200, <http://dx.doi.org/10.1021/acs.jpca.6b02230>.
- [10] B.A. Maron, S.-S. Tang, J. Loscalzo, S-nitrosothiols and the S-nitrosoproteome of the cardiovascular system, *Antioxid. Redox Signal.* 18 (2013) 270–287, <http://dx.doi.org/10.1089/ars.2012.4744>.
- [11] E. Belcastro, W. Wu, I. Fries-Raeth, A. Corti, A. Pompella, P. Leroy, I. Lartaud, C. Gaucher, Oxidative stress enhances and modulates protein S-nitrosation in smooth muscle cells exposed to S-nitrosoglutathione, *Nitric Oxide Biol. Chem.* 69 (2017) 10–21, <http://dx.doi.org/10.1016/j.niox.2017.07.004>.
- [12] F. Dabboul, P. Leroy, K. Maguin Gate, A. Boudier, C. Gaucher, P. Liminana, I. Lartaud, A. Pompella, C. Perrin-Sarrado, Endothelial  $\gamma$ -glutamyltransferase contributes to the vasorelaxant effect of S-nitrosoglutathione in rat aorta, *PLoS One* 7 (2012) e43190, <http://dx.doi.org/10.1371/journal.pone.0043190>.
- [13] M.H. Krieger, K.F.R. Santos, S.M. Shishido, A.C.B.A. Wanschel, H.F.G. Estrela, L. Santos, M.G. De Oliveira, K.G. Franchini, R.C. Spadari-Bratfisch, F.R.M. Laurindo, Antiatherogenic effects of S-nitroso-N-acetylcysteine in hypercholesterolemic LDL receptor knockout mice, *Nitric Oxide Biol. Chem.* 14 (2006) 12–20, <http://dx.doi.org/10.1016/j.niox.2005.07.011>.
- [14] M. Khan, B. Sekhon, S. Giri, M. Jatana, A.G. Gil, K. Ayasolla, C. Elango, A.K. Singh, I. Singh, S-nitrosoglutathione reduces inflammation and protects brain against focal cerebral ischemia in a rat model of experimental stroke, *J. Cereb. Blood Flow Metab. Off. J. Int. Soc. Cereb. Blood Flow Metab.* 25 (2005) 177–192, <http://dx.doi.org/10.1038/sj.jcbfm.9600012>.
- [15] M. Khan, M. Jatana, C. Elango, A.S. Paintlia, A.K. Singh, I. Singh, Cerebrovascular protection by various nitric oxide donors in rats after experimental stroke, *Nitric Oxide Biol. Chem.* 15 (2006) 114–124, <http://dx.doi.org/10.1016/j.niox.2006.01.008>.
- [16] M. Khan, T.S. Dhammu, M. Baarane, J. Kim, M.K. Paintlia, I. Singh, A.K. Singh, GSNO promotes functional recovery in experimental TBI by stabilizing HIF-1 $\alpha$ , *Behav. Brain Res.* 340 (2018) 63–70, <http://dx.doi.org/10.1016/j.bbr.2016.10.037>.
- [17] L.C. Pinheiro, J.H. Amaral, G.C. Ferreira, R.L. Portella, C.S. Ceron, M.F. Montenegro, J.C. Toledo, J.E. Tanus-Santos, Gastric S-nitrosothiol formation drives the antihypertensive effects of oral sodium nitrite and nitrate in a rat model of renovascular hypertension, *Free Radic. Biol. Med.* 87 (2015) 252–262, <http://dx.doi.org/10.1016/j.freeradbiomed.2015.06.038>.
- [18] M. Levin (Ed.), *Pharm. Process Scale-Up*, Informa Healthcare, 2001, <http://dx.doi.org/10.1201/9780824741969.axh>.
- [19] Y. Peng, P. Yadava, A.T. Heikkinen, N. Parrott, A. Railkar, Applications of a 7-day Caco-2 cell model in drug discovery and development, *Eur. J. Pharm. Sci. Off. J. Eur. Fed. Pharm. Sci.* 56 (2014) 120–130, <http://dx.doi.org/10.1016/j.ejps.2014.02.008>.
- [20] W. Wu, C. Perrin-Sarrado, H. Ming, I. Lartaud, P. Maincent, X.-M. Hu, A. Sapin-Minet, C. Gaucher, Polymer nanocomposites enhance S-nitrosoglutathione intestinal absorption and promote the formation of releasable nitric oxide stores in rat aorta, *Nanomed. Nanotechnol. Biol. Med.* 12 (2016) 1795–1803, <http://dx.doi.org/10.1016/j.nano.2016.05.006>.
- [21] K.A. Broniowska, A.R. Diers, N. Hogg, S-nitrosoglutathione, *Biochim. Biophys. Acta* 2013 (1830) 3173–3181, <http://dx.doi.org/10.1016/j.bbagen.2013.02.004>.
- [22] P. Teixeira, P. Napoleão, G. Saldanha, S-nitrosoglutathione efflux in the erythrocyte, *Clin. Hemorheol. Microcirc.* 60 (2015) 397–404, <http://dx.doi.org/10.3233/CH-141855>.
- [23] L.F. Prescott, R.N. Illingworth, J.A. Critchley, M.J. Stewart, R.D. Adam, A.T. Proudfoot, Intravenous N-acetylcysteine: the treatment of choice for paracetamol poisoning, *Br. Med. J.* 2 (1979) 1097–1100.

- [24] Y. Wang, J. Cao, X. Wang, S. Zeng, Stereoselective transport and uptake of propranolol across human intestinal Caco-2 cell monolayers, *Chirality* 22 (2010) 361–368, <http://dx.doi.org/10.1002/chir.20753>.
- [25] M. Parent, A. Boudier, F. Dupuis, C. Nouvel, A. Sapin, I. Lartaud, J.-L. Six, P. Leroy, P. Maincent, Are in situ formulations the keys for the therapeutic future of S-nitrosothiols? *Eur. J. Pharm. Biopharm. Off. J. Arbeitsgemeinschaft Pharm. Verfahrenstechnik EV* 85 (2013) 640–649, <http://dx.doi.org/10.1016/j.ejpb.2013.08.005>.
- [26] E.H. Kerns, L. Di, S. Petusky, M. Farris, R. Ley, P. Jupp, Combined application of parallel artificial membrane permeability assay and Caco-2 permeability assays in drug discovery, *J. Pharm. Sci.* 93 (2004) 1440–1453, <http://dx.doi.org/10.1002/jps.20075>.
- [27] C. Zhu, L. Jiang, T.-M. Chen, K.-K. Hwang, A comparative study of artificial membrane permeability assay for high throughput profiling of drug absorption potential, *Eur. J. Med. Chem.* 37 (2002) 399–407.
- [28] S.I. Khan, E.A. Abourashed, I.A. Khan, L.A. Walker, Transport of harman alkaloids across Caco-2 cell monolayers, *Chem. Pharm. Bull. (Tokyo)* 52 (2004) 394–397.
- [29] B. Srinivasan, A.R. Kolli, M.B. Esch, H.E. Abaci, M.L. Shuler, J.J. Hickman, TEER measurement techniques for in vitro barrier model systems, *J. Lab. Autom.* 20 (2015) 107–126, <http://dx.doi.org/10.1177/2211068214561025>.
- [30] W.S. Jobgen, S.C. Jobgen, H. Li, C.J. Meininger, G. Wu, Analysis of nitrite and nitrate in biological samples using high-performance liquid chromatography, *J. Chromatogr. B Analyt. Technol. Biomed. Life. Sci.* 851 (2007) 71–82, <http://dx.doi.org/10.1016/j.jchromb.2006.07.018>.
- [31] H.K. Kim, J.H. Hong, M.S. Park, J.S. Kang, M.H. Lee, Determination of propranolol concentration in small volume of rat plasma by HPLC with fluorometric detection, *Biomed. Chromatogr. BMC* 15 (2001) 539–545, <http://dx.doi.org/10.1002/bmc.110>.
- [32] G.S. Rekhi, S.S. Jambekar, P.F. Souney, D.A. Williams, A fluorimetric liquid chromatographic method for the determination of propranolol in human serum/plasma, *J. Pharm. Biomed. Anal.* 13 (1995) 1499–1505.
- [33] J.M. Ryu, S.J. Chung, M.H. Lee, C.K. Kim, C.K. Shim, Increased bioavailability of propranolol in rats by retaining thermally gelling liquid suppositories in the rectum, *J. Control. Release Off. J. Control. Release Soc.* 59 (1999) 163–172.
- [34] T. Galaon, S. Udrescu, I. Sora, V. David, A. Medvedovici, High-throughput liquid-chromatography method with fluorescence detection for reciprocal determination of furosemide or norfloxacin in human plasma, *Biomed. Chromatogr.* 21 (2007) 40–47, <http://dx.doi.org/10.1002/bmc.715>.
- [35] O. Parodi, R. De Maria, E. Roubina, Redox state, oxidative stress and endothelial dysfunction in heart failure: the puzzle of nitrate-thiol interaction, *J. Cardiovasc. Med.* 8 (2007) 765–774, <http://dx.doi.org/10.2459/JCM.0b013e32801194d4>.
- [36] E.C. Sherrer, A. Verras, M. Madeira, W.K. Hagmann, R.P. Sheridan, D. Roberts, K. Bleasby, W.D. Cornell, QSAR prediction of passive permeability in the LLC-PK1 cell line: trends in molecular properties and cross-prediction of Caco-2 permeabilities, *Mol. Inform.* 31 (2012) 231–245, <http://dx.doi.org/10.1002/minf.201100157>.
- [37] S. Yamashita, T. Furubayashi, M. Kataoka, T. Sakane, H. Sezaki, H. Tokuda, Optimized conditions for prediction of intestinal drug permeability using Caco-2 cells, *Eur. J. Pharm. Sci. Off. J. Eur. Fed. Pharm. Sci.* 10 (2000) 195–204.
- [38] P.-A. Billat, E. Roger, S. Faure, F. Lagarce, Models for drug absorption from the small intestine: where are we and where are we going? *Drug Discov. Today* 22 (2017) 761–775, <http://dx.doi.org/10.1016/j.drudis.2017.01.007>.
- [39] T. Han, R.S. Everett, W.R. Proctor, C.M. Ng, C.L. Costales, K.L.R. Brouwer, D.R. Thakker, Organic cation transporter 1 (OCT1/mOct1) is localized in the apical membrane of caco-2 cell monolayers and enterocytes, *Mol. Pharmacol.* 84 (2013) 182–189, <http://dx.doi.org/10.1124/mol.112.084517>.
- [40] T. Hirano, S. Yasuda, Y. Osaka, M. Kobayashi, S. Itagaki, K. Iseki, Mechanism of the inhibitory effect of zwitterionic drugs (levofloxacin and grepafloxacin) on carnitine transporter (OCTN2) in Caco-2 cells, *Biochim. Biophys. Acta BBA – Biomembr.* 1758 (2006) 1743–1750, <http://dx.doi.org/10.1016/j.bbmem.2006.07.002>.
- [41] G. Fethi, F. Habib, H. Katsumi, N. Okada, T. Fujita, M. Attia, A. Yamamoto, Excellent absorption enhancing characteristics of NO donors for improving the intestinal absorption of poorly absorbable compound compared with conventional absorption enhancers, *Drug Metab. Pharmacokinet.* 21 (2006) 222–229.
- [42] A. Yamamoto, H. Tatsumi, M. Maruyama, T. Uchiyama, N. Okada, T. Fujita, Modulation of intestinal permeability by nitric oxide donors: implications in intestinal delivery of poorly absorbable, *Drugs* 7 (2018).
- [43] A.L. Salzman, M.J. Menconi, N. Unno, R.M. Ezzell, D.M. Casey, P.K. Gonzalez, M.P. Fink, Nitric oxide dilates tight junctions and depletes ATP in cultured Caco-2BBE intestinal epithelial monolayers, *Am. J. Physiol.* 268 (1995) G361–373, <http://dx.doi.org/10.1152/ajpgi.1995.268.2.G361>.
- [44] N. Numata, K. Takahashi, N. Mizuno, N. Utoguchi, Y. Watanabe, M. Matsumoto, T. Mayumi, Improvement of intestinal absorption of macromolecules by nitric oxide donor, *J. Pharm. Sci.* 89 (2000) 1296–1304.
- [45] D.-Z. Xu, Q. Lu, E.A. Deitch, Nitric oxide directly impairs intestinal barrier function, *Shock Augusta Ga* 17 (2002) 139–145.
- [46] N. Hogg, R.J. Singh, E. Konorev, J. Joseph, B. Kalyanaraman, S-Nitrosoglutathione as a substrate for gamma-glutamyl transpeptidase, *Biochem. J.* 323 (Pt 2) (1997) 477–481.
- [47] B. Alberts, A. Johnson, J. Lewis, M. Raff, K. Roberts, P. Walter, Carrier Proteins and Active Membrane Transport, 2002. <https://www.ncbi.nlm.nih.gov/books/NBK26896/> (accessed January 23, 2018).
- [48] A. Daiber, T. Münzel, Organic nitrate therapy, nitrate tolerance, and nitrate-induced endothelial dysfunction: emphasis on redox biology and oxidative stress, *Antioxid. Redox Signal.* 23 (2015) 899–942, <http://dx.doi.org/10.1089/ars.2015.6376>.
- [49] E. Le Ferrec, C. Chesne, P. Artusson, D. Brayden, G. Fabre, P. Gires, F. Guillo, M. Rousset, W. Rubas, M.L. Scarino, In vitro Models of the Intestinal Barrier. The Report and Recommendations of ECVAM Workshop 46, European Centre for the Validation of Alternative methods, *Altern. Lab. Anim. ATLA*, 2001, pp. 649–668.
- [50] J.E. Gonçalves, M. Ballerini Fernandes, C. Chiann, M.N. Gai, J. De Souza, S. Storpirtis, Effect of pH, mucin and bovine serum on rifampicin permeability through Caco-2 cells, *Biopharm. Drug Dispos.* 33 (2012) 316–323, <http://dx.doi.org/10.1002/bdd.1802>.
- [51] W. Wu, C. Gaucher, R. Diab, I. Fries, Y.-L. Xiao, X.-M. Hu, P. Maincent, A. Sapin-Minet, Time lasting S-nitrosoglutathione polymeric nanoparticles delay cellular protein S-nitrosation, *Eur. J. Pharm. Biopharm. Off. J. Arbeitsgemeinschaft Pharm. Verfahrenstechnik EV* 89 (2015) 1–8, <http://dx.doi.org/10.1016/j.ejpb.2014.11.005>.
- [52] W. Wu, C. Gaucher, I. Fries, X.-M. Hu, P. Maincent, A. Sapin-Minet, Polymer nanocomposite particles of S-nitrosoglutathione: a suitable formulation for protection and sustained oral delivery, *Int. J. Pharm.* 495 (2015) 354–361, <http://dx.doi.org/10.1016/j.jipharm.2015.08.074>.
- [53] K.U. Shah, S.U. Shah, N. Dilawar, G.M. Khan, S. Gibaud, Thiomers and their potential applications in drug delivery, *Expert Opin. Drug Deliv.* 14 (2017) 601–610, <http://dx.doi.org/10.1080/17425247.2016.1227787>.



S-nitrosothiols medium permeability might be not enough to envisage an oral treatment with those molecules. However, their intestinal permeability might be increased using nanoformulations such as GSNO nanocomposite particles consisting in polymeric nanoparticles (Eudragit RL<sup>®</sup>) encapsulating GSNO (GSNO-NP) embedded in an alginate/chitosan matrix. These nanocomposite particles with a GSNO encapsulation efficiency of 72% induced the formation of a NO store in the aorta of Wistar rats 18 h after the oral administration of an unique dose of 15 mg/kg [60]. Therefore, GSNO was absorbed by the intestine and transport into the systemic circulation to the vessel wall.

In this introduction, the links between atherosclerosis and NO has been discussed. NO is a vasodilator with anti- or pro-inflammatory properties depending on its concentration. The different pathways implicated in atherosclerosis development and the nitro redox interconnections has been clarified. In this context, the objectives of the work presented in this PhD manuscript were to *i*) establish a model of monocytes differentiation into macrophages, which are then polarized to M1-like macrophages or M2-like macrophages, *ii*) to study the impact of NO, and more specifically of GSNO, on the formation of foam cells and *iii*) to develop a vSMCs model of dedifferentiation using different stimuli such as AngII and oxLDLs.

## CHAPTER 2

*S*-NITROSOTHIOLS POTENTIAL *vs.* MACROPHAGES  
DERIVED FOAM CELLS FORMATION AND  
MONOCYTES/MACROPHAGES  
DIFFERENTIATION/POLARIZATION

# I. Production of oxidized low-density lipoproteins

## 1. Oxidation of low-density lipoproteins

Oxidation of low-density lipoproteins (oxLDLs) plays a central role in the development of atherosclerosis. oxLDLs are up taken by macrophages and vSMCs “macrophage-like” leading to the formation of foam cells. LDLs oxidation is commonly performed on LDLs isolated from heparinized plasma and produced by exposure to different oxidants such as  $\text{CuSO}_4$  (the most used),  $\text{FeSO}_4$  or even 2,2'-azobis(2-methylpropionamidine) dihydrochloride (AAPH). Parameters (*e.g.* time, concentration, *etc*) slightly vary among different protocols and present some critical variables that are not clearly described in literature. Part of this PhD was thus spent in the setup of a suitable and reproducible protocol for LDLs oxidation.

The main issues are:

- a. The source of LDLs: due to technical problems for the isolation of LDLs from donor's plasma and to have a better reproducibility of the starting material, we decided to buy purified LDLs. Products from Sigma and Millipore were tested;
- b. The need of a dialysis step in order to remove the high concentrations of EDTA that are commonly used to preserve commercial LDLs from oxidation and that might chelate copper and iron ions;
- c. The buffer used for LDLs oxidation. Some phosphate buffers may prevent/delay LDLs oxidation by hampering the formation of copper-LDL or iron-LDL complexes that are required for LDLs oxidation;
- d.  $\text{CuSO}_4$  concentration, volume of the sample, time and type of incubation (static *vs.* dynamic). In many protocols, these parameters are not specified resulting in different levels of LDLs oxidation or even their partial aggregation/precipitation;
- e. Levels of LDLs oxidation. In many protocols, LDLs oxidation is only confirmed by the variation of their electrophoretic mobility. We decided to better evaluate the extent of our LDLs oxidation with a quantification of peroxidised lipids (TBARS assay).

Several experiments were performed in order to define all these parameters and a summary of the final protocol is presented in **Table 2**.

**Table 2:** protocol of LDLs oxidation by copper sulfate

Parameters	Encountered problems	Final protocol
[LDLs]	/	0.5 mg/mL
[CuSO <sub>4</sub> ]	/	10 µM
Volume of the LDLs sample	No oxidation (or under limit of quantification) with volume < 1 mL	Minimum 1 mL (final volume)
Temperature, time, with or without agitation	Agglomeration of LDLs with rotative agitation	37°C, 24 h, without agitation
Buffer used for the dilution	PBS or NaCl 0.9% (commercial LDLs are conditioned in NaCl)	NaCl 0.9%
Number of dialysis		Two dialysis: one before and one after the oxidation

### **Final protocol**

Purified LDLs (Sigma, L7914 or Millipore 437644) at 5 mg/mL in NaCl 150 mM; 0.01% EDTA were diluted to 1 mg/mL in NaCl 0.9% prior dialysis with a 20 kDa MWCO membrane (Mini Dialysis Devices) against NaCl 0.9% (v/v) to remove EDTA. The dialysis was performed on an orbital shaker (150 rpm), at 4 °C, the dialysis solution was changed every hour during 5 h followed by an overnight dialysis. After dialysis, protein concentration was determined using the bicinchoninic acid (BCA) method and considered as a reference for LDLs concentration. Then, 0.5 mg/mL of LDLs were oxidized with 10 µM CuSO<sub>4</sub> during 24 h at 37 °C, in the dark. The reaction was stopped with EDTA by dialysis against NaCl 0.9%; EDTA 1 mM. Protein concentration as well as the degree of lipid peroxidation (TBARS method) were finally determined and oxLDLs were conserved in the dark at 4 °C until use.

## **2. Peroxidised lipids quantification**

Thiobarbituric Acid Reactive Substance (TBARS) is used to determine the oxidation level of LDLs. oxLDLs diluted 2 times in 0.2 M sulphuric acid (final volume 200 µL) are vigorously mixed with 200 µL of TBA reagent (0.92 M trichloroacetic acid and 0.026 M 2-thiobarbituric acid in HCl 0.25 M) and 2 µL of 2% BHT. After 60 min of incubation at 95 °C, the MDA-TBA adduct produced is extracted with 400 µL of 1-butanol and centrifuged at 15,000 g for 3 min. Then, fluorescence intensity of the supernatant is read at 553 nm after excitation at 532 nm (BioTek, Synergy 2 model). MDA standard is produced by 1,1,3,3-tetramethoxypropane (TMP) hydrolysis in 0.2 M H<sub>2</sub>SO<sub>4</sub> during 2 h in the dark and at room temperature. MDA



standard concentration is measured by absorbance at 245 nm ( $\epsilon = 13,700 \text{ mol}^{-1}.\text{L}^{-1}.\text{cm}^{-1}$ ) to build a calibration curve from 0.075  $\mu\text{M}$  to 3.000  $\mu\text{M}$ . Peroxidised lipids are expressed as nmol of MDA per mg of proteins.

The quantity of peroxidised lipids is determined after each assay of LDLs oxidation. For all batches ( $n = 9$ ), results were  $10.49 \pm 4.71$  nmol of oxLDLs/mg of proteins (mean  $\pm$  SD).

## II. Article 4: S-nitrosoglutathione impact on oxLDLs phagocytosis by M0-macrophages

### Article 4: S-nitrosoglutathione impact on oxLDLs phagocytosis by M0-macrophages

#### **Impact du S-nitrosoglutathion sur la phagocytose des oxLDLs par les macrophages M0**

Justine Bonetti<sup>1</sup>, Alessandro Corti<sup>2</sup>, Isabelle Fries<sup>1</sup>, Alfonso Pompella<sup>2</sup>, Caroline Gaucher<sup>1</sup>

*(to be submitted in Nitric Oxide Journal)*

<sup>1</sup>Université de Lorraine, CITHEFOR, F-54000 Nancy, France; justine.bonetti@univ-lorraine.fr

<sup>2</sup>Dept. of Translational Research NTMS, University of Pisa Medical School, 56126 Pisa, Italy; alessandro.corti@med.unipi.it

L'athérosclérose est décrite comme une pathologie chronique complexe associée à une inflammation et un stress oxydant, entraînant l'induction et la progression des lésions athérosclérotiques dans la paroi vasculaire *via* des altérations cellulaires et moléculaires. Ces lésions conduisent à la formation de plaques d'athérome. Celles-ci sont composées de cellules spumeuses dérivées des macrophages et des cellules musculaires lisses ayant internalisés des lipides oxydés (oxLDL). L'infiltration des oxLDL génère un stress oxydant ainsi qu'une inflammation dans le sous-endothélium, ce qui entraîne une activation des cellules endothéliales et augmente l'expression de molécules d'adhésion comme la molécule d'adhésion intracellulaire 1 (ICAM-1), la molécule d'adhésion vasculaire 1 (VCAM-1) sur leur membrane plasmique, et la production de chimiokines telles que la protéine chimio-attractante monocytaire 1 (MCP-1) et l'interleukine 8. Au sein des plaques, la population de macrophages est hétérogène dû à la présence du facteur stimulant les macrophages (M-CSF) qui induit la différenciation des monocytes en macrophages M0. Au cours du développement des plaques d'athérome, la présence d'oxLDL et de cytokines pro-inflammatoires augmentent la production de M-CSF et du facteur stimulant les granulocyte-macrophage (GM-CSF) avec un déséquilibre entre les deux facteurs en faveur du M-CSF. Le GM-CSF présent en forte concentration dans les lésions avancées, induit quant à lui, la différenciation des monocytes en macrophages M0 et favorise leur polarisation en macrophages M1. Les oxLDL interagissent avec les macrophages *via* des récepteurs tels que le CD36, une glycoprotéine membranaire, récepteur de classe B de 88 kDa dont l'expression est plus élevée dans les macrophages M1, ou le

récepteur 1 lectine-like aux lipoprotéines oxydées de faible poids moléculaire (Lox-1), une protéine membranaire de type II dont l'expression est plus élevée dans les macrophages M2. Ces récepteurs ont été identifiés au niveau de la membrane plasmique des macrophages et sont responsables de plus de 90 % de la fixation et de l'internalisation des oxLDL. La formation de cellules spumeuses est directement liée à l'expression de CD36 et l'expression de CD36 est directement liée aux oxLDL. Le développement de l'athérosclérose est également lié à une diminution de la biodisponibilité en monoxyde d'azote (NO). Outre son rôle direct dans l'homéostasie vasculaire, NO présente des propriétés antioxydantes. En effet, il a été démontré que NO réduit l'oxydation des LDL et la formation de plaques d'athérome dans un modèle murin d'athérosclérose. De plus, les statines donneuses de NO présentent une activité hypolipémiante et anti-inflammatoire supérieure à celle des statines. Par conséquent, la connexion entre NO, oxydation des lipides et leur accumulation dans la paroi vasculaire est établie. Cependant, aucune donnée n'est connue sur les mécanismes induits. L'effet antioxydant de NO est médié par la *S*-nitrosation des résidus cystéine des protéines. En effet, le *S*-nitrosogluthation (GSNO) qui est la forme physiologique de stockage et de transport de NO, est capable de protéger du stress oxydant, les résidus de cystéine des protéines. En effet, GSNO réduit les ponts disulfures *via* la *S*-nitrosation des atomes de soufre. De plus, GSNO est composé de glutathion (GSH), le principal tampon redox intracellulaire formant un couple redox avec le glutathion oxydé (GSSG).

L'expression de CD36 étant étroitement liée au stress oxydant et sa voie de signalisation utilisant des ROS, nous avons émis l'hypothèse dans cette étude que GSNO pourrait limiter la formation des cellules spumeuses en diminuant l'expression de CD36. Le statut redox des macrophages M0 a été analysé après pré-traitement avec GSH ou GSNO, cela nous a permis de déterminer un effet du NO, en présence ou non d'oxLDL. Le GSNO va potentiellement diminuer la formation de cellules spumeuses et l'induction du stress oxydant par les oxLDL.

## 1. Introduction

Atherosclerosis is described as a complex chronic disease associated with inflammation and oxidative stress, which modulate the initiation and the progression of lesions in the vascular wall *via* cellular and molecular alterations. Those lesions lead to the formation of atherosclerotic plaques that in most cases are silent with a slow development explaining why patients are asymptomatic until acute events – like myocardial infarction or stroke – occur. These events are due to a sudden ischemia produced either by a thrombus (myocardial infarction) or a plaque rupture (stroke).

Atherosclerotic plaques are composed of foam cells derived from macrophages and smooth muscle cells that internalized oxidized low-density lipoproteins (oxLDLs) infiltrated in the subendothelium. OxLDLs infiltration generate oxidative stress and inflammation in the subendothelium that lead to endothelial cells activation increasing the expression of adhesion molecules like the intracellular adhesion molecule 1 (ICAM-1) and the vascular adhesion molecule 1 (VCAM-1) on their plasma membrane [1], and the production of chemokines such as monocyte chemoattractant protein-1 (MCP-1) and interleukine-8. Both phenomena are implicated in monocytes recruitment, adhesion and transmigration in the subendothelium where they differentiate into macrophages to phagocyte oxLDLs. Macrophage population in atherosclerotic plaques is heterogenous due to the presence of macrophage colony-stimulating factor (M-CSF), which induces the differentiation of monocytes into M0-macrophages and favours their polarization into M2-macrophages. During plaques progression, the presence of oxLDLs and pro-inflammatory cytokines increase the production of M-CSF and granulocyte-macrophage colony-stimulating factor (GM-CSF) with an imbalance between the two factors in favour of M-CSF [2]. GM-CSF present in high concentration in advance lesions, induces the differentiation of monocytes into M0-macrophages and favours their polarization into M1-macrophages. Another specific macrophage type is polarized from M0-macrophages after the presence of oxLDLs, the Mox phenotype, identified only in mice. Indeed, oxLDLs phagocytosis by M0-macrophages lead to the formation of Mox-macrophages that present a decrease phagocytic activity, express a panel of antioxidant enzymes under the control of the KLF-2 transcription factor [3]. Mox macrophages represent around 30% of all macrophages found in advance atherosclerotic lesions of LDLR<sup>-/-</sup> mice [3]. Foam cells and oxLDLs may drive cell death, thus contributing to the formation of the necrotic core within atherosclerotic plaques.



Therefore, M0-macrophages are at the intersection of monocytes differentiation into different subtypes of macrophages. Interaction of oxLDLs with macrophages occurs *via* scavenger receptors such as CD36, a membrane glycoprotein and class B scavenger receptor of 88 kDa (higher in M1-macrophages), or Lectin-like oxidized low-density lipoprotein receptor-1 (Lox-1), a type II membrane protein (higher in M2-macrophages). They were all identified at the plasma membrane of macrophages as responsible for over 90% of oxLDLs binding and uptake [4]. CD36 expression is increased through the activation of PPAR $\gamma$  and Nrf2 transcription factors after macrophages exposition to oxLDLs [5]. Foam cells formation is directly linked to CD36 expression and CD36 expression is directly linked to oxLDLs. Indeed, Febbraio *et al.* [6] showed, in genetically altered mice that do not express CD36, a lack of foam cells formation after oxLDLs exposure. Furthermore, CD36 expression is upregulated by oxLDLs and contributes to macrophage trapping inside atherosclerotic lesions [7]. In macrophages, CD36 forms a “mega complex” with other proteins at the plasma membrane like the Toll-like receptor or the Na-K ATPase pump. Upon oxLDLs binding, CD36 promotes the recruitment and the activation of Src family kinases. The induced signal transduction promotes cytoskeletal rearrangement *via* focal adhesion kinases phosphorylation, loss of cellular locomotion and macrophage trapping. The binding of oxLDLs on CD36 also promotes Rac activity modulating non-muscle myosin II and regulating cellular locomotion. OxLDLs uptake is linked to MAP kinase activation (JNK1/2) who is essential for CD36-mediated macrophage foam cells formation. The mechanistic connection between CD36 and the other membrane proteins (in particular Toll-like receptor or Na-K ATPase pump) has been shown to be linked to pro-inflammatory pathways activation like NK- $\kappa$ B, promoting atherosclerosis, cholesterol deposition and foam cells formation [8]. CD36 signaling promotes also the generation of intracellular reactive oxygen species (ROS) from NADPH oxidase. Downstream consequences of macrophage ROS generation are the oxidation of critical cysteine residues in proteins such as tyrosine phosphatase SHP2 leading to the disruption of actin cytoskeletal rearrangements and macrophage migration that might be reversed by an antioxidant such as *N*-acetylcysteine [7,9].

Atherosclerosis development is correlated with a decrease of nitric oxide (NO) bioavailability. Besides its direct role in vascular homeostasis, NO shows antioxidant properties [10]. Indeed, NO has been shown to reduce LDLs oxidation [11] and the formation of atherosclerotic plaques in a murine model of atherosclerosis [12]. Moreover, NO-donating statins have superior lipid-lowering and anti-inflammatory activity than statins [13,14].

Therefore, the connexion between NO, lipid oxidation and accumulation in the vascular wall is established. However, nothing is known on about the mechanisms induced. NO mainly express its antioxidant effect through the *S*-nitrosation of proteins cysteine residues. Those formed *S*-nitrosoproteins are protected from cysteine overoxidation to disulphide bound or sufenylation/sulfinylation/sulfonylation. We have shown that *S*-nitrosoglutathione (GSNO), a NO donor, which is the physiological form of NO storage and transport, was able to protect cysteine residues under oxidative stress [15]. Indeed, GSNO was able to reduce reverse disulphide bound within proteins by their *S*-nitrosation. Moreover, GSNO is composed of glutathione (GSH), the main low-molecular-weight thiol-containing peptide found in cytoplasm forming a redox couple with glutathione disulfide (GSSG) considered as the main cellular redox buffer [16]. GSH plays an antioxidant role as a scavenger of electrophilic and oxidant species either in a direct way or through enzymatic catalysis. Indeed, GSH is the co-substrate of glutathione peroxidases (EC 1.11.1.9; GPx), permitting the reduction of peroxides (hydrogen and lipid peroxides) and producing GSSG.

As CD36 expression is closely linked to oxidative stress and its signaling pathway uses ROS, we hypothesized in the present study that GSNO might limited foam cells formation with a decrease expression of CD36. The cellular redox status of M0-macrophages was analysed after pre-treatment with GSH or GSNO, allowing us to determine an effect of NO, and in presence or not of oxLDLs. GSNO will potentially decrease foam cells formation and the induction of oxidative stress by oxLDLs.

## 2. Materials and methods

### 2.1. Materials

#### 2.1.1. Chemicals

Sulfuric acid was purchased from Prolabo, hydrochloric acid from VWR Chemicals, ethanol absolute from Carlo Erba Reagents and trichloroacetic acid from Acros Organics. Sodium nitrite (NaNO<sub>2</sub>) and 1-butanol are from Merck. Slide-A-Lyser<sup>®</sup> MINI Dialysis Devices (Ref. 88402) and Pierce<sup>™</sup> BCA<sup>™</sup> protein assay kit from ThermoFisher Scientific (Ref. 23227). Clarity<sup>™</sup> Western ECL substrate from Bio-Rad. All other reagents were purchased from Sigma, France.

### 2.1.2. S-nitrosoglutathione powder synthesis

GSNO powder was synthesized, purified, isolated and stored as previously described [17]. Briefly, GSH is incubated with one equivalent of sodium nitrite under acidic condition. Reaction is kept on agitation and on ice for 40 min under N<sub>2</sub>. Then, GSNO is precipitated with acetone and purified as a solid. The solid was then washed with acetone and diethyl ether. Powder aliquots are stored at -20 °C in bottles filled with N<sub>2</sub>.

### 2.2. Human monocytes culture, differentiation and treatments

Human monocytes THP-1 (ATCC® TIB-202™) from passage 3 to 13 were grown in a complete medium consisting of RPMI-1640 supplemented with 10% (v/v) of heat-inactivated foetal bovine serum, 100 U/mL of penicillin, 100 U/mL of streptomycin, 0.05 mM of  $\beta$ -mercaptoethanol. Cells were cultivated at 37 °C under 5% of CO<sub>2</sub> (v/v) in a humidified incubator. THP-1 are seeded at  $1.8 \times 10^5$  cells/well in 6-wells plate with 100 nM of Phorbol 12-myristate 13-acetate (PMA), 24 h before experiment. PMA is removed and M0-macrophages were then pre-incubated with 25  $\mu$ M of GSNO or GSH diluted in complete medium for 6 h at 37 °C. PBS is used as control. After this pre-incubation, the medium is removed and cells are incubated with 25  $\mu$ g/mL of oxLDLs in complete medium during 48 h at 37 °C.

### 2.3. Oxidation of low-density lipoproteins

Purified LDLs (Sigma, L7914 or Millipore 437644) at 5 mg.mL<sup>-1</sup> in NaCl 150 mM; 0.01% EDTA were diluted to 1 mg.mL<sup>-1</sup> in NaCl 0.9% prior dialysis with a 20 kDa MWCO membrane against NaCl 0.9% (v/v) to remove EDTA. The dialysis is performed on an orbital shaker (150 rpm), at 4 °C, overnight and the dialysis solution is changed every hour during 5 h. After dialysis, protein concentration (section 2.6.) was determined and considered as LDLs concentration. Then, 0.5 mg.mL<sup>-1</sup> of LDLs were oxidized with 10  $\mu$ M CuSO<sub>4</sub> during 24 h at 37 °C, in the dark. The reaction was stopped with EDTA by dialysis against NaCl 0.9%; EDTA 1 mM. Protein concentration as well as the degree of lipid peroxidation (section 2.4.) are finally determined and oxLDLs are conserved in the dark at 4 °C until use.

### 2.4. Peroxidised lipids quantification

OxLDLs diluted 2 times in 0.2 M sulphuric acid (final volume 200  $\mu$ L) are vigorously mixed with 200  $\mu$ L of 0.92 M trichloroacetic acid and 0.026 M 2-thiobarbituric acid in HCl 0.25 M (TBA reagent) and 2  $\mu$ L of 2% BHT. After 60 min of incubation at 95 °C, the malondialdehyde (MDA)-TBA adduct produced is extracted with 400  $\mu$ L of 1-butanol and centrifuged at

15,000 g for 3 min. Then, fluorescence intensity of the supernatant is read at 553 nm after excitation at 532 nm (BioTek, Synergy 2 model). MDA standard is produced by 1,1,3,3-tetramethoxypropane (TMP) hydrolysis in 0.2 M H<sub>2</sub>SO<sub>4</sub> during 2 h in the dark and at room temperature. MDA standard concentration is measured by absorbance at 245 nm ( $\epsilon = 13,700 \text{ mol}^{-1} \cdot \text{L}^{-1} \cdot \text{cm}^{-1}$ ) to build a calibration curve from 0.075  $\mu\text{M}$  to 3.000  $\mu\text{M}$ . Peroxidised lipids are expressed as nmol of MDA per mg of proteins.

## 2.5. DiI-oxLDLs synthesis

Labelled oxLDLs (oxLDLs from protocol in section 2.3) are obtained according to Innerarity *et al.*, with minor modifications [18]. Briefly, lipoprotein-free serum is produced starting from foetal calf serum integrated with 1% (v/v) of 0.15 M NaCl/0.1 M EDTA/0.2 M NaN<sub>3</sub>. Then, 3.17 g of KBr is added in 10.1 mL of plasma (final density of 1.23 g.mL<sup>-1</sup>) and the plasma is centrifuged at 100,000 g for 22 h. The lipoprotein-free serum is collected from the bottom of the vial and dialysed against NaCl 0.9%, at 4 °C, overnight. The lipoprotein-free serum is then sterile-filtered (0.22  $\mu\text{m}$ ) and kept at -20 °C until use. 1 mg of oxLDLs diluted in lipoprotein-free serum is labelled with 50  $\mu\text{L}$  of 3 mg.mL<sup>-1</sup> DiI in DMSO and incubated at 37 °C overnight, in the dark. Finally, the DiI-oxLDLs density is increased to 1.065 g.mL<sup>-1</sup> using KBr and centrifuged at 100,000 g 16 h at 4 °C. DiI-oxLDLs are collected on the top of the solution and dialysed against NaCl-EDTA 1 mM and sterile-filtered. DiI-oxLDLs are kept at 4 °C, protected from the light.

## 2.6. Total proteins quantification

Total proteins determination is performed using Pierce<sup>TM</sup> BCA<sup>TM</sup> protein assay kit, following manufacturer's instructions. Protein concentration is calculated upon a bovine serum albumin standard curve ranging from 25 to 1000  $\mu\text{g/mL}$ .

## 2.7. Cells redox status

### 2.7.1. Quantification of reduced cellular glutathione

Intracellular GSH was quantified as previously described [15]. Briefly, cells are lysed in 3.3% (v/v) perchloric acid solution and centrifuged at 10,000 g; 4 °C for 15 min. Acidic supernatants are neutralised with 40% NaOH and diluted 10 times in 0.1 M HCl containing 2 mM of EDTA. 60  $\mu\text{L}$  of diluted samples or standard GSH solutions (from 0.65 to 3.25  $\mu\text{M}$ ) are transferred in triplicate in a 96-wells black plate. 120  $\mu\text{L}$  of 0.4 M borate buffer (pH 9.2) and 20  $\mu\text{L}$  of 5.4 mM NDA solution are added into each well and incubated 25 min on ice in the dark. The



fluorescence intensity of GSH-NDA adduct is read at 485 nm after an excitation at 485 nm (BioTek, Synergy 2 model). The values are expressed as nmol of GSH per mg of proteins.

#### 2.7.2. Quantification of reduced cellular thiols, intracellular low and high molecular weight reduced thiols

Reduced thiol functions are oxidized by 5-5'-dithio-bis(2-nitrobenzoic) acid (DTNB) producing 5-thio-2-nitrobenzoate, which absorbs at 412 nm. Reduced thiols concentration is calculated upon a GSH standard curve ranging from 3.25  $\mu$ M to 32.5  $\mu$ M. Cells are washed twice with PBS and lysed with 250  $\mu$ L of 3.3% (v/v) perchloric acid solution. Lysates are then centrifuged for 15 min at 10,000 g and 4°C. The supernatant is used for low molecular weight (LMW) thiols quantification and the pellet is used for high molecular weight (HMW, proteins) thiols quantification.

Then, 200  $\mu$ L of supernatant are neutralized with 11.5  $\mu$ L of 40% NaOH and diluted with 800  $\mu$ L of PBS/5 mM EDTA; pH 7.5. The pellet is resuspended in 700  $\mu$ L of PBS/5 mM EDTA containing 0.5% (v/v) sodium dodecyl sulphate. 200  $\mu$ L of each sample are transferred in triplicate in a 96-wells black plate and incubated 10 min in the dark at room temperature with 40  $\mu$ L of 1 mM DTNB. The absorbance is read at 405 nm (BioTek, EL 800). The values are expressed as nmol of LMW or HMW thiols per mg of proteins.

#### 2.7.3. Extracellular nitrite ions and *S*-nitrosothiols quantification

Extracellular nitrite ions ( $\text{NO}_2^-$ ) and *S*-nitrosothiols (RSNOs) are quantified using a colorimetric method, Griess and Griess-Saville methods. Griess assay works in two steps:  $\text{NO}_2^-$  form diazonium salt with sulfanilamide, reacting with N-(1-naphthyl)ethylenediamine solution to form a chromophoric azo product that absorb at 540 nm. For RSNOs quantification, sulfanilamide is supplemented with mercuric ions, used to cleave the S-NO bond. The concentrations of  $\text{NO}_2^-$  and RSNOs are quantified using standard curves (1 – 10  $\mu$ M) of  $\text{NO}_2^-$  or GSNO, respectively. To calculate RSNOs concentration, free  $\text{NO}_2^-$  quantified by Griess assay are subtracted from those obtained with Griess-Saville assay. Results are expressed as  $\mu$ M of  $\text{NO}_2^-$  or RSNOs.

#### 2.7.4. Intracellular nitrite ions and *S*-nitrosothiols quantification

Nitrite ions and *S*-nitrosothiols are quantified using a fluorometric method [19,20]. Quantification of intracellular nitrite ions ( $\text{NO}_2^-$ ) is based on the direct reaction between 2,3-diaminonaphthalene (DAN) and nitrite ions to yield 2,3-naphotriazole (NAT). For

*S*-nitrosothiols (RSNO) quantification, mercuric ions are used to cleave the S-NO bond allowing the release of nitrite ions that are quantified with DAN. The fluorescent intensity is read on 100  $\mu$ L of sample at 375 nm ( $\lambda_{\text{ex}} = 375$  nm/ $\lambda_{\text{em}} = 415$  nm; JASCO, FP-83000iRM).  $\text{NO}_2^-$  and RSNO concentrations are determined using  $\text{NO}_2^-$  or GSNO standard curve (0.1 – 1  $\mu$ M), respectively. The RSNO concentration (DAN- $\text{Hg}^{2+}$  assay) is obtained by the subtraction of the nitrite ions concentration (DAN assay). Results are expressed as nmol of nitrite ions or RSNO per mg of proteins.

#### 2.7.5. Extracellular and intracellular peroxynitrites ions quantification

Quantification of peroxynitrite ions ( $\text{ONOO}^-$ ) (adapted from [21,22]) is based on the oxidation of dihydrorhodamine-123 (DHR-123) into fluorescent rhodamine-123 (Rh-123) by  $\text{ONOO}^-$ . Extracellular  $\text{ONOO}^-$  are quantified by directly incubating 10  $\mu$ M of DHR-123 with cells during 20 min at 37 °C. For intracellular  $\text{ONOO}^-$  quantification, cells are washed twice with PBS, and lysed with 700  $\mu$ L of lysis buffer (50 mM Tris, 150 mM NaCl, 1% NP-40 (v/v), 0.1% SDS (w/v), 1 mM EDTA, 0.1 mM neocuproine). The fluorescent intensity is read at 485 nm after an excitation at 530 nm (BioTek, Synergy 2 model) on 200  $\mu$ L of sample deposited in triplicate in a 96-wells black plate.  $\text{ONOO}^-$  concentrations are calculated using a Rh-123 standard curve ranging from 0.01 to 0.5  $\mu$ M. Values are expressed as  $\mu$ M of  $\text{ONOO}^-$  per mg of proteins. Sydnominine (SIN-1) has been used as positive control of  $\text{ONOO}^-$  production.

#### 2.7.6. Western blot

Cells are lysed with 10 mM Tris-HCl; pH 7.8. 30  $\mu$ g of proteins are deposited on a SDS-PAGE gel composed of a 10% separative gel and a 4% stacking gel. After migration, proteins are transferred onto a polyvinyl membrane and incubated with rabbit polyclonal anti-CD36 antibody (1/5000; Origene) or anti-actin antibody (1/2000; A2547 Santa Cruz). Visualization of proteins bands was obtained using an HRP conjugated goat anti-rabbit IgG antibody (1/2000; Santa Cruz Biotechnology, USA) and the revelation was performed with ECL solution. Bands were analysed with a Bio-Rad ChemiDoc and quantified by ImageJ.

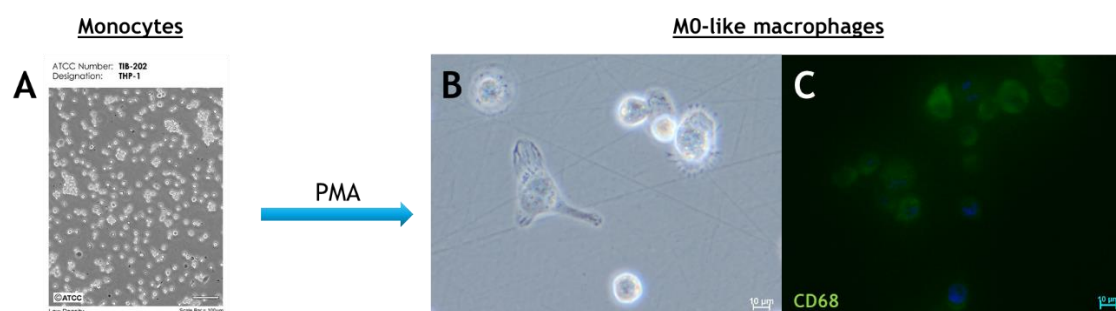
#### 2.7.7. Statistical analysis

Results are shown as mean  $\pm$  standard error of the mean. Values were compared with one-way ANOVA or two-way ANOVA followed by a Bonferroni's post-test using the Graphpad Prism 9 software;  $p < 0.05$  was considered as statistically significant.

### 3. Results

#### 3.1. GSNO impact on oxLDLs internalization by M0-macrophages

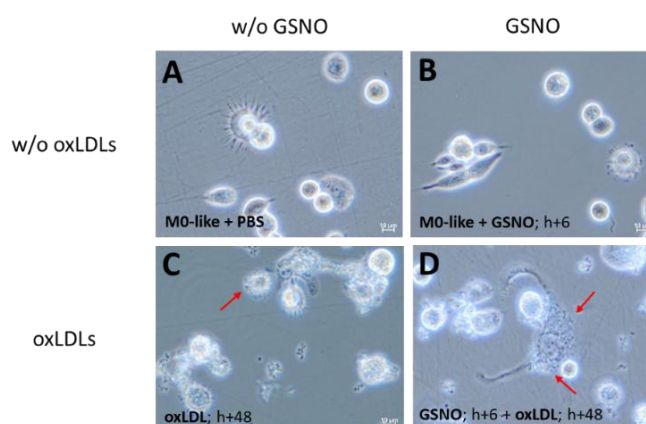
Monocytes stimulation with PMA induced their differentiation from monocytes into M0-macrophages (**Fig. 7A**) attested by their morphology and adherence as well as plasma membrane expression of CD68, a macrophage marker (**Fig. 7B** and **7C**).



**Figure 7:** Optical microscopy of monocytes (picture from ATCC) (A) and M0-like macrophages (Magnification: 40x, scale bar: 10 μm) (B); fluorescent microscopy of CD68 in M0-like macrophages (Magnification: 40x, scale bar: 10 μm) (C)

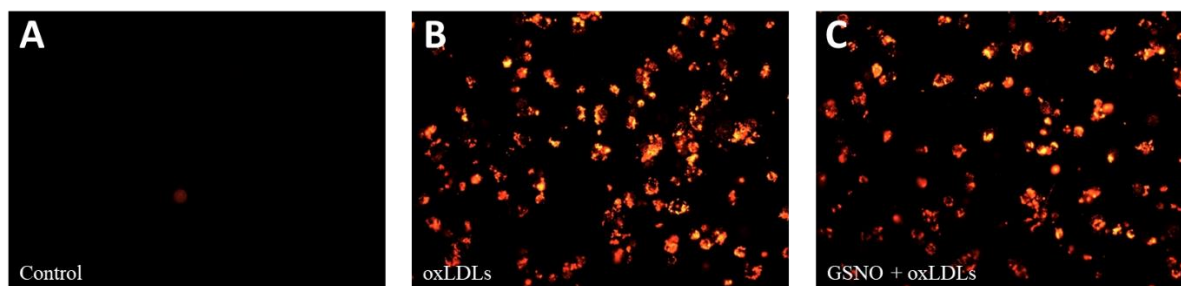
After 6 h of M0-macrophages pre-treatment with 25 μM of GSNO, only  $1.43 \pm 0.40$  μM of nitrite ions and  $0.84 \pm 0.07$  μM of GSNO are still present in the culture medium representing around 90 % of GSNO decrease compared to the initial concentration. The intracellular concentrations of nitrite ions and *S*-nitrosothiols were under the limit of quantification ( $< 0.25$  μM). These results showed that M0-macrophages metabolised almost all the available GSNO.

The pre-treatment of M0-macrophages with GSNO was followed by an incubation with oxLDLs. Figure 8 shows the morphology of M0-macrophages with no effect of GSNO incubation on their morphology (**Fig. 8A** and **8B**) and with the appearance of droplets (red arrows) only in the presence of oxLDLs either without and with GSNO preincubation (**Fig. 8C** and **8D**). Those droplets suppose the internalization of oxLDLs and the formation of foam cells.



**Figure 8:** Optical microscopy of M0-like macrophages before and after pre-treatment with 25  $\mu$ M of GSNO and 25  $\mu$ g/mL of oxLDLs (Magnification: 40x, scale bar: 10  $\mu$ m)

To confirm that droplets are originating from lipids contained by oxLDLs, labelled DiI-oxLDLs were incubated with M0-macrophages.



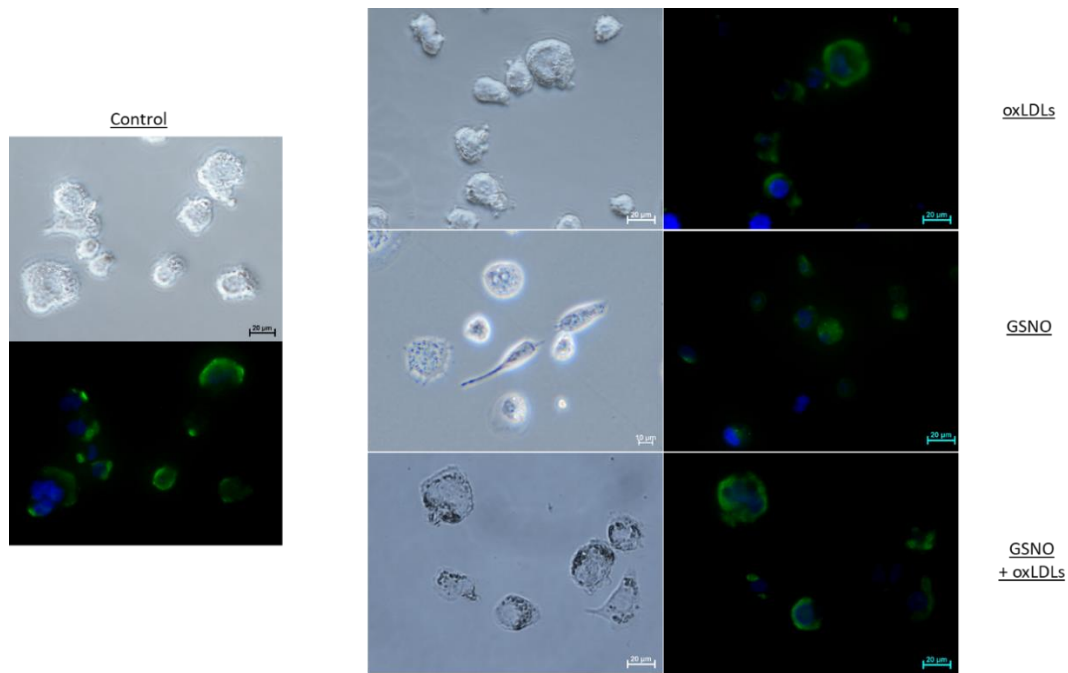
**Figure 9:** Fluorescent microscopy of M0-macrophages pre-treated with GSNO at 25  $\mu$ M and incubated with 25  $\mu$ g/mL of DiI-oxLDLs (Magnification: 40x) (n=1)

Figure 3 shows an interaction between labelled-oxLDLs and M0-macrophages (**Fig. 9B** and **9C**), validating the presence of oxLDLs in contact with the plasma membrane or inside M0-macrophages. However, no difference in oxLDLs internalisation can be visualized after pre-GSNO treatment.

### 3.2. Impact of *S*-nitrosoglutathione on CD36 expression

To further explain the implication of GSNO in oxLDLs internalization, the expression of CD36 on M0-macrophages plasma membrane was visualized by immunofluorescence (**Fig. 10**). CD36 is expressed on the plasma membrane of M0-macrophages, whatever the treatment is.





**Figure 10:** Immunofluorescent detection of CD36 in M0-macrophages. Cells were pre-treated with GSH or GSNO for 6 h and incubated with oxLDLs at 25  $\mu\text{g/mL}$  for 48 h in fresh complete medium. Cells were fixed with paraformaldehyde and incubated first with CD36 primary antibody followed by a secondary antibody coupled to Alexa<sup>®</sup> 488. Finally, nuclei were labelled with Hoechst 33258 (Magnification: 40x, scale bar: 20  $\mu\text{m}$ )

To quantify CD36 expression within M0-Macrophages, a western-blot analysis was performed (**Fig. 11**). Figure 11A shows an example of bands obtained for CD36 and actin in the different conditions.

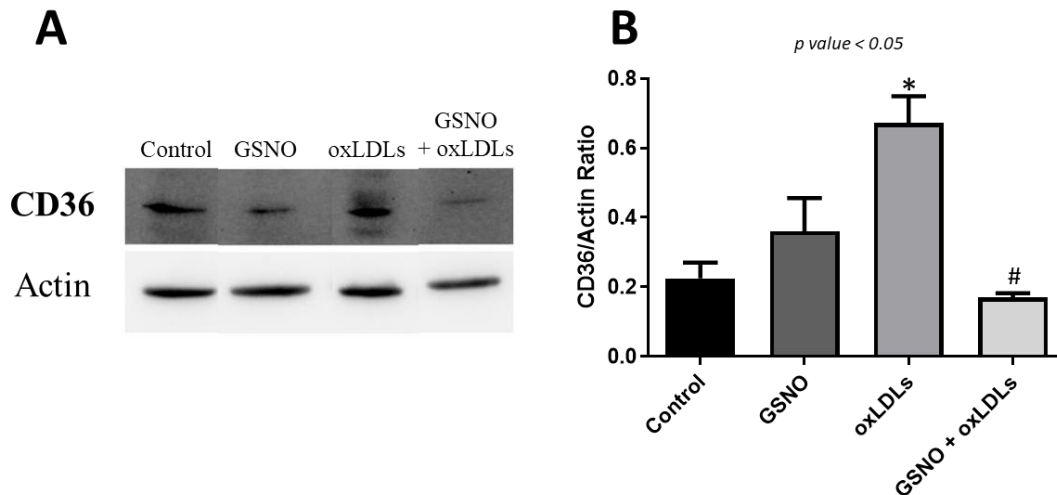


**Figure 11:** Expression of CD36 after M0-macrophages pre-treatment with 25  $\mu\text{M}$  of GSNO and incubation with 25  $\mu\text{g/mL}$  of oxLDLs. Ratio of proteins of CD36 vs.  $\alpha$ -actin bands were quantified by ImageJ. Results are presented as mean  $\pm$  SEM of 3 independent experiments and analysed by One-way ANOVA and Bonferroni's post-test; \* vs. control; # vs. oxLDLs;  $p < 0.05$ .

GSNO pre-treatment alone had no effect on CD36 expression (**Fig. 11B**). As expected, CD36 expression is increased 3 times by oxLDLs alone. However, GSNO pre-treatment was able to

abolish the oxLDLs-induced overexpression of CD36. As GSNO has antioxidant properties and CD36 signaling is mediated by ROS, cell redox status was then evaluated.

### 3.3. Cell redox status

First of all, the production of peroxynitrite ions was quantified either in the culture medium and in M0-macrophages. The intracellular concentration of peroxynitrite ions was under the limit of quantification whatever the condition was. In the culture medium, no variation of peroxynitrite ions concentration was observed (**Fig. 12**). Therefore, even with a pre-treatment with GSNO or with oxLDLs-induced overexpression of CD36, nitrosative stress was not detected.

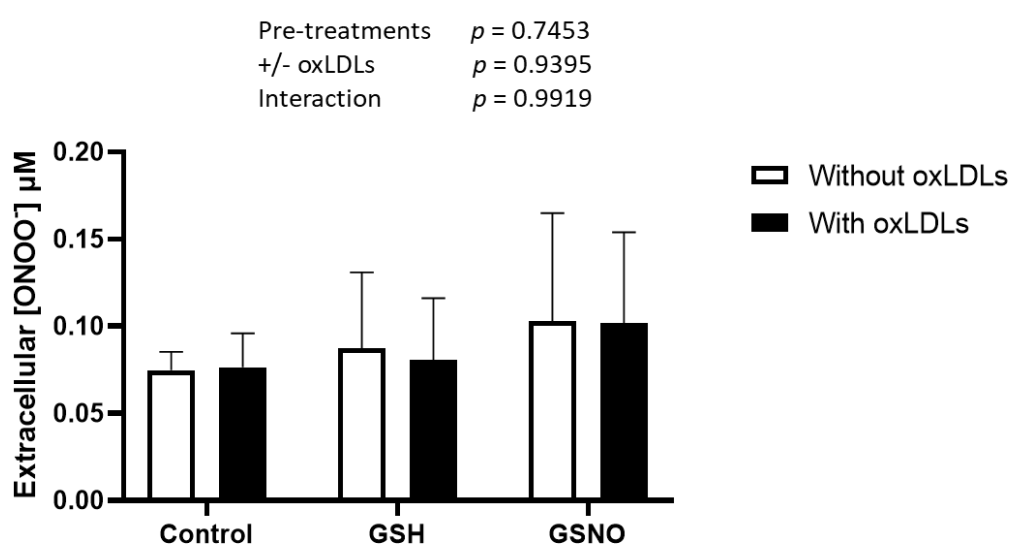


**Figure 12:** Extracellular quantification of peroxynitrite ions. Cells were pre-treated with GSH or GSNO for 6 h and incubated with oxLDLs at 25 μg/mL for 48 h in fresh complete medium. Results are presented as mean ± SEM of 2-3 independent experiments and analysed by Two-way ANOVA

ROS signaling passes mostly through the modification of thiol functions of aminoacids, peptides and proteins. Therefore, the thiol redox status of cells (**Fig. 13**) was evaluated upon the quantification of low molecular weight (LMW) thiols (**Fig. 13A**) corresponding essentially to free cysteine residues and cysteine-containing peptides such as GSH, intracellular GSH concentration (**Fig. 13B**) as well as intracellular GSH/GSSG ratio (**Fig. 13C**), extracellular GSH concentration (**Fig. 13D**), and proteins containing thiol function named high molecular weight (HMW) thiols (**Fig. 13E**).

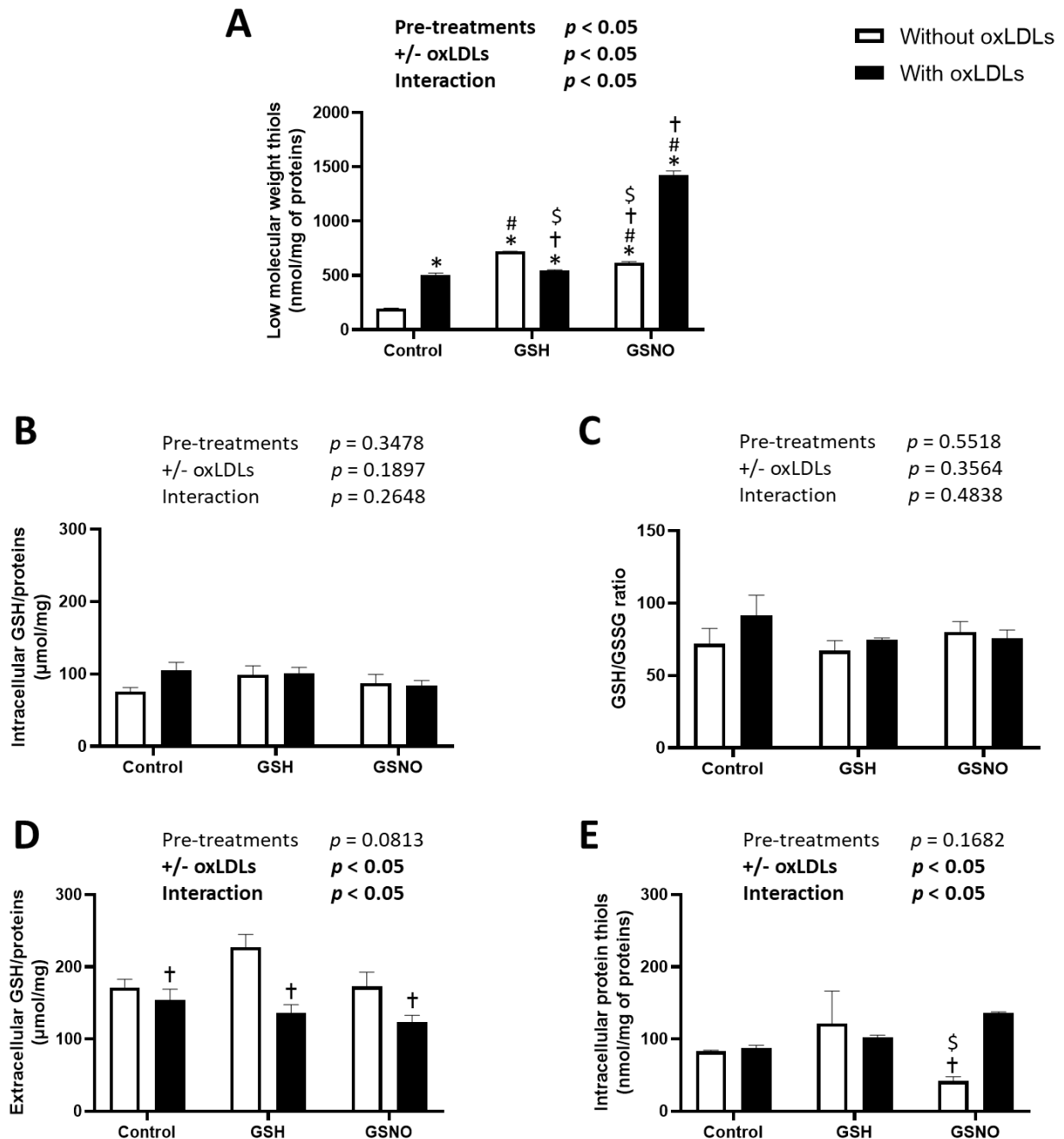


**Figure 13:** Thiol redox status of M0-macrophages. Cells were pre-treated with GSH or GSNO for 6 h and incubated with oxLDLs at 25  $\mu\text{g/mL}$  for 48 h in fresh complete medium. **A:** intracellular low molecular weight (LMW) thiols concentration; **B:** intracellular GSH concentration; **C:** intracellular GSH/GSSG ratio; **D:** extracellular GSH concentration and **E:** intracellular protein thiols concentration. Results are presented as mean  $\pm$  SEM of 3 independent experiments and analysed by Two-way ANOVA and Tukey's multiple comparison; \* vs. control without oxLDLs; # vs. control with oxLDLs; † vs. GSH without oxLDLs; § vs. GSNO with oxLDLs;  $p < 0.05$

The intracellular concentration of LMW thiols is affected by GSH and GSNO pre-treatment as well as by the presence of oxLDLs (**Fig. 13A**). Indeed, under GSH or GSNO pre-treatments, and without oxLDLs incubation, the concentration of intracellular LMW thiols is increased compared to the control in the same amount between GSH and GSNO. This result is not surprising as GSH and GSNO contain cysteine residues that might have been delivered to

M0-macrophages during the pre-treatment. After oxLDLs incubation, this increase is not observed into M0-macrophages pre-treated with GSH followed by oxLDLs incubation, possibly suggesting that the oxidative stress induced by oxLDLs consumes the LMW thiols brought by GSH. However, a GSNO pre-treatment on M0-macrophages undergoing oxLDLs incubation highly increase their LMW thiols content. As no modification in LMW thiol intracellular content was seen with GSH pre-treatment, we can assume that NO is responsible of the 3 times increase in LMW thiol observed with GSNO pre-treatment. So, GSNO pre-treatment helps M0-macrophages to fight against the oxidative stress induced by oxLDLs incubation by increasing their production of LMW thiols. As already said, LMW thiols are composed of cysteine residues and cysteine-containing peptides such as GSH. Glutathione is the major intracellular antioxidant and considered as the main intracellular redox buffer regarding the GSH/GSSG redox couple. GSH intracellular concentration as well as the GSH/GSSG ratio are not affected by any of the pre-treatments or oxLDLs incubation (**Fig. 13B** and **13C**) indicating that glutathione is still able to maintain the intracellular redox potential of M0-macrophages. The only variation observed within GSH balance is the decrease in its efflux after incubation with oxLDLs in the GSH pre-treatment condition compared to a GSH-pre-treatment without oxLDLs incubation (**Fig. 13D**). As the efflux of GSH is decreased, the intracellular concentration might increase. No increase in either intracellular LMW thiols nor intracellular GSH concentration or GSH/GSSG ratio was observed. This suggests that GSH is metabolized by the cells and probably oxidized to counteract the oxidative stress induced by oxLDLs incubation.

The intracellular HMW thiols representing proteins containing reduced cysteine residues is not impacted by GSH pre-treatment followed by an incubation with or without oxLDLs compared to control conditions (**Fig. 13E**). On the contrary, GSNO pre-treatment without oxLDLs incubation decreases the amount of HMW thiols compared to GSH pre-treatment without oxLDLs incubation or GSNO pre-treatment followed by oxLDLs incubation (**Fig. 13E**). This might suggest that GSNO pre-treatment induces either the oxidation of proteins thiol function or protein *S*-nitrosation as a NO store or protein activity modification, which is not seen after oxLDLs incubation because NO is remobilized.

#### 3.4. Intracellular formation of nitrite ions and *S*-nitrosothiols in presence of oxLDLs

Intracellular NO<sub>2</sub><sup>-</sup> concentration is decreased by oxLDLs incubation whatever the pre-treatment is compared to incubation without oxLDLs (**Fig. 14A**). As M0-macrophages contains nitrite ions after each pre-treatment without oxLDLs incubation, we can hypothesize that



oxLDLs consumes the intracellular nitrite ions stock. This consumption is not due to nitrite ions oxidation into peroxynitrite ions as no variation of the intracellular concentration of peroxynitrite ions was observed (section 3.3). An oxidation into nitrate ions is not envisaged because the cytosol is known to be reductive [18] and its redox potential was not affected by oxLDLs incubation as showed by the GSH/GSSG ratio (**Fig. 13C**).

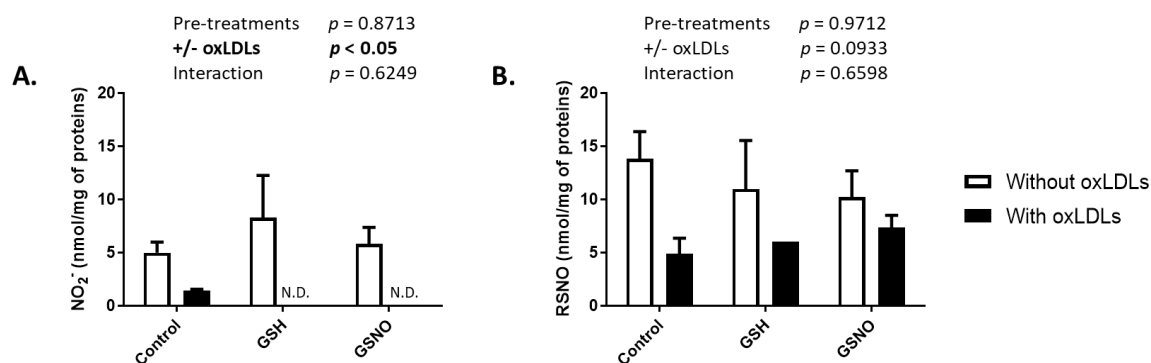


**Figure 14:** **A:** Intracellular formation of nitrite ions (NO<sub>2</sub><sup>-</sup>) and **B:** S-nitrosothiols (RSNOs), quantified by DAN and DAN-Hg<sup>2+</sup> assay. N.D.: not detected. Cells were pre-treated with GSH or GSNO for 6 h and incubated with oxLDLs at 25 µg/mL for 48 h in fresh complete medium. Results are presented as mean ± SEM of 3 independent experiments and analysed by Two-way ANOVA;  $p < 0.05$

Incubation of M0-macrophages with oxLDLs induces a decrease tendency on intracellular RSNOs content compared to the condition with oxLDLs without any statistical difference (**Fig. 14B**).

#### 4. Discussion

Atherosclerosis is one of the most common cardiovascular diseases. The implication of M0-macrophages in the development of atheroma plaques is well known and demonstrated. Internalisation of oxLDLs by macrophages leads to the formation of foam cells, composing the lipid necrotic core of plaques. In the present study, the experiments were planned to demonstrate the potential of GSNO, a NO donor, to counteract M0-macrophages internalization of oxLDLs by modulating oxidative stress. OxLDLs induce the activation of a plethora of cellular pathways like NF-κB or PPAR-γ, block macrophage migration (via alterations of cytoskeleton) and induce an overexpression of CD36 [23]. Interaction of CD36 with oxLDLs triggers a pro-inflammatory and pro-atherogenic signaling response [24].

The suitability of our M0-macrophage model obtained from THP-1 cell line and its interaction with oxLDLs has been validated by contrast phase microscopy as well as by fluorescence microscopy. The presence of lipid droplets and the internalization of DiI-oxLDLs suggest the formation of foam cells. The incubation with 25 µM GSNO seems to have no impact on the

morphology of M0-macrophages which were nevertheless able to metabolise almost 90% of the GSNO available in the medium after 6 h. To better understand the effects of GSNO in foam cells formation, the expression of CD36 on M0-macrophages was studied. We confirmed that oxLDLs induce an overexpression of CD36 in M0-macrophages [25] and we showed that GSNO pre-treatment was able to abolish this overexpression of CD36 induced by oxLDLs. Even if we did not see any variation in oxLDLs binding on M0-macrophages (DiI oxLDLs experiment), others showed that in CD36-deficient subjects, 50% of oxLDLs binding to human macrophages is reduced [26]. CD36 is regulated by oxidative stress, its overexpression is induced by oxLDLs and activates oxidative stress-related signalization pathways as well as downregulates the activity of antioxidants factors like Nrf2. GSNO is known to be a strong antioxidant linked to its ability to release NO and GSH. The GSH part will bring cysteine aminoacids to the cell that will be participate to the intracellular thiol pool and part will be used for GSH intracellular synthesis. Moreover, we previously showed that GSNO protects proteins thiol functions from oxidation by increasing their *S*-nitrosation [15]. Therefore, the antioxidant activity of GSNO might explain the abolishment of oxLDLs-induced CD36 overexpression. GSH and GSH/GSSG status have also been implicated in the regulation of macrophage CD36 expression as well as GSH-dependent antioxidant system has anti-atherogenic functions. Indeed, decreased intracellular GSH concentration and GSH/GSSG ratio, using *L*-buthionine-*S,R*-sulfoximine, increased ROS production, CD36 expression and enhances oxLDLs uptake [27]. CD36, in response to oxLDLs, alters cytoskeletal dynamics and inhibits macrophages migration [7]. Moreover, the inhibition of macrophage migration induced by oxLDLs can be restored, *in vitro*, by treating cells with antioxidant like *N*-acetyl-cysteine. In macrophages, oxLDLs/CD36 signaling induces a chronic inflammation through a dysregulation of fatty acid metabolism to oxidative stress from mitochondria. Indeed, in ApoE<sup>-/-</sup> mice, mitochondrial ROS generation is correlated with CD36 expression in lesioned macrophages [28]. As CD36 signaling is mediated and promotes ROS formation and is linked with the migration inhibition, we studied the redox status of the cells. Even if oxLDLs induced an overexpression of CD36 and ROS production, no nitrosative stress was detected in the intracellular or extracellular compartments. As the major part of ROS signaling acts through the modification of thiol functions of amino-acids, proteins or peptides, the M0-macrophages thiol status was evaluated. Usually, pre-treatment with GSNO and incubation with oxLDLs should increase oxidative stress through the production of peroxynitrite ions. In our model, no production of peroxynitrite ions was detected, in presence or absence of oxLDLs, inside M0-macrophages or in the culture medium. LMW thiols of which cysteine and GSH are the major components, are increased by

GSH and GSNO pre-treatments, and upon the incubation with oxLDLs. This increase is higher with GSNO pre-treatment followed by an incubation with oxLDLs supposing an effect of NO and not only an effect of the GSH moiety. This NO effect could be explained by a transnitrosation reaction. Pre-treatment with GSNO could induce protein *S*-nitrosation, an important post-translational modulation of protein function [29,30] and a modification of antioxidant signaling pathways (*i.e.* Nrf2). Indeed, GSNO is able to transfer its nitroso group to another thiol function, *i.e.* cysteine, allowing the obtention of GSH and a low molecular weight RSNO, the *S*-nitroso-*L*-cysteine (L-CysNO). L-CysNO is transported inside the cells and can *S*-nitrosate cellular GSH to reform GSNO or *S*-nitrosate protein [31]. Protein *S*-nitrosation could be a mean to restore and to reconstitute NO store in tissues. This *S*-nitrosation of proteins could not be quantified in our study due to its low stability, this mechanism is transitory and might have disappeared after 6 h of GSNO pre-treatment followed by 48 h of incubation with oxLDLs. M0-macrophages used GSNO to counteract the oxidative stress induced by oxLDLs like the overexpression of CD36 or ROS production.

Glutathione, a strong antioxidant, plays an important role in the maintenance of cells redox status. Pre-treatments or oxLDLs incubation as well as the GSH/GSSG ratio, an indicator of cell redox potential, have not impact on intracellular GSH concentration [16]. The stability of the GSH/GSSG ratio whatever the conditions were, reflects a stable redox signaling and no impact on GSH-related detoxification enzymes [32] in M0-macrophages. Another study demonstrated that oxLDLs promotes ROS formation and protein *S*-glutathionylation by a mechanism independent from its effect on GSH depletion [33]. Macrophages death induced by oxLDLs is mediated by peroxides and/or peroxy radicals but peroxide formation is not sufficient suggesting a second mechanism. This second mechanism would be involved in the disruption of the intracellular glutathione buffering, initiated by the oxLDL-induced depletion of GSH and inhibition of glutathione reductase.

## 5. Conclusion

In the present study, we have demonstrated that a pre-treatment with GSNO abolishes oxLDL-induced overexpression of CD36 through its antioxidant properties. M0-macrophage used GSNO to counteract the oxLDL-induced oxidative stress with a supposing protein *S*-nitrosation and restoration of “NO stores” in tissues. Targeting CD36, its effectors and the induced pathways can be a new possible strategy to counteract atherosclerotic diseases progression.

- [1] P. Libby, Inflammation in atherosclerosis, *Nature*. 420 (2002) 868–874.  
<https://doi.org/10.1038/nature01323>.
- [2] S.W. Waldo, Y. Li, C. Buono, B. Zhao, E.M. Billings, J. Chang, H.S. Kruth, Heterogeneity of human macrophages in culture and in atherosclerotic plaques, *Am. J. Pathol.* 172 (2008) 1112–1126. <https://doi.org/10.2353/ajpath.2008.070513>.
- [3] A. Kadl, A.K. Meher, P.R. Sharma, M.Y. Lee, A.C. Doran, S.R. Johnstone, M.R. Elliott, F. Gruber, J. Han, W. Chen, T. Kensler, K.S. Ravichandran, B.E. Isakson, B.R. Wamhoff, N. Leitinger, Identification of a novel macrophage phenotype that develops in response to atherogenic phospholipids via Nrf2, *Circ Res.* 107 (2010) 737–746.  
<https://doi.org/10.1161/CIRCRESAHA.109.215715>.
- [4] L.J.H. van Tits, R. Stienstra, P.L. van Lent, M.G. Netea, L. a. B. Joosten, A.F.H. Stalenhoef, Oxidized LDL enhances pro-inflammatory responses of alternatively activated M2 macrophages: a crucial role for Krüppel-like factor 2, *Atherosclerosis*. 214 (2011) 345–349. <https://doi.org/10.1016/j.atherosclerosis.2010.11.018>.
- [5] T. Ishii, K. Itoh, E. Ruiz, D.S. Leake, H. Unoki, M. Yamamoto, G.E. Mann, Role of Nrf2 in the regulation of CD36 and stress protein expression in murine macrophages: activation by oxidatively modified LDL and 4-hydroxynonenal, *Circ Res.* 94 (2004) 609–616. <https://doi.org/10.1161/01.RES.0000119171.44657.45>.
- [6] M. Febbraio, E.A. Podrez, J.D. Smith, D.P. Hajjar, S.L. Hazen, H.F. Hoff, K. Sharma, R.L. Silverstein, Targeted disruption of the class B scavenger receptor CD36 protects against atherosclerotic lesion development in mice, *J Clin Invest.* 105 (2000) 1049–1056.
- [7] Y.M. Park, M. Febbraio, R.L. Silverstein, CD36 modulates migration of mouse and human macrophages in response to oxidized LDL and may contribute to macrophage trapping in the arterial intima, *J Clin Invest.* 119 (2009) 136–145.  
<https://doi.org/10.1172/JCI35535>.
- [8] M. Yang, R.L. Silverstein, CD36 signaling in vascular redox stress, *Free Radical Biology and Medicine*. 136 (2019) 159–171.  
<https://doi.org/10.1016/j.freeradbiomed.2019.02.021>.
- [9] Y.M. Park, J.A. Drazba, A. Vasanji, T. Egelhoff, M. Febbraio, R.L. Silverstein, Oxidized LDL/CD36 interaction induces loss of cell polarity and inhibits macrophage locomotion, *Mol Biol Cell*. 23 (2012) 3057–3068. <https://doi.org/10.1091/mbc.E11-12-1051>.
- [10] D.A. Wink, H.B. Hines, R.Y.S. Cheng, C.H. Switzer, W. Flores-Santana, M.P. Vitek, L.A. Ridnour, C.A. Colton, Nitric oxide and redox mechanisms in the immune response, *J Leukoc Biol.* 89 (2011) 873–891. <https://doi.org/10.1189/jlb.1010550>.
- [11] W. Martinet, V. Croons, J.-P. Timmermans, A.G. Herman, G.R.Y. De Meyer, Nitric oxide selectively depletes macrophages in atherosclerotic plaques via induction of endoplasmic reticulum stress, *Br. J. Pharmacol.* 152 (2007) 493–500.  
<https://doi.org/10.1038/sj.bjp.0707426>.
- [12] M.H. Krieger, K.F.R. Santos, S.M. Shishido, A.C.B.A. Wanschel, H.F.G. Estrela, L. Santos, M.G. De Oliveira, K.G. Franchini, R.C. Spadari-Bratfisch, F.R.M. Laurindo, Antiatherogenic effects of S-nitroso-N-acetylcysteine in hypercholesterolemic LDL receptor knockout mice, *Nitric Oxide*. 14 (2006) 12–20.  
<https://doi.org/10.1016/j.niox.2005.07.011>.
- [13] S. Momi, F. Impagnatiello, M. Guzzetta, R. Caracchini, G. Guglielmini, R. Olivieri, A. Monopoli, P. Gresele, NCX 6560, a nitric oxide-releasing derivative of atorvastatin, inhibits cholesterol biosynthesis and shows anti-inflammatory and anti-thrombotic properties, *European Journal of Pharmacology*. 570 (2007) 115–124.  
<https://doi.org/10.1016/j.ejphar.2007.05.014>.



- [14] E. Ongini, F. Impagnatiello, A. Bonazzi, M. Guzzetta, M. Govoni, A. Monopoli, P. Del Soldato, L.J. Ignarro, Nitric oxide (NO)-releasing statin derivatives, a class of drugs showing enhanced antiproliferative and antiinflammatory properties, *Proc Natl Acad Sci U S A.* 101 (2004) 8497–8502. <https://doi.org/10.1073/pnas.0401996101>.
- [15] E. Belcastro, W. Wu, I. Fries-Raeth, A. Corti, A. Pompella, P. Leroy, I. Lartaud, C. Gaucher, Oxidative stress enhances and modulates protein S-nitrosation in smooth muscle cells exposed to S-nitrosoglutathione, *Nitric Oxide.* 69 (2017) 10–21. <https://doi.org/10.1016/j.niox.2017.07.004>.
- [16] C. Gaucher, A. Boudier, J. Bonetti, I. Clarot, P. Leroy, M. Parent, Glutathione: Antioxidant Properties Dedicated to Nanotechnologies, *Antioxidants (Basel).* 7 (2018). <https://doi.org/10.3390/antiox7050062>.
- [17] M. Parent, F. Dahboul, R. Schneider, I. Clarot, P. Maincent, P. Leroy, A. Boudier, A Complete Physicochemical Identity Card of S-nitrosoglutathione, *Current Pharmaceutical Analysis.* 9 (2013) 31–42. <https://doi.org/10.2174/157341213804806098>.
- [18] T.L. Innerarity, R.E. Pitas, R.W. Mahley, Lipoprotein-receptor interactions, *Methods Enzymol.* 129 (1986) 542–565. [https://doi.org/10.1016/0076-6879\(86\)29091-6](https://doi.org/10.1016/0076-6879(86)29091-6).
- [19] J. Bonetti, Y. Zhou, M. Parent, I. Clarot, H. Yu, I. Fries-Raeth, P. Leroy, I. Lartaud, C. Gaucher, Intestinal absorption of S-nitrosothiols: Permeability and transport mechanisms, *Biochem. Pharmacol.* 155 (2018) 21–31. <https://doi.org/10.1016/j.bcp.2018.06.018>.
- [20] W.S. Jobgen, S.C. Jobgen, H. Li, C.J. Meininger, G. Wu, Analysis of nitrite and nitrate in biological samples using high-performance liquid chromatography, *J. Chromatogr. B Analyt. Technol. Biomed. Life Sci.* 851 (2007) 71–82. <https://doi.org/10.1016/j.jchromb.2006.07.018>.
- [21] E.F.C. Simões, J.M.M. Leitão, J.C.G.E. da Silva, Reduced fluoresceinamine for peroxynitrite quantification in the presence of nitric oxide, *J Fluoresc.* 22 (2012) 1127–1140. <https://doi.org/10.1007/s10895-012-1051-3>.
- [22] J.L. Knepler, L.N. Taher, M.P. Gupta, C. Patterson, F. Pavalko, M.D. Ober, C.M. Hart, Peroxynitrite causes endothelial cell monolayer barrier dysfunction, *American Journal of Physiology-Cell Physiology.* 281 (2001) C1064–C1075. <https://doi.org/10.1152/ajpcell.2001.281.3.C1064>.
- [23] J. Bonetti, A. Corti, L. Lerouge, A. Pompella, C. Gaucher, Phenotypic Modulation of Macrophages and Vascular Smooth Muscle Cells in Atherosclerosis-Nitro-Redox Interconnections, *Antioxidants (Basel).* 10 (2021) 516. <https://doi.org/10.3390/antiox10040516>.
- [24] R.L. Silverstein, W. Li, Y.M. Park, S.O. Rahaman, Mechanisms of Cell Signaling by the Scavenger Receptor CD36: Implications in Atherosclerosis and Thrombosis, *Trans Am Clin Climatol Assoc.* 121 (2010) 206–220.
- [25] B. Fuhrman, N. Volkova, M. Aviram, Oxidative stress increases the expression of the CD36 scavenger receptor and the cellular uptake of oxidized low-density lipoprotein in macrophages from atherosclerotic mice: protective role of antioxidants and of paraoxonase, *Atherosclerosis.* 161 (2002) 307–316. [https://doi.org/10.1016/s0021-9150\(01\)00646-3](https://doi.org/10.1016/s0021-9150(01)00646-3).
- [26] S. Nozaki, H. Kashiwagi, S. Yamashita, T. Nakagawa, B. Kostner, Y. Tomiyama, A. Nakata, M. Ishigami, J. Miyagawa, K. Kameda-Takemura, Reduced uptake of oxidized low density lipoproteins in monocyte-derived macrophages from CD36-deficient subjects, *J Clin Invest.* 96 (1995) 1859–1865. <https://doi.org/10.1172/JCI118231>.
- [27] X. Yang, H. Yao, Y. Chen, L. Sun, Y. Li, X. Ma, S. Duan, X. Li, R. Xiang, J. Han, Y. Duan, Inhibition of Glutathione Production Induces Macrophage CD36 Expression and

- Enhances Cellular-oxidized Low Density Lipoprotein (oxLDL) Uptake, *J Biol Chem.* 290 (2015) 21788–21799. <https://doi.org/10.1074/jbc.M115.654582>.
- [28] Y. Chen, M. Yang, W. Huang, W. Chen, Y. Zhao, M.L. Schulte, P. Volberding, Z. Gerbec, M.T. Zimmermann, A. Zeighami, W. Demos, J. Zhang, D.A. Knaack, B.C. Smith, W. Cui, S. Malarkannan, K. Sodhi, J.I. Shapiro, Z. Xie, D. Sahoo, R.L. Silverstein, Mitochondrial metabolic reprogramming by CD36 signaling drives macrophage inflammatory responses, *Circ Res.* 125 (2019) 1087–1102. <https://doi.org/10.1161/CIRCRESAHA.119.315833>.
- [29] B. Huang, S.C. Chen, D.L. Wang, Shear flow increases S-nitrosylation of proteins in endothelial cells, *Cardiovascular Research.* 83 (2009) 536–546. <https://doi.org/10.1093/cvr/cvp154>.
- [30] M. Ibáñez-Vea, H. Huang, X. Martínez de Morentin, E. Pérez, M. Gato, M. Zuazo, H. Arasanz, J. Fernández-Irigoyen, E. Santamaría, G. Fernandez-Hinojal, M.R. Larsen, D. Escors, G. Kochan, Characterization of Macrophage Endogenous S-Nitrosoproteome Using a Cysteine-Specific Phosphonate Adaptable Tag in Combination with TiO<sub>2</sub> Chromatography, *J Proteome Res.* 17 (2018) 1172–1182. <https://doi.org/10.1021/acs.jproteome.7b00812>.
- [31] K.A. Broniowska, A.R. Diers, N. Hogg, S-nitrosoglutathione, *Biochim. Biophys. Acta.* 1830 (2013) 3173–3181. <https://doi.org/10.1016/j.bbagen.2013.02.004>.
- [32] D.P. Jones, Redox potential of GSH/GSSG couple: assay and biological significance, *Methods Enzymol.* 348 (2002) 93–112. [https://doi.org/10.1016/s0076-6879\(02\)48630-2](https://doi.org/10.1016/s0076-6879(02)48630-2).
- [33] Y. Wang, M. Qiao, J.J. Mieyal, L.M. Asmis, R. Asmis, Molecular mechanism of glutathione-mediated protection from oxidized low-density lipoprotein-induced cell injury in human macrophages: role of glutathione reductase and glutaredoxin, *Free Radic Biol Med.* 41 (2006) 775–785. <https://doi.org/10.1016/j.freeradbiomed.2006.05.029>.

### III. Development of a primary model of monocytes differentiation into macrophages and their polarization

#### 1. Differentiation of monocytes into M0-macrophages

The previous co-tutelle project was focused on the elaboration of a protocol to differentiate monocytes into M1-like macrophages (pro-inflammatory) or M2-like macrophages (anti-inflammatory). The model has been published with a differentiation obtained by GM-CSF or M-CSF stimulation followed by an incubation with IL-10, TNF $\alpha$  or TNF $\alpha$ /IL-1 $\beta$  [11]. One goal of my PhD was to improve this model considering both the protocol of monocytes isolation and the combination of growth factors and cytokines to induce a more suitable M1 and M2 polarization according to the literature [61,62]. The protocols commonly used for monocytes isolation start from isolated blood mononuclear cells (lymphocytes and monocytes) and are based on the known property of monocytes to adhere to culture plastic dishes or on the employment of magnetic beads grafted with specific antibody. Moreover, according to literature, cultures of basal M0-macrophages can be obtained by cultivating isolated monocytes in the presence of M-CSF at 50 ng/mL for 5-7 days. Then, the polarization of M0-macrophages is obtained using pro-inflammatory factors, *i.e.* IFN $\gamma$  + LPS for M1-macrophages and anti-inflammatory factors, *i.e.* IL-4 or IL-10 for M2-macrophages.

Blood from healthy donors was collected and peripheral blood mononuclear cells (PBMCs) were isolated by Histopaque-1077<sup>®</sup> density centrifugation. The Institutional Ethics Committee of the University of Pisa approved the protocol that was conformed to the Declaration of Helsinki. Patients gave their verbal informed consent to participate and the data were analysed anonymously.

On these bases, the two different methods for monocytes isolation were compared [11,63]:

- ❖ **Isolation with magnetic beads** (Miltenyi kit (MACS, Pan Monocytes Isolation kit)): allowing the collection of classical monocytes CD14<sup>+</sup>/CD16<sup>-</sup>. The process is based on a negative selection. Mononuclear cells labelled with a cocktail of biotin-conjugated antibody (against T cells, natural killer cells, B cells, dendritic cells and basophiles) are separated from unlabelled cells using a column and a magnetic field. Cells of interest, here monocytes, remains unlabelled and in their native state, unlike unwanted cells (lymphocytes and non-monocytes) which are labelled by the biotin antibody specific for their cell surface receptors and are thus retained in the column.

- ❖ **Adherence method:** PBMCs are left to adhere to the plastic plate for 24 h in RPMI 1640 medium supplemented with 10% (v/v) of fetal calf serum, 2 mmol/L of *L*-glutamine, 100 U/mL of penicillin and 100 µg/mL of streptomycin. After 24 h of culture, non-adherent cells are removed to keep only adherent cells, the monocytes.

In both cases, monocytes are cultured for 7 days more in complete medium supplemented with 50 ng/mL of M-CSF allowing the differentiation of monocytes into M0-macrophages (CD68<sup>+</sup>).

#### a. Polarization of M0-macrophages

M0-macrophages are stimulated and polarized towards a M1 or M2 phenotype with a 48 h- incubation with a mix of interferon-γ (IFNγ) at 20 ng/mL and lipopolysaccharide (LPS) at 100 ng/mL for M1-macrophages polarization or, IL-4 or IL-10 at 20 ng/mL for M2-macrophages polarization.

To validate the polarization of M0-macrophages into M1 or M2 subtypes, the expression of CD80 (surface receptor for LDLs) a phenotypical marker of M1-macrophages and CD206 (mannose receptor) a specific marker of M2-macrophages have been analysed by flow-cytometry. Similar levels of cell viability (about 98%) and purity (about 86% of CD14<sup>+</sup> cells, a marker of monocytes/macrophages) were found for both techniques. The expression of CD80 in IFNγ/LPS treated cells and CD206 in IL-4 or IL-10 macrophages was confirmed (**Table 3**) without any impact of the technique used for isolation. On these bases and due to the requirement of a large number of cells for further experiments, we decided to use the less expensive method, the adhesion method.


**Table 3:** expression of M1- and M2-macrophages markers after analysis by flow-cytometry

Types of macrophages expected	Growth factors/Cytokines	Isolation with magnetic beads	Adherence method
M1	IFNγ/LPS	80% CD80 <sup>+</sup> / CD206 <sup>-</sup>	80% CD80 <sup>+</sup> / CD206 <sup>-</sup>
M2	IL-4	95% CD80 <sup>-</sup> / CD206 <sup>+</sup>	95% CD80 <sup>-</sup> / CD206 <sup>+</sup>
M2	IL-10	90% CD80 <sup>-</sup> / CD206 <sup>+</sup>	96% CD80 <sup>-</sup> / CD206 <sup>+</sup>

This model has been validated and published in *Toxicological Sciences* in 2020 “*Induction of gamma-glutamyltransferase activity and consequent pro-oxidant reactions in human macrophages exposed to crocidolite asbestos*” (**Appendix 1**).



## Induction of Gamma-Glutamyltransferase Activity and Consequent Pro-oxidant Reactions in Human Macrophages Exposed to Crocidolite Asbestos

Alessandro Corti <sup>\*,†</sup>, Justine Bonetti,<sup>†</sup> Silvia Dominici,<sup>\*</sup> Simona Piaggi,<sup>\*</sup> Vanna Fierabracci,<sup>\*</sup> Rudy Foddìs,<sup>\*</sup> and Alfonso Pompella<sup>\*</sup>

<sup>\*</sup>Department of Translational Research NTMS, University of Pisa Medical School, Pisa 56126, Italy; and

<sup>†</sup>Université de Lorraine, CITHEFOR, F-54000 Nancy, France

The authors certify that all research involving human subjects was done under full compliance with all government policies and the Helsinki Declaration.

<sup>‡</sup>To whom correspondence should be addressed. Fax: (+39) 050 2218557; E-mail: alessandro.corti@med.unipi.it.

### b. Antioxidant defences

To further characterize the antioxidant defences of our M1/M2 macrophages and to determine their implication in the oxidative stress context of atheroma plaques, we have also evaluated the expression of some key enzymes involved in GSH metabolism:  $\gamma$ -glutamyl-transferase (GGT), glutathione peroxidase (GPx), glutathione reductase (GR) and glutathione *S*-transferase (GST). These enzymes are involved in the maintenance of cell redox status and in the GSH-dependent modulation of several functions involved in cell homeostasis such as the maintenance of low levels of ROS or of the balance GSH/GSSG, including the synthesis and the degradation of GSNO. Indeed, GGT is involved in the antioxidant defences and implicated in the GSH/GSNO catabolism. In atherosclerosis, GGT is used as a predictor of cardiovascular risks with an association of higher GGT levels and the progression of atherosclerosis [64]. An interaction between the fraction b-GGT and cardiovascular risk factors (LDL cholesterol, triglycerides...) has been demonstrated [11]. GGT is also involved in the decomposition of GSNO with hydrolysis and transpeptidase reactions. GPx, another antioxidant enzyme family, are used to detoxify from ROS, mainly H<sub>2</sub>O<sub>2</sub> and lipids into H<sub>2</sub>O or O<sub>2</sub>. GR is able to reduce one GSSG into two GSH molecules, allowing the maintenance of the supply of GSH. GSTs are a family of enzymes involved in antioxidant defences and also in the detoxification of endogenous/exogenous compounds. GST can reduce lipid hydroperoxides through their selenium-dependent GPx activity [65]. Their role in the redox regulation of intracellular signaling pathways implicated in cell survival and apoptosis (MAPK family) has been suggested [66,67].

Therefore, we evaluated the activity of these four enzymes in monocytes, M0-, M1- and M2-macrophages as follows. Cells were seeded in Petri dish at  $400.10^6$  cells/mL and differentiated into the different macrophage types (see parts “*differentiation of monocytes into M0-macrophages*” and “*Polarization of M0-macrophages*”). Then, cells were lysed and scraped in Tris-HCl buffer (10 mM; pH = 7.8), this followed by 5 cycles of freezing/defrosting (-80 °C/37 °C), 50 strokes of Dounce homogenizer. Samples were conserved at -80 °C until use.

- ❖ GGT activity was evaluated according to Huseby and Strömme [68–70]. Briefly, 1 mL of gamma-glutamyl-p-nitroanilide (GPNA) solution was mixed with 100 µL of glycylglycine (GlyGly). The reaction was started by the addition of 50 µL of the sample and incubated at 37 °C. The sample is ready when a clearly different colour was observed compared to the corresponding blank. The absorbance was read at 405 nm.
- ❖ GPx activity was evaluated using the method of Paglia and Valentine, with minor modifications [71]. Briefly, 100 µL of cell lysate was mixed in 0.1 M of potassium phosphate buffer, pH=7, with 1 mM of EDTA, 1 mM of sodium azide, 1 mM of reduced glutathione, 2 U/mL of glutathione reductase and 0.2 mM of NADPH. The enzymatic reaction was started by addition of 0.1 mL of 1.5 M cumene hydroperoxide. We followed the oxidation of NADPH spectrophotometrically at 340 nm for 5 minutes after the beginning of the reaction.
- ❖ GR activity was measured using 100 µL of cell lysate mixed with 0.06 M of sodium phosphate buffer, pH=7.6, containing 3 mM of EDTA and 2 mg/mL of bovine serum albumin and added with 3.25 mM of GSSG and 0.1 mM of NADPH. The oxidation of the NADPH was followed spectrophotometrically at 340 nm for 5 minutes after the beginning of the reaction [72].
- ❖ GST activity was performed using 10 µL of cell lysate diluted in 0.1 M potassium phosphate buffer, pH=6.5 and mixed with 1 mM of reduced glutathione and 1 mM of chloro-2,4 dinitrobenzene (CDNB). The absorption of GS-dinitrobenzene (GS-DNB) adduct was followed spectrophotometrically at 340 nm for 5 minutes after the beginning of the reaction [73].

We thus evaluated the activity of these enzymes in our M1-like and M2-like macrophages. As expected, we observed a certain level of biological variability among samples obtained from different donors. To decrease the variability between the samples and to better compare the

effect of cytokines on their activity, we decided to express our data as a ratio of the proteins (Fig. 15).

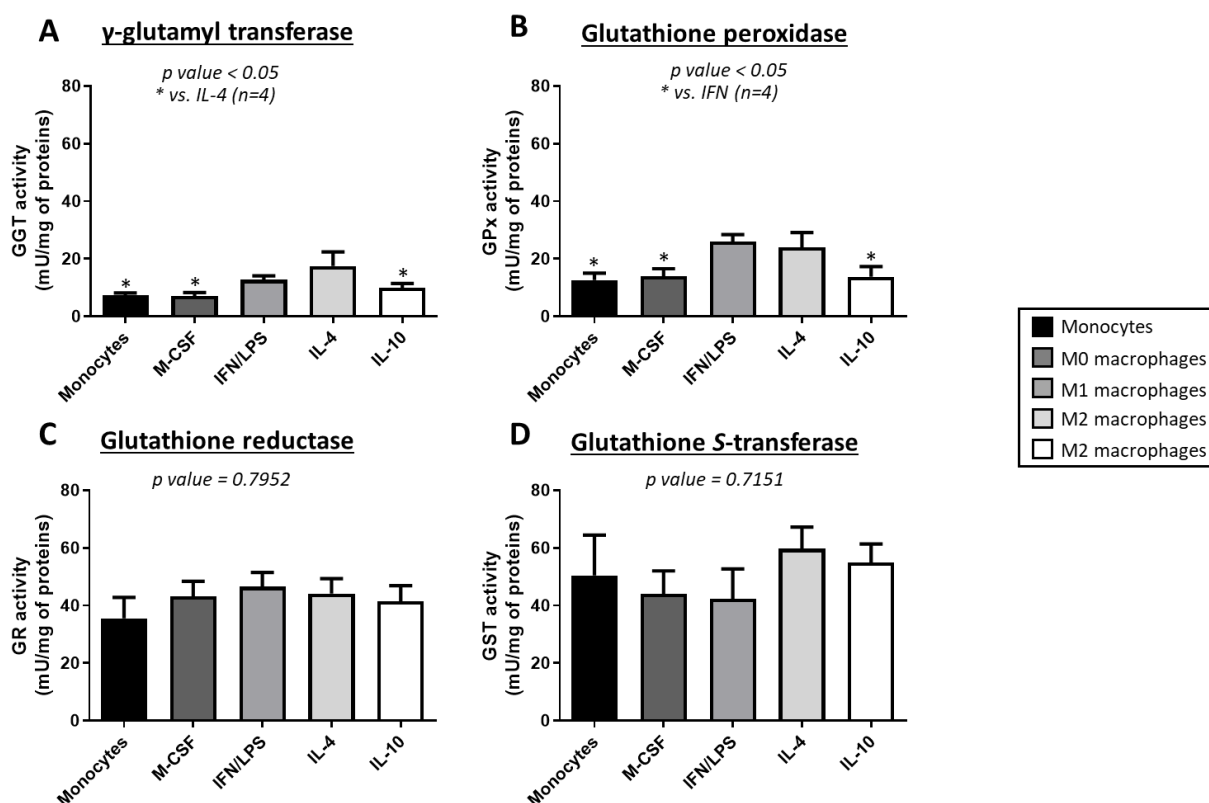


**Figure 15:** Enzyme activity of the  $\gamma$ -glutamyl transferase (GGT) (A), the glutathione peroxidase (GPx) (B), the glutathione reductase (GR) (C) and the glutathione S-transferase (GST) (D). Results are presented as mean  $\pm$  SEM of 3-4 independent experiments and analysed by One-way ANOVA – Tukey’s post test; \* vs. IL-4 or IFN $\gamma$ ;  $p < 0.05$ .

GGT activity was 1.5 to 2 times higher in M1- and M2-macrophages than in monocytes and M0-macrophages (Fig. 15A). These data are in agreement with those previously obtained in our lab [11]. However, GGT activity was the same in M1-macrophages (cells treated with IFN $\gamma$ /LPS) and in M2-macrophages (cells treated with IL-4 or IL-10). A recent study showed that in asymptomatic individuals, elevated serum GGT levels were significantly associated with advance atherosclerotic plaques [74]. Indeed, GGT is induced by oxidative stress and pro-inflammatory cytokines and could be involved in the function of “pro-inflammatory” M1-macrophages [11]. It has been shown that degranulation of M1-macrophages release large amount of GGT [11]. Interestingly, GPx activity is 2 times higher in M1-macrophages and M2-macrophages (treated with IL-4) than in monocytes and M0-macrophages (Fig. 15B). The higher levels of GPx could play a role in the antioxidant defences of “pro-inflammatory” M1 macrophages involved in the oxidative burst using GSH as co-substrate. Indeed, GPx4 is the only antioxidant enzyme implicated in the inhibition of lipid peroxidation with the reduction of phospholipid hydroperoxides within membrane and lipoproteins [75].

GR and GST activities are the same in monocytes, M0-macrophages, M1-macrophages or M2-macrophages (**Fig. 15C** and **15D**). However, our results showed two times higher activities for GR and GST compared to GGT and GPx.

The higher activities of GGT and GPx in M2-macrophages (treated with IL-4) than in M0-macrophages can induce a better metabolism of GSNO, inducing a higher level of NO in the cells, limit lipid peroxidation and ROS production.



# CHAPTER 3

## DEVELOPMENT OF A SMOOTH MUSCLE CELLS MODEL OF DEDIFFERENTIATION

In healthy arteries, vSMCs are located in the tunica media of the vessel wall where they are responsible for vasoactivity (contraction/relaxation), vascular diameter and blood pressure. Differentiated contractile vSMCs have low migration and proliferation abilities. They express specific contractile markers like  $\alpha$ -smooth muscle actin ( $\alpha$ -SMA), smooth muscle myosin heavy chain (SM-MHC), transgelin, H1-calponin and smoothelin. However, unlike other muscle cells, vSMCs do not terminally differentiate and retain a high level of plasticity while remaining in a quiescent phenotype. In response to vascular injury and inflammatory stimuli, such as during atherosclerosis, contractile vSMCs are able to undergo de-differentiation to a secretory/proliferative (“pro-atherosclerotic”) phenotype, which is implicated in vascular wall hyperplasia occurring during progression of atherosclerotic plaques [76]. De-differentiated vSMCs are characterized by a decreased expression of contractile markers and increased proliferation, migration and secretory abilities, and can even express markers of macrophagic as well as skeletal muscle phenotypes. De-differentiated vSMCs act in all steps of atherosclerosis development, until the formation of advanced plaques presenting a necrotic core and varying degrees of calcification. The vSMCs’ phenotypic switch allows their migration and infiltration from the media to intima due to secretion of matrix metalloproteinases (MMP-2, MMP-9) [12], as well as their capacity to internalise oxLDLs through the expression of the pro-low density lipoprotein receptor-related protein 1 (LRP-1). During their phenotypic switch, in a pro-inflammatory context, vSMCs acquire macrophagic properties and express macrophage markers, such as CD68 [34], as well as mesenchymal stem cells markers (*e.g.*, Sca1 and CD105) [35,77], suggesting the presence of a vSMC progenitor population within the vessel wall that proliferates and accumulates along with the development of atherosclerosis. The switch to a macrophage-like phenotype is likely driven by lipids accumulation and is the main step in the formation of foam cells and the necrotic core of plaques [35]. Foam cells encountered in plaques have been shown in fact to derive from both macrophages and vSMCs, through oxLDLs accumulation [36–38]. Allahverdian *et al.* previously demonstrated that, of the foam cells present in human plaques, 40% are of vSMC origin *vs.* 60% of a macrophagic one [78].

The following chapter will focus the development of a vSMCs dedifferentiated model using AngII.

## I. Validation of vascular smooth muscle cells contractile phenotype

During this PhD, several cell types have been used in this part of the project. Many problems such as slow growth, contaminations, no reactivity have been encountered with the human aortic vascular smooth muscle cells (HA-VSMC; ATCC® CRL-1999™) and aortic primary smooth muscle cells from Wistar rat (SMC-I).

Then we focused on human aortic SMCs (HAoSMCs, CC2571 from Lonza®) because they are primary and from human origin (**Fig. 16**) so more adapted to our purpose.

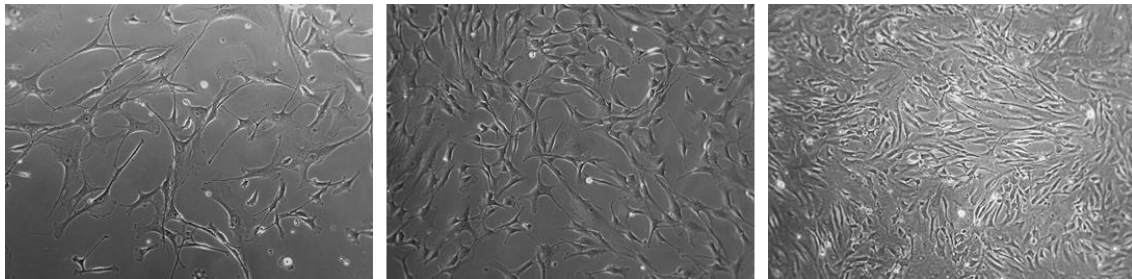


**Figure 16:** Optical microscopy of Human Aortic smooth muscle cells – CC2571 Lonza® (pictures from Lonza®)

First, the phenotype of HAoSMCs was validated using specific markers:

- ❖ Myosin heavy chain, a contractile protein of muscle: lost during dedifferentiation
- ❖  $\alpha$ -actin playing a major role in cell anchoring: lost during dedifferentiation
- ❖ Transgelin, a precocious marker of vSMCs differentiation (calponin analogous, SM22 $\alpha$ ), playing a role in actin cross-linking/gelling: lost during dedifferentiation
- ❖ Vimentin, essential for organelle support and anchoring.

All these markers play a role in maintaining the cytoskeleton structure and the contractility of primary vSMCs. The presence of  $\alpha$ -actin, transgelin and vimentin was validated by immunofluorescence (**Fig. 17**). Myosin was not detected even with two distinct primary antibodies.

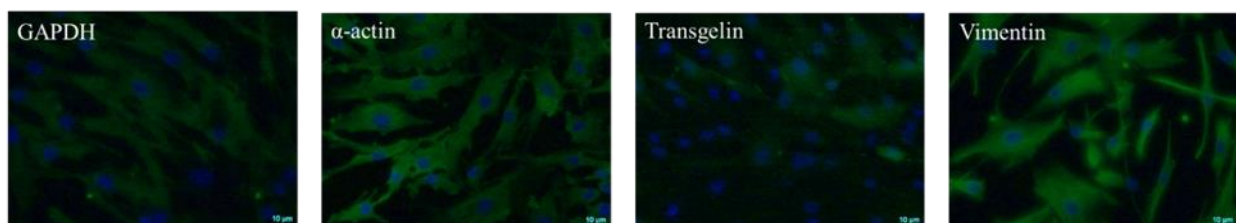


**Figure 17:** Immunofluorescent detection of differentiation markers of vSMCs:  $\alpha$ -actin, transgelin, vimentin and reference protein: GAPDH. Cells were fixed with paraformaldehyde 4% (w/v) and labelled with 1:50  $\alpha$ -actin/transgelin/vimentin for 45 minutes in blocking solution (Triton 0.1% (w/v), PBS/BSA 0.5% (w/v)). Then, secondary antibody Alexa® 488 diluted at 1:100 was incubated 45 minutes. Finally, nuclei are labelled by Hoechst 33258 for 15 minutes (Magnification: 40x, scale bar: 10  $\mu$ m)

The expression of the three differentiation markers was semi-quantified by Western-blot (Fig. 18). These two experiments validated the contractile phenotype of vSMCs.

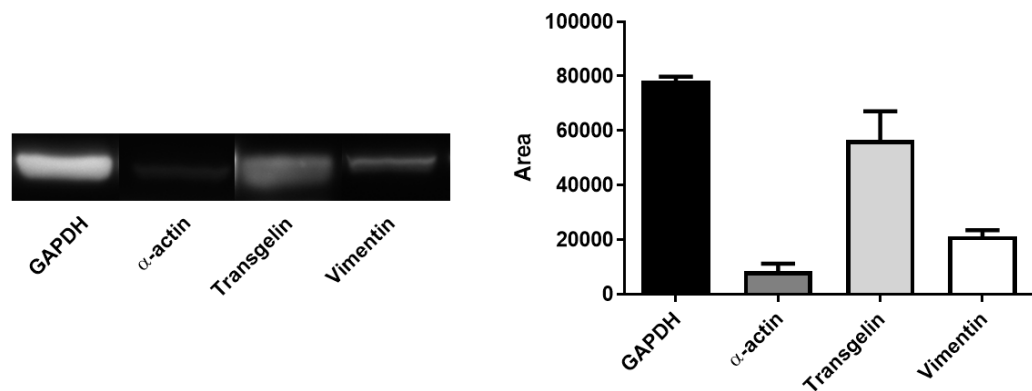


**Figure 18:** Quantification of the expression of differentiation markers of vSMCs by Western blot analysis; GAPDH,  $\alpha$ -actin, transgelin and vimentin (n=3)

We also studied the impact of cell passage on those markers of differentiation (Fig. 19). The number of passages seems to have a slight effect on  $\alpha$ -actin expression, no effect on transgelin expression but a huge effect on vimentin expression with an expression decreased by four after passage 4. Vimentin regulates vSMCs phenotype and its increase in secretory phenotype. However, the number of experiments need to be increased and confirmed by further analysis.

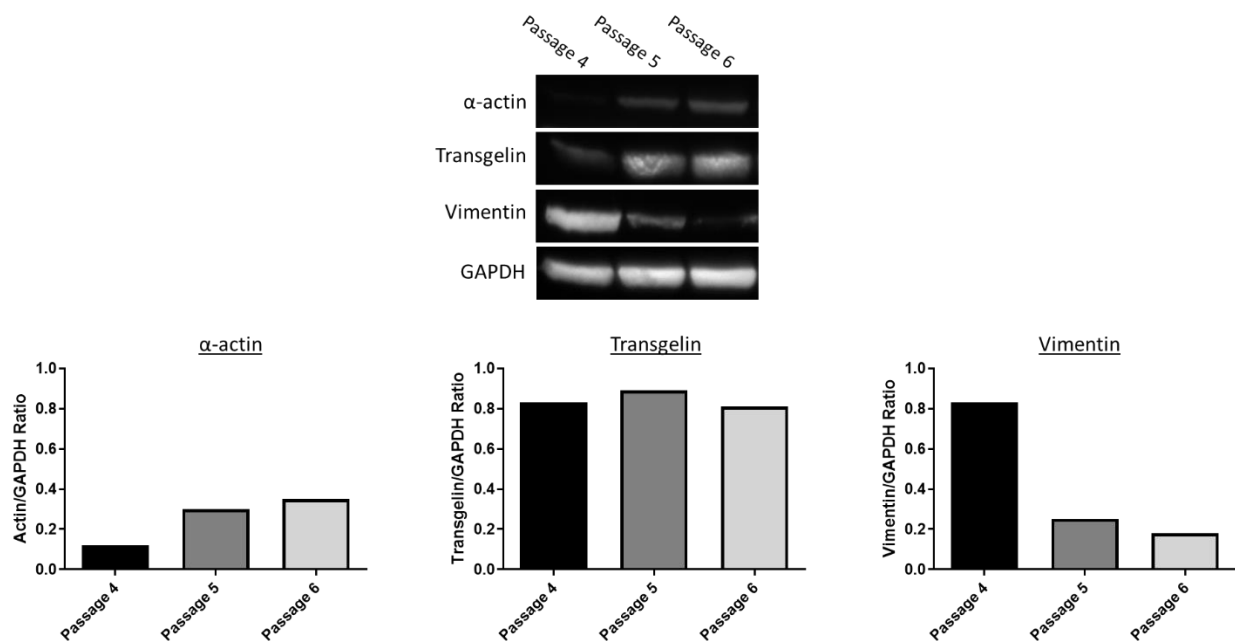


**Figure 19:** Impact of cell passages of the expression of differentiation markers:  $\alpha$ -actin, transgelin and vimentin (n=1)



## II. Development of the smooth muscle cells dedifferentiation model

In the literature, few models of vSMCs dedifferentiation are available. These models are all based on primary rat SMCs and propose to stimulate cells with oxidative stress (deprivation of foetal bovine serum, AngII) or inflammation (lipopolysaccharide stimulus) or both with oxLDLs (**Table 4**).

**Table 4:** Synthesis of dedifferentiation protocols in literature

Methods	Conditions	Cell type (Rat)	Dedifferentiation markers	Dedifferentiation cell type
<b>Fetal Bovine Serum (FBS)</b> <b>Dong N. <i>et al.</i>; 2017</b>	0.5% – 48 h	Aorta (abdominal/thoracic) primary SMC	Calponin Smoothelin	/
<b>Lipopolysaccharide (LPS)</b> <b>Leimgruber C. <i>et al.</i>; 2016</b>	1 µg/mL 48 h	Prostate primary SMC	Calponin Vimentin	Myofibroblast
<b>oxLDLs (PAPC, POVPC, oxPAPC, PGPC)</b> <b>Pidkovka N. <i>et al.</i>; 2007</b>	1 to 30 µg/mL 24 h to 72 h	Aorta primary SMC	α-actin Myosin heavy chain	/
<b>Angiotensin II</b> <b>Guo X. <i>et al.</i>; 2017</b>	100 nM – 48 h	Cardiac primary fibroblasts	β-catenin Collagen I	Myofibroblast
<b>Synchronization of cell cycles + Angiotensin II</b> <b>Tang <i>et al.</i>; 2019</b>	100 nM – 48 h	Aorta (thoracic) primary SMC	p22phox Smooth Muscle 22 α α-actin KLF4	/

Three dedifferentiation protocols were tried (FBS deprivation [79], LPS [80] and AngII [81]). FBS and LPS protocols were excluded because not conclusive and not representative of the disease even if they are used in the literature.

Dedifferentiation induced by AngII has been retained, adapted to the protocol from Tang *et al.*, 2019 [81,82]. First, cells are seeded at  $60.10^3$  cells/mL in complete culture medium (FBS 5%). When cells reach 70-80% of confluency (after around 24 h), cell cycles are synchronized by FBS deprivation (0.5%) during 24 h, followed by a 48-h stimulation with AngII at 100 nM (**Fig. 20**).

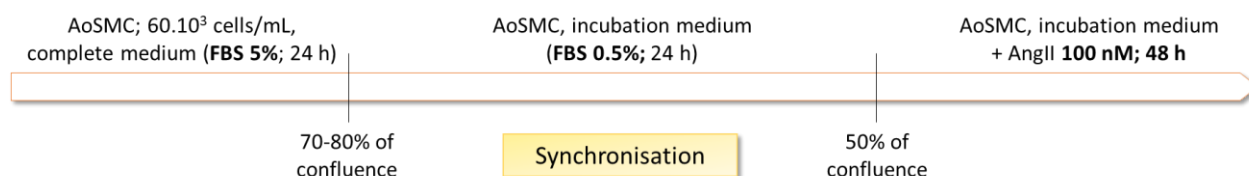


**Figure 20:** Protocol for SMC dedifferentiation based on Tang *et al.* [82]

As GAPDH, a metabolic enzyme, is used as the reference protein to quantify phenotypic markers variation, we first verified the stability of GAPDH expression at different passages and after AngII stimulation. Densitometric quantification was performed using the ImageJ software and showed no difference between different passages, control and AngII stimulation (**Fig. 21**). This result validated GAPDH as the reference protein.

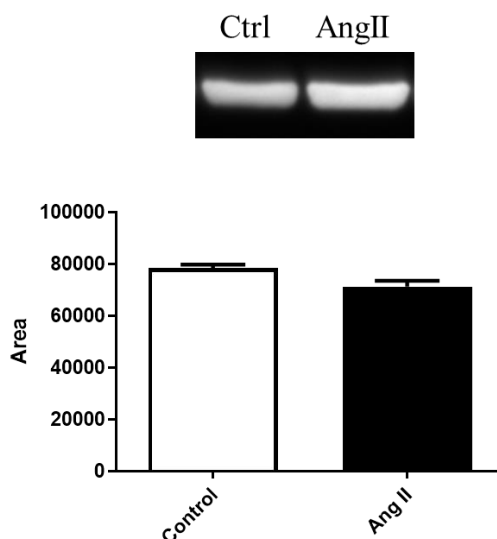


**Figure 21:** Effect of passage and AngII stimulation on GAPDH expression in AoSMCs. Analysis were performed by Western-blot and bands quantify by ImageJ; Mean ± SEM (n=3)

## 1. Synchronisation of the cells and impact of Angiotensin II

The experiments dealing with AngII-induced dedifferentiation (**Fig. 20**) were performed at passages 5 and 6 (thawing at passage 4). Cells morphology was followed after synchronisation (FBS deprivation) and after 4 h, 24 h or 48 h of AngII treatment (**Fig. 22**). There was no impact of FBS deprivation nor AngII treatment on cell morphology.

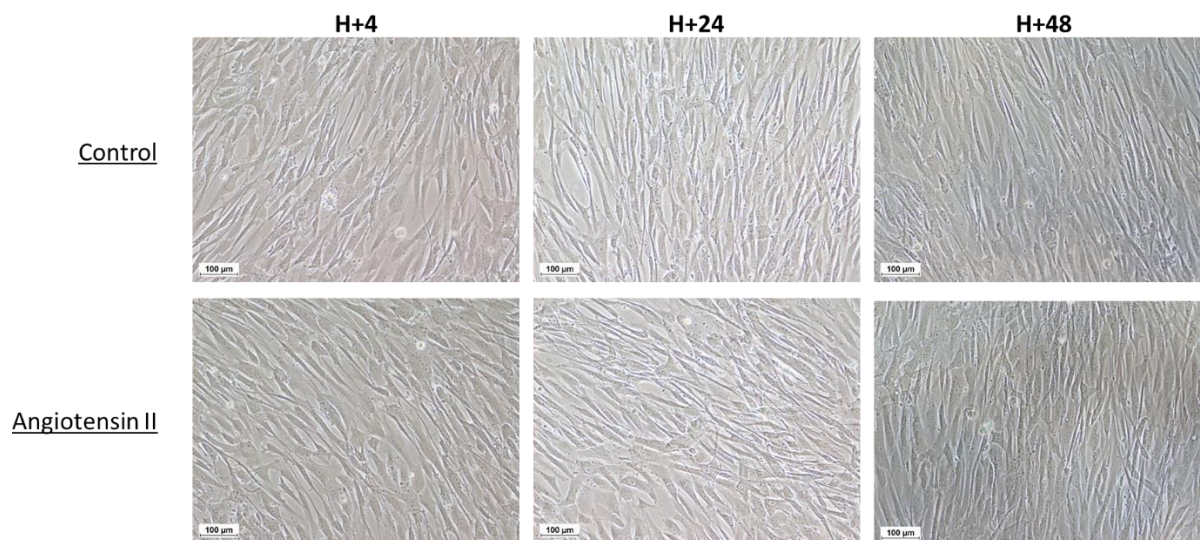


**Figure 22:** Optical microscopy of vSMCs. Cells are synchronised at J+1 during 24 h with complete medium by FBS deprivation (0.5% FBS) and are treated with AngII at 100 nM for 48 h (Magnification: 20x, scale bar: 100  $\mu$ m)

The impact of AngII treatment was studied on the expression of differentiation markers ( $\alpha$ -actin, transgelin and vimentin). As shown in **Fig. 23**, there is no effect on the expression of the markers after AngII treatment.

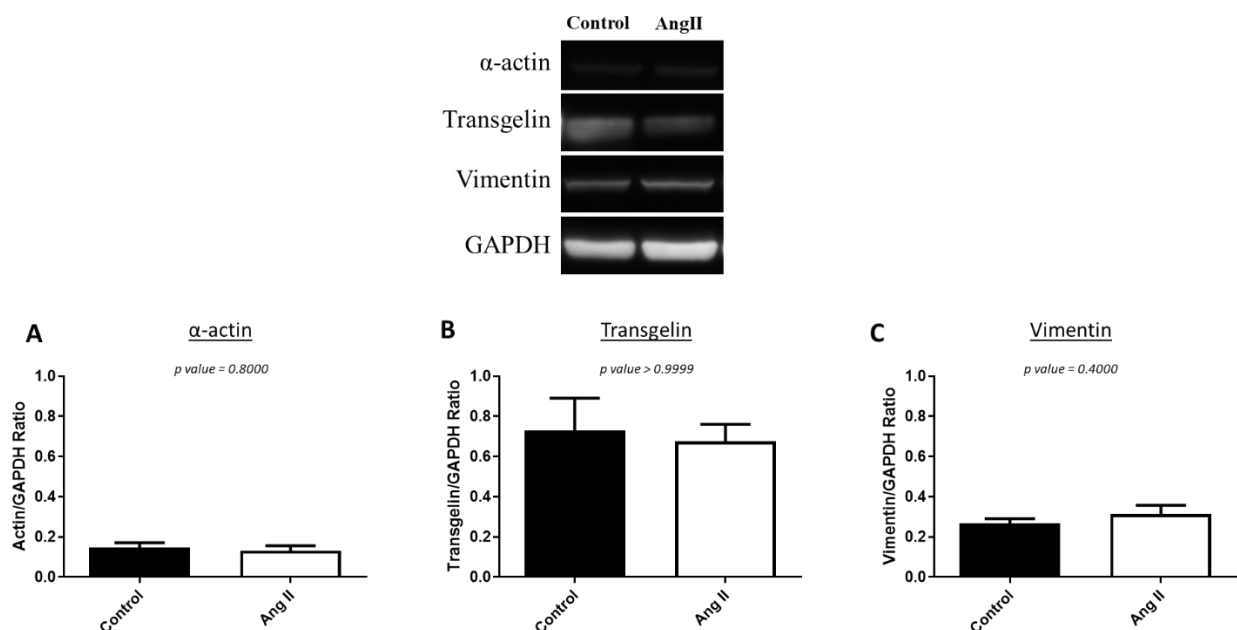


**Figure 23:** Expression of differentiation markers after 48h of AngII stimulation. Ratio of protein of interest vs. GAPDH after Western-blot:  $\alpha$ -actin (A), transgelin (B) and vimentin (C). Results are presented as mean  $\pm$  SEM of 3 independent experiments and analysed by *t*-test; Mann-Whitney test

As it seems that protein expression is not impacted by AngII treatment. In the future, we should have a look at genes variation of expression. To go further in the AngII model, we had a look at cell redox status to validate the ability of AngII stimulation to induce oxidative stress in our model.

### a. NOX species production

To better understand the impact of AngII of vSMCs, medium was collected for the quantification of nitrite ions ( $\text{NO}_2^-$ ) and RSNOs using Griess and Griess-Saville method (see part “*extracellular nitrite ions and S-nitrosothiols quantification; Chapter 2*”).

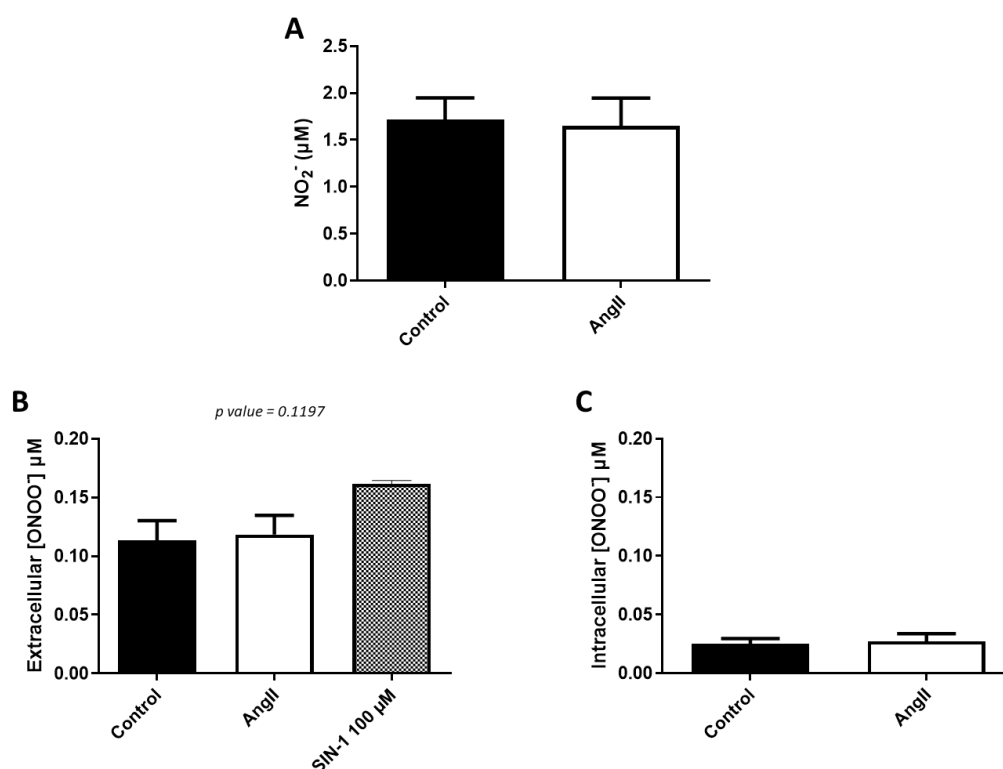


**Figure 24:** Extracellular quantification of nitrite ions by Griess assay (A). vSMCs were synchronised 24 h with FBS 0.5% and incubated for 48 h with AngII; Extracellular (B) and intracellular (C) quantification of peroxynitrite ions in vSMCs after incubation with 100 nM of AngII for 48 h. Results are presented as mean  $\pm$  SEM of 2-3 independent experiments and analysed by One-way ANOVA

As shown in **Fig. 24A**, there was no statistical difference between the incubation medium with or without AngII and RSNOs level was undetectable. The incubation for 48 h with 100 nM of AngII has no impact on endogenous production of nitric oxide. Intracellular  $\text{NO}_2^-$  and RSNOs has been quantified and were under the limit of quantification.

To validate that the oxidative (nitrosative) stress was no so intense, peroxynitrite ions ( $\text{ONOO}^-$ ) were quantified. Indeed, in an oxidative stress context, NO can form  $\text{ONOO}^-$  in combination with superoxide anion. Sydnominine (SIN-1) has been used as positive control of  $\text{ONOO}^-$  production (**Fig. 24B**).



Results showed that incubation with 100 nM of AngII for 48 h seems to not induce the production of extracellular or intracellular ONOO<sup>-</sup> (**Fig. 24B and C**). An increasing tendency is observed for ONOO<sup>-</sup> production after SIN-1 treatment but without statistical difference.

#### b. Cell redox status

##### ❖ Reduced cellular thiols quantification

Reduced cellular thiols were quantified as protocol described in part “*redox status of the cells*” (**Fig. 25**).

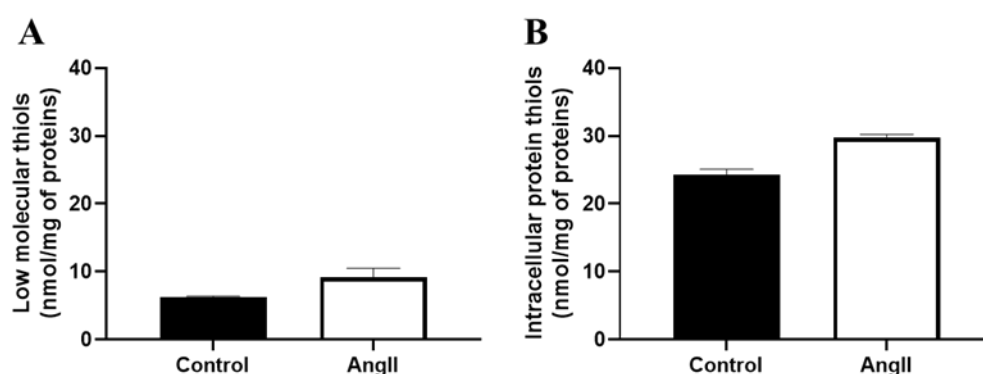


**Figure 25:** Intracellular thiols status after incubation with 100 nM of AngII (n=1 in triplicate)

Low molecular weight thiols and intracellular proteins seems to be increased after the incubation of AngII at 100 nM compared to the basal condition. However, those results need to be confirmed by further analysis (n=1).

The development of a vSMCs model of dedifferentiation is still in progression. The number of experiments need to be increased. The protein variations observed by Western-blot will be confirmed by the gene expression study of these proteins of differentiation.

# DISCUSSION GENERALE, CONCLUSIONS ET PERSPECTIVES

## I. Discussion générale

À l'heure actuelle, les maladies cardiovasculaires dont l'athérosclérose sont la première cause de décès dans le monde. Des facteurs de risque tels que l'hypertension artérielle, le diabète, le tabac, l'obésité, le manque d'activité physique ou la génétique (hypercholestérolémie familiale) augmentent le risque de développer une pathologie cardiovasculaire. L'athérosclérose est décrite comme une maladie chronique, complexe se développant lentement et silencieusement durant plusieurs dizaines d'années jusqu'à l'apparition de plaques d'athérome. Durant son développement, plusieurs facteurs entrent en jeu : *i)* les cellules inflammatoires telles que les monocytes, macrophages, lymphocytes *ii)* les cellules musculaires lisses de la paroi artérielle, *iii)* les cellules endothéliales, *iv)* les lipides oxydés. Ces différents facteurs, associés à une inflammation et un stress oxydant, sont responsables de l'ensemble des différentes étapes de développement de la maladie allant de l'apparition de stries lipidiques (dès l'enfance dans les couches internes de la paroi artérielle) jusqu'au noyau nécrotique et sa rupture. L'inflammation et le stress oxydant engendrent également un dysfonctionnement de l'endothélium qui induit une diminution de la biodisponibilité en NO, une oxydation des LDL, la prolifération/dédifférenciation des CML induisant la progression de la plaque d'athérome.

NO joue un rôle central dans le maintien de l'homéostasie vasculaire. En fonction de sa concentration, de son lieu de production et de sa cible, NO aura différentes fonctions. À faible concentration (10 nM), NO aura un rôle dans la signalisation ou un rôle anti-apoptotique. À forte concentration ( $> 1 \mu\text{M}$ ), NO aura un rôle dans l'induction de l'inflammation (dommages au niveau des CML), sera pro-apoptotique, pro-athérosclérotique (*via* l'inhibition de NF- $\kappa$ B) et entraînera des effets cytotoxiques. Il a été démontré que de fortes concentrations en NO augmentent l'accumulation des oxLDL et du cholestérol au sein des macrophages [83]. En déficit ou en excès, NO est impliqué dans diverses pathologies telles que l'athérosclérose, le cancer, les hémorragies intracérébrales, le psoriasis ou encore le choc septique [84].

Afin de pallier cette diminution en NO, l'utilisation de *S*-nitrosothiols a été envisagée. Formés par *S*-nitrosation (formation d'une liaison covalente entre NO et un résidu cystéine d'une protéine), ils permettent d'augmenter la demi-vie de NO de quelques secondes à plusieurs heures. Parmi les *S*-nitrosothiols, nous nous sommes intéressés au GSNO, forme physiologique de transport et de stockage de NO, permettant ainsi de mimer l'un des réservoirs physiologiques de NO.

Au cours du développement de l'athérosclérose, la combinaison inflammation/stress oxydant/diminution de la concentration en NO entraîne une différenciation des monocytes en macrophages, une dédifférenciation des CML vers un phénotype sécrétoire et une oxydation des LDL. Cet ensemble de modifications conduit à la formation de cellules spumeuses et du cœur nécrotique.

Basé sur l'ensemble de ce qui précède, ce travail de thèse s'est focalisé dans un premier temps sur la mise en place de deux modèles cellulaires de cellules spumeuses à partir de macrophages ou de CML, les deux types cellulaires majoritairement impliqués dans la formation des plaques d'athérome. Dans un second temps, l'impact du GSNO sur ces cellules spumeuses, d'un point de vue morphologique et redox. Pour se faire, le plan expérimental de cette thèse a été divisé en trois parties :

- Un premier objectif visant à développer un modèle de différenciation des monocytes en macrophages, à partir d'une lignée cellulaire, et de la formation des cellules spumeuses. Une fois ce modèle développé, nous nous sommes intéressés à la capacité de GSNO à restaurer la biodisponibilité en NO, son impact sur l'internalisation des oxLDL ainsi que l'effet au niveau du statut redox des cellules.
- Un deuxième objectif très proche du précédent, consistant à développer un modèle de différenciation des monocytes en macrophages mais cette fois à partir de donneurs sains humains. Cette différenciation est suivie d'une polarisation des macrophages et de l'étude des enzymes impliquées dans le métabolisme du GSH.
- Un troisième objectif, suivant la ligne directrice du premier, consistant à développer un modèle de dédifférenciation des CML et étudier leur statut redox.

Des études précédentes ont démontré l'intérêt de l'utilisation des *S*-nitrosothiols dans la prévention de l'athérosclérose. Des *S*-nitrosothiols tels que *S*-nitroso-D-pénicillamine ont montré des capacités à réduire le taux de LDL oxydés et d'élimination des macrophages au sein des plaques d'athérome [51]. D'autres études ont prouvé une diminution de la taille des plaques d'athérome, du stress oxydant ainsi que du cholestérol circulant suite à une administration de *S*-nitroso-N-acétylcystéine dans un modèle d'athérosclérose chez la souris (souris LDLR<sup>-/-</sup>) [53].

Il est connu qu'au cours du développement de l'athérosclérose, les monocytes infiltrant le sous-endothélium suite à une expression à la surface des cellules endothéliales de molécules d'adhérence (ICAM-1 et VCAM-1), se différencient en macrophages et phagocytent les oxLDL

induisant la formation de cellules spumeuses. La différenciation de monocytes à partir d'une lignée cellulaire (ici THP-1) est bien documentée dans la littérature ainsi que la formation des cellules spumeuses. Cependant, une supplémentation en NO *via* le GSNO n'a jamais été étudié, tout comme le statut redox des cellules. GSNO, en plus de NO, possède un squelette glutathion, un antioxydant majeur, qui pourrait permettre de limiter le stress oxydant présent dans les plaques d'athérome et ainsi diminuer la formation des cellules spumeuses.

Au cours du premier objectif, nous avons donc établi un modèle de différenciation de monocytes en macrophages à l'aide de PMA. Ces macrophages ont ensuite été pré-traités avec du GSH ou du GSNO durant 6 h. Après incubation, un dosage des ions nitrite et du GSNO a été réalisé et a démontré que 90% du GSNO avait été métabolisé par les cellules. Le pré-traitement a été suivi d'une incubation pendant 48 h avec des oxLDL. Un protocole d'oxydation des LDL à l'aide de sulfate de cuivre a été mis au point et validé en amont. Nous avons démontré, après observation microscopique, une interaction entre les oxLDL et les macrophages supposant l'internalisation des oxLDL et la formation de cellules spumeuses. À ce stade, aucune différence n'est visible entre le contrôle et le pré-traitement avec GSNO. Afin de mieux évaluer l'implication de GSNO dans l'internalisation des oxLDL, nous avons étudié l'expression de CD36, un récepteur membranaire responsable de la fixation et de l'internalisation des oxLDL par les macrophages. L'analyse par western-blot a confirmé les données de la littérature avec une surexpression de CD36 en présence des oxLDL [10,85]. Lorsque les macrophages sont pré-traités avec GSNO, nous avons démontré que la surexpression de CD36 induite par les oxLDL était abolie. Ces résultats indiquent un effet de GSNO sur la formation des cellules spumeuses. L'expression de CD36 étant connue pour être liée au stress oxydant et à la présence d'espèces réactives de l'oxygène, nous avons jugé important d'étudier le statut redox des cellules et plus particulièrement le statut des thiols. Nous avons démontré que les thiols de faible poids moléculaire, majoritairement composé de GSH et de cystéine, augmentaient après les pré-traitements GSH et GSNO et également en présence de oxLDL. Cette augmentation est plus importante suite au pré-traitement GSNO suivi de l'incubation avec les oxLDL, ce qui nous laisse supposer un effet NO et non seulement un effet du GSH. Malgré la présence des oxLDL, nous avons démontré que cela n'avait pas d'impact sur la concentration intracellulaire en GSH ni sur le ratio GSH/GSSG, laissant penser à une stabilité de la signalisation redox au sein des cellules.

Le second objectif a été de développer un modèle de différenciation monocytes/macrophages mais en se rapprochant au maximum de la physiopathologie de l'athérosclérose et de



l'hétérogénéité macrophagique. À partir de donneurs de sang sains, les monocytes ont été isolés et mis en culture durant 7 jours en présence de M-CSF permettant ainsi l'obtention de macrophages M0. Ces macrophages ont ensuite été polarisés en macrophages M1 ou M2 à l'aide d'IFN $\gamma$ /LPS et IL-4 ou IL-10, respectivement. Afin de mieux caractériser les défenses antioxydantes de ces macrophages et leur implication dans le contexte pro-oxydant des plaques d'athérome, nous avons étudié l'activité de quatre enzymes impliquées dans le métabolisme du GSH : la GGT, la GPx, la GR et la GST. Les résultats ont révélé une activité GGT et GPx plus importante dans les macrophages M1 et dans les macrophages M2 (traités avec IL-4). Il a déjà été démontré que les macrophages M1 étaient capables de libérer, par dégranulation, de la GGT suite à un stimulus pro-inflammatoire [11] contribuant ainsi à la progression et l'instabilité des plaques d'athérome en impactant le processus inflammatoire. En revanche, la présence de GGT dans les macrophages M2 pourrait permettre un meilleur métabolisme de GSNO permettant d'augmenter le niveau de NO intracellulaire et peut-être de restaurer sa biodisponibilité au sein des plaques d'athérome.

Enfin, le troisième objectif de cette thèse s'est focalisé sur l'autre type cellulaire majeur impliqué dans la formation des plaques d'athérome, les CML. À partir de cellules aortiques primaires humaines et après avoir validé leur phénotype contractile, nous avons développé un modèle de dédifférenciation de ces cellules contractiles vers un phénotype sécrétoire/prolifératif selon deux protocoles. Le premier protocole est basé sur l'utilisation de l'angiotensine II [81]. Les cellules sont mises en culture dans du milieu complet, 5% de SVF puis synchronisées au même stade du cycle cellulaire par déprivation de SVF (0,5%), s'en suit une incubation de 48h en présence d'angiotensine II. Nous avons démontré que l'angiotensine II n'impactait pas la morphologie cellulaire ni l'expression des marqueurs de différenciation ( $\alpha$ -actine, transgeline et vimentine). L'étude du statut redox des cellules a montré une légère augmentation des thiols de faible poids moléculaire ainsi que des protéines thiolées intracellulaires après incubation avec l'angiotensine II, cependant ces résultats restent à être confirmés. L'incubation avec l'angiotensine ne produit pas de stress oxydant intense, aucune formation d'ions peroxy-nitrite n'a été observée. Cependant, ces résultats devront être confirmés par la suite.

## II. Conclusions et perspectives

Ces travaux de doctorat visaient à étudier l'impact du *S*-nitrosoglutathion sur la métaplasie des macrophages et des cellules musculaires lisses en cellules spumeuses. Un premier objectif a consisté à développer un modèle de différenciation des monocytes en macrophages M0. L'effet d'un pré-traitement avec GSNO sur l'internalisation de oxLDLs et sur le statut redox des macrophages M0 ont été évalués. Un second objectif, proche du premier, a consisté à développer un modèle de différenciation de monocytes humain primaires provenant de donneurs sains en macrophages M0, puis de les polariser en macrophages M1 (pro-inflammatoires) et macrophages M2 (anti-inflammatoires). La validation de ce modèle a fait l'objet d'une publication (**Annexe 1**). Enfin, l'activité des enzymes impliquées dans le métabolisme du GSH a été caractérisée au sein de ce modèle.

Cela nous a permis de démontrer que :

- Le pré-traitement de macrophages M0 avec GSNO abolit la surexpression de CD36 induite par les oxLDL supposant un effet sur les cellules spumeuses. Le pré-traitement GSNO permet d'augmenter la quantité de thiols de faible poids moléculaires (GSH et cystéine) présents dans les macrophages après incubation avec les oxLDL. Cet effet étant absent suite à un pré-traitement avec GSH, il suppose un effet d'association entre NO et le glutathion de GSNO. Ainsi, Les macrophages M0 utiliseraient GSNO pour contrer le stress oxydant induit par les oxLDL. Cette partie fera l'objet d'une publication dans le journal *Nitric oxide*.
- L'activité GGT et GPx est augmentée au sein des macrophages M1 et des macrophages M2 (traités à l'IL-4) comparé aux monocytes et aux macrophages M0. Ainsi, ces macrophages polarisés seraient plus à même de métaboliser GSNO *via* la GGT ce qui augmenterait la libération de NO au sein de la plaque d'athérome et donc un ciblage du traitement. De plus, grâce à l'activité GPx, les macrophages M1 et les macrophages M2 seront plus efficaces pour réduire les lipides oxydés que les monocytes et les macrophages M0.

Ces résultats prometteurs méritent cependant d'être approfondis. En effet, malgré l'abolition de la surexpression de CD36 par un pré-traitement GSNO nous n'avons pas réussi à mettre en évidence une diminution de l'internalisation des oxLDLs par les macrophages M0. Ainsi, dans un premier temps, il faudrait valider CD36 comme récepteur clé des oxLDL. Pour cela, un antagoniste du CD36 pourrait être utilisé pour empêcher la reconnaissance des oxLDLs par ce

récepteur. Ainsi, une diminution de la formation de cellules spumeuses devrait être observée, validant le CD36 comme récepteur clé des oxLDL. Ensuite, il me semble important d'étudier l'internalisation de CD36 afin de comprendre par quels mécanismes passe la diminution de sa surexpression. Pour cela, le récepteur ainsi que les vésicules intracellulaires peuvent être marqués à l'aide d'anticorps fluorescents afin d'identifier un éventuel mécanisme d'internalisation. Pour valider le phénotype des cellules spumeuses et ainsi confirmer leur capacité à internaliser les oxLDL, une quantification intracellulaire de ces oxLDL est nécessaire. Celle-ci a déjà été réalisée par utilisation de la méthode TBARS, sans résultats concluants. La quantification de la fluorescence des DiI-oxLDL est une possibilité (selon [86]).

L'implication de NO dans le développement de l'athérosclérose (diminution de sa biodisponibilité) ainsi que son impact sur le stress oxydant est connu, tout comme son impact sur les gènes pro-apoptotiques et pro-athérosclérotiques. Afin de confirmer l'impact du GSNO sur les macrophages, il serait nécessaire d'étudier d'autres espèces impliquées dans le stress oxydant (autres que GSH) tels que le couple NADPH/NAD<sup>+</sup> ainsi que les voies de signalisation et facteurs de transcription sous-jacents tels que NF-κB. Pour finir, étudier l'impact de l'apport de NO *via* la S-nitrosation des protéines permettraient d'avoir davantage de données sur la formation d'un stock de NO et sur les voies de signalisation potentiellement impactées au sein des macrophages ou des cellules spumeuses limitant ainsi leur progression. Pour cela, un Biotin-Switch pourra être réalisé afin de purifier les protéines S-nitrosées qui seront ensuite identifiées par spectrométrie de masse.

Dans cette première partie du projet, nous nous sommes focalisés sur le lien entre stress oxydant et athérosclérose avec la présence des oxLDL. Les macrophages M1 et M2 étant retrouvés au sein des plaques d'athérome, établir le statut redox (thiols de faible poids moléculaire, ratio GSH/GSSG, GSH...) de ces types cellulaires sera primordial, tout comme étudier leur réponse suite à un pré-traitement avec GSNO. L'inflammation ayant également un impact important dans le développement de la pathologie, cet aspect devra être étudié afin d'en connaître l'impact sur les cellules. Une quantification des cytokines anti- et pro-inflammatoires sera nécessaire. Afin de confirmer l'effet du GSNO sur les macrophages et de mettre en évidence les voies de signalisation qui pourraient être impactées, permettant ainsi de connaître le mécanisme d'action de NO, il sera nécessaire d'étudier qu'elles sont les protéines S-nitrosées.

Le second type cellulaire impliqué majoritairement au sein des plaques d'athérome, les cellules musculaires lisses, a également été étudié. Un modèle basé sur la synchronisation des cellules suivi d'une induction de stress oxydant grâce à l'angiotensine II est, à ce jour, toujours en cours

de développement. Afin de poursuivre sa validation, l'étude des gènes impliqués dans la dédifférenciation devra être réalisé. Les gènes de ménage ainsi que les amorces des gènes de dédifférenciation sont déjà validés. Un intérêt particulier sera porté au facteur de transcription KLF-4 étant donné son implication dans la dédifférenciation des cellules musculaires lisses ainsi que l'impact, déjà démontré, du NO sur celui-ci. A plus long terme, l'étude du profil des enzymes impliquées dans le métabolisme de GSH sera nécessaire. La formation des cellules spumeuses devra également être étudiée suite à une incubation avec les oxLDL tout comme l'impact du GSNO.

Dans les années à venir, plusieurs perspectives sont possibles afin de poursuivre ce projet. La mise en place de co-cultures, macrophages/cellules musculaires lisses afin de se replacer au mieux dans les conditions pathophysiologiques de l'athérosclérose, ces deux types cellulaires évoluant en symbiose lors du développement de la pathologie. Ces co-cultures permettront ainsi de mettre en évidence différentes cytokines libérées et leurs impacts sur les différents types cellulaires. Une étude *in vivo* peut également être mise en place avec l'utilisation de souris LDLR<sup>-/-</sup> afin d'étudier la capacité de GSNO à limiter le développement de l'athérosclérose. En effet, nous avons démontré l'absorption intestinale des S-nitrosothiols et la possibilité d'une administration par voie orale avec une absorption majoritaire sous forme d'espèces dérivées de NO (ions nitrite et nitrate).

## REFERENCES



- [1] WHO | Cardiovascular diseases (CVDs), WHO. (n.d.). [http://www.who.int/cardiovascular\\_diseases/en/](http://www.who.int/cardiovascular_diseases/en/) (accessed August 28, 2018).
- [2] M.C. Fishbein, G.A. Fishbein, Arteriosclerosis: facts and fancy, *Cardiovascular Pathology*. 24 (2015) 335–342. <https://doi.org/10.1016/j.carpath.2015.07.007>.
- [3] F.O. Martinez, S. Gordon, The M1 and M2 paradigm of macrophage activation: time for reassessment, *F1000Prime Rep*. 6 (2014) 13. <https://doi.org/10.12703/P6-13>.
- [4] M. Stein, S. Keshav, N. Harris, S. Gordon, Interleukin 4 potently enhances murine macrophage mannose receptor activity: a marker of alternative immunologic macrophage activation, *J. Exp. Med*. 176 (1992) 287–292. <https://doi.org/10.1084/jem.176.1.287>.
- [5] S.W. Waldo, Y. Li, C. Buono, B. Zhao, E.M. Billings, J. Chang, H.S. Kruth, Heterogeneity of human macrophages in culture and in atherosclerotic plaques, *Am. J. Pathol*. 172 (2008) 1112–1126. <https://doi.org/10.2353/ajpath.2008.070513>.
- [6] E. Sierra-Filardi, M.A. Vega, P. Sánchez-Mateos, A.L. Corbí, A. Puig-Kröger, Heme Oxygenase-1 expression in M-CSF-polarized M2 macrophages contributes to LPS-induced IL-10 release, *Immunobiology*. 215 (2010) 788–795. <https://doi.org/10.1016/j.imbio.2010.05.020>.
- [7] L.J.H. van Tits, R. Stienstra, P.L. van Lent, M.G. Netea, L. a. B. Joosten, A.F.H. Stalenhoef, Oxidized LDL enhances pro-inflammatory responses of alternatively activated M2 macrophages: a crucial role for Krüppel-like factor 2, *Atherosclerosis*. 214 (2011) 345–349. <https://doi.org/10.1016/j.atherosclerosis.2010.11.018>.
- [8] T. Kazawa, T. Kawasaki, A. Sakamoto, M. Imamura, R. Ohashi, S. Jiang, T. Tanaka, H. Iwanari, T. Hamakubo, J. Sakai, T. Kodama, M. Naito, Expression of liver X receptor alpha and lipid metabolism in granulocyte-macrophage colony-stimulating factor-induced human monocyte-derived macrophage, *Pathol. Int*. 59 (2009) 152–160. <https://doi.org/10.1111/j.1440-1827.2009.02343.x>.
- [9] M. Febbraio, E.A. Podrez, J.D. Smith, D.P. Hajjar, S.L. Hazen, H.F. Hoff, K. Sharma, R.L. Silverstein, Targeted disruption of the class B scavenger receptor CD36 protects against atherosclerotic lesion development in mice, *J Clin Invest*. 105 (2000) 1049–1056.
- [10] Y.M. Park, M. Febbraio, R.L. Silverstein, CD36 modulates migration of mouse and human macrophages in response to oxidized LDL and may contribute to macrophage trapping in the arterial intima, *J Clin Invest*. 119 (2009) 136–145. <https://doi.org/10.1172/JCI35535>.
- [11] E. Belcastro, M. Franzini, S. Cianchetti, E. Lorenzini, S. Masotti, V. Fierabracci, A. Pucci, A. Pompella, A. Corti, Monocytes/macrophages activation contributes to b-gamma-glutamyltransferase accumulation inside atherosclerotic plaques, *J Transl Med*. 13 (2015) 325. <https://doi.org/10.1186/s12967-015-0687-6>.
- [12] D. Gomez, G.K. Owens, Smooth muscle cell phenotypic switching in atherosclerosis, *Cardiovasc. Res*. 95 (2012) 156–164. <https://doi.org/10.1093/cvr/cvs115>.
- [13] J.H. Fountain, S.L. Lappin, Physiology, Renin Angiotensin System, in: *StatPearls*, StatPearls Publishing, Treasure Island (FL), 2020. <http://www.ncbi.nlm.nih.gov/books/NBK470410/> (accessed February 8, 2021).
- [14] P. Madiraju, E. Hossain, M.B. Anand-Srivastava, Natriuretic peptide receptor-C activation attenuates angiotensin II-induced enhanced oxidative stress and hyperproliferation of aortic vascular smooth muscle cells, *Mol. Cell. Biochem*. 448 (2018) 77–89. <https://doi.org/10.1007/s11010-018-3316-x>.
- [15] A. Nguyen Dinh Cat, A.C. Montezano, D. Burger, R.M. Touyz, Angiotensin II, NADPH Oxidase, and Redox Signaling in the Vasculature, *Antioxid Redox Signal*. 19 (2013) 1110–1120. <https://doi.org/10.1089/ars.2012.4641>.

- [16] J.M. Kim, H.-S. Heo, Y.M. Ha, B.H. Ye, E.K. Lee, Y.J. Choi, B.P. Yu, H.Y. Chung, Mechanism of Ang II involvement in activation of NF- $\kappa$ B through phosphorylation of p65 during aging, *Age (Dordr)*. 34 (2012) 11–25. <https://doi.org/10.1007/s11357-011-9207-7>.
- [17] T. Liu, L. Zhang, D. Joo, S.-C. Sun, NF- $\kappa$ B signaling in inflammation, *Signal Transduct Target Ther*. 2 (2017) 17023. <https://doi.org/10.1038/sigtrans.2017.23>.
- [18] R. Kranzhöfer, M. Browatzki, J. Schmidt, W. Kübler, Angiotensin II activates the proinflammatory transcription factor nuclear factor-kappaB in human monocytes, *Biochem Biophys Res Commun*. 257 (1999) 826–828. <https://doi.org/10.1006/bbrc.1999.0543>.
- [19] S. Keidar, M. Kaplan, A. Hoffman, M. Aviram, Angiotensin II stimulates macrophage-mediated oxidation of low density lipoproteins, *Atherosclerosis*. 115 (1995) 201–215. [https://doi.org/10.1016/0021-9150\(94\)05514-j](https://doi.org/10.1016/0021-9150(94)05514-j).
- [20] J.M. Proudfoot, K.D. Croft, I.B. Puddey, L.J. Beilin, Angiotensin II type 1 receptor antagonists inhibit basal as well as low-density lipoprotein and platelet-activating factor-stimulated human monocyte chemoattractant protein-1, *J Pharmacol Exp Ther*. 305 (2003) 846–853. <https://doi.org/10.1124/jpet.102.047795>.
- [21] T.S. Hakim, K. Sugimori, E.M. Camporesi, G. Anderson, Half-life of nitric oxide in aqueous solutions with and without haemoglobin, *Physiol Meas*. 17 (1996) 267–277.
- [22] J.T. Groves, C.C.Y. Wang, Nitric oxide synthase: Models and mechanisms, *Current Opinion in Chemical Biology*. 4 (2000) 687–695. [https://doi.org/10.1016/S1367-5931\(00\)00146-0](https://doi.org/10.1016/S1367-5931(00)00146-0).
- [23] M.-C. Broillet, S-Nitrosylation of proteins, *CMLS, Cell. Mol. Life Sci*. 55 (1999) 1036–1042. <https://doi.org/10.1007/s000180050354>.
- [24] S. Miersch, B. Mutus, Protein S-nitrosation: Biochemistry and characterization of protein thiol–NO interactions as cellular signals, *Clinical Biochemistry*. 38 (2005) 777–791. <https://doi.org/10.1016/j.clinbiochem.2005.05.014>.
- [25] J. SUN, C. STEENBERGEN, E. MURPHY, S-Nitrosylation: NO-Related Redox Signaling to Protect Against Oxidative Stress, *Antioxid Redox Signal*. 8 (2006) 1693–1705. <https://doi.org/10.1089/ars.2006.8.1693>.
- [26] E. Belcastro, W. Wu, I. Fries-Raeth, A. Corti, A. Pompella, P. Leroy, I. Lartaud, C. Gaucher, Oxidative stress enhances and modulates protein S-nitrosation in smooth muscle cells exposed to S-nitrosoglutathione, *Nitric Oxide*. 69 (2017) 10–21. <https://doi.org/10.1016/j.niox.2017.07.004>.
- [27] R. Radi, Protein Tyrosine Nitration: Biochemical Mechanisms and Structural Basis of its Functional Effects, *Acc Chem Res*. 46 (2013) 550–559. <https://doi.org/10.1021/ar300234c>.
- [28] M.H. Shishehbor, R.J. Aviles, M.-L. Brennan, X. Fu, M. Goormastic, G.L. Pearce, N. Gokce, J.F. Keaney, M.S. Penn, D.L. Sprecher, J.A. Vita, S.L. Hazen, Association of nitrotyrosine levels with cardiovascular disease and modulation by statin therapy, *JAMA*. 289 (2003) 1675–1680. <https://doi.org/10.1001/jama.289.13.1675>.
- [29] D. Tousoulis, A.-M. Kampoli, C. Tentolouris, N. Papageorgiou, C. Stefanadis, The role of nitric oxide on endothelial function, *Curr Vasc Pharmacol*. 10 (2012) 4–18. <https://doi.org/10.2174/157016112798829760>.
- [30] C. Farah, L.Y.M. Michel, J.-L. Balligand, Nitric oxide signalling in cardiovascular health and disease, *Nature Reviews Cardiology*. 15 (2018) 292–316. <https://doi.org/10.1038/nrcardio.2017.224>.
- [31] E. Belcastro, C. Gaucher, A. Corti, P. Leroy, I. Lartaud, A. Pompella, Regulation of protein function by S-nitrosation and S-glutathionylation: processes and targets in

- cardiovascular pathophysiology, *Biological Chemistry*. 398 (2017) 1267–1293. <https://doi.org/10.1515/hsz-2017-0150>.
- [32] M.M. Cortese-Krott, M. Kelm, Endothelial nitric oxide synthase in red blood cells: Key to a new erythrocrine function?, *Redox Biol*. 2 (2014) 251–258. <https://doi.org/10.1016/j.redox.2013.12.027>.
- [33] P. Kleinbongard, R. Schulz, T. Rassaf, T. Lauer, A. Dejam, T. Jax, I. Kumara, P. Gharini, S. Kabanova, B. Ozüyan, H.-G. Schnürch, A. Gödecke, A.-A. Weber, M. Robenek, H. Robenek, W. Bloch, P. Rösen, M. Kelm, Red blood cells express a functional endothelial nitric oxide synthase, *Blood*. 107 (2006) 2943–2951. <https://doi.org/10.1182/blood-2005-10-3992>.
- [34] S. Feil, B. Fehrenbacher, R. Lukowski, F. Essmann, K. Schulze-Osthoff, M. Schaller, R. Feil, Transdifferentiation of vascular smooth muscle cells to macrophage-like cells during atherogenesis, *Circ. Res*. 115 (2014) 662–667. <https://doi.org/10.1161/CIRCRESAHA.115.304634>.
- [35] M.R. Bennett, S. Sinha, G.K. Owens, Vascular Smooth Muscle Cells in Atherosclerosis, *Circ. Res*. 118 (2016) 692–702. <https://doi.org/10.1161/CIRCRESAHA.115.306361>.
- [36] X.-H. Yu, Y.-C. Fu, D.-W. Zhang, K. Yin, C.-K. Tang, Foam cells in atherosclerosis, *Clin. Chim. Acta*. 424 (2013) 245–252. <https://doi.org/10.1016/j.cca.2013.06.006>.
- [37] C. Chaabane, M. Coen, M.-L. Bochaton-Piallat, Smooth muscle cell phenotypic switch: implications for foam cell formation, *Curr. Opin. Lipidol*. 25 (2014) 374–379. <https://doi.org/10.1097/MOL.0000000000000113>.
- [38] D.A. Chistiakov, A.A. Melnichenko, V.A. Myasoedova, A.V. Grechko, A.N. Orekhov, Mechanisms of foam cell formation in atherosclerosis, *J. Mol. Med*. 95 (2017) 1153–1165. <https://doi.org/10.1007/s00109-017-1575-8>.
- [39] K. Ashina, Y. Tsubosaka, K. Kobayashi, K. Omori, T. Murata, VEGF-induced blood flow increase causes vascular hyper-permeability in vivo, *Biochemical and Biophysical Research Communications*. 464 (2015) 590–595. <https://doi.org/10.1016/j.bbrc.2015.07.014>.
- [40] R.G. Tilton, K.C. Chang, W.S. LeJeune, C.C. Stephan, T.A. Brock, J.R. Williamson, Role for nitric oxide in the hyperpermeability and hemodynamic changes induced by intravenous VEGF., *Invest. Ophthalmol. Vis. Sci*. 40 (1999) 689–696.
- [41] P.A. Cahill, E.M. Redmond, Vascular endothelium – Gatekeeper of vessel health, *Atherosclerosis*. 248 (2016) 97–109. <https://doi.org/10.1016/j.atherosclerosis.2016.03.007>.
- [42] K. Theodorou, R.A. Boon, Endothelial Cell Metabolism in Atherosclerosis, *Front Cell Dev Biol*. 6 (2018). <https://doi.org/10.3389/fcell.2018.00082>.
- [43] M. Le Bras, M.-V. Clément, S. Pervaiz, C. Brenner, Reactive oxygen species and the mitochondrial signaling pathway of cell death, *Histol Histopathol*. 20 (2005) 205–219. <https://doi.org/10.14670/HH-20.205>.
- [44] M. Valko, D. Leibfritz, J. Moncol, M.T.D. Cronin, M. Mazur, J. Telser, Free radicals and antioxidants in normal physiological functions and human disease, *Int J Biochem Cell Biol*. 39 (2007) 44–84. <https://doi.org/10.1016/j.biocel.2006.07.001>.
- [45] D.A. Wink, H.B. Hines, R.Y.S. Cheng, C.H. Switzer, W. Flores-Santana, M.P. Vitek, L.A. Ridnour, C.A. Colton, Nitric oxide and redox mechanisms in the immune response, *J Leukoc Biol*. 89 (2011) 873–891. <https://doi.org/10.1189/jlb.1010550>.
- [46] X. Yang, Y. Li, Y. Li, X. Ren, X. Zhang, D. Hu, Y. Gao, Y. Xing, H. Shang, Oxidative Stress-Mediated Atherosclerosis: Mechanisms and Therapies, *Front Physiol*. 8 (2017). <https://doi.org/10.3389/fphys.2017.00600>.
- [47] D. Lapenna, S. de Gioia, G. Ciofani, A. Mezzetti, S. Ucchino, A.M. Calafiore, A.M. Napolitano, C. Di Ilio, F. Cuccurullo, Glutathione-Related Antioxidant Defenses in

- Human Atherosclerotic Plaques, *Circulation*. 97 (1998) 1930–1934.  
<https://doi.org/10.1161/01.CIR.97.19.1930>.
- [48] M. Torzewski, V. Ochsenhirt, A.L. Kleschyov, M. Oelze, A. Daiber, H. Li, H. Rossmann, S. Tsimikas, K. Reifenberg, F. Cheng, H.-A. Lehr, S. Blankenberg, U. Förstermann, T. Münzel, K.J. Lackner, Deficiency of Glutathione Peroxidase-1 Accelerates the Progression of Atherosclerosis in Apolipoprotein E-Deficient Mice, *ATVB*. 27 (2007) 850–857. <https://doi.org/10.1161/01.ATV.0000258809.47285.07>.
- [49] D.H. Kwon, H. Lee, C. Park, S.-H. Hong, S.H. Hong, G.-Y. Kim, H.-J. Cha, S. Kim, H.-S. Kim, H.-J. Hwang, Y.H. Choi, Glutathione Induced Immune-Stimulatory Activity by Promoting M1-Like Macrophages Polarization via Potential ROS Scavenging Capacity, *Antioxidants (Basel)*. 8 (2019). <https://doi.org/10.3390/antiox8090413>.
- [50] T. Kondo, M. Hirose, K. Kageyama, Roles of Oxidative Stress and Redox Regulation in Atherosclerosis, *JAT*. 16 (2009) 532–538. <https://doi.org/10.5551/jat.1255>.
- [51] W. Martinet, V. Croons, J.-P. Timmermans, A.G. Herman, G.R.Y. De Meyer, Nitric oxide selectively depletes macrophages in atherosclerotic plaques via induction of endoplasmic reticulum stress, *Br. J. Pharmacol.* 152 (2007) 493–500.  
<https://doi.org/10.1038/sj.bjp.0707426>.
- [52] M. Parent, A. Boudier, F. Dupuis, C. Nouvel, A. Sapin, I. Lartaud, J.-L. Six, P. Leroy, P. Maincent, Are in situ formulations the keys for the therapeutic future of S-nitrosothiols?, *Eur J Pharm Biopharm.* 85 (2013) 640–649. <https://doi.org/10.1016/j.ejpb.2013.08.005>.
- [53] M.H. Krieger, K.F.R. Santos, S.M. Shishido, A.C.B.A. Wanschel, H.F.G. Estrela, L. Santos, M.G. De Oliveira, K.G. Franchini, R.C. Spadari-Bratfisch, F.R.M. Laurindo, Antiatherogenic effects of S-nitroso-N-acetylcysteine in hypercholesterolemic LDL receptor knockout mice, *Nitric Oxide*. 14 (2006) 12–20.  
<https://doi.org/10.1016/j.niox.2005.07.011>.
- [54] M. Khan, B. Sekhon, S. Giri, M. Jatana, A.G. Gilg, K. Ayasolla, C. Elango, A.K. Singh, I. Singh, S-Nitrosoglutathione reduces inflammation and protects brain against focal cerebral ischemia in a rat model of experimental stroke, *J. Cereb. Blood Flow Metab.* 25 (2005) 177–192. <https://doi.org/10.1038/sj.jcbfm.9600012>.
- [55] M. Khan, M. Jatana, C. Elango, A.S. Paintlia, A.K. Singh, I. Singh, Cerebrovascular protection by various nitric oxide donors in rats after experimental stroke, *Nitric Oxide*. 15 (2006) 114–124. <https://doi.org/10.1016/j.niox.2006.01.008>.
- [56] M. Khan, T.S. Dhammu, F. Matsuda, A.K. Singh, I. Singh, Blocking a vicious cycle nNOS/peroxynitrite/AMPK by S-nitrosoglutathione: implication for stroke therapy, *BMC Neurosci.* 16 (2015) 42. <https://doi.org/10.1186/s12868-015-0179-x>.
- [57] M. Khan, T.S. Dhammu, M. Baarine, J. Kim, M.K. Paintlia, I. Singh, A.K. Singh, GSNO promotes functional recovery in experimental TBI by stabilizing HIF-1 $\alpha$ , *Behav. Brain Res.* 340 (2018) 63–70. <https://doi.org/10.1016/j.bbr.2016.10.037>.
- [58] L.C. Pinheiro, J.H. Amaral, G.C. Ferreira, R.L. Portella, C.S. Ceron, M.F. Montenegro, J.C. Toledo, J.E. Tanus-Santos, Gastric S-nitrosothiol formation drives the antihypertensive effects of oral sodium nitrite and nitrate in a rat model of renovascular hypertension, *Free Radic. Biol. Med.* 87 (2015) 252–262.  
<https://doi.org/10.1016/j.freeradbiomed.2015.06.038>.
- [59] J. Bonetti, Y. Zhou, M. Parent, I. Clarot, H. Yu, I. Fries-Raeth, P. Leroy, I. Lartaud, C. Gaucher, Intestinal absorption of S-nitrosothiols: Permeability and transport mechanisms, *Biochem. Pharmacol.* 155 (2018) 21–31.  
<https://doi.org/10.1016/j.bcp.2018.06.018>.
- [60] W. Wu, C. Perrin-Sarrado, H. Ming, I. Lartaud, P. Maincent, X.-M. Hu, A. Sapin-Minet, C. Gaucher, Polymer nanocomposites enhance S-nitrosoglutathione intestinal absorption



- and promote the formation of releasable nitric oxide stores in rat aorta, *Nanomedicine*. 12 (2016) 1795–1803. <https://doi.org/10.1016/j.nano.2016.05.006>.
- [61] Y. Yao, X.-H. Xu, L. Jin, Macrophage Polarization in Physiological and Pathological Pregnancy, *Front Immunol*. 10 (2019) 792. <https://doi.org/10.3389/fimmu.2019.00792>.
- [62] N. Wang, H. Liang, K. Zen, Molecular Mechanisms That Influence the Macrophage M1–M2 Polarization Balance, *Front. Immunol*. 0 (2014). <https://doi.org/10.3389/fimmu.2014.00614>.
- [63] F. Raggi, S. Pelassa, D. Pierobon, F. Penco, M. Gattorno, F. Novelli, A. Eva, L. Varesio, M. Giovarelli, M.C. Bosco, Regulation of Human Macrophage M1–M2 Polarization Balance by Hypoxia and the Triggering Receptor Expressed on Myeloid Cells-1, *Frontiers in Immunology*. 8 (2017). <https://doi.org/10.3389/fimmu.2017.01097>.
- [64] A. Pompella, M. Emdin, C. Passino, A. Paolicchi, The significance of serum gamma-glutamyltransferase in cardiovascular diseases, *Clin Chem Lab Med*. 42 (2004) 1085–1091. <https://doi.org/10.1515/CCLM.2004.224>.
- [65] S.S. Singhal, S.P. Singh, P. Singhal, D. Horne, J. Singhal, S. Awasthi, Antioxidant Role of Glutathione S-Transferases: 4-Hydroxynonenal, a Key Molecule in Stress-Mediated Signaling, *Toxicol Appl Pharmacol*. 289 (2015) 361–370. <https://doi.org/10.1016/j.taap.2015.10.006>.
- [66] G. Filomeni, G. Rotilio, M.R. Ciriolo, Cell signalling and the glutathione redox system, *Biochem. Pharmacol*. 64 (2002) 1057–1064. [https://doi.org/10.1016/s0006-2952\(02\)01176-0](https://doi.org/10.1016/s0006-2952(02)01176-0).
- [67] E. Laborde, Glutathione transferases as mediators of signaling pathways involved in cell proliferation and cell death, *Cell Death Differ*. 17 (2010) 1373–1380. <https://doi.org/10.1038/cdd.2010.80>.
- [68] N.E. Huseby, J.H. Strömme, Practical points regarding routine determination of gamma-glutamyl transferase (gamma-GT) in serum with a kinetic method at 37 degrees C, *Scand J Clin Lab Invest*. 34 (1974) 357–363. <https://doi.org/10.3109/00365517409049892>.
- [69] F. Dahboul, P. Leroy, K. Maguin Gate, A. Boudier, C. Gaucher, P. Liminana, I. Lartaud, A. Pompella, C. Perrin-Sarrado, Endothelial  $\gamma$ -glutamyltransferase contributes to the vasorelaxant effect of S-nitrosoglutathione in rat aorta, *PLoS ONE*. 7 (2012) e43190. <https://doi.org/10.1371/journal.pone.0043190>.
- [70] C. Perrin-Sarrado, M. Pongas, F. Dahboul, P. Leroy, A. Pompella, I. Lartaud, Reduced Activity of the Aortic Gamma-Glutamyltransferase Does Not Decrease S-Nitrosoglutathione Induced Vasorelaxation of Rat Aortic Rings, *Front Physiol*. 7 (2016) 630. <https://doi.org/10.3389/fphys.2016.00630>.
- [71] D.E. Paglia, W.N. Valentine, Studies on the quantitative and qualitative characterization of erythrocyte glutathione peroxidase, *J Lab Clin Med*. 70 (1967) 158–169.
- [72] V. Massey, C.H. Williams, On the Reaction Mechanism of Yeast Glutathione Reductase, *Journal of Biological Chemistry*. 240 (1965) 4470–4480. [https://doi.org/10.1016/S0021-9258\(18\)97085-7](https://doi.org/10.1016/S0021-9258(18)97085-7).
- [73] W.H. Habig, M.J. Pabst, W.B. Jakoby, Glutathione S-transferases. The first enzymatic step in mercapturic acid formation, *J Biol Chem*. 249 (1974) 7130–7139.
- [74] Y.-G. Kim, G.-M. Park, S.B. Lee, D.H. Yang, J.-W. Kang, T.-H. Lim, H.-K. Kim, J. Choe, S.-W. Lee, Y.-H. Kim, Association of gamma-glutamyl transferase with subclinical coronary atherosclerosis and cardiac outcomes in non-alcoholics, *Sci Rep*. 10 (2020) 17994. <https://doi.org/10.1038/s41598-020-75078-6>.
- [75] A.A. Sneddon, H.-C. Wu, A. Farquharson, I. Grant, J.R. Arthur, D. Rotondo, S.-N. Choe, K.W.J. Wahle, Regulation of selenoprotein GPx4 expression and activity in



- human endothelial cells by fatty acids, cytokines and antioxidants, *Atherosclerosis*. 171 (2003) 57–65. <https://doi.org/10.1016/j.atherosclerosis.2003.08.008>.
- [76] S. Allahverdian, C. Chaabane, K. Boukais, G.A. Francis, M.-L. Bochaton-Piallat, Smooth muscle cell fate and plasticity in atherosclerosis, *Cardiovasc Res*. 114 (2018) 540–550. <https://doi.org/10.1093/cvr/cvy022>.
- [77] L.S. Shankman, D. Gomez, O.A. Cherepanova, M. Salmon, G.F. Alencar, R.M. Haskins, P. Swiatlowska, A.A.C. Newman, E.S. Greene, A.C. Straub, B. Isakson, G.J. Randolph, G.K. Owens, KLF4 Dependent Phenotypic Modulation of SMCs Plays a Key Role in Atherosclerotic Plaque Pathogenesis, *Nat Med*. 21 (2015) 628–637. <https://doi.org/10.1038/nm.3866>.
- [78] S. Allahverdian, A.C. Chehroudi, B.M. McManus, T. Abraham, G.A. Francis, Contribution of intimal smooth muscle cells to cholesterol accumulation and macrophage-like cells in human atherosclerosis, *Circulation*. 129 (2014) 1551–1559. <https://doi.org/10.1161/CIRCULATIONAHA.113.005015>.
- [79] N. Dong, W. Wang, J. Tian, Z. Xie, B. Lv, J. Dai, R. Jiang, D. Huang, S. Fang, J. Tian, H. Li, B. Yu, MicroRNA-182 prevents vascular smooth muscle cell dedifferentiation via FGF9/PDGFR $\beta$  signaling, *International Journal of Molecular Medicine*. 39 (2017) 791–798. <https://doi.org/10.3892/ijmm.2017.2905>.
- [80] C. Leimgruber, A.A. Quintar, N. Peinetti, M.V. Scalerandi, J.P. Nicola, J.M. Miano, C.A. Maldonado, Testosterone Rescues the De-Differentiation of Smooth Muscle Cells Through Serum Response Factor/Myocardin, *Journal of Cellular Physiology*. 232 (2017) 2806–2817. <https://doi.org/10.1002/jcp.25679>.
- [81] X. Guo, F. Yan, X. Shan, J. Li, Y. Yang, J. Zhang, X. Yan, P. Bu, SIRT3 inhibits Ang II-induced transdifferentiation of cardiac fibroblasts through  $\beta$ -catenin/PPAR- $\gamma$  signaling, *Life Sci*. 186 (2017) 111–117. <https://doi.org/10.1016/j.lfs.2017.07.030>.
- [82] Y. Tang, Q. Huang, C. Liu, H. Ou, D. Huang, F. Peng, C. Liu, Z. Mo, p22phox promotes Ang-II-induced vascular smooth muscle cell phenotypic switch by regulating KLF4 expression, *Biochem. Biophys. Res. Commun*. 514 (2019) 280–286. <https://doi.org/10.1016/j.bbrc.2019.04.128>.
- [83] J.-F. Zhao, S.-K. Shyue, S.-J. Lin, J. Wei, T.-S. Lee, Excess nitric oxide impairs LXR( $\alpha$ )-ABCA1-dependent cholesterol efflux in macrophage foam cells, *J Cell Physiol*. 229 (2014) 117–125. <https://doi.org/10.1002/jcp.24429>.
- [84] V. (Wai C. Wong, E. Lerner, Nitric oxide inhibition strategies, *Future Sci OA*. 1 (2015) FSO35. <https://doi.org/10.4155/fso.15.35>.
- [85] M.D. Lopez-Carmona, M.C. Plaza-Seron, A. Vargas-Candela, F.J. Tinahones, R. Gomez-Huelgas, M.R. Bernal-Lopez, CD36 overexpression: a possible etiopathogenic mechanism of atherosclerosis in patients with prediabetes and diabetes, *Diabetol Metab Syndr*. 9 (2017) 55. <https://doi.org/10.1186/s13098-017-0253-x>.
- [86] T. Takahashi, Y. Huang, K. Yamamoto, G. Hamano, A. Kakino, F. Kang, Y. Imaizumi, H. Takeshita, Y. Nozato, S. Nozato, S. Yokoyama, M. Nagasawa, T. Kawai, M. Takeda, T. Fujimoto, K. Hongyo, F. Nakagami, H. Akasaka, Y. Takami, Y. Takeya, K. Sugimoto, H.Y. Gaisano, T. Sawamura, H. Rakugi, The endocytosis of oxidized LDL via the activation of the angiotensin II type 1 receptor, *IScience*. 24 (2021) 102076. <https://doi.org/10.1016/j.isci.2021.102076>.

# Appendix 1




**SOT** | Society of  
Toxicology  
www.toxsci.oxfordjournals.org

TOXICOLOGICAL SCIENCES, 2019, 1–7

doi: 10.1093/toxsci/kfz175  
Advance Access Publication Date: August 6, 2019  
Research Article

## Induction of Gamma-Glutamyltransferase Activity and Consequent Pro-oxidant Reactions in Human Macrophages Exposed to Crocidolite Asbestos

Alessandro Corti <sup>\*,1</sup>, Justine Bonetti,<sup>†</sup> Silvia Dominici,<sup>\*</sup> Simona Piaggi,<sup>\*</sup> Vanna Fierabracci,<sup>\*</sup> Rudy Foddìs,<sup>\*</sup> and Alfonso Pompella<sup>\*</sup>

<sup>\*</sup>Department of Translational Research NTMS, University of Pisa Medical School, Pisa 56126, Italy; and

<sup>†</sup>Université de Lorraine, CITHEFOR, F-54000 Nancy, France

The authors certify that all research involving human subjects was done under full compliance with all government policies and the Helsinki Declaration.

<sup>1</sup>To whom correspondence should be addressed. Fax: (+39) 050 2218557; E-mail: alessandro.corti@med.unipi.it.

### ABSTRACT

Asbestos is the main causative agent of malignant pleural mesothelioma. The variety known as crocidolite (blue asbestos) owns the highest pathogenic potential, due to the dimensions of its fibers as well as to its content of iron. The latter can in fact react with macrophage-derived hydrogen peroxide in the so called Fenton reaction, giving rise to highly reactive and mutagenic hydroxyl radical. On the other hand, hydroxyl radical can as well originate after thiol-dependent reduction of iron, a process capable of starting its redox cycling. Previous studies showed that glutathione (GSH) is one such thiol, and that cellular gamma-glutamyltransferase (GGT) can efficiently potentiate GSH-dependent iron redox cycling and consequent oxidative stress. As GGT is expressed in macrophages and is released upon their activation, the present study was aimed at verifying the hypothesis that GSH/GGT-dependent redox reactions may participate in the oxidative stress following the activation of macrophages induced by crocidolite asbestos. Experiments in acellular systems confirmed that GGT-mediated metabolism of GSH can potentiate crocidolite-dependent production of superoxide anion, through the production of highly reactive dipeptide thiol cysteinyl-glycine. Cultured THP-1 macrophagic cells, as well as isolated monocytes obtained from healthy donors and differentiated to macrophages *in vitro*, were investigated as to their expression of GGT and the effects of exposure to crocidolite. The results show that crocidolite asbestos at subtoxic concentrations (50–250 ng/1000 cells) can upregulate GGT expression, which raises the possibility that macrophage-initiated, GSH/GGT-dependent pro-oxidant reactions may participate in the pathogenesis of tissue damage and inflammation consequent to crocidolite intoxication.

**Key words:** crocidolite asbestos; macrophages; gamma-glutamyltransferase; glutathione; iron reduction; oxidative injury.

Exposure to asbestos—a family of hydrated silicate minerals with fibrillar structure at microscopic level—represents the main risk factor for the onset of pleural mesothelioma, a highly malignant and aggressive neoplasia of the lung. The highest carcinogenic potential is owned by the mineral varieties termed amosite and crocidolite (also known as blue asbestos), whose fibers are relatively longer. Once inhaled microscopic fibers reach the lung parenchyma, where resident macrophages become activated in a

typical foreign body reaction and produce reactive oxygen species (ROS: superoxide anion, hydrogen peroxide) and cytokines. Macrophages also attempt to phagocytose the fibers—but the dimensions of the latter do not allow formation of complete phagosomes, and cause rather plasma membrane ruptures leading to macrophage death (reviewed by Jiang *et al.*, 2008).

Pathogenicity of asbestos is closely related with the presence of iron associated with fibers, particularly in the case of

crocidolite asbestos (CR-A). Iron can in fact react with macrophage-derived  $H_2O_2$  and catalyze a typical Fenton reaction giving rise to highly reactive hydroxyl radical. In addition, a series of agents are capable of reducing ionic iron and starting its so called "redox cycling," leading to the production of ROS (Kappus and Sies, 1981). Previous studies from our laboratory have shown that thiol-dependent reduction of iron is greatly enhanced in the presence of gamma-glutamyltransferase (GGT) enzyme activity (Dominici et al., 1999). Interestingly, activated macrophages display such activity and can release GGT extracellularly (Belcastro et al., 2015). The present study was aimed therefore to verify the hypothesis that macrophagic GGT can further promote—in a thiol-dependent way—the pro-oxidant reactions ensuing from the redox cycling of iron associated with CR-A fibers.

## MATERIALS AND METHODS

**Chemicals.** Unless otherwise indicated, all reagents were from Sigma Chemical Co (St Louis, Missouri). Recombinant human cytokines and growth factors were purchased from PeproTech (London, UK). The specific GGT inhibitor GGsToP was obtained from Tocris (UK); purified human GGT was obtained from Lee Biosolutions (St Louis, Missouri). CR-A standard by the Union Internationale Contre le Cancer (UICC) was kindly provided by Dr F. Turci, Department of Chemistry of the University of Turin (Italy).

**NBT reduction assay.** Nitroblue tetrazolium (NBT) assay is used to estimate the superoxide production through the generation of purple-colored formazan precipitates (Uy et al., 2011). Incubations (100  $\mu$ l) were carried out in 100 mM Tris-HCl buffer, pH 7.4, at 37°C in the dark and, where indicated, contained glutathione (GSH) (0.5 mM) and glycyl-glycine as GGT cosubstrate (2 mM), purified GGT (100 mU/ml), cysteinyl-glycine (0.5 mM), specific GGT inhibitor GGsToP (30  $\mu$ M), the iron chelator deferoxamine mesylate (DFO; 3 mM), CR-A (20  $\mu$ g/ml), and NBT (0.33 mg/ml). After 60 min, DMSO (50  $\mu$ l) was added to dissolve the formazan crystals and the absorbance was recorded at 560 nm using a multilabel counter (Wallac 1420-Victor3, Perkin-Elmer).

**Cells of macrophagic lineage.** The human monocytic leukemia cell line THP-1 was purchased from the Interlab Cell Line Collection (ICLC, Genova, Italy). Cells were routinely grown in suspension in RPMI 1640 medium supplemented with 2 mM L-glutamine and 10% fetal bovine serum (vol/vol) in a humidified 37°C, 5%  $CO_2$  incubator, and were plated in the presence of phorbol 12-myristate-13-acetate (PMA; 100 nM) for 24 h to achieve their differentiation into macrophage-like cells (Daigneault et al., 2010).

Human peripheral blood mononuclear cells (PBMCs) were isolated by Histopaque-1077 density centrifugation from the blood of healthy donors obtained by the Blood Transfusion Center of the University of Pisa Hospital. The study was approved by the Institutional Ethics Committee of the University of Pisa Hospital, and conformed to the Declaration of Helsinki. Written informed consent was obtained from all subjects enrolled in the study and the data were analyzed anonymously. Monocytes were isolated from PBMCs as previously described (Belcastro et al., 2015), by negative selection with the Pan Monocyte Isolation Kit (Miltenyi Biotec, Bergisch Gladbach, Germany), according to manufacturer's instructions. Monocytes were then cultured for 6 days in complete medium (RPMI 1640 medium, 2 mM L-glutamine, 100 U/ml penicillin, 100  $\mu$ g/ml streptomycin, 10% vol/vol fetal calf serum) integrated with 50 ng/ml

recombinant human macrophage colony stimulating factor (M-CSF) in order to obtain their differentiation into M2-like macrophages (M0 cells). Confirmation of the M0 phenotype was obtained by cytokine profile (Belcastro et al., 2015) and by conventional flow cytometry techniques (data not shown) according to others (eg. Jaguin et al., 2013; Raggi et al., 2017).

**Cell viability assay.** Cell viability was evaluated by the WST-1 assay (Roche) according to the manufacturer's instructions, and the results were expressed as percentages of control. The Trypan blue exclusion test was also used.

**Western blot analyses.** Samples were harvested in sodium dodecyl sulfate (SDS) sample buffer (62.5 mM Tris-HCl [pH 6.8], 2% wt/vol SDS, 10% glycerol, 50 mM dithiothreitol [DTT], 0.01% [wt/vol] bromophenol blue) and heated at 95°C for 5 min. Samples were separated by 10% SDS-PAGE and incubated with a rabbit anti-GGT antibody directed against the C-terminal 20 amino acids of human GGT heavy chain prepared as described (Hanigan and Frierson, 1996). A rabbit antiactin antibody (1:1000; Cell Signaling) was used as loading control. Visualization of protein bands was obtained using a horseradish peroxidase-conjugated antirabbit IgG antibody (Santa Cruz Biotechnology, Santa Cruz, California) and the ECL detection system (Roche, Basel, Switzerland). Bands were analyzed with a Bio-Rad ChemiDoc apparatus equipped with the Quantity One software.

**Cytochemical staining for GGT activity.** Samples were fixed in a phosphate buffered acetone formaldehyde mixture and the cytochemical revelation of GGT activity was obtained using gamma-glutamyl-4-methoxy-2-naphthylamide as a substrate and glycyl-glycine as cosubstrate, with Fast Garnet GBC as a chromogen (Khalaf and Hayhoe, 1987).

**Other determinations.** GGT activity was determined according to Huseby and Strömme (1974). Determinations of GSH reductase and GSH peroxidase were performed as described (Paolicchi et al., 2002). Protein content was determined by using the Pierce BCA Protein Assay Kit (ThermoFisher Scientific), following the manufacturer's instructions.

**Statistical analysis of data.** The Student's t test or one-way ANOVA with Newman-Keuls test for multiple comparisons were used, as detailed for each experiment.

## RESULTS

The ability of CR-A to catalyze thiol-dependent production of superoxide anion was verified *in vitro*, using the NBT reduction assay. As shown in Figure 1, the addition to CR-A of GSH alone produced some stimulation of NBT reduction, and the effect was greatly enhanced by the addition of GGT. The same was observed in the presence of cysteinyl-glycine alone, ie, the redox-active thiol dipeptide originating from GGT-dependent metabolism of GSH. The role of GGT activity in the phenomenon was confirmed using the specific GGT inhibitor GGsToP, whose presence abolished the observed stimulation of NBT reduction. The involvement of iron was confirmed using the iron chelator deferoxamine mesylate, which inhibited the GGT-induced production of superoxide anion (Figure 1).

GGT enzyme activity was determined in 2 distinct cellular models of macrophagic lineage, THP-1 monocytic leukemia cells (differentiated to macrophages by exposure to PMA) and



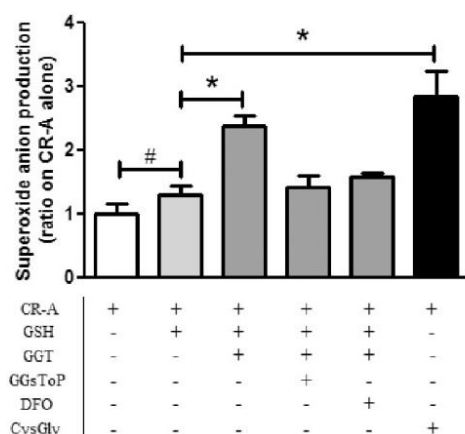


**Figure 1.** Production of superoxide anion (nitroblue tetrazolium reduction) in an acellular system including crocidolite asbestos plus the indicated reagents. Incubations were carried out as detailed in Materials and Methods section and the absorbance was recorded at 560 nm. Data are expressed as ratios on values obtained from the incubation with crocidolite asbestos (CR-A) alone. Where indicated purified human gamma-glutamyltransferase (GGT), the GGT inhibitor GGsToP or the iron chelator deferoxamine mesylate (DFO) were added to the incubation mixtures. Data are means  $\pm$  SD of 4 determinations and were analyzed by one-way ANOVA with Newman-Keuls test for multiple comparisons. # $p < .005$ ; \* $p < .0001$ .

peripheral blood monocytes obtained from healthy donors, differentiated *in vitro* to macrophages by treatment with M-CSF (M0 cells). Basal levels of GGT activity were significantly different, being remarkably higher in THP-1 as compared to M0 cells (Figure 2). Cells were then exposed to nontoxic concentrations of CR-A, corresponding to 0.05 and 0.25  $\mu$ g/1000 cells for THP-1 (viability:  $92.9 \pm 8.9$ ) and M0 cells (viability:  $97.5 \pm 8.7$ ), respectively, and GGT protein expression was evaluated by immunoblot. In such conditions, a remarkable induction of GGT was observed in both THP-1 and M0 cells (approximately +40%). The phenomenon was observed as both enzyme activity (Figure 3) as well as expression of GGT protein (Figure 4).

The 2 cellular models under examination presented with different sensitivities to CR-A cytotoxicity, M0 cells being approximately 5-fold more resistant than THP-1 cells (Figure 5). The possibility that the difference might result from different antioxidant defenses was investigated by analyzing the GSH status in the 2 cellular models. Indeed, basal intracellular GSH levels were markedly higher in M0 cells. Exposure to CR-A caused a significant increase of total GSH in THP-1 cells, but not in M0 cells (Figure 6). Levels of GSSG were also significantly increased in THP-1 cells (GSSG/GSH ratio, CR-A treated vs controls:  $5.0 \pm 0.1\%$  vs  $3.6 \pm 0.6\%$ , ie, +38%,  $p < .05$ ), whereas they were undetectable in M0 cells, irrespective of treatment. Analysis of GSH-related enzymes showed that both GSH reductase and GSH peroxidase activities were markedly higher in M0 cells (Figure 7). The increased GSH reductase activity of M0 cells can account for their higher basal GSH content, and this in turn suggests that the higher resistance of M0 cells to CR-A cytotoxicity can be an effect of their stronger GSH-dependent antioxidant defenses.

The possible implication of GGT-mediated pro-oxidant reactions in the cytotoxic effects of CR-A was tested in more

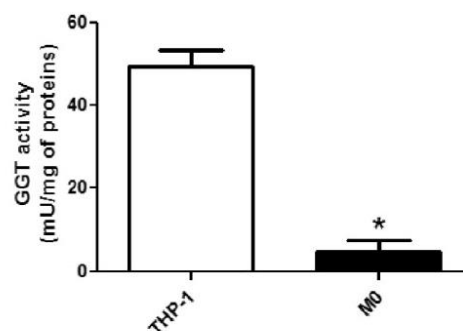


**Figure 2.** Gamma-glutamyltransferase (GGT) enzyme activity in the 2 cellular models under evaluation. GGT activity was evaluated after differentiation with phorbol 12-myristate-12 acetate (PMA) or macrophage colony stimulating factor (M-CSF) (see text for details). Data are expressed as means  $\pm$  SD of 3–6 determinations. \* $p < .001$ .

sensitive THP-1 cells. However, the inhibition of GGT activity with the specific inhibitor GGsToP did not protect cells from CR-A cytotoxicity (data not shown).

## DISCUSSION

CR-A fibers include up to 30% iron as an integral component of their chemical structure, and additional iron deriving from dead macrophages as well as hemolysis accumulates onto fibers during decades of permanence in tissue (Nagai et al., 2011). As recognized in earlier studies (Governa et al., 1999), iron plays a central role in pathogenicity of asbestos: activated macrophages in fact release  $H_2O_2$  and thus CR-A associated iron can promote a typical Fenton reaction originating highly reactive and harmful hydroxyl radical. On the other hand, the reduction of ferric Fe(III) to ferrous Fe(II) ions followed by autooxidation of the latter (the so called “iron redox cycling”), can also give rise to ROS production (Kappus and Sies, 1981). Among other compounds, endogenous thiols (R-SH) are capable of reducing iron and promote iron-dependent ROS production, with varying efficiency depending on the reactivity of their SH groups (Spear and Aust, 1994). Altogether, such iron-dependent pro-oxidant reactions could concur to tissue damage induced by CR-A intoxication, as well as to the mutagenic effects resulting at later times in carcinogenesis (Toyokuni, 2019).

The well-known thiol tripeptide GSH is also capable of sustaining iron redox cycling to some extent, and previous studies from our laboratory have shown that this ability is remarkably boosted in cysteinyl-glycine, the dipeptide resulting from GSH metabolism by GGT (Dominici et al., 1999). GGT activity is present in serum, and is expressed at varying levels in several cell types. We documented thus the ability of GGT to catalyze thiol-dependent pro-oxidant reactions in a series of experimental models of pathophysiological relevance (reviewed by Dominici et al., 2005). GGT-mediated pro-oxidant reactions are well evident after addition of exogenous GSH (Dominici et al., 1999), but it is important to note here that they also spontaneously occur in basal condition. Cellular GGT is in fact present on the outer aspect of the cell membrane and continuously metabolizes the GSH effluxing from the cell itself—a step in what was termed “the gamma-glutamyl cycle” (Griffith and Meister, 1979; Meister, 1974). Previous work from our laboratory has demonstrated that

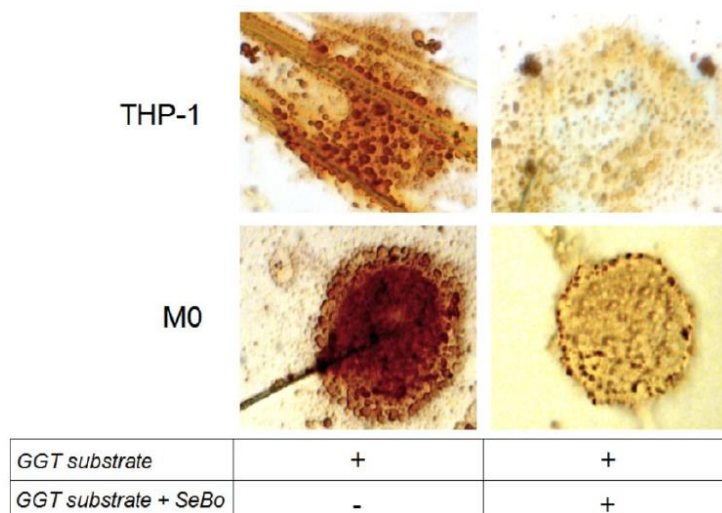


**Figure 3.** Cytochemical demonstration of gamma-glutamyltransferase (GGT) activity in THP-1 and M0 cells exposed to crocidolite asbestos. GGT activity (dark stain) is present in association with cells. Negative control: inhibition of GGT activity with serine/boric acid (20/20 mM) complex (SeBo) added to the complete incubation mixture (Dominici *et al.*, 2005). Magnification:  $\times 100$ .

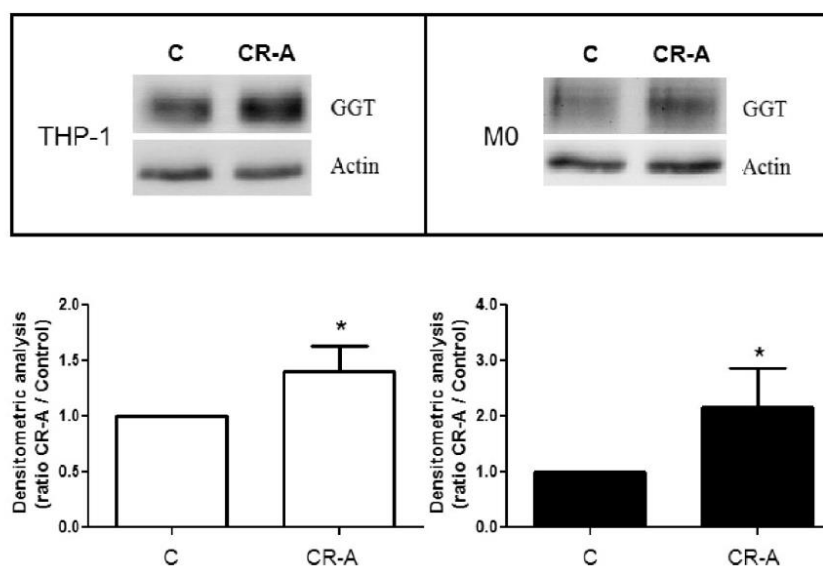


**Figure 4.** Effects of exposure to crocidolite asbestos on the cellular expression of gamma-glutamyltransferase (GGT). Representative immunoblots out of 3–4 experiments are shown. Cells were incubated for 48 h with or without control (C) a noncytotoxic concentration of crocidolite asbestos (CR-A) (0.05  $\mu\text{g}/1000$  cells for THP-1 and 0.25  $\mu\text{g}/1000$  cells for M0). Data are means  $\pm$  SD of 3–4 experiments and are expressed as ratios on untreated controls. \* $p < .005$ .

the continuous cleavage of effluxing GSH by cell membrane GGT indeed imposes a continuous, low level oxidative stress to cells (Corti *et al.*, 2009). The significance of GGT thus extends beyond its recognized function in the cellular supply

of thiols (the "antioxidant" role of GGT), and the possibility that it may paradoxically promote oxidative stress in selected conditions (ie, availability of metal cations) should be considered.



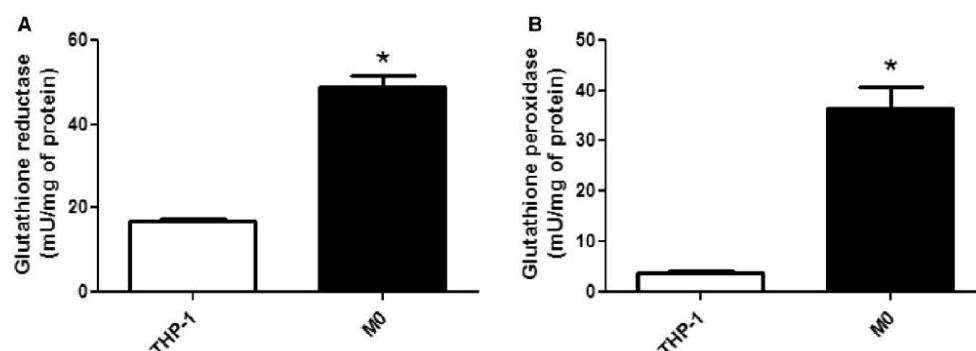


Figure 7. Glutathione (GSH)-dependent enzyme activities in THP-1 and M0 cells. See Materials and Methods section for details. Data are means  $\pm$  SD of 3 determinations. A, Glutathione reductase, \* $p < .001$ . B, Glutathione peroxidase, \* $p < .005$ .

University of Pisa Hospital and with the 1964 Helsinki declaration and its later amendments or comparable ethical standards.

**Informed consent:** Written informed consent was obtained from all subjects enrolled in the study and the data were analyzed anonymously.

## ACKNOWLEDGMENTS

The authors are indebted to Dr F. Turci, Department of Chemistry of the University of Turin (Italy), for providing material and discussing laboratory procedures. A special thanks to Dr C. Pileggi and Dr M. Lanza of Azienda Ospedaliera Universitaria Pisana (Pisa, Italy) for their help in blood samples collection.

## FUNDING

This study was funded by the University of Pisa (PRA 2017 funds). We also acknowledge the financial support from the Program VINCI 2018—Université Franco Italienne (project number: C2-796).

## REFERENCES

- Belcastro, E., Franzini, M., Cianchetti, S., Lorenzini, E., Masotti, S., Fierabracci, V., Pucci, A., Pompella, A., and Corti, A. (2015). Monocytes/macrophages activation contributes to  $\gamma$ -glutamytransferase accumulation inside atherosclerotic plaques. *J. Transl. Med.* **13**, 325.
- Corti, A., Bergamini, G., Menegazzi, M., Piaggi, S., Bramanti, E., Scatagli, I., Cianchetti, S., Paggiaro, P., Melotti, P., and Pompella, A. (2013).  $\gamma$ -Glutamyltransferase catabolism of S-nitrosoglutathione modulates IL-8 expression in cystic fibrosis bronchial epithelial cells. *Free Radic. Biol. Med.* **65**, 360–370.
- Corti, A., Duarte, T. L., Giommarelli, C., De Tata, V., Paolicchi, A., Jones, G. D., and Pompella, A. (2009). Membrane gamma-glutamyl transferase activity promotes iron-dependent oxidative DNA damage in melanoma cells. *Mutat. Res.* **669**, 112–121.
- Corti, A., Paolicchi, A., Franzini, M., Dominici, S., Casini, A. F., and Pompella, A. (2005). The S-thiolating activity of membrane gamma-glutamyltransferase: Formation of cysteinyl-glycine mixed disulfides with cellular proteins and in the cell microenvironment. *Antioxid. Redox Signal.* **7**, 911–918.
- Daigneault, M., Preston, J. A., Marriott, H. M., Whyte, M. K., and Dockrell, D. H. (2010). The identification of markers of macrophage differentiation in PMA-stimulated THP-1 cells and monocyte-derived macrophages. *PLoS One* **5**, e8668.
- Dominici, S., Paolicchi, A., Corti, A., Maellaro, E., and Pompella, A. (2005). Prooxidant reactions promoted by soluble and cell-bound gamma-glutamyltransferase activity. *Meth. Enzymol.* **401**, 484–501.
- Dominici, S., Valentini, M., Maellaro, E., Del Bello, B., Paolicchi, A., Lorenzini, E., Tongiani, R., Comporti, M., and Pompella, A. (1999). Redox modulation of cell surface protein thiols in U937 lymphoma cells: The role of gamma-glutamyl transpeptidase-dependent  $H_2O_2$  production and S-thiolation. *Free Radic. Biol. Med.* **27**, 623–635.
- Governa, M., Amati, M., Fontana, S., Visona, I., Botta, G. C., Mollo, F., Bellis, D., and Bo, P. (1999). Role of iron in asbestos-body-induced oxidant radical generation. *J. Toxicol. Environ. Health A* **58**, 279–287.
- Griffith, O. W., and Meister, A. (1979). Translocation of intracellular glutathione to membrane-bound gamma-glutamyl transpeptidase as a discrete step in the gamma-glutamyl cycle: Glutathionuria after inhibition of transpeptidase. *Proc. Natl. Acad. Sci. U.S.A.* **76**, 268–272.
- Hanigan, M. H., and Frierson, H. F., Jr (1996). Immunohistochemical detection of gamma-glutamyl transpeptidase in normal human tissue. *J. Histochem. Cytochem.* **44**, 1101–1108.
- Hanigan, M. H., Gillies, E. M., Wickham, S., Wakeham, N., and Wirsig-Wiechmann, C. R. (2015). Immunolabeling of gamma-glutamyl transferase 5 in normal human tissues reveals that expression and localization differ from gamma-glutamyl transferase 1. *Histochem. Cell Biol.* **143**, 505–515.
- Heisterkamp, N., Groffen, J., Warburton, D., and Sneddon, T. P. (2008). The human gamma-glutamyltransferase gene family. *Hum. Genet.* **123**, 321–332.
- Huseby, N. E., and Strömme, J. H. (1974). Practical points regarding routine determination of gamma-glutamyl transferase (gamma-GT) in serum with a kinetic method at 37 degrees C. *Scand. J. Clin. Lab. Invest.* **34**, 357–363.
- Jaguin, M., Houlbert, N., Fardel, O., and Lecureur, V. (2013). Polarization profiles of human M-CSF-generated macrophages and comparison of M1-markers in classically activated macrophages from GM-CSF and M-CSF origin. *Cell. Immunol.* **281**, 51–61.

- Jiang, L., Nagai, H., Ohara, H., Hara, S., Tachibana, M., Hirano, S., Shinohara, Y., Kohyama, N., Akatsuka, S., and Toyokuni, S. (2008). Characteristics and modifying factors of asbestos-induced oxidative DNA damage. *Cancer Sci.* **99**, 2142–2151.
- Kappus, H., and Sies, H. (1981). Toxic drug effects associated with oxygen metabolism: Redox cycling and lipid peroxidation. *Experientia* **37**, 1233–1241.
- Khalaf, M. R., and Hayhoe, F. G. J. (1987). Cytochemistry of gamma-glutamyltransferase in haemic cells and malignancies. *Histochem. J.* **19**, 385–395.
- Kugelman, A., Choy, H. A., Liu, R., Shi, M. M., Gozal, E., and Forman, H. J. (1994). Gamma-glutamyl transpeptidase is increased by oxidative stress in rat alveolar L2 epithelial cells. *Am. J. Respir. Cell Mol. Biol.* **11**, 586–592.
- Lee, D. H., and Jacobs, D. R., Jr (2009). Is serum gamma-glutamyltransferase a marker of exposure to various environmental pollutants? *Free Radic. Res.* **43**, 533–537.
- Lu, E., Wolfreys, F. D., Muppidi, J. R., Xu, Y., and Cyster, J. G. (2019). S-geranylgeranyl-L-glutathione is a ligand for human B cell-confinement receptor P2RY8. *Nature* **567**, 244–248.
- Maellaro, E., Dominici, S., Del Bello, B., Valentini, M. A., Pieri, L., Perego, P., Supino, R., Zunino, F., Lorenzini, E., Paolicchi, A., et al. (2000). Membrane gamma-glutamyl transpeptidase activity of melanoma cells: Effects on cellular H<sub>2</sub>O<sub>2</sub> production, cell surface protein thiol oxidation and NF-kappa B activation status. *J. Cell. Sci.* **113**, 2671–2678.
- Meister, A. (1974). Glutathione, metabolism and function via the gamma-glutamyl cycle. *Life Sci.* **15**, 177–190.
- Nagai, H., Ishihara, T., Lee, W. H., Ohara, H., Okazaki, Y., Okawa, K., and Toyokuni, S. (2011). Asbestos surface provides a niche for oxidative modification. *Cancer Sci.* **102**, 2118–2125.
- Paolicchi, A., Lorenzini, E., Perego, P., Supino, R., Zunino, F., Comporti, M., and Pompella, A. (2002). Extra-cellular thiol metabolism in clones of human metastatic melanoma with different gamma-glutamyl transpeptidase expression: Implications for cell response to platinum-based drugs. *Int. J. Cancer* **97**, 740–745.
- Paolicchi, A., Minotti, G., Tonarelli, P., Tongiani, R., De Cesare, D., Mezzetti, A., Dominici, S., Comporti, M., and Pompella, A. (1999). Gamma-glutamyl transpeptidase-dependent iron reduction and LDL oxidation—a potential mechanism in atherosclerosis. *J. Investig. Med.* **47**, 151–160.
- Paolicchi, A., Tongiani, R., Tonarelli, P., Comporti, M., and Pompella, A. (1997). Gamma-glutamyl transpeptidase-dependent lipid peroxidation in isolated hepatocytes and HepG2 hepatoma cells. *Free Radic. Biol. Med.* **22**, 853–860.
- Raggi, F., Pelassa, S., Pierobon, D., Penco, F., Gattorno, M., Novelli, F., Eva, A., Varesio, L., Giovarelli, M., and Bosco, M. C. (2017). Regulation of human macrophage M1-M2 polarization balance by hypoxia and the triggering receptor expressed on myeloid cells-1. *Front. Immunol.* **8**, 1097.
- Spear, N., and Aust, S. D. (1994). Thiol-mediated NTA-Fe(II) reduction and lipid peroxidation. *Arch. Biochem. Biophys.* **312**, 198–202.
- Toyokuni, S. (2019). Iron addiction with ferroptosis-resistance in asbestos-induced mesothelial carcinogenesis: Toward the era of mesothelioma prevention. *Free Radic. Biol. Med.* **133**, 206–215.
- Uy, B., McGlashan, S. R., and Shaikh, S. B. (2011). Measurement of reactive oxygen species in the culture media using Acridan Lumigen PS-3 assay. *J. Biomol. Tech.* **22**, 95–107.
- Wickham, S., Regan, N., West, M. B., Thai, J., Cook, P. F., Terzyan, S. S., Li, P. K., and Hanigan, M. H. (2013). Inhibition of human  $\gamma$ -glutamyl transpeptidase: Development of more potent, physiologically relevant, uncompetitive inhibitors. *Biochem. J.* **450**, 547–557.
- Zhang, H., and Forman, H. J. (2009). Redox regulation of gamma-glutamyl transpeptidase. *Am. J. Respir. Cell Mol. Biol.* **41**, 509–515.

## **Potentiel thérapeutique des S-nitrosothiols dans la prévention de l'athérosclérose : modulation de la métaplasie des monocytes et cellules musculaires lisses en cellules spumeuses**

L'athérosclérose est une maladie chronique, silencieuse, à évolution lente, caractérisée par la formation de plaques d'athérome. Celles-ci se forment suite à une accumulation de lipoprotéines de faible densité (LDL), de monocytes et de cellules musculaires lisses (CML) précédant leur métaplasie en cellules spumeuses. Cela conduit à la formation d'un noyau nécrotique et une possible calcification de l'artère. L'évolution de ces phénomènes est due à une combinaison entre l'inflammation et le stress oxydant. Deux types cellulaires majeurs sont impliqués dans la formation des plaques d'athérome : *i*) les monocytes qui se différencient en deux sub-populations de macrophages : pro-inflammatoires (M1) et anti-inflammatoires (M2) ainsi que *ii*) les CML, perdant leur phénotype contractile pour se dédifférencier vers un phénotype sécrétoire/prolifératif. Ainsi différenciées/dédifférenciées, les cellules acquièrent la capacité à internaliser les LDL oxydés (oxLDL) conduisant à la formation de cellules spumeuses. Le stress oxydant et l'inflammation engendrent également un dysfonctionnement de l'endothélium menant à une diminution de la biodisponibilité en monoxyde d'azote (NO), une oxydation des LDL et une prolifération/dédifférenciation des CML. Afin de pallier cette diminution de NO, l'utilisation de donneurs de NO, les S-nitrosothiols est envisagée. Formés par S-nitrosation, ils permettent d'augmenter la demi-vie de NO et de limiter le stress oxydant. Parmi eux, le S-nitrosoglutathion (GSNO), forme physiologique de transport et de stockage de NO, permettant ainsi de mimer des réservoirs physiologiques en NO. La première partie de ce manuscrit a été consacrée au développement d'un modèle cellulaire de différenciation monocytes/macrophages suivi de leur polarisation en macrophages M1 ou M2. Une deuxième partie s'est axée sur l'étude de l'impact de NO, et plus particulièrement de GSNO, sur la formation des cellules spumeuses. Enfin, en troisième partie, le développement d'un modèle cellulaire de dédifférenciation des CML à partir d'un stimulus induisant un stress oxydant, l'angiotensine II.

**Mots-clés :** athérosclérose, S-nitrosoglutathion, stress oxydant, inflammation, monoxyde d'azote

## **Therapeutic potential of S-nitrosothiols in the prevention of atherosclerosis: modulation of monocytes and smooth muscle cells metaplasia**

Atherosclerosis is a chronic disease, quiet, with a slow evolution, characterized by the formation of atherosclerotic plaques. These are formed further to an accumulation of low-density lipoproteins (LDLs), monocytes and smooth muscle cells (SMCs), followed by their metaplasia into foam cells. The whole leads to the formation of the necrotic *core* and a possible artery calcification. The evolution of these phenomena is due to a combination of inflammation and oxidative stress. Two major cell types are involved in atherosclerotic plaques formation: *i*) monocytes, differentiated into two sub-populations of macrophages: pro-inflammatory (M1) and anti-inflammatory (M2) as well as *ii*) SMCs, losing their contractile phenotype to dedifferentiate into a secretory/proliferative phenotype. Differentiated/dedifferentiated cells purchase the capacity to internalize oxidized LDLs (oxLDLs), allowing foam cells formation. Oxidative stress and inflammation cause also an endothelial dysfunction leading to a decrease of nitric oxide (NO) bioavailability, LDLs oxidation and a proliferation/dedifferentiation of SMCs. In order to compensate this decrease of NO, the use of NO donors, such as S-nitrosothiols, is considered. Formed by S-nitrosation, they increase NO half-life and limit oxidative stress. Among them, S-nitrosoglutathione (GSNO), a physiological storage form and transport of NO, allows to mimic physiological reservoirs of NO. The first part of this manuscript was devoted to the development of a cellular model of monocytes/macrophages differentiation followed by their polarization into M1- and M2-macrophages. The second part of this manuscript was centred on the study of the impact of NO, and more specifically of GSNO, on foam cells formation. Finally, in a third part, the development of a cellular model of SMC dedifferentiation from a stimulus inducing oxidative stress, angiotensin II.

**Key words:** atherosclerosis, S-nitrosoglutathione, oxidative stress, inflammation, nitric oxide